ANNUAL REVIEW

INSTITUTE FOR MOLECULAR SCIENCE

1983

ANNUAL REVIEW

INSTITUTE FOR MOLECULAR SCIENCE

1983

Published by
Okazaki National Research Institutes
Institute for Molecular Science
Myodaiji, Okazaki 444, Japan
Phone 0564-54-1111
Telex 4537-475 KOKKEN J
December 27, 1983

Editorial Committee 1983: Nobuyuki Nishi (Chairman),
Keiichiro Nasu, Chikashi Yamada,
Hisanori Shinohara, Gunzi Saito,
Noboru Kaga, Keisaku Kimura,
Toshihiro Takagi, and Noriko Hosoi

IMS 1983

As Director-General I am pleased to issue the Annual Review 1983 reporting on the present situation of IMS and scientific activities accomplished during the past year.

As this Review shows, scientific activity at IMS has continued to increase during the past year. In particular, I am glad to report that the Ultraviolet Synchrotoron Orbital Radiation (UVSOR) Project has made great progress and has succeeded in the test operation of our UVSOR machine. I hope its regular operation will start in the coming January.

During the past year, several young scientists in IMS have moved to new positions outside and we have had new scientists join us. Among them a senior research staff member was Dr. T. Kitagawa as Professor of Molecular Dynamics. He transferred from Osaka University to the chair as the successor to the late Professor T. Fujiyama.

Two research laboratories for foreign visiting scientists have been newly established. I am glad to have had Dr. G. Saxon (Daresbury Laboratory, UK) as Professor of the Synchrotron Radiation Research Laboratory and Professor S.H. Bauer (Cornell University, USA) as Professor of the Molecular Energy Conversion Laboratory.

Professor Sir George Porter (Royal Institution, UK) completed his term of service as a foreign member of the IMS Council at the end of last May. I would like to take this opportunity to extend my hearty thanks to him for his excellent services to IMS. I am glad that IMS has Professor Per Olov Löwdin (University of Uppasla, Sweden) as a new foreign member of the Council.

December 1983

Saburo Nagakura
Director-General

CONTENTS

IMS 1983 ..... Saburo Nagakura iii

CONTENTS v

ORGANIZATION AND STAFF 1

COUNCIL 8

BUILDINGS AND CAMPUS 10

RESEARCH ACTIVITIES I DEPARTMENT OF THEORETICAL STUDIES 12

A. Characterization of Potential Energy Surfaces 12

1. Intramolecular Vibrational Relaxation in $CHCl_3$: A Classical Trajectory Study 12
2. The Structure and Stability of Oxyallyl: An MCSCF Study 12
3. Ab Initio Study of m-Benzoquinodimethane 12
4. Ab Initio MO Calculations of Isotope Effects in Model Processes of Neopentyl Ester Solvolysis 13
5. Theoretical Studies of the Gas-Phase Proton Affinities of Molecules Containing Phosphorus-Carbon Multiple Bonds 13

B. Problems of Molecular Structure 13

1. The Effective Fragment Potential Method – An Approximate ab initio MO Method for Large Molecules 14
2. Role of Sulfur d Orbitals in the S...N Bond Stability of Ammonioalkylsulfuranes 14
3. Relative Conformer Stability of Diphosphine and Phosphinodifluoreophosphine: An Ab Initio Study 14
4. Force Field in the Hydrazine Molecule from Ab Initio MO Calculation 14
5. Vibrational Analysis of Ethylamines: Trans and Gauche Forms 15
6. **Ab initio** Molecular Orbital Study on the Formic Acid Dimer 15
7. Ab Initio Molecular Orbital Study on the Thermostability of the Extreme Thermophile tRNA: Role of the Base Stacking 15

C. Structure, Bonding and Reactivity of Transition Metal Complexes 16

1. Reaction Mechanisms of Oxidative Addition: $H_2 + Pt(0)(PH_3)_2 \rightarrow Pt(II)(H)(PH_3)_2$ and Reductive Elimination: $Pt(II)(H)(CH_3)(PH_3)_2 \rightarrow CH_4 + Pt(0)(PH_3)_2$: Ab initio MO Study 16
2. Intramolecular CH...M Interaction: A Theoretical Study for Three-coordinate $Pd(H)(C_2H_5)(PH_3)$ and Six-coordinate $Ti(H)_3(CH_3)(PH_3)_2$ and $Ti(H)_3(C_2H_5)(PH_3)_2$ 16

D. Development and Application of the LCAO-Xα Direct Force Calculation Method 17

1. Force and Virial Formula in the LCAO-Xα Method and its Application to Oxygen Chemisorption on Metal Surfaces 17
2. The Role of d-Orbitals in Dissociative Chemisorption of Hydrogen Molecule on Metal Surfaces 17

E. Chemical Reaction in Liquid Phase 18

1. Energy Relaxation of Ethylene in Solvents 18

F. Nonadiabatic Transitions in Atomic and Molecular Processes 18

1. Semiclassical Theory of Predissociation Induced by Rotational (Coriolis) Coupling 18
2. Dynamical-state Representation and Its Application to the $Li^+ + Na$ and $Li + Na^+$ Collisions 19

G. Theoretical Studies of Chemical Reaction Dynamics 19

1. A New Semiclassical Scattering Theory in Phase Space 19
2. Applicability of the LZS and the RZ formulas to Collinear Chemical Reactions 19

H. Potential Energy Curves of Low Lying Excited States of CN 20

I. Electron-Correlation and Electron-Phonon Coupling in One-Dimensional Many-Electron Systems 21
1. Extended Peierls-Hubbard Model for One-Dimensional N-Sites N-Electrons System. I. – Phase Diagram by Mean Field Theory – 21
2. Extended Peierls-Hubbard Model for One-Dimensional N-Sites N-Electrons System. II. – Effects of Fluctuation, Optical and Magnetic Excitations – 21
3. Extended Peierls-Hubbard Model for One-Dimensional N-Sites N-Electrons System. III. – Lattice Relaxation after Optical Excitation in CDW – 21

J. Paths and Rates of Chemical Reactions 22
1. Ab initio MO CI Study of the Hydrogen Abstruction by $NH(a^1\Delta)$ 22
2. SCF MO Studies of the Reaction of $NH(^3\Sigma^-)$ with Ethylene 22
3. Potential Energy Profile and the Rates of the Reaction $H + HN_3 \rightarrow NH_2 + N_2$ 23

RESEARCH ACTIVITIES II DEPARTMENT OF MOLECULAR STRUCTURE 25

A. High Resolution Spectroscopy of Transient Molecules 25
1. Microwave Spectroscopy of the CD_3O Radical 25
2. Rovibronic Interaction in the $^2\Pi$ Linear Triatomic Molecule: Microwave Spectroscopic Investigation of the NCO Radical in the $\tilde{X}(000)^2\Pi$, $\tilde{X}(010)^2\Delta$, and $X(020)^2\Phi$ States 25
3. Laser Excitation Spectrum and Microwave Optical Double Resonance Spectrum of the 3_0^1 Band in the $\tilde{a}^3A_2$-$\tilde{X}^1A_1$ System of H_2CS: The Hyperfine Structure of the $\tilde{a}^3A_2$ State 26
4. Third-Order Anharmonic Potential Constants and Equilibrium Structure of HNO 27
5. Rovibronic Interaction in the NO_3 Radical 27
6. Doppler-Limited Dye Laser Excitation Spectroscopy of the HSO Radical: the $\tilde{A}^2A'(001) - \tilde{X}^2A''(000)$ Band 28
7. Coriolis Interaction between the (020) $K_a = 2$ and (100) $K_a = 1$ Levels of HNO in the A^1A'' State 28
8. Far-Infrared Laser Magnetic Resonance Spectroscopy of the PH and PD Radicals in the $X^3\Sigma^-$ State 29
9. Far-Infrared Laser Magnetic Resonance Detection and Microwave Spectroscopy of the PO Radical 29
10. Far-Infrared Laser Magnetic Resonance Spectroscopy of the PO_2 Radical 30
11. Difference Frequency Laser Spectroscopy of the ν_1 Band of the HO_2 Radical 31
12. The Microwave Spectrum of the Fluoromethyl Radical, CH_2F 31
13. The Microwave Spectrum of an Unstable Molecule, HPO 31
14. The Microwave Spectrum of the $N^{35}Cl$ Radical in the $X^3\Sigma^-$ State 32
15. The Microwave Spectrum of the FeO Free Radical 32
16. The ν_2 Band of the FO_2 Radical Investigated by Infrared Diode Laser Spectroscopy 33
17. Infrared Diode Laser Spectroscopy of the BrO Radical 34
18. Infrared Diode Laser Spectroscopy of the PO Radical 34
19. Infrared Diode Laser Spectroscopy of the FO Radical 34
20. Detection of the ν_2 Bands of CD_2 and CH_2 by Infrared Diode Laser Spectroscopy 35
21. Zeeman and Stark Effects of the HCF $\tilde{A}^1A''(000) - \tilde{X}^1A'(000)$ Band 35
22. Far-Infrared Laser Magnetic Resonance Spectroscopy of the AsH Radical in the $X^3\Sigma^-$ State 36
23. The Infrared Diode Laser Spectrum of the SCl Radical 36
24. Microwave Spectroscopy of the PF Radical 36
25. Microwave Spectroscopy of the GeF Radical 37
26. Infrared Diode Laser Spectroscopy of the Coriolis-Coupled ν_2/ν_3 Bands of DO_2 37
27. Electric Dipole Moments of the H_2CS Molecule in the $\tilde{A}^1A_2$ v = 0 and $\tilde{a}^3A_2$ v_3 = 1 States 38
28. Third-Order Anharmonic Potential Constants and Equilibrium Structure of HCO 39
29. Microwave Spectroscopy of Boron Chloride (BCl). The Chlorine Nuclear Quadrupole Coupling Constant 39

B. Development of New Instruments and New Experimental Methods for High Resolution Spectroscopy 40
1. Extension of the Wavelength Region for a cw Dye Laser Spectrometer 40
2. Data Processing System for Dye Laser Excitation Spectroscopy 40
3. Data Processing System for an Infrared Diode Laser Spectrometer 41
4. Infrared Diode Laser Spectroscopic System for Transient Molecules Generated by an Excimer Laser 41

C. High Resolution Spectroscopy of Molecules of Fundamental Importance 42
1. Microwave Spectrum and Internal Rotation of 2-Butyne-1,1,1-d_3 (Dimethylacetylene), $CH_3C \equiv CCD_3$ 42
2. Microwave Spectroscopy of Deuterated Silanes 43
3. Ananlysis of the High-Resolution Infrared Spectrum of Methane-d_2 in the 2000 ~ 2400 cm^{-1} Region 43
4. Stark Modulation Infrared Diode Laser Spectroscopy of the $\nu_6 + \nu_8$ Band of Diacetylene 44

D. Raman Spectroscopy of Macromolecules and Molecular Aggregates 44
1. Raman Spectroscopic Studies of Submillimolar Surfactant Solution; Concentration Dependence of the C-H Stretching Raman Lines 45
2. PO_2^- Symmetric-Stretching Raman Line and Molecular Aggregation States of Barium Dialkyl Phosphates 45
3. Resonance Raman Spectra of the Reaction Intermediates of Horseradish Peroxidase Catalysis 45
4. Distinct Heme-Substrate Interactions of Lactoperoxidase Probed by Resonance Raman Spectroscopy: Difference between Animal and Plant Peroxidases 46
5. Resonance Raman Study of Plant Tissue Peroxidases: Common Characteristics in Iron Coordination Environments 46
6. Resonance Raman Studies of Hemoglobin M: Evidence for Iron-Tyrosine Charge-Transfer Interactions in the Abnormal Subunits of Hb M Boston and Hb M Iwate 46
7. Resonance Raman Study of an aa_3-Type Cytochrome Oxidase of Thermophilic Bacterium PS3 47
8. Subunit Assembly Dependent Photoreduction of Heme of Giant Hemoglobin Probed by Resonance Raman Spectroscopy 47
9. Iron-Histidine Stretching Raman Line of the aa_3-Type Cytochrome Oxidases 48

E. Structures of Liquids and Noncrystalline Solids 48
1. X-Ray Diffraction Study of Mixing States in the Carbon Tetrachloride Solutions of Methanol and Pentane 48
2. On the Effect of the Finite Size of the Solvent Molecule in Dielectric Friction Theory 49
3. Catalyst Preparation Procedure Probed by EXAFS Spectroscopy I. Nickel on Silica 49
4. A Study of Orientational Pair Correlation of Pyridine and 2,4-Dimethylpyridine in Water by Depolarized Rayleigh Scattering and NMR Spectra 49
5. Kirkwood-Buff Parameters and Correlation Length in Aqueous Solutions of n-Alkoxyethanols 49

RESEARCH ACTIVITIES III DEPARTMENT OF ELECTRONIC STRUCTURE 51

A. Photochemical Formation and Reactions of Vibrationally Highly Excited ("Hot") Molecules and Radicals 51
1. Laser Flash Photolysis of Benzene. VIII. Formation of Hot Benzene from the S_2 State and Its Collisional Deactivation 51
2. Formation of Hot Hexafluorobenzene in the 193 nm Photolysis 52
3. Nanosecond Laser Photolysis of Phenyl Halide at 193 nm in the Gas Phase: Formation of Hot Radical and its Reaction 52
4. Photodissociation of Benzyl Chloride at 193 nm in the Gas Phase: the Absorption Spectra of Hot and Relaxed Benzyl Radical 52
5. Direct Measurement of Formation Rates of Allyl-type Radicals from Ethylene Derivartives 53
6. ArF Laser Flash Photolysis of Ethylene Derivatives: Substituents Dependence of Allyl Radical Formation 53

B. Radiationless Processes in Large Molecules — Channel Three in Benzene 54
1. Laser Flash Photolysis of Benzene. VII. Fluorescence Decay in the Channel 3 Region 54
2. Fluorescence Quantum Yields of S_1 Benzene in the Channel 3 Region 55
3. Fluorescence Spectra from Highly Excited Vibrational Levels in Benzene 55
4. Channel Three Decay in Benzene: A Fluorescence Investigation 56
5. Assignment of the E Absorption Transitions in C_6D_6 by Means of Isolated-Molecule Fluorescence Spectra 58

C. Dynamic Behavior of Excited States 58
1. Picosecond Fluorescence Measurement of Submono- and Monolayer of Adsorbed Rhodamine B on a Single Crystal of Naphthalene and on Glass 58
2. Interaction of Cationic Dye and Anionic Detergent above and below the Critical Micelle Concentration as Revealed by Fluorescence Characteristics 59
3. Photoreduction of Polyhalogenated Anthraquinones by Direct Electron Transfer from Alcohol 60
4. Photoionization Mechanism of TMPD in Acetonitrile 60
5. Picosecond Dynamic Stokes Shift of α-Naphthylamine 61
6. Solvent Effects on the Nonradiative Relaxation Processes of the Lowest Excited Singlet States of Mesosubstituted Bromoanthracenes 61
7. Decomposition Rate of Benzyl Chloride Excited at 266 nm in the Vapor Phase 61

D. Solar Energy Conversion by Using Photocatalytic Effects of Semiconductors and Dyes — Decomposition of Water and Hydrogen Evolution— 62
1. Mechanism of Hydrogen Production from Water with Fluorescein Derivatives as Photocatalysts 62
2. Photoelectrochemical Cell Composed of Fluorescein Derivatives 63
3. Photocatalytic Reactions of Aliphatic Hydrocarbons with Water 63
4. Photocatalytic Oxidation of Benzene in Water 64
5. The Valence Band Position of Anatase TiO_2 64
6. Difference in Photocatalytic Activity between Rutile and Anatase TiO_2 65
7. Application of Photocatalytic Reaction to Organic Synthesis 66
8. The Catalytic Role of RuO_2 on n-Type Semiconductor for Photocatalytic Oxygen Evolution 66
9. Analysis of the Transient Response of a Semiconductor – Electrolyte Circuit to a Short Light Pulse: Application to CdSe Electrodes 67

E. Dynamical Processes in Electronically and/or Vibrationally Excited Molecules 68
1. Vibrational Randomization and Predissociation of Benzene Dimer 68
2. Translational Energy Distribution of Benzene Produced by the Infrared-photodissociation of Benzene Dimer 69
3. The S_1, $^1A_2(n,\pi^*)$ state of Acetone Supersonic Nozzle Beam 69
4. Intensity of Local Mode Transition 70

F. Study on Photochemical Processes Related to Planetary Space Chemistry 70
1. Photodetachment of Surface Molecules from Ice 70
2. Formation of Heterocyclic Compounds Induced by UV Light Irradiation on Low Temperature Solids Containing Ammonia and Acetonitrile 71
3. Photochemistry of Solid Acetylene 72
4. Detection of Hot-Hydrogen Atoms from UV Laser Photodissociation of Ammonia at 193 nm 73

G. Photodissociation and Multiphoton Ionization Dynamics of Molecular Beams Initiated by UV Excimer Lasers 74
1. Photodissociation of Molecular Beams of Alkyl and Alkyne Halides 74
2. Photofragmentation Dynamics of Cl_2SO at 193 nm 74
3. Multiphoton Ionization and Fragmentations of Acetone and Cyclic Ketones: Effects of One-photon Dissociation 75
4. Multiphoton-Ionization Mass Spectroscopy of 2,4-hexadiyne at 248 and 193 nm: Wavelength Dependence on H atom Detachment 75

H. Formation and Properties of Hydrogen-Bonded Molecular Clusters Both in Supersonic Nozzle Beams and Inert-Gas Matrices at Low Temperatures 76
1. Infrared Spectra of Cryodeposited Thin Film of Ammonia: Temperature Dependence on Solid NH_3 Phases 76

2. Infrared Spectra of Ammonia Clusters Trapped in an Argon Matrix at 16K: Deposition from Pulsed Nozzle Beam 77
3. Two-Photon-Ionization Mass Spectroscopy of Ammonia Clusters in a Pulsed Supersonic Nozzle Beam 78
4. Photoionization of Ammonia Clusters by Vacuum UV Photons 78

I. Proton Transfer in the Excited States of Salycilaldehyde 80
1. Investigation of the Dynamic Processes of the Excited States of o-Hydroxybenzaldehyde and o-Hydroxyacetophenone by Emission and Picosecond Spectroscopy 80

J. Studies on Electronic Structure, Energy Transfer, Dissociation and Recombination of Small Molecules 81
1. Effects of External Magnetic Field on Laser-Induced Fluorescence of NaK 81
2. Laser-Induced Fluorescence of the NaCs Molecule 81

RESEARCH ACTIVITIES IV DEPARTMENT OF MOLECULAR ASSEMBLIES 82

A. Photoelectron Spectroscopy of Organic Solids in Vacuum Ultraviolet Region 82
1. UV Photoelectron Spectroscopy of Photoconducting Polymers 82
2. Ultraviolet Photoelectron Spectra of α- and β-Polymorphs of Copper Phthalocyanine 82
3. Ionization Potentials and Polarization Energies of Tetraselenafulvalene (TSF) Derivatives 83
4. Ultraviolet Photoelectron Spectroscopy of Fluorosubstituted Polyethylenes 83

B. Electric- and Photo-conduction in Organic Solids 84

C. Energy Transfer in Cytochrome c_3 and Hydrogenase 84
1. Magnetic Resonance Study of Hydrogenase and Cytochrome c_3 84

D. Physics and Chemistry of Graphite and its Intercalates 84
1. Chemisorption of Hydrogen in Graphite-Alkali Metal Intercalation Compounds 84
2. Responsible Layer for Superconductivity in the First Stage Potassium Graphite Intercalation Compound 85
3. Sulfur-Bridged Polycyclic Aromatic Compounds 85

E. Organic Metals 85
1. Organic Conductors: Electrical Properties of HMTTeF (Hexamethylenetetratellurafulvalene) Complexes 86
2. Crystal Structure of a New Type of Two-Dimensional Organic Metal, $(BEDT\text{-}TTF)_2ClO_4(C_2H_3Cl_3)_{0.5}$ 87
3. X-Ray Evidence for a Structural Phase Transition in the Organic Two-Dimensional Conductor $(BEDT\text{-}TTF)_2ClO_4(C_2H_3Cl_3)_{0.5}$ 88
4. Two-Dimensional Band Structure of an Organic Metal, $(BEDT\text{-}TTF)_2ClO_4\text{-}(C_2H_3Cl_3)_{0.5}$ 88
5. Crystal Structure of α-$(BEDT\text{-}TTF)_2PF_6$ 89
6. Transverse Conduction and Metal-Insulator Transition in β-$(BEDT\text{-}TTF)_2\text{-}PF_6$ 90
7. Tunneling Spectroscopic Study on the Superconductivity of $(TMTSF)_2ClO_4$ Crystals 90
8. Precise Determination of Critical Field Anisotropy in $(TMTSF)_2ClO_4$ 91
9. Anomalous Longitudinal Magnetoresistance in $(TMTSF)_2ClO_4$ 92
10. Superconducting Transition of Organic Metal $(TMTSF)_2ClO_4$: Effects of Thermally Induced Microcracks 92
11. Kink Deformation of $(TMTSF)_2ClO_4$ Single Crystal and Its Influence on Electrical Resistivity 92
12. Spin-Density-Wave and Superconducting States in Thermally Quenched $(TMTSF)_2ClO_4$ 93
13. Quenching Effect on the Anion Ordering in $(TMTSF)_2ClO_4$ ... An X-Ray Study ... 94
14. The Synthesis of 2,7-Bis(dimethylamino)pyrene and -tetrahydropyrene and the Electrical Conductivities of Their Complexes 94
15. Synthesis of Cyclobutane-fused Tetracyanoquinodimethanes 95
16. New Wurster-Type Acceptors Isoelectronic with 2,6-Anthraquinone 95
17. Poly (Carbon Diselenide); A Metallic Polymer? 95

F. Studies of Ion-Molecule Reactions by Threshold Electron-Secondary Ion Coincidence (TESICO) Technique 95
1. State Selected Charge Transfer Reactions: $NO^+(a^3\Sigma^+,v;\ b^3\Pi,v) + H_2 \rightarrow H_2^+ + NO$ and $H_2^+(X^2\Sigma_g^+,v) + NO \rightarrow NO^+ + H_2$ 96
2. State Selected Charge Transfer Reactions: $O_2^+(X^2\Pi_g,v;\ a^4\Pi_u,v) + Ar \rightarrow Ar^+ + O_2$ and $Ar^+(^2P_{3/2},^2P_{1/2}) + O_2 \rightarrow O_2^+ + Ar$ 96
3. Vibrational-State Selected Study of the Reaction of $O_2^+(v)$ with CH_4 97
4. Vibrational-State Selected Reaction Cross Sections for $C_2H_2^+(v) + D_2$ 98
5. An *ab initio* Study of Potential Energy Surfaces for the Reaction $NO^+(a^3\Sigma^+) + Ar \rightarrow Ar^+ + NO$ 98

G. Photoionization Processes in Small Molecules 99

H. Spectroscopy and Chemical Dynamics Using Supersonic Nozzle Beams 100
1. Characterization of Seeded Molecular Beams: Translational Nonequilibrium and Velocity Slip 100

I. HeI Photoelectron Spectroscopic Studies of Gaseous Molecules 100
1. A Photoelectron Spectroscopic Study of a Series of Ferrocene Compounds 101

J. Studies of Ionization of Hydrogen Bonded Dimers by Photoelectron Spectroscopy 101
1. Photoelectron Spectroscopic Study of Simple Hydrogen-Bonded Dimers. I. Supersonic Nozzle Beam Photoelectron Spectrometer and the Formic Acid Dimer 101
2. Photoelectron Spectroscopic Study of Simple Hydrogen-Bonded Dimers. II. The Methanol Dimer 101
3. A Photoelectron Spectroscopic Estimation of the Concentrations of Simple Hydrogen-Bonded Dimers Produced in the Temperature-controlled Supersonic Nozzle Beam 102
4. Ionization Energies of the Water Dimer and Clusters 102
5. Electronic and Molecular Structure of the Water Dimer Cation. A Theoretical Study 102
6. Proton-transfer Potential-energy Surfaces of the Water Dimer Cation $(H_2O)_2^+$ in the $1^2A''$ and $1^2A'$ States 103

K. Development of Multiphoton Ionization Photoelectron Spectroscopy and Its Application 103
1. A Photoelectron Spectroscopic Study of (3 + 1) Resonant Multiphoton Ionization of NO and NH_3 103
2. Multiphoton Ionization Photoelectron Spectroscopic Study on Autoionization Processes of NO Molecule 104
3. A Photoelectron Spectroscopic Study of Ionization Selectivity in Resonantly Enhanced Multiphoton Ionization of Xe and Kr 104
4. Resonant Multiphoton Ionization Photoelectron Spectroscopic Study of Benzene. Evidence for Fast Intramolecular Vibrational Relaxation within the $^1E_{1u}$ State 105
5. Multiphoton Ionization Photoelectron Spectroscopic Study on Intramolecular Relaxation Processes of Naphthalene 106
6. Multiphoton Dissociation of Ferrocene and Iron Pentacarbonyl. A Multiphoton Ionization Photoelectron Study 106

L. Production, Characterization, and Spectroscopic Studies of Molecualr Complexes and Clusters 107
1. Differential Cross Section of NO Scattered from Ar at Thermal Collision Energies 107

M. Molecular Beam Studies of Reaction Dynamics Involving Chemically Reactive Atoms and Free Radicals 108
1. Molecular Beam Chemiluminescence Studies Involving Active Nitrogen Atoms $N^*(^2D,^2P)$. I. $N^*(^2D,^2P) + HX \rightarrow NH(A^3\Pi) + X$ (X=I and Br) 108
2. Construction of a Crossed Molecular Beams Apparatus with an Electron Bombardment Ionization Mass Spectrometer (MBC-I) 109

RESEARCH ACTIVITIES V DEPARTMENT OF APPLIED MOLECULAR SCIENCE 110

A. Molecular Design of Bridged Aromatic Compounds and High-Spin Organic Compounds 110

1. Transient Absorption Spectra of the Excited States of Triptycene and 3-Acetyltriptycene 110
2. Contrasting ESR and UV Spectroscopic Properties and Reactivities between the Conformationally Fixed *o*-(9-Fluorenyl)phenylnitrenes at Cryogenic Temperatures 111
3. Time-Resolved Absorption Spectroscopic Detection of 10,10-Dimethyl-10-silaanthracen-9(10H)-one Oxide 111
4. Design, Preparation, and ESR Detection of a Ground-State Nonet Hydrocarbon as a Model for One-Dimensional Organic Ferromagnets 112

B. Stereochemical Consequences of the Non-bonded Interaction in Overcrowded Molecules 113
1. Crystal and Molecular Structure of Bis(9-triptycyl) Ether 113
2. Molecular Structure of Bis(9-triptycyl) Ether by Molecular Mechanical Calculations 114
3. Correlated Internal Rotation in Bis(2,6-dichloro-9-triptycyl)methane. Separation, Optical Resolution and Identification of Five Possible Phase Isomers. 114
4. Recognition of the Phase Relationship between Remote Substituents in 9,10-Bis(3-chloro-9-triptycyloxy)triptycene Molecules Undergoing Rapid Internal Rotation 115

C. Structural and Mechanistic Studies by Means of NMR of the Less Common Nuclei 116
1. The Conformations of Several 1-Phenylethyl and 1-Phenylpropyl Aryl Sulfoxides. Evidence for Attractive Aryl/Aryl Interaction 116
2. Selenium-77 NMR Studies of 9H-Selenoxanthenium Derivatives 116

D. Zinc(II)-Tetraazacycloalkane Complexes 117
1. CO_2-uptake by Zn(II)-tetraazacycloalkane Complexes 118
2. X-ray Structural and Ab Initio MO Studies on Molecular Stereochemistries of Six-coordinate Zn(II) Complexes of *trans*-ZnX_2N_4 Type. Flat Potential Surface with respect to Out-of-plane Displacement of Zn(II) from a Plane formed by In-plane Four Nitrogens 118

E. One-Dimensional M(II)-M(IV) Mixed Valence Complexes of Palladium and Nickel 119
1. Syntheses, Electronic Spectra, Electric Conductivities, and X-Ray Photoelectron Spectra of One-Dimensional Pd(II)-Pd(IV) Mixed Valence Complexes with Linear Tetramines or Tetraazacycloalkanes 119
2. Structures of One-Dimensional Pd(II)-Pd(IV) Mixed Valence Complexes and Their Parent Pd(II) and Pd(IV) Complexes with 1,4,8,11-Tetraazacyclotetradecane 120
3. Syntheses, Electronic Spectra, Electric Conductivities, and X-ray Photoelectron Spectra of Ni(II)-Ni(IV) Mixed Valence Complexes with Linear Tetramines or Tetraazacycloalkanes 121
4. Structural Study of Ni(II)-Ni(IV) Mixed Valence Complexes by Means of Extended X-ray Absorption Fine Structure 122

F. Nuclear Magnetic Study of Ion-Ion Interaction in Solutions of Metal Complex Salts 122
1. Proton Chemical Shift Study of the Hydrophobic Interaction between Tris-(1,10-phenanthroline)ruthenium(II) Ions in Aqueous Solution 123
2. Rotational Motion of the Tris(1,10-phenanthroline) and Tris(2,2-bipridine) Complexes of Ruthenium(II) and Cobalt(III) Ions in Solutions 123

G. Organic Reactions Initiated by Photoinduced Electron Transfer 124
1. Photocyclization of ω-Anilinoalkyl *m*-Nitrophenyl Ethers 124

RESEARCH ACTIVITIES VI 125

COMPUTER CENTER 125

A. Theoretical Investigations of Metalloporphyrins by the *Ab Initio* SCF MO Method 125
1. *Ab initio* MO Study of Mössbauer Spectra of Fe-Porphyrin Complexes 125

CHEMICAL MATERIALS CENTER 125

B. Synthesis and Characterization of 1-[Bis-(cyclopentadienyl)zircona]-2-oxacyclopentanes. X-Ray Crystal Structure of $[(\eta\text{-}C_5H_5)_2\overline{ZrOCH_2CH_2CHCH_3}]_2$ 125

C. Characterization of the New Platinacycle Compounds Derived from Bicyclo[1.1.0] butanes and Platinum Complexes. An Isolation of a Novel Carbene — Pt(0) Complex 126

D. Synthesis of New Atropisomeric Diphosphine Ligands and Their Use in Transition Metal Catalyzed Asymmetric Reactions 127

INSTRUMENT CENTER 127

E. Photophysical Dynamics of Highly-Ordered Molecular Assemblies 127

1. Picosecond Time-Resolved Fluorescence Spectroscopy of Photosynthetic Bile-pigments 128
2. Picosecond Time-Resolved Fluorescence Spectroscopy of Liquid Crystals 128

F. Development of Picosecond Time-Resolved Fluorescence Spectophotometer 129

G. Magnetic Resonance Study of Hydrogenase and Cytochrome c_3 129

H. The Study of Metal Fine Particles in Organic Solvents 130

1. Preparation Method and Optical Properties of Metal Particles 130
2. Reaction of Metal Fine Particles in Organic Solvents 130

I. Development of Experimental Devices and Techniques 131

1. Spectrofluorimeter with Nanosecond Time Resolution by Means of a Transient Digital Memory 131

LOW TEMPERATURE CENTER 132

J. Hydrogen Chemisorption in Alkali Metal Complexes of Polycyclic Aromatic Hydrocarbons and Graphite 132

1. Chemisorption of Hydrogen in Graphite-Alkali Metal Intercalation Compounds 132

K. Solid State Properties of Organic Conductors 132

1. Synthesis of Cyclobutane-fused Tetracyanoquinodimethanes 132
2. The Synthesis of 2,7-Bis(dimethylamino)pyrene and -tetrahydropyrene and the Electrical Conductivities of Their Complexes 132

EQUIPMENT DEVELOPMENT CENTER 133

L. Development of Optical Apparatus 133

1. Design and Construction of a Vacuum-UV Spectrophotometer 133
2. Pressure Apparatus for Optical measurements at low temperatures 134
3. Electroreflectance Spectrometer 134

M. Experimental Confirmation of the Spin-Orbit Coupling-Assisted d-d Transition in Transition Metal Complex Ions 134

N. Picosecond High-Power Continuously Tunable Laser Ranging between 214 nm and 4.4 μm 135

ULTRAVIOLET SYNCHORTRON ORBITAL RADIATION FACILITY 136

O. Construction of UVSOR (Ultraviolet Synchrotron Orbital Radiation) Light Source 136

RESEARCH FACILITIES 137

Computer Center 137

Chemical Materials Center 137

Instrument Center 137

Low-Temperature Center 138

Equipment Development Center 138

Ultraviolet Synchrotron Orbital Radiation Facility 138

SPECIAL RESEARCH PROJECTS 140

OKAZAKI CONFERENCES 146

JOINT STUDIES PROGRAMS 149

1. Joint Studies 149
2. Research Symposia 150
3. Cooperative Research 150
4. Use of Facility 150

FOREIGN SCHOLARS 151

AWARD 154

LIST OF PUBLICATIONS 156

ORGANIZATION AND STAFF

Organization

The Institute for Molecular Science comprises 15 research laboratories —each staffed by a professor, an associate professor, two research associates and a few technical associates—, two research laboratories with foreign visiting professors, and six research facilities. The laboratories are grouped into five departments as follows:

Department of Theoretical Studies	Theoretical Studies I
	Theoretical Studies II
	Theoretical Studies III
Department of Molecular Structure	Molecular Structure I
	Molecular Structure II[2]
	Molecular Dynamics
Department of Electronic Sturcture	Excited State Chemistry
	Excited State Dynamics
	Electronic Structure[2]
	Molecular Energy Conversion[3]
Department of Molecular Assemblies	Solid State Chemistry
	Photochemistry
	Molecular Assemblies Dynamics[1]
	Molecular Assemblies[2]
	Synchrotron Radiation Research[3]
Department of Applied Molecular Science	Applied Molecular Science I
	Applied Molecular Science II[2]

Research Facilities are:

- Computer Center
- Instrument Center
- Low-Temperature Center
- Chemical Materials Center
- Equipment Development Center
- Ultraviolet Synchrotron Orbital Radiation (UVSOR) Facility[3]

1) To be established.

2) Professors and associate professors are adjunct professors from universities.

3) Research Laboratories with foreign visiting professors established in April, 1983.

Scientific Staff

Saburo NAGAKURA	**Professor, Director-General**

Department of Theoretical Studies

Theoretical Studies I

Keiji MOROKUMA	Professor
Iwao OHMINE	Associate Professor (December '82—)
Shigeki KATO	Research Associate
Chikatoshi SATOKO	Research Associate
Shigeru OBARA	Technical Associate (—July '83)[1]
Nobuyuki SHIMA	Technical Associate (—March '83)[2]
Nobuaki KOGA	Technical Assistant (September '83 —)
Yoshihiro OSAMURA	Research Fellow (—March '83)[3]
Kenshu KAMIYA	Graduate Student from Univ. of Tokyo (April '83—)

Theoretical Studies II

Hiroki NAKAMURA	Professor
Keiichiro NASU	Associate Professor
Kazuo TAKATSUKA	Research Associate
Hidemitsu HAYASHI	Research Associate (February '83—)

Theoretical Studies III

Takayuki FUENO	Adjunct Professor from Osaka Univ. (April '81—March '83)
Kimio OHNO	Adjunct Professor from Hokkaido Univ. (April '83—)
Masaru TSUKADA	Adjunct Associate Professor from Univ. of Tokyo (April '82—)
Katsuhisa OHTA	Research Associate

Department of Molecular Structure

Molecular Structure I

Eizi HIROTA	Professor
Shuji SAITO	Associate Professor
Chikashi YAMADA	Research Associate
Yasuki ENDO	Research Associate
Tetsuo SUZUKI	Technical Associate
Hideto KANAMORI	Technical Associate (March '83—)
Shi-aki HYODO	Graduate Student from Tokyo Metropolitan Univ. (October '79—March '83)
Koichi TSUKIYAMA	Graduate Student from Tokyo Inst. of Tech.* (October '81—)

Molecular Structure II

Ikuzo TANAKA	Adjunct Professor from Tokyo Inst. of Tech. (April '81—March '83)
Soji TSUCHIYA	Adjunct Professor from the Univ. of Tokyo (April '83—)
Hiroyasu NOMURA	Adjunct Associate Professor from Nagoya Univ. (April '82—)
Kentarou KAWAGUCHI	Research Associate

Molecular Dynamics

Teizo KITAGAWA	Professor (April '83—)
Yasuo UDAGAWA	Associate Professor
Tadashi KATO	Research Associate
Keiji KAMOGAWA	Research Associate
Kazuyuki TOHJI	Technical Associate
Ryosaku IGARASHI	Research Fellow (April '81—March '83)[4]
Nobuyuki ITO	Graduate Student from Tokyo Metropolitan Univ.* (October '79—March '83)
Hideji TANABE	Graduate Student from Toyohashi Univ. of Technology* (October '82—)
Takashi OGURA	Graduate Student from Osaka Univ.* (April '83—)
Shinji HASHIMOTO	Graduate Student from Osaka Univ.* (April '83—)
Junji TERAOKA	Graduate Scientist from Osaka Univ. (April '83—September '83)

Department of Electronic Structure

Excited State Chemistry

Keitaro YOSHIHARA	Professor
Tadayoshi SAKATA	Associate Professor
Nobuaki NAKASHIMA	Research Associate
Tomoji KAWAI	Research Associate (—March '83)[5]
Minoru SUMITANI	Technical Associate
Kazuhito HASHIMOTO	Technical Associate
Nobuo SHIMO	Visiting Research Fellow from Idemitsu Kosan Co., Ltd. (June '81—)
Shigemasa NAKAMURA	Graduate Student from Nagoya Univ.* (April '81—March '83)
Noriaki IKEDA	Research Fellow (April '82—)

Excited State Dynamics

Ichiro HANAZAKI	Professor
Nobuyuki NISHI	Associate Professor
Iwao NISHIYAMA	Research Associate
Hisanori SHINOHARA	Research Associate
Masaaki BABA	Technical Associate
Tohru OKUYAMA	Technical Associate
Susumu KUWABARA	Graduate Student from Osaka Univ.* (April '79—March '83)
Kanekazu SEKI	Graduate Student from Univ. of Tokyo* (October '83—)

Electronic Structure

Noboru HIROTA	Adjunct Professor from Kyoto Univ. (April '82—)
Hajime KATO	Adjunct Associate Professor from Kobe Univ. (April '81—March '83)
Yoshibumi TANIMOTO	Adjunct Associate Professor from Kanazawa Univ. (April '83—)
Ryoichi NAKAGAKI	Research Associate
Takeshi WATANABE	Technical Assistant (April '83—)
Mitsuo HIRAMATSU	Visiting Research Fellow from Hamamatsu Photonics Co., Ltd. (April '83—)

Molecular Energy Conversion

Simon H. BAUER	Visiting Professor from Cornell Univ., U.S.A.

Department of Molecular Assemblies

Solid State Chemistry

Hiroo INOKUCHI	Professor
Inosuke KOYANO	Associate Professor
Kenichiro TANAKA	Research Associate
Kazuhiko SEKI	Research Associate
Naoki SATO	Technical Associate
Tatsuhisa KATO	Technical Associate
Mototada KOBAYASHI	IMS Fellow (February '83)
Akiharu HIOKI	Graduate Student from Nagoya Univ.* (October '81—)
Eisuke NISHITANI	Graduate Student from Tokyo Inst. of Tech.* (October '81—September '83)
Hiromichi YAMAMOTO	Graduate Student from Nagoya Univ.* (April '83—)
Hiroaki KUMAGAI	Graduate Student from Nagoya Univ.* (April '82—)
Shinsuke NAKAJIMA	Graduate Student from Yokohama National Univ.* (October '82—March '83)
Akira ISHIKAWA	Visiting Research Fellow from Kao Soap Co., Ltd. (May '82—May '83)
Hitoshi HAYASHI	Visiting Research Fellow from Nippondenso Co., Ltd. (April '83—)

Photochemistry

Katsumi KIMURA	Professor
Kosuke SHOBATAKE	Associate Professor
Yohji ACHIBA	Research Associate
Kiyohiko TABAYASHI	Research Associate
Kenji SATO	Technical Associate
Shigeru OHSHIMA	Technical Associate (April '83—)
Shinji TOMODA	Research Fellow (April '80—July '83)[6]
Yatsuhisa NAGANO	Graduate Student from Osaka Univ.* (April '82—)
Atsunari HIRAYA	Graduate Student from Tohoku Univ.* (April '83—)

Molecular Assemblies

Motohiro KIHARA	Adjunct Professor from Nat. Lab. for High Energy Phys. (April '81—March '83)
Yusei MARUYAMA	Adjunct Professor from Ochanomizu Univ. (April '83—)
Yasuhiko SHIROTA	Adjunct Associate Professor from Osaka Univ. (April '81—March '83)
Naohiko MIKAMI	Adjunct Associate Professor from Tohoku Univ. (April '83—)
Gunzi SAITO	Research Associate

Synchrotron Radiation Research

Godfrey SAXON	Visiting Professor from Daresbury Laboratory, SERC, U.K.

Department of Applied Molecular Science

Applied Molecular Science I

Hiizu IWAMURA	Professor
Tasuku ITO	Associate Professor
Tadashi SUGAWARA	Research Associate
Koshiro TORIUMI	Research Associate
Masako KATO	Technical Associate

Shigeru MURATA	Technical Associate
Hideyuki TUKADA	IMS Fellow (March '82—)
Akira IZUOKA	Research Fellow (April '83—)
Masahiro YAMASHITA	JSPS Fellow (April '82—September '83)[7]
Masamichi ATO	Graduate Student from Nagoya Univ.* (October '81—)
Tohru NAKANISHI	Graduate student from Tokyo Metropolitan Univ.* (October '82—)
Toshiaki KANAO	Graduate Student from Kumamoto Univ.* (April '83—)

Applied Molecular Science II

Hideo YAMATERA	Adjunct Professor from Nagoya Univ. (April '81—March '83)
Akio YAMAMOTO	Adjunct Professor from Tokyo Inst. of Tech. (April '83—)
Kiyoshi MUTAI	Adjunct Associate Professor from Univ. of Tokyo (April '82—)
Noboru KOGA	Research Associate

Research Facilities

Computer Center

Keiji MOROKUMA	Director
Hiroshi KASHIWAGI	Associate Professor
Unpei NAGASHIMA	Research Associate (September '83—)
Shigeyoshi YAMAMOTO	Technical Associate
Minoru SAITO	Graduate Student from Nagoya Univ. (April '82—)

Instrument Center

Keitaro YOSHIHARA	Director
Iwao YAMAZAKI	Associate Professor
Keisaku KIMURA	Research Associate
Naoto TAMAI	Research Associate (September '83—)
Toshiro MURAO	Technical Associate (—March '83)[8]

Low-Temperature Center

Hiroo INOKUCHI	Director
Toshiaki ENOKI	Research Associate

Chemical Materials Center

Hiizu IWAMURA	Director
Hidemasa TAKAYA	Associate Professor
Kazushi MASHIMA	Research Associate
Masashi YAMAKAWA	Technical Associate

Equipment Development Center

Eizi HIROTA	Director
Tadaoki MITANI	Associate Professor
Yoshihiro TAKAGI	Research Associate
Yoshiki WADA	Graduate Student from Univ. of Tokyo* (—March '83)

Ultraviolet Synchrotron Orbital Radiation Facility

Hiroo INOKUCHI	Director
Makoto WATANABE	Associate Professor
Toshio KASUGA	Associate Professor
Takatoshi MURATA	Adjunct Associate Professor from Kyoto Univ. of Education (May '82—)

Hiroto YONEHARA Research Associate (May '83—)

* Conduct graduate studies at IMS on the Cooperative Education Programs of IMS with graduate schools.
1) Present address: Dept. of Chemistry, Kyoto Univ., Kitashirakawa, Sakyoku, Kyoto 606.
2) Present address: Dept. of Physics, Univ. of Tokyo, Hongo, Bunkyoku, Tokyo 113.
3) Present address: Dept. of Chemistry, Keio Univ., Hiyoshi, Yokohama 223.
4) Present address: Fuji Xerox Co., Ltd. Minamiashigara, Kanagawa 250-01.
5) Present address: Institute of Scientific and Industrial Research, Osaka Univ., Mihogaoka, Ibaraki, Osaka 567.
6) Present address: Dept. of Chemistry, Faculty of Science, Osaka Univ., Machikaneyama, Toyonaka, Osaka 560.
7) Present address: College of General Education, Kyushu Univ., Ropponmatsu, Chuoku, Fukuoka 810.
8) Present address: Hitachi Instrument Engineering Co., Ichige, Katsuta, Ibaraki 312.

Technical Staff

Akira UCHIDA	Technical Division Head
Keiichi HAYASAKA	Technical Section Chief
Kusuo SAKAI	Technical Section Chief
Satoshi INA	Computer Center (Unit Chief)
Fumio NISHIMOTO	Computer Center
Takaya YAMANAKA	Instrument Center
Shunji BANDO	Instrument Center
Kenichi IMAEDA	Low-Temperature Center
Kazuo HAYAKAWA	Equipment Development Center
Hisashi YOSHIDA	Equipment Development Center
Masaaki NAGATA	Equipment Development Center
Toshio HORIGOME	Equipment Development Center
Nobuo MIZUTANI	Equipment Development Center
Norio OKADA	Equipment Development Center
Mitsukazu SUZUI	Equipment Development Center
Shinji KATO	Equipment Development Center
Osamu MATSUDO	UVSOR Facility (Unit Chief)
Masami HASUMOTO	UVSOR Facility
Toshio KINOSHITA	UVSOR Facility (April '83—)

Foreign Visiting Staff

Ewa Lipczyńska-Kochany	Tech. Univ. of Warsaw, Warsaw, Poland	Apr. 1, 1981—Sept. 30, 1982
Desmond V. O'Connor	The Royal Institution, London, U.K.	Jan. 12, 1982—Mar. 31, 1983
Chen Shangxian	Institute of Chemistry, Academia Sinica, Beijing, P.R. China	Apr. 16, 1982—Apr. 10, 1983
Klaus Kemnitz	Univ. Erlangen-Nuernberg, West Germany	Apr. 20, 1982—
Jean Demuynck	Univ. of Strasbourg, France	July 1—Sept. 30, 1982
Donald Bethell	Univ. of Liverpool, U.K.	July 19—Oct. 29, 1982
A. Robert W. McKellar	NRC, Canada	Aug. 1—Oct. 15, 1982

Oliver Johnson	Univ. of Pittsburg,	Sept. 1, 1982—Apr. 15, 1983
Bernhard M. Schmid	Physikalisches Institute, Univ. Stuttgart, West Germany	Nov. 1, 1982—July 10, 1983
James E. Butler	Naval Research Lab., U.S.A.	Nov. 1, 1982—Nov. 14, 1983
Kalidas D. Sen	Univ. of Hyderabad, India	Nov. 15, 1982—Jan. 6, 1983
Manfred Faubel	MPI Für Strömungs-forschung, Göttingen, West Germany	Nov. 16, 1982—Mar. 31, 1983
Ronald H. Wilson	General Electric, New York, U.S.A.	Dec. 1, 1982—Feb. 28, 1983
Frans C. De Schryver	Katholic Univ. Leuven, Belgium	Feb. 21—Mar. 6, 1983
Robert J. Butcher	Univ. of Cambridge, U.K.	Mar. 1—June 30, 1983
Henryk Ratajczak	Univ. of Wrolaw, Poland	Mar. 30—Apr. 7, 1983
John T. Hougen	NBS, Maryland, U.S.A.	Apr. 1—30, 1983
Imre G. Csizmadia	Univ. of Toronto, Canada	May 2—June 30, 1983
Ronald D. McKelvey	Univ. of Wisconsin-La Crosse, U.S.A.	May 30—Nov. 30, 1983
Eva M. Voigt	Simon Fraser Univ. Burnaby, B.C., Canada	May 9—Aug. 17, 1983
Odile Eisenstein	Univ. of Michigan, U.S.A.	May 10—June 28, 1983
Raymond A. Poirier	Univ. of Toronto, Canada	May 23—June 18, 1983
Weston T. Borden	Univ. of Washington, U.S.A.	June 15—July 15, 1983
Terry A. Miller	Bell Lab., U.S.A.	June 28—Sept. 24, 1983
Robert J. Donovan	Univ. of Edinburgh, Edinburgh, U.K.	July 4—Sept. 23, 1983
Sang Chul Shim	KAIST, Korea	July 9—Aug. 8, 1983

COUNCIL

Saburo NAGAKURA, Director-General

Councillors

Chairman	Yasutada UEMURA	Professor, The Science University of Tokyo
Vice-Chairman	Kenichi FUKUI	President, Kyoto University of Industrial Arts and Textile Fibers
	Hideo AKAMATU	Professor Emeritus, The University of Tokyo and IMS
	Soichi IIJIMA	President, Nagoya University
	Masao KAKUDO	President, Himeji Institute of Technology
	Tetsuji KAMETANI	President, Hoshi University
	Noboru KOMATSU	President, Toyota Central Research & Development Laboratories, INC.
	Kazuo SAITO	Professor, Tohoku University
	Yoneichiro SAKAKI	President, Toyohashi University of Technology
	Osamu SHIMAMURA	Director, Sagami Chemical Research Center
	Ikuzo TANAKA	Professor, Tokyo Institute of Technology
	Sadao NAKAJIMA	Director, The Institute for Solid State Physics, The University of Tokyo
	Hiroaki BABA	Professor, The Research Institute of Applied Electricity, Hokkaido University
	Masao FUJIMAKI	President, Ochanomizu University
	Daikichiro MORI	Director-General, The Institute of Space and Astronautical Science
	Michael KASHA	Professor, Florida State University,
	Per-Olov LÖWDIN	Professor, University of Florida and Professor Emeritus, Uppsala University

The Council is the advisory board for the Director-General. Two of the councillors are selected among distinguished foreign scientists.

Professor Emeritus

Professor Hideo AKAMATU, *ex*-Director-General of IMS, was named the first Professor Emeritus of this Institute in September, 1982.

Distinguished Research Consultants

Kenichi FUKUI	President, Kyoto University of Industrial Arts and Textile Fibers
Masao KOTANI	Professor Emeritus, The University of Tokyo

Administration Bureau

Akira MUROYA	Director-General, Administration Bureau
Katsuhiko HISAO	Director, General Affairs Department
Seigo MIURA	Director, Finance and Facilities Department
Haruhiko IWASA	Head, General Affairs Division
Shigeyoshi ONO	Head, Personnel Division
Takeru YAMAKAWA	Head, Research Cooperation and International Affairs Division
Shunsuke YAMAKI	Head, Budget Division
Wataru KOUCHI	Head, Accounts Division
Takashi YOKOYAMA	Head, Construction Division
Shoichi SATO	Head, Equipment Division

BUILDINGS AND CAMPUS

The IMS campus covering 62,561 m^2 is located on a low hill in the middle of Okazaki City. The inequality in the surface of the hill and growing trees are preserved as much as possible, and low-storied buildings are adopted for conservation of the environment. The buildings of IMS are separated according to their functions as shown in the map. The Research Office Building and all Research Facilities except for the Computer Center are linked organically to the Main Laboratory Building by corridors. Computer Center, Library, and Administration Buildings are situated between IMS and the neighboring National Institute for Basic Biology and National Institute for Physiological Sciences, because the latter two facilities are common to these three institutes.

The lodging facility of IMS called Yamate Lodge, located within 10 min. walk, has sleeping accommodations for 20 guests. Since June 1, 1981 a new lodging facility called Mishima Lodge has been opened. Mishima Lodge, located within four minutes' walk east of IMS can accommodate 30 guests and six families. Scientists who visit IMS as well as the two other institutes can make use of these facilities. Foreign visiting scientists can also live at these lodgings with their families during their stay.

The Institute for Molecular Science

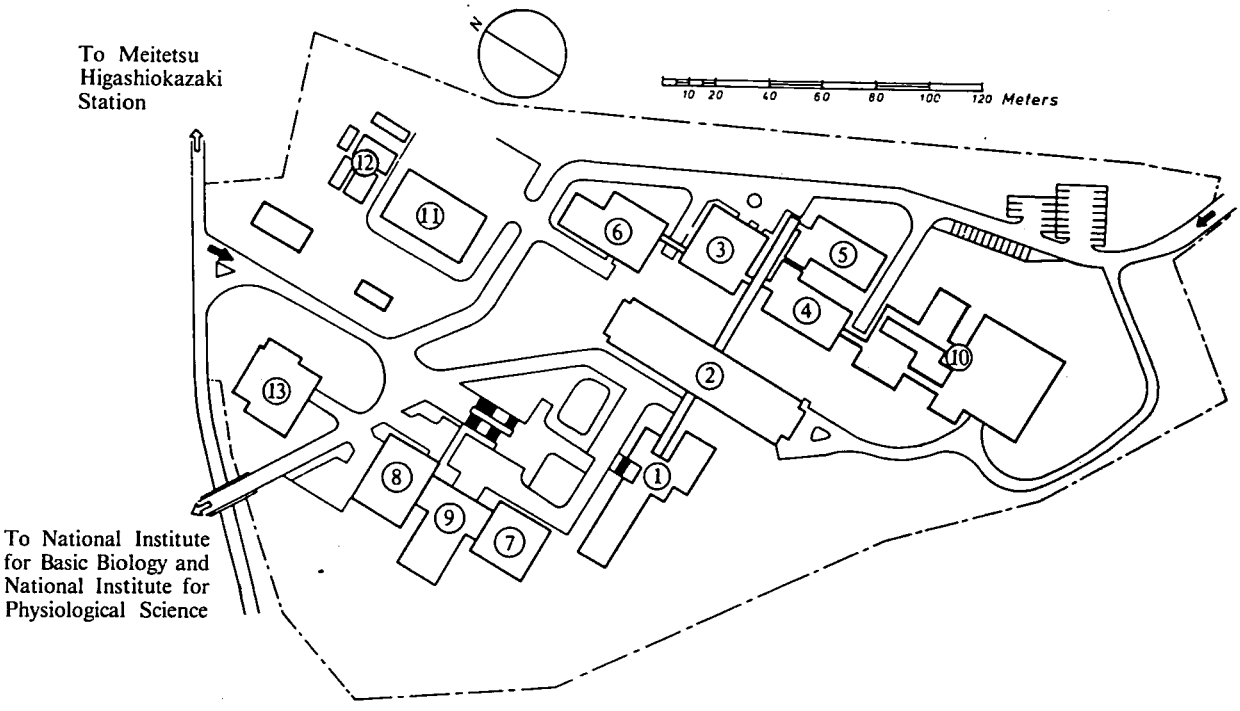

1. Research Office Building
2. Main Laboratory Building
3. Equipment Development Center
4. Instrument Center
5. Chemical Materials Center
6. Low-Temperature Center
7. Computer Center
8. Library
9. Central Administration
10. UVSOR Facility
11. Power Station
12. Waste-Water Disposition Facilities
13. Faculty Club

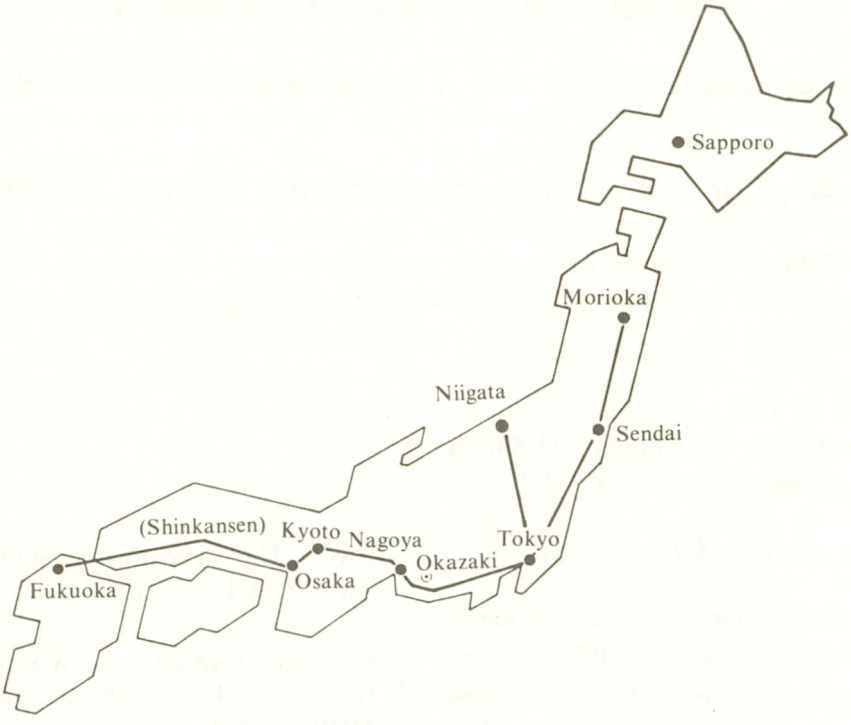

Okazaki (population 276,000) is 260 km southwest of Tokyo, and can be reached by train in about 3 hours from Tokyo via New Tokaido Line (Shinkansen) and Meitetsu Line.
The nearest large city is Nagoya, about 40 km west of Okazaki.

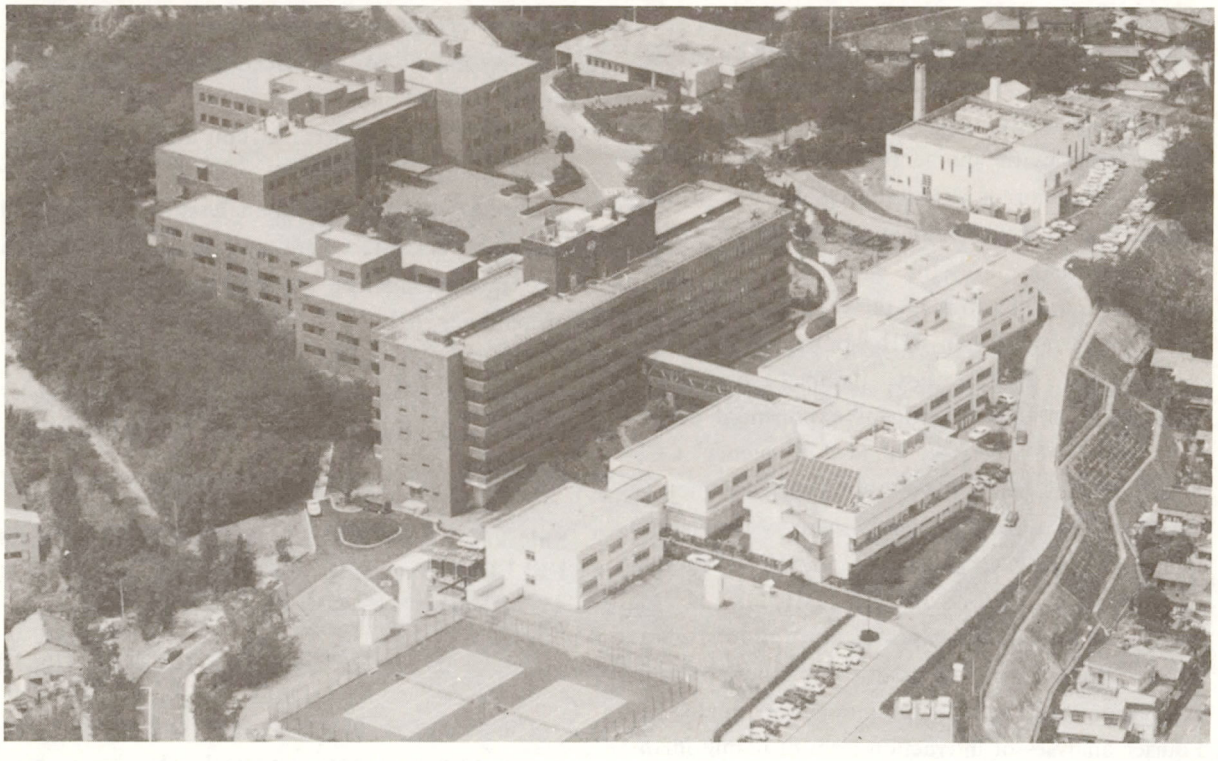

IMS, 1983

RESEARCH ACTIVITIES I
Department of Theoretical Studies

I—A Characterization of Potential Energy Surfaces

Our theoretical study of potential energy surfaces has widened its scope to varieties of problems of chemical reactions, energy transfer and molecular interactions. This development is partly due to collaboration with visiting foreign scholars and through the joint studies program.

I-A-1 Intramolecular Vibrational Relaxation in $CHCl_3$: A Classical Trajectory Study

Shigeki KATO and Keiji MOROKUMA

The mechanism of intramolecular vibrational relaxation (IVR) in chloroform ($CHCl_3$) has been studied by a classical trajectory method. The initial vibrational excited states were prepared by exciting the CH stretching normal mode and the IVR processes from these states were examined. Ab initio SCF calculations have been carried out to determine the harmonic and cubic force constants of $CHCl_3$. These force constants were utilized to construct the potential energy function given by an analytic form. The results were analyzed on the basis of zero-th order hamiltonian picture constructed by the normal coordinates. The distributions of energy in each vibrational mode were characterized by the moments of energy. It is shown that the behavior of IVR critically depends on the amount of energy initially supplied in the CH stretching mode. For the cases where the CH stretching is excited to the 5 or 7th vibrational level, the average energy in CH stretching mode is characterized by a fast damped oscillation ($0<t<0.3$ps) and a subsequent exponential decay ($t>0.3$ps). The energies in low frequency CCl stretching and bending vibrations increase monotonically. On the other hand, there is no energy transfer to the CCl vibrational modes when the CH stretching mode is excited to the 1st or 3rd vibrational level. The shapes of absorption spectra have been calculated by the vibrational level populations evaluated by the moment method. The Fourier analyses of interaction term of hamiltonian were performed to elucidate the mechanism of IVR process.

I-A-2 The Structure and Stability of Oxyallyl. An MCSCF Study

Yoshihiro OSAMURA, Weston T. BORDEN *(Univ. of Washington and IMS),* **and Keiji MOROKUMA**

[*J. Am. Chem. Soc.*, in press]

The structures of several low-lying states of oxyallyl ($.CH_2COCH_2.$) have been determined by ab initio MCSCF calculations. The ground state of oxyallyl is found to be $^3B_2$, but the first excited state ($^1A_1$) is located only 6 kcal/mole higher in energy. The $^1A_1$ state is best described as a diradical, with a strong C-O π bond and an electron largely localized at each of the peripheral carbon atoms. Two other singlet states, $^1B_2$ and $^1B_1$, lie 10–20 kcal/mole above $^1A_1$. The vibrational analysis of $^1A_1$ shows all real frequencies; therefore, oxyallyl appears to be a true intermediate of the ring opening of cyclopropanone.

I-A-3 Ab Initio Study of m-Benzoquinodimethane

Shigeki KATO, Keiji MOROKUMA, David FELLER*, Ernest R. DAVIDSON*, and Weston T. BORDEN* *(*Univ. of Washington)*

[*J. Am. Chem. Soc.*, **105**, 1791 (1983)]

The geometries of the $^3B_2$ and $^1A_1$ states of the *m*-benzoquinodimethane diradical (**1**) have been optimized by, respectively, UHF and TCSCF

calculations, using the STO-3G basis set. The energies at the optimal geometries have been computed with the Dunning split-valence basis set, using two different schemes for correlation energy recovery. Both schemes lead to the prediction of a $^3B_2$ ground state for **1**, with $^1A_1$ computed to be 10 kcal/mol higher in energy. The geometry of *p*-benzoquinodimethane (**2**) has also been optimized and the energy of its closed-shell ^1A_g ground state computed. The relative energies of the ground states of **1** and **2** are found to depend on the method used for recovering correlation energy. Evidence is presented that variational π configuration interaction (CI) energy differences are likely to be more reliable than estimates made from all-valence-electron CI calculations that use a small number of selected single and double excitations. The energy difference between the two ground states is computed to be 24 kcal/mol by CI calculations involving all π configulations through quadruply excited in an 11-orbital subspace of the full 16-orbital π space. This calculated energy difference is discussed in context of a recent experimental determination.

I-A-4 Ab Initio MO Calculations of Isotope Effects in Model Processes of Neopentyl Ester Solvolysis

Hiroshi YAMATAKA*, Takashi ANDO* *(*Osaka Univ.),* **Shigeru NAGASE** *(Yokohama National Univ.),* **Mitsuyasu HANAMURA, and Keiji MOROKUMA**

Ab Initio molecular orbital calculations were carried out for the isotope effects on ionizations of 1-propanol to a series of propyl cations, model reactions of the neighboring group assisted (k_Δ) and non-assisted (k_c) processes of neopentyl ester solvolysis. Calculated carbon-14 isotope effects of the migrating methyl group were normal (larger than unity) for all the model processes, suggesting that the experimentally observed normal carbon isotope effect at the position can not be decisive evidence supporting the k_Δ mechanism for the neopentyl solvolysis. On the other hand, deuterium isotope effects of the methyl group were calculated to be normal for the k_Δ process as expected but inverse (smaller than unity) for the k_c model process; the inverse effect is incompatible with experiment. From these results, it was concluded that the mechanism of the neopentyl solvolysis is k_Δ.

I-A-5 Theoretical Studies of the Gas-Phase Proton Affinities of Molecules Containing Phosphorus-Carbon Multiple Bonds

Lawrence L. LOHR *(Univ. of Michigan),* **H. Bernhard SCHLEGEL** *(Wayne State Univ.),* **and Keiji MOROKUMA**

[*J. Am. Chem. Soc.*, in press]

Theoretical values for the gas-phase proton affinities (PA's) of phosphaethyne, phosphaethene, and phosphabenzene have been obtained from ab initio SCF calculations employing analytic gradient techniques for geometry optimization. The sensitivity of the results to the choice of basis set and to the inclusion of correlation is discussed. The PA's for P-site and C-site protonation are found to be nearly equal in both phosphaethene and phosphabenzene at the split-valence SCF level; however, polarization functions and electron correlation both act to favor P-site protonation over C-site protonation, resulting in an isomerization energy of approximately 50 kJ mol^{-1}.

By contrast we find C-site protonation to be strongly favored over P-site protonation for phosphaethyne even at the split-valence SCF level. Comparisons are made to computed and observed PA's both for saturated C-P systems and for saturated and unsaturated C-N systems.

I—B Problems of Molecular Structure

Various problems of molecular structure have been investigated. Many of these problems have been brought over to us by collaborators who actually carried out experiment. We also have some similar projects which have not yet resulted in successful conclusions.

I-B-1 The Effective Fragment Potential Method — An Approximate ab initio MO Method for Large Molecules

Katsuhisa OHTA, Kazuo KITAURA *(Osaka City Univ.),* **Yasunori YOSHIOKA, and Keiji MOROKUMA**

[*Chem. Phys. Lett.*, **101**, 12 (1983)]

The effective fragment potential (EFP) approximation within the ab initio MO method is proposed. Only the active electrons of a molecule are explicitly taken into account, the rest of the molecule being replaced by an effective potential. Considering NH_3 as a two-electron system, the potential parameters have been determined and tested for various complexers. Figure 1 is the

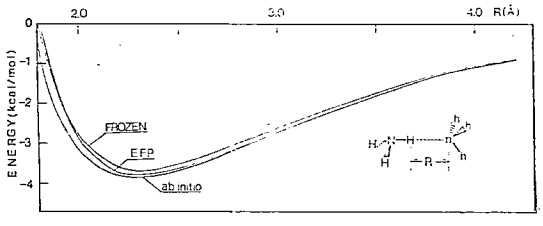

Figure 1. Potential energy curves for H_2NH ... nh_3. The geometry of NH_3 is fixed with one of the NH bond on the C_{3v} axis of nh_3.

potential energy curves for $H_2NH...NH_3$, where the proton acceptor ammonia molecule nh_3 is represented with full ab initio, the frozen core and the EFP approximation.

I-B-2 Role of Sulfur d Orbitals in the S...N Bond Stability of Ammonioalkylsulfuranes

Keiji MOROKUMA, Mitsuyasu HANAMURA *(Tohoku Univ.),* **and Kin-ya AKIBA** *(Hiroshima Univ.)*

Using $H_2NCH_2OCH_2SHX^+$ (X=H and Cl) as model compounds, we examined the role of sulfur d orbitals on the stability of S...N bonded cyclic ammonioalkylsulfuranes. The ab initio Hartree-Fock calculation with sulfur d orbitals gives a cyclic structure (shown in Figure 1), while the calculation without d causes breaking of the S...N bond. The origin of the S...N bond stability and the role of d

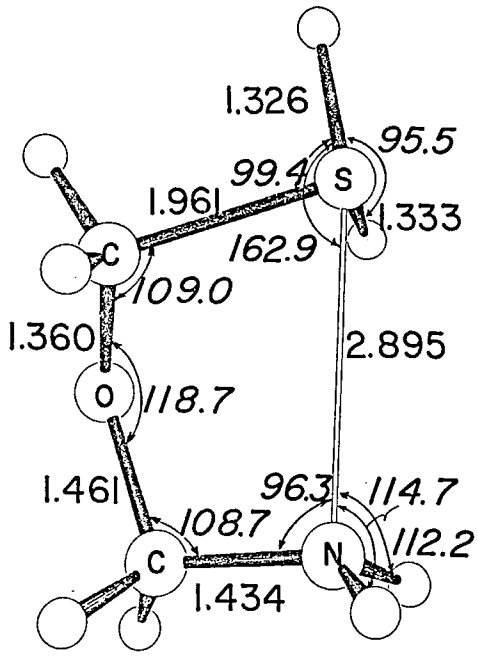

Figure 1. Optimized structure of $H_2NCH_2OCH_2SH_2$.

orbitals in it have been analysed and attributed to both electrostatic and charge transfer interactions.

I-B-3 Relative Conformer Stability of Diphosphine and Phosphinodifluoreophosphine: An Ab Initio Study

K.D. SEN *(Univ. of Hyderabad, India and IMS),* **Katsuhisa OHTA, and Keiji MOROKUMA**

The geometry and the energy of confomers of H_2PPH_2 and H_2PPF_2 have been studied with the ab initio HF and CI method. The order of stability has been found to decrease in the order gauche > trans > cis for H_2PPH_2 and gauch ~ trans > cis for H_2PPF_2. The barrier for internal rotation has also been calculated.

I-B-4 Force Field in the Hydrazine Molecule from Ab Initio MO Calculation

Naoki TANAKA,* Yoshiaki HAMADA,* Yoko SUGAWARA,* Masamichi TSUBOI* *(*Univ. of Tokyo),* **Shigeki KATO, and Keiji MOROKUMA**

[*J. Mol. Spectr.*, **99**, 245 (1983)]

Ab initio MO calculations were applied to hydrazine to obtain a reliable molecular force field and to clear up some complexities in the observed spectrum and contradictions in the assignments reported by previous investigators. Various levels of ab initio MO methods, namely the Hartree-Fock (HF) SCF methods wit STO-3G, 4-31G, and 4-31G* (in which polarization functions of the nitrogen atoms were added) basis sets, and the configuration interaction (CI) method with a 6-31G* basis set were compared with one another with respect to the calculated molecular parameters. It has been concluded that the HFSCF-4-31G* is, in general, significant and useful, and the improvement caused by elevating the level of calculation up to CI-6-31G* is not very great. For instance, most of the off-diagonal force constant values calculated with HFSCF-4-31G* are already found to be reliable. On the other hand, however, with the 6-31G* CI method, and with anharmonic corrections, nearly perfect reproduction of the observed fundamental frequencies of N_2H_4 has been achieved. Guided by this calculation, a few pieces of new interpretation of te N_2D_4 spectrum have been presented.

I-B-5 Vibrational Analysis of Ethylamines: Trans and Gauche Forms

Yoshiaki HAMADA,* Kazuko HASHIGUCHI,* Akiko Y. HIRAKAWA,* Masamichi TSUBOI,* Munetaka NAKATA,* Mitsuo TASUMI *(*Univ. of Tokyo),* **Shigeki KATO, and Keiji MOROKUMA**

Starting from force constant values calculated by an ab initio MO method (4-31G(N*)), and by adjusting the diagonal elements, a practical force constant matrix (**F**) has been reached, which could explain the observed infrared and Raman spectra (in the lower frequency range than 2000 cm^{-1}) of gauche form of the ethylamine $CH_3CH_2NH_2$ molecule and five isotopic species $CH_3^{13}CH_2NH_2$, $CH_3CH_2^{15}NH_2$, $CH_3CD_2NH_2$, $CH_3CH_2ND_2$, and $CH_3CD_2NH_2$. The $\underset{\sim}{F}$ matrix for the trans form of ethylamine was constructed by transferring ab initio 4-31G(N*) values and by revising diagonal elements with conversion factors whose values are equal to the corresponding values of gauche form. A nearly complete set of assignments was achieved of the variational bands of ethylamines, observed so far in the 2000 − 100 cm^{-1} spectral range. In matrix isolation spectroscopy, two bands assignable to the NH_2 wagging vibrations of gauche and trans forms have been found at 755 and 782 cm^{-1}, respectively, for $CH_3CH_2NH_2$. They are at 768 and 774 cm^{-1}, respectively for $CD_3CD_2NH_2$. From the intensity changes of these bands observed on changing the nozzle temperature in the matrix formation, the energy difference ΔE (gauche-trans) of these two conformers has been estimated to be 100 ± 10 cm^{-1}.

I-B-6 Ab initio Molecular Orbital Study on the Formic Acid Dimer

Soichi HAYASHI*, Junzo UMEMURA* *(*Kyoto Univ.),* **Shigeki KATO, and Keiji MOROKUMA**

[*J. Phys. Chem.*, in press]

Ab initio MO calculation has been performed on formic acid dimer to elucidate the potential barrier height for the double proton transfer in formic acid dimer. Full geometry optimization has been made both on the energy minimum (equilibrium) C_{2h} structure and the energy maximum (transition state) D_{2h} structure, using the Hartree-Fock method with the 4-31G basis set. A configuration interaction calculation and a Hartree-Fock calculation at the 6-31G* basis set were performed to improve the barrier height. Normal coordinate calculation has been made using the force constants obtained by the ab initio method to take into account the diference in zero-point energy between the C_{2h} and D_{2h} structures. The effective barrier height calculated is 7.1 kcal/mol (4-31G) − 11.7 kcal/mol (6-31G* estimated), the lowest ever calculated. A discussion on the double proton transfer rate is also presented.

I-B-7 Ab Initio Molecular Orbital Study on the Thermostability of the Extreme Thermophile tRNA: Role of the Base Stacking

Misako AIDA,* Chikayoshi NAGATA* *(*National Cancer Center Research Institute),* **Iwao OHMINE, and Keiji MOROKUMA**

[*J. Theo. Biol.* **99**, 599 (1982)]

In extremely thermophilic tRNA, ribosylthymine is replaced by 2-thioribosylthymine at the key site in tRNA. By means of the *ab initio* molecular orbital (MO) calculation using the 4-31G basis set, we evaluate how this replacement brings about an increment of stacking enery, and how this increment in stacking energy is responsible for the stability of the thermophile tRNA. Calculated stacking energy for $G{:}s^2T{:}\Psi$ is larger by 4.85 kJ/mol (1.16 kcal/mol) than that for $G{:}T{:}\Psi$. Taking account of the thermodynamical data of yeast tRNAs by Privalov & Filimonov (1978), such an increment in stacking energy seems to considerably contribute to the increase of the midpoint melting temperature (T_m) in the thermophile tRNA, although other factors such as hydrogen bonding, ribose puckering and magnesium ions can not be excluded. It is found that the dispersion force mainly contributes to the stacking energies for $G{:}T{:}\Psi$ and $G{:}s^2T{:}\Psi$, especially for the latter. From the decomposition of the SCF energy, electrostatic and charge transfer energies are found to contribute to the stabilization of the thermophile tRNA, though the contribution of the former is larger than the latter.

I—C Structure, Bonding, and Reactivity of Transition Metal Complexes

Theoretical studies of transition metal complexes remain to be challenging but exciting problems to our group. We have found the first ab initio theoretical evidence of the activation of an alkyl C-H bond by a transition metal.

I-C-1 Reaction Mechanisms of Oxidative Addition: H_2 + Pt (0)$(PH_3)_2$ → Pt(II)$(H)_2(PH_3)_2$ and Reductive Elimination: Pt(II)(H)(CH_3)-$(PH_3)_2$ → CH_4 + Pt(0)$(PH_3)_2$: Ab initio MO Study

Shigeru OBARA, Kazuo KITAURA, and Keiji MOROKUMA

Reaction mechanisms of the oxidative addition of H_2 to two-coordinate Pt(0)$(PH_3)_2$ and the reductive elimination of CH_4 from four-coodinate Pt(II)(H)$(CH_3)(PH_3)_2$ are studied by ab initio RHF and CI calculations with the energy gradient method within the frame work of the relativistic effective core potential approximation for Pt core electrons. Fully optimized geometries of transition states of both reactions as well as the reactants and products have been obtained. The fact that the oxidative addition more commonly takes place for H_2 and the reductive elimination for CH_4 can be explained in terms of calculated exothermicity. The H_2 oxidative addition reaction is suggested to pass through an early transition state that would lead directly to a cis product, and then to be pushed toward a trans product by a steric repulsion between bulky phosphine ligands. Large deuterium kinetic isotope effects experimentally found in the reductive elimination reaction of CH_3D from Pt(D)$(CH_3)(PPh_3)_2$ is accoutned for in terms of the calculated four-coordinate transition state, where the reaction coordinate is the CPtH bending. A decrease in the interligand angle has been found to increase the reactivity of the metal center by selectively activating a d orbital. Both donation and backdonation between the metal and H_2 have been found to be important at the transition state.

I-C-2 Intramolecular CH...M Interaction: A Theoretical Study for Three-coordinate Pd(H)$(C_2H_5)(PH_3)$ and Six-coordinate Ti(H)$_3$-$(CH_3)(PH_3)_2$ and Ti(H)$_3(C_2H_5)(PH_3)_2$

Shigeru OBARA, Kazuo KITAURA, and Keiji MOROKUMA

We report the first ab initio molecular orbital result in which the intramolecular CH...M interaction is found between an inert alkyl group and a transition metal. The optimized geometry for Pd(H)$(C_2H_5)(PH_3)$ has a distorted ethyl group with

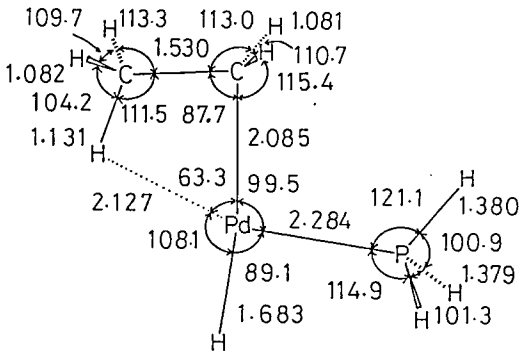

a short ethyl H^{β}...Pd distance, as shown in Figure 1. For $Ti(H)_3(R)(PH_3)_2$, ($R=CH_3$ and C_2H_5), the calculation gives the optimized geometries with normal undistorted alkyl groups.

I—D Development and Application of the LCAO-Xα Direct Force Calculation Method

An energy gradient method is developed for the LCAO-Xα scheme, which is quite convenient for the numerical calculations of forces acting on each ions in the cluster. This method is applied for various problems including chemisorption systems.

I-D-1 Force and Virial Formula in the LCAO-Xα Method and its Application to Oxygen Chemisorption on Metal Surfaces

Chikatoshi SATOKO

The method of the gradient of the electronic total energy with respect to nuclear coordinates has been formulated and related with the virial in the LCAO-Xα methods. These formulae are extended to the linear combination of the plane-waves (LCPW) method. Our method is applied to the chemisorption of an oxygen atom on the Al(111) surface and the Mg(0001) surface. The calculated forces explain the experiments that the oxygen atom is not absorbed in the Al surface but absorbed in the Mg surface.

According to the calculated force and virial, an activation energy for the oxygen penetration into the surface is about 1 eV on the Al suface, while zero on the Mg surface. This is due to the difference in the properties of the surface bonding.

The virials are equal to zero, if all the atoms in the cluster is displaced to the equillibrium positions. In our model cluster, however, the metal atoms are assumed to be fixed at the bulk positions, so that the virials are non vanishing. The full optimization of the geometry is nonsense in the cluster approximation, because the atoms of the cluster surface are bound with the surrounding metal atoms. The pressure of the cluster against the surrounding atoms is estimated from the virials. The pressure of the cluster at the Al surface is always higher than that at the Mg surface when the oxygen atom approaches the surface. This means that the oxygen atom is more easily chemisorbed on the Mg surface than on the Al surface.

I-D-2 The Role of d-Orbitals in Dissociative Chemisorption of Hydrogen Molecule on Metal Surfaces

Chikatoshi SATOKO and Masaru TSUKADA

[*Surface Science*, in press]

The dissociative chemisorption processes of hydrogen molecule on metal surfaces such as Ni,Cu,Mg and Ca are studied by the cluster model using the LCAO-Xα energy gradient method. The calculated forces acting on the hydrogen atoms along the reaction path of the dissociation reveal that the hydrogen dissociates on on-top site of the Ni and Ca surfaces. The dissociative forces on the Ni and Ca surface are derived mainly from the

interaction between H_2 antibonding orbital and the lobe shaped orbital of the 3 dyz electons of the metal. The chemisorption of the hydrogen molecule on the Cu and Mg surface is not dissociative, as the d electrons do not contribute to the force acting on the hydrogen molecule.

For the case of the chemisorption on the bridge site, the d-orbitals interacting with the H-H antibonding orbital are the antibonding combination of the dz^2 orbitals of the two metal atoms. The distance between the hydrogen atoms and these dz^2 orbitals is not so close to cause the strong interaction for the hydrogen dissociation, and besides the force acting on the hydrogen atoms due to the 3 dyz orbital is not available for the dissociation on the bridge site. Thus the hydrogen molecule on the bridge site on the Ni surface does not dissociate without the activation barrier.

I—E Chemical Reaction in Liquid Phase

An understanding of the dynamical mechanism of chemical reactions in solvents is an ultimate goal of the theoretical chemistry. This program involves the potential surface and molecular dynamics calculations for a system with many degrees of freedom. As the first step of this study, we have chosen a photoisomerization process of a polyene in liquid phase.

I-E-1 Energy Relaxation of Ethylene in Solvents

Iwao OHMINE

The dynamics of vibrational relaxation of highly excited polyenes (ethylene) in solvents is studied by the molecular dynamics (MD) calculation. Upon excitation, such molecules undergo a C-C torsional isomerization with the concominante intra- and inter-molecular vibrational relaxation. We have previously studied the intramolecular relaxation of polyenes in this photoisomerization process.[1] Presently, we extend our investigation to analyze the mechanism of the intermolecular relaxation of polyenes caursed by the interaction with the solvent molecules. We chose an ethylene in Ar or H_2O solvent as a model system, and performed the full three-dimensional molecular dynamics calculation. It was found that (1) The ethylene vibrational energy dissipation is mainly due to the hard repulsive collisions with solvent molecules. (2) The frequency of these hard collisions depends critically on the interaction strength between solvent molecules. (3) The Langevin equation does not work. (4) When the ethylene is protonated, inducing the coulomb interaction with solvent molecules (H_2O), the C-C torsional dissipation is greatly enhanced. We are now extending our analysis to include the effects of the sudden polarization in the singlet mechanism.

Reference

1. I. Ohmine and K. Morokuma, *J. Chem. Phys.* **73**, 1907 (1980) and **74**, 564 (1981).

I—F Nonadiabatic Transitions in Atomic and Molecular Processes

We have proposed a general analytical procedure, a semiclassical theory in the dynamical-state representation, which makes a unified treatment of nonadiabatic transitions possible. This method can be applied not only to collision but also to spectroscopic problems.

I-F-1 Semiclassical Theory of Predissociation Induced by Rotational (Coriolis) Coupling

Hiroki NAKAMURA

[*Chem. Phys.*, **78**, 235 (1983)]

The dynamical-state representation and the multichannel quantum-defect theory of predissociation are used to formulate a semiclassical theory of predissociation of a diatomic molecule induced by Coriolis coupling. It is demonstrated that the simple perturbation theory becomes invalid when the rotational angular momentum quantum number is large, and that the non-perturbative formula developed in this paper should be employed.

I-F-2 Dynamical-state Representation and Its Application to the $Li^+ + Na$ and $Li + Na^+$ Collisions

Reiko HIROKAWA *(Ochanomizu Univ.),* **Hiroki NAKAMURA, and Eiichi ISHIGURO** *(Ochanomizu Univ.)*

Differential as well as total cross sections are calculated for the following processes:

$$Li + Na \rightarrow Li^+ + Na,\ Li^*(2p) + Na^+,$$

and

$$Li^+ + Na \rightarrow Li + Na^+,\ Li^*(2p) + Na^+.$$

In these processes both radial and rotational couplings play an important role. There have been reported some theoretical studies based on the simplified versions of the semiclassical methods. None of them, however, can be free from ambiguities with respect to the treatment of rotational coupling. Our formalism based on the dynamical-state representation takes into account properly the multi-trajectory effect and the rotational coupling effect without any ambiguity. Adiabatic potential energies are taken from Wijnaendts van Resandt et al.[1] The rotational coupling matrix element is taken from Melius and Goddard.[2] The results are in good agreement with experiment.

References

1) R.W. Wijnaendts van Resandt, C. de Vreugd, R.L. Champion, and J. Los, *Chem. Phys.*, **29**, 151 (1978).
2) C.F. Melius and W.A. Goddard III, *Phys. Rev.*, **A10**, 1541 (1974).

I—G Theoretical Studies of Chemical Reaction Dynamics

I-G-1 A New Semiclassical Scattering Theory in Phase Space

Kazuo TAKATSUKA and Hiroki NAKAMURA

A new semiclassical scattering theory is proposed to describe heavy particle collisions including chemical reactions. A dynamical characteristic function (DCF) which is an integral transform of the density operator is defined in a phase space. A semiclassical approximation to the equation of motion satisfied by the exact DCF leads to a classical Liouville equation with an inhomogeneous term which is proportional to Lagrangian. As a result, the semiclassical DCF can be obtained easily in terms of the classical trajectories and the phase integrals along them. Important physical quantities such as wavefunction, density and flux at an arbitarary time can be calculated from a Fourier transform of the DCF. Our analysis shows that these quantities calculated from the semiclassical DCF must be quite accurate in general. The relationship between Schrödinger equation defined in a configuration space and our phase space theory will also be clarified. Our formalism has the following advantages compared to the classical S-matrix theory and the semiclassical theory based on the Wigner phase space function: (i) There is no need to search for special classical trajectories which satisfy the quantized boundary conditions. (i) The DCF does not involve a divergent factor such as the Van Vleck determinant which appears in the primitive semiclassical approximation. (iii) Our formalism is free from the so-called dangerous cross terms which cause an error in the semiclassical Wigner phase space funciton, and is consequently expected to be more accurate. (iv) The DCF can yield a local flux with much fewer classical trajectories than the Wigner phase space function.

I-G-2 Applicability of the LZS and the RZ

formulas to Collinear Chemical Reactions

Hiroki NAKAMURA

The Landau-Zener-Stueckelberg and the Rosen-Zener formulas are shown to be invariant under the following scaling of energy and length:

$$E = \bar{E}/\beta \quad \text{and} \quad R = \bar{R}\sqrt{\beta} \ ,$$

where β is a scaling factor. This means that it is worthwhile to think about an application of these formulas to simple chemical reactions by using the hyperspherical coordinate system. As an example, the RZ formula is demonstrated to be applicable with high accuracy to asymmetric hydrogen-atom-transfer reactions. The model system employed mimicks the reaction

$$Br + HCl\ (v{=}4) \rightarrow Cl + HBr\ (v{=}2)\ .$$

As is seen from Figure 1, the RZ formula works very well compared to the one proposed by Babamov et al.[1]

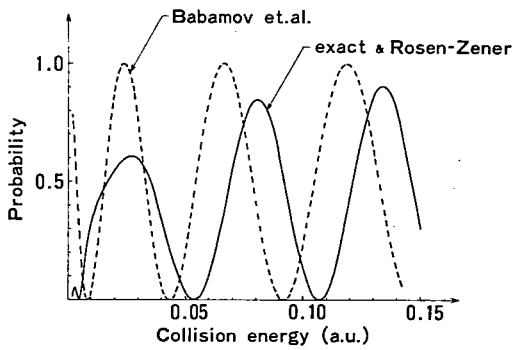

Figure 1. Transition probabilities as a function of collision energy for the collinear reaction

Br + HCl (v=4) → Cl + HBr (v=2)

——— : exact quantum-mechanical close-coupling calculation and Rosen-Zener approximation (indistinguishable in the figure) (two-state approximation)

– – – – – : approximation by Babamov et al.[1]

Reference

1) V.K. Babamov, V. Lopez, and R.A. Marcus, *J. Chem. Phys.*, **78**, 5621 (1983).

I—H Potential Energy Curves of Low Lying Excited States of CN

Kazuo TAKATSUKA, Haruhiko ITO,* Yoshihiro OSAMURA, Yasushi OZAKI,*** Takashi NAGATA,* Tamotsu KONDOW,* Hiroki NAKAMURA, and Kozo KUCHITSU*** *(*Tokyo Univ., **Keio Univ., ***National Institute for Environment Studies)*

In the experiments on the collisions of BrCN with Ar metastables,[1] intensity anomalies have been observed in the emission ($B^2\Sigma^+ \rightarrow X^2\Sigma^+$) bands of the product CN. Based on the CI calculations of Schaefer and Heil,[2] these anomalies have been identified to be due to the rotational perturbations between $B^2\Sigma^+$ and $^4\Pi$ states, the latter being observed experimentally for the first time. To examine this idea we have carried out more extensive calculations of the potential curves of low lying excited states of CN ($X^2\Sigma^+$, $A^2\Pi_i$, $B^2\Sigma^+$, $^4\Sigma^+$, and $^4\Pi$), since the results of Schaefer and Heil are not accurate enough to interpret the details of the experimental results.

MCSCF calculations with about 550 configurations using double-zeta and polarization bases have been performed. The vibrational states v = 12, 14 and 17 of $B^2\Sigma^+$ are found to energetically match with v′ = 3, 6, and 11 of $^4\Pi$, respectively. The computed molecular constants are in good agreement with the experimental values. In addition to the above vibrational states our potential curves suggested that v = 10 of $B^2\Sigma^+$ was likely to be perturbed by v′ = 0 of $^4\Pi$. In fact a new anomalous peak due to this perturbation has been found later. Thus our calculated curves have confirmed the experimental analysis.

References

1) J. Yencha, Y. Ozaki, T. Kondow and K. Kuchitsu, *Chem. Phys.*, **51**, 343 (1980); Y. Ozaki et al. *Chem. Phys.*, accepted for publication.
2) H.F. Schaefer III and T.G. Heil, *J. Chem. Phys.*, **54**, 2573 (1971).

I—I Electron-Correlation and Electron-Phonon Coupling in One-Dimensional Many-Electron Systems

To clarify optical, magnetic and electric properties of various newly synthesized one-dimensional materials from unified theoretical point of view, we study the phase diagram, optical and magnetic excitations of a one-dimensional many-electron system with the electron-electron repulsion and the electron-phonon coupling.

I-I-1 Extended Peierls-Hubbard Model for One-Dimensional N-Sites N-Electrons System. I. — Phase Diagram by Mean Field Theory —

Keiichiro NASU

[*J. Phys. Soc. Jpn.*, **52**, No. 11 (1983)]

The phase diagram of a one-dimensional many-electron system with a site-diagonal electron-phonon(e-p) coupling and a short-ranged inter-site electron-electron(e-e) repulsion as well as intra-site one is studied within the mean field theory for electrons and in the adiabatic limit for phonons. This theory covers the whole region of four basic parameters characterizing the system: the transfer energy of electron T, the e-p coupling energy S, the intra- and inter-site e-e repulsive energies U and V, and the phase diagram is given in a tetrahedral coordinate space spanned by T, U, S and V. It is proved that the "T-U-S-V tetrahedron" divided into SDW and CDW regions by the interface $U = S+2V$, that is, "S" competes with "U" but cooperates with "V". The "S↔U" and "S↔T" competitions appeared in the energy gap of CDW can well explain the experimental results of halogen-bridged mixed-valence metal complex chains.

I-I-2 Extended Peierls-Hubbard Model for One-Dimensional N-Sites N-Electrons System. II. — Effects of Fluctuation, Optical and Magnetic Excitations —

Keiichiro NASU

[*J. Phys. Soc. Jpn.*, **53**, No. 1 (1984)]

A one-dimensional many-electron system with a site-diagonal electron-phonon coupling, intra- and inter-site electron-electron(e-e) repulsions is studied within the RPA for electrons and in the adiabatic limit for phonons, so as to clarify effects of fluctuation on the phase diagram of the ground state within the mean field theory(MFT), and also on various excitations therefrom. Energies of bound electron-hole(e-h) pairs in the MFT energy-gap such as magnon and charge-transfer(CT) excitons are calculated together with the ground-state energy-gain due to the virtual excitations of these quasi-particles. The resultant new phase diagram is such that the SDW phase erodes the CDW region given by the MFT because of the virtual excitation of magnons. It is shown that the inter-site e-e repulsion always gives a stable singlet CT exciton that dominates the optical property of the CDW. This result can well explain the light absorption spectral shape of halogen-bridged mixed-valence metal complex chains.

I-I-3 Extended Peierls-Hubbard Model for One-Dimensional N-Sites N-Electrons System. III. — Lattice Relaxation after Optical Excitation in CDW —

Keiichiro NASU

[*J. Phys. Soc. Jpn.*, **53**, No. 1 (1984)]

The self-trapping of charge-transfer exciton in the CDW phase of one-dimensional many-electron system with short-ranged electron(e-p) and electron-electron(e-e) interactions is studied by a variational method for the exciton and in the adiabatic limit for phonons, so as to clarify its lattice relaxation process after the light excitation. The adiabatic potential energy surface describing the lattice relaxation process is calculated in a wide region of four basic parameters characterizing the system: the transfer energy of electron T, the e-p coupling energy S, intra- and inter-site e-e repulsive energies

U and V. It is shown that in the strong coupling case S ≫ 2T, the exciton relaxes to metastable ground states such as an *island of SDW phase* or a *kink-antikink pair* in the phase of Peierls distortion, and only in the intermediate case S ~ 2T, it relaxes to a luminescent state localized in the middle of the energy-gap. These results can well explain the luminescence of Wolffram's red salt.

I—J Paths and Rates of Chemical Reactions

I-J-1 Ab initio MO CI Studies of the Hydrogen Abstraction by NH ($a^1\Delta$)

Takayuki FUENO[1] *(Osaka Univ. and IMS),* **Okitsugu KAJIMOTO** *(Tokyo Univ.)* **and V. BONAČIĆ-KOUTECKÝ** *(Freie Universität Berlin)*

Clear-cut evidence[2] exists indicating that NH($a^1\Delta$) can directly abstract a hydrogen atom from paraffins in a manner more or less competitive to the insertion into C-H bonds. Obviously, it is the open-shell configuration $(1\sigma)^2(2\sigma)^2(3\sigma)^2(p_x)(p_y)$ which is responsible to this radical character of NH($a^1\Delta$).

We have examined

$$NH(a^1\Delta) + H_2 \rightarrow NH_2(\tilde{X}^2B_1) + H$$

as a prototype of the NH($a^1\Delta$) abstraction reactions. The path of the reaction was traced by the singlet UHF SCF procedure with the 4-31G basis set. It has proved that the reaction proceeds maintaining the planar A″(C_s) structure throughout.

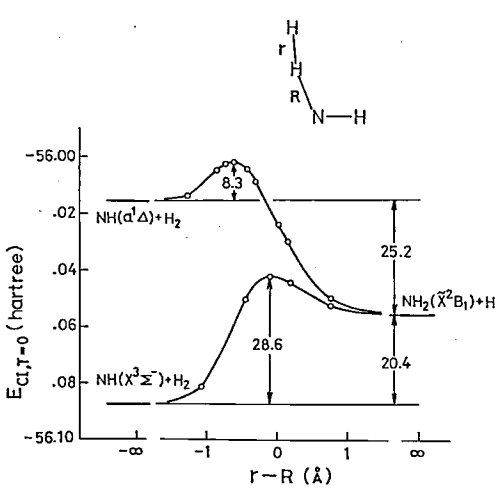

Figure 1. Potential energy profiles calculated for the abstraction reactions of NH($a^1\Delta$) and NH($^3\Sigma^-$) from H_2. The energies were calculated by the MRD-CI procedure on the minimum-energy path points deduced from the UHF SCF geometry optimizations. The energy gaps indicated are in kcal/mol.

The multi-reference double-excitation configuration-interaction (MRD-CI) calculations[3] were then conducted at several points on the SCF minimum-energy path.

Figure 1 illustrates the change in the CI energy $E_{CI,T=0}$ calculated as the function of $r_{HH} - R_{HN}$ chosen as a principal reaction coordinate. The activation barrier height $\Delta E^{\neq}$ calculated for the singlet reaction in question is 8.3 kcal/mol, which is considerably smaller than 28.6 kcal/mol[4] obtained for the corresponding triplet reaction. The effects of polarization functions were found to be immaterial.

Calcualtions have been extended to the reaction of methane:

$$NH(a^1\Delta) + CH_4 \rightarrow NH_2(\tilde{X}^2B_1) + H$$

The results have proved to be much the same as in the case of H_2.

References

1) IMS Adjunct Professor for 1981–1983.
2) (a) O. Kajimoto and T. Fueno, *Chem. Phys. Lett.*, **80**, 484 (1981); (b) O. Kondo, J. Miyata, O. Kajimoto and T. Fueno, *ibid.*, **88**, 424 (1982).
3) R.J. Buenker and S.D. Peyerimhoff, *Theoret. Chim. Acta*, **35**, 33 (1974); **39**, 217 (1975).
4) T. Fueno, V. Bonačić-Koutecký and J. Koutechý, *J. Am. Chem. Soc.*, **105**, 5547 (1983).

I-J-2 SCF MO Studies of the Reaction of NH($^3\Sigma^-$) with Ethylene

Takayuki FUENO[1] *(Osaka Univ. and IMS),* **Kizashi YAMAGUCHI and Osamu KONDO** *(Osaka Univ.)*

The addition reaction of the NH($^3\Sigma^-$) radical toward ethylene and the isomerization – fragmentation processes for the resulting triplet adduct have been investigated by the 4-31G UHF SCF method.

Full geometry optimization of the adduct triplet diradical $\dot{C}H_2CH_2\dot{N}H$ has shown that there exist four stable conformations as local energy minima.

The most stable of these is found to be the "face-CH_2 and edge-NH cis (FE_t)" conformer:

The transition state geometry (FE_c) for the addition has already been reported.[2] The barrier height calculated using the 4-31G** basis is 8.1 kcal/mol.

The triplet diradical will be subject to isomerization or fragmentation, unless it is effectively converted into the singlet state. The α C-H bond cleavage (a), 1,2-hydrogen shift (b) and 1,3-hydrogen shift (c) are conceivable:

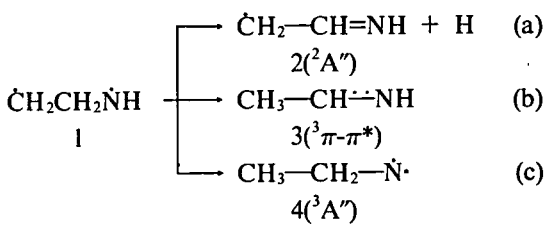

The transition states for processes (a) to (c) have been located by computation. Shown in Table I are the barrier heights $\Delta E^{\neq}$ and the energy charges for reaction ΔE. Apparently, the α C-H bond cleavage is the most favorable, despite the least stability of its product system.

The product radicals 2 to 4 are eventually led to $CH_3CH = \dot{N}(^2A')$. The route via the triplet nitrene 4 has proved to be energetically the most favorable.

References

1) IMS Adjunct Professor for 1981–1983.
2) T. Fueno, V. Bonačić-Koutecký and J. Koutecký, *J. Am. Chem. Soc.*, **105**, 5547 (1983).

Table I. Unimolecular reactions of the triplet CH_2CH_2NH diradical.

Reaction	Product	Energy (kcal/mol)	
		$\Delta E^{\neq}$	ΔE
(a)	$2(^2A') + H$	26.3	20.5
(b)	$3(\pi\text{-}\pi^*)$	60.5	−3.5
(c)	$4(^3A'')$	35.6	−30.9

I-J-3 Potential Energy Profile and the Rates of the Reaction $H + HN_3 \rightarrow NH_2 + N_2$

Takayuki FUENO[1] *(Osaka Univ. and IMS)*

Hydrazoic acid(HN_3) reacts with the hydrogen atom in the gas phase to give the NH_2 radical and molecular N_2.[2,3] The reaction appears to involve the intermediacy of an energized HHN_3 adduct radical.

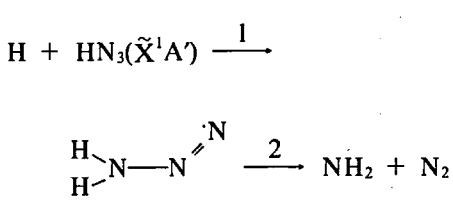

Geometry optimization by the UHF SCF procedure with the 4-31G basis set has shown that the adduct is the most stable in the planar $A'(C_s)$ structure and is 71.4 kcal/mol more stable than the reactant system. The transition states (TS) for Stages 1 and 2 are both found to be nonplanar, with the energy barriers of 4.1 and 5.0 kcal/mol, respectively. Clearly, Stage 1 must be the rate-controlling step, barrier height corrected for the vibrational zero-point energy being E_0 = 4.3 kcal/mol.

The MRD-CI calculations with the same basis set have been carried out for the various SCF energy minima as well as the saddle points involved. Neither of the barrier heights is altered appreciably from the corresponding UHF SCF result.

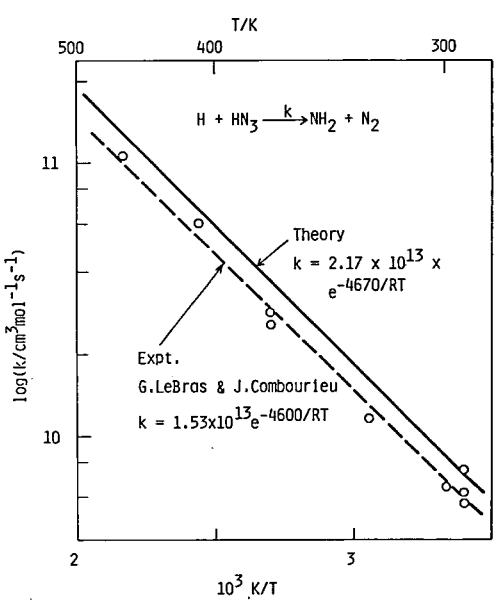

Figure 1. The bimolecular rate constant for the reaction $H + HN_3 \rightarrow NH_2 + N_2$. —, ab initio MO TST; O, experiment.

The vibrational frequency analysis has been worked out for the transition state of Stage 1. The bimolecular reaction rate constants have been calculated in the temperature range 300 to 500K, using the conventional (κ=1) transition state theory (TST) combined with the SCF results of the transition state characteristics. In Figure 1, the results are compared with the experimental data.[2] The agreement between the ab initio MO TST and experiment is excellent, even though it is perhaps somewhat fortuitous.

References

1) IMS Adjunct Professor for 1981–1983.
2) G. Le Bras and J. Combourieu, *Int. J. Chem. Kinet.*, **5**, 559 (1973).
3) O. Kajimoto, T. Kawajiri and T. Fueno, *Chem. Phys. Lett.*, **76**, 315 (1980).

RESEARCH ACTIVITIES II
Department of Molecular Structure

II—A High Resolution Spectroscopy of Transient Molecules

During the course of chemical reactions many transient molecules appear as intermediates. However, because of their high reactivities (i.e. short lifetimes), the knowledge on these transients is still very much limited. Many of them have open-shell electronic structures, which characterize such species as free radicals and cause splittings in their high-resolution spectra because of fine structure and/or hyperfine structure interactions of unpaired electrons. Analyses of these structures provide us with information on the electronic properties of molecules which is not obtainable for molecules without unpaired electrons. High resolution spectroscopy not only provides molecular constants of transient molecules at very high precision, but also allows us to unambiguously identify such species in chemical reaction systems and to unravel the details of the reaction mechanisms. The present project will also be of some significance in related fields such as astrophysics and environmental researches.

II-A-1 Microwave Spectroscopy of the CD_3O Radical

Yasuki ENDO, Shuji SAITO, and Eizi HIROTA

We have previously studied the CH_3O radical by microwave spectroscopy.[1] The measurement has been extended to CD_3O to test the validity of the rotational Hamiltonian for a symmetric top in a ^2E state that was employed in analyzing the CH_3O spectrum, and also to determine the molecular structure.

The presence of three deuterium nuclei makes the magnetic hyperfine interaction extremely complicated; the A_1/A_2 and E states are split into 11 and 8 components, respectively, and a few lines appear as hyperfine doublets. The matrix elements of the hyperfine interaction Hamiltonian have been derived in terms of reduced matrix elements $\langle\Gamma' ; I' | |T^1(I-\alpha)| |\Gamma ; I\rangle$ where Γ and Γ' are A_1 or E, and I and I' designate the total nuclear spin quantum number of 0, 1, 2, or 3. Because the coupling constants are not large, many hyperfine components are not completely resolved, as exemplified by the $E_{3/2}$ $J = 3.5 \leftarrow 2.5$, $K = 1$ transition shown in Figure 1; a simulation method assuming a Lorentzian lineshape was employed in analyzing unresolved hyperfine structures.

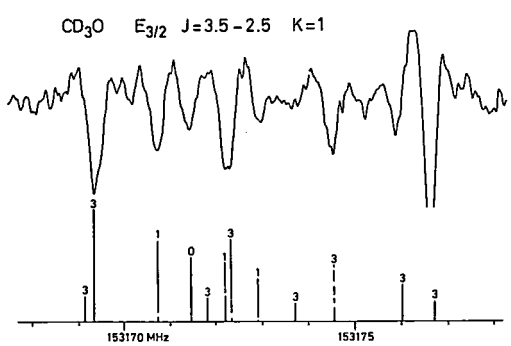

Figure 1. The $J = 3.5 \leftarrow 2.5$ $K = 1$ transition of CD_3O in $^2E_{3/2}$. The number shown on the top of each calculated line (designated by a stick below the observed spectrum) is the total nuclear spin quantum number.

The hyperfine coupling constants obtained for CH_3O, when multiplied by the factor 1/6.51438, were found to account for the hyperfine structure of CD_3O satisfactorily.

Reference

1) Y. Endo, S. Saito, and E. Hirota, IMS Ann. Rev., 22 (1982).

II-A-2 Rovibronic Interaction in the $^2\Pi$ Linear Triatomic Molecule: Microwave Spectroscopic Investigation of the NCO Radical in the $\tilde{X}(000)^2\Pi$, $\tilde{X}(010)^2\Delta$, and $\tilde{X}(020)^2\Phi$ States.

Kentarou KAWAGUCHI, Shuji SAITO, and Eizi HIROTA

In a previous paper,[1] we have investigated rovibronic interactions in the NCO radical by observing its microwave spectra in the $\tilde{X}(010)$ $\mu^2\Sigma$ and $\kappa^2\Sigma$ states. The present study extends the measurements to the three states of NCO shown in the title, and molecular constants obtained from an analysis of the observed spectra are listed in Table I. The precision of each constant has been much improved in comparison with those of earlier measurements where available. It is interesting to note that eQq_2, the non-axially symmetric component of the N nuclear quadrupole coupling tensor, was determined for the ground state and was found to be positive. This can be understood if one notes three electrons (including one unpaired electron) to be present in the highest occupied π orbital in NCO. Another interesting feature of the present result is that A_J considerably changes with the ν_2 excitation.

Table I. Molecular Constants of NCO in $\tilde{X}(000)^2\Pi$, $\tilde{X}(010)^2\Delta$, and $\tilde{X}(020)^2\Phi$ (MHz)[a]

Constant	$\tilde{X}(000)^2\Pi$	$\tilde{X}(010)^2\Delta$	$\tilde{X}(020)^2\Phi$
B	11 677.334 1(42)	11 708.272 9(72)	11 739.902 6(89)
D	0.004 572(66)	0.004 77(12)	0.004 81(11)
A_J	−0.130 0(19)	−0.314 2(27)	−0.565 3(25)
p	78.99(15)		
q	−1.484(56)		
$a-(b+c)/2$	70.45(17)	68.35(23)	65.87(81)
$a+(b+c)/2$	53.50(12)	52.80(18)	51.82(57)
b	31.2(16)	31.5(43)	[31.22][b]
d	88.494(75)		
eQq_1	−2.185(68)	−2.20(25)	−2.16(66)
eQq_2	16.2(29)		

a. Values in parentheses denote three standard errors and apply to the last digits of the constants.
b. Assumed.

Reference

1) K. Kawaguchi, S. Saito, and E. Hirota, Mol. Phys., **49**, 663 (1983).

II-A-3 Laser Excitation Spectrum and Microave Optical Double Resonance Spectrum of the 3_0^1 Band in the $\tilde{a}^3A_2$ — $\tilde{X}^1A_1$ System of H_2CS: The Hyperfine Structure of the $\tilde{a}^3A_2$ State

Tetsuo SUZUKI, Shuji SAITO, and Eizi HIROTA

[*J. Chem. Phys.*, **79**, 1641 (1983)]

The dye laser excitation spectrum with the Doppler-limited resolution and the microwave optical double resonance spectrum of the 3_0^1 band in the $\tilde{a}^3A_2 - \tilde{X}^1A_1$ system of H_2CS were observed in order to obtain detailed and precise information on the excited triplet state. The excitation spectrum observed in the region 15280 to 15400 cm^{-1} yielded molecular constants listed in Table I; the ν_3'/ν_6' Coriolis interaction as revealed in the $K_a' = 4$ and 5 lines was taken into account. Fifteen K-type doubling transitions and two a-type R branch transitions in the $\tilde{a}$ state were observed by rf or microwave optical double resonance; two K-

Table I. Molecular Constants of H_2CS in $\tilde{a}^3A_2$ $\nu_3 = 1$ (MHz)[a]

A	280 457.6(87)	Spin-spin interaction constants	
B	16 401.74(28)	α	−43 474.6(61)
C	15 488.75(31)	β	2 550.2(61)
Δ_N	0.024 46(19)	Spin-rotation interaction constants	
Δ_{NK}	0.936(14)	a_0	4 880.2(45)
Δ_K	23.44(41)	a	4 685.9(50)
δ_N	0.001 48(10)	b	−82.87(26)
δ_K	0.66(11)		
ν [$\tilde{a}$ $\nu_3 = 1 \leftarrow \tilde{X}$ $\nu = 0$]		15 389.0317(37)	cm^{-1}
$\nu_6 = 1$[b]			
$B + C$	32 189.5(24)	$\lvert G_{36}{}^c \rvert$	5307(41)
$\nu_3 - \nu_6$	99.341(24)	cm^{-1}	

a. Values in parentheses denote three standard errors and apply to the last digits of the constants.
b. Other parameters were fixed to those of the ground state.

doubling transitions with $K_a' = 1$ and two R branch transitions (all F_3 components) were resolved into three hyperfine components. The observed splittings gave the proton hyperfine coupling constants to be $a_F = 27.7(25)$, $T_{bb} + T_{cc} = 12.8(44)$, and $T_{bb} - T_{cc} = 7.89(19)$ MHz with one standard error in parentheses. These constants can be interpreted in terms of a model that one unpaired electron occupies a non-bonding orbital mainly consisting of a sulfur in-plane $3p_b$ orbital and the other lies in an anti-bonding π^* orbital approximated by an out-of-phase linear combination of a sulfur $3p_c$ and a carbon $2p_c$ orbital.

II-A-4 Third-Order Anharmonic Potential Constants and Equilibrium Structure of HNO

Eizi HIROTA

The anharmonic potential constants F_{ijk} and the equilibrium structure were derived previously[1] using laser Stark spectroscopic data[2] on the HNO ν_2 and ν_3 bands and on the DNO ν_2 band with some preliminary informaiton on the ν_1 state. Johns et al.[3] have recently carried out a more extensive observation on the ν_1 and ν_2 bands of both HNO and DNO, leaving only the ν_3 band of DNO to be observed. A program has been written which computes harmonic (F_{ij}) and third-order (F_{ijk}) potential constants and the equilibrium bond lengths (r_e) and bond angle (θ_e) from experimental data available, i.e. the vibrational frequencies (ν_i), ground-state rotational constants (B_0), vibration-rotation constants (α_s), Coriolis coupling constants (ζ_{ij}), and centrifugal distortion constants (Δ_J etc.) by the least-squares method. The observed rotational constants were corrected for electron contributions using rotational g factors. The analysis was performed in two steps; in the first step, F_{11}, F_{22}, F_{23}, and F_{33} were determined from ν_i, ζ_{ij}, and Δ_J, ..., and the structure parameters and F_{ijk} were derived in the second step from B_0 and α_s. It was still not possible to determine all F_{ijk}, and Table I summarizes one of the most plausible sets of molecular parameters thus obtained.

References

1) E. Hirota, IMS Ann. Rev., 29 (1983).
2) J. W. C. Johns and A. R. W. McKellar, J. Chem. Phys., 66, 1217 (1977).
3) J. W. C. Johns, A. R. W. McKellar, and E. Weinberger, to be published.

Table I. Third-Order Anharmonic Potential Constants Equilibrium Structure of HNO

F_{111}	−27.44(29) md/A^2	F_{112}	6.6(44) md/A^2
F_{222}	−74(22) md/A^2	F_{223}	−0.6(17) md/A
F_{333}	−1.17(17) mdA	F_{123}	6.32(48) md/A

other $F_{ijk} = 0$ assumed.

	HNO		DNO	
(MHz)	obs.	calc.	obs.	calc.
α_1^A	24 074.9	24 063.1	8 622.4	8 658.6
α_1^B	−232.4	−165.3	−10.4	49.8
α_1^C	−15.3	−87.2	82.5	61.4
α_2^A	−2 923.6	−2 923.1	2 082.1	2 101.0
α_2^B	303.7	255.4	352.6	328.0
α_2^C	−91.6	6.7	273.4	290.1
α_3^A	−10 356.4	−10 355.7		−7 650.5
α_3^B	41.5	−46.2		−180.2
α_3^C	759.5	507.5		178.7

	Present (r_e)	Dalby (r_0)[a]	Ogilvie (r_0)[b]
r(H-N) (Å)	$1.061_5 \pm 0.004$	1.062_8	1.09026(H-N) 1.0795(D-N)
r(N-O) (Å)	1.207 ± 0.004	1.211_6	1.2090
θ(HNO) (Å)	$108.9_5 \pm 0.4$	108.5_8	108.047

a. F. W. Dalby, Can. J. Phys., 36, 1336 (1958).
b. J. F. Ogilvie, J. Mol. Struct., 31, 407 (1976).

II-A-5 Rovibronic Interaction in the NO_3 Radical

Eizi HIROTA, Kentarou KAWAGUCHI, Takashi ISHIWATA *(Tokyo Inst. Tech.)*, **and Ikuzo TANAKA** *(Tokyo Inst. Tech. and IMS)*

We have recently observed ν_3 (N–O degenerate stretching) band of the NO_3 radical by infrared tunable diode laser spectroscopy.[1] The observed spectrum clearly indicates that NO_3 is a D_{3h} planar molecule. There are, however, several anomalies in the observed spectrum or in the molecular constants obtained therefrom. For example, as shown in Table I, the observed centrifugal distortion constants are much larger in magnitude than the calculated values, and the first-order Coriolis coupling constant which is observed differs much from the calculated value. The observed spin-rotation interaction constants are also difficult to

interpret.

The present study explains the anomalies by the spin-orbit interaction and the orbital-rotation interaction between the lowest excited state ($\tilde{A}$) of $^2E''$ symmetry and $\tilde{X}$ state; the perturbed energy of the $\tilde{X}$ state is given by

$$E(X) = [E^0(X) + E^0(A)]/2 - (1/2)\,[(\Delta E)^2 + 8e_+e_-]^{1/2}, \qquad (1)$$

where ΔE denotes the difference between the unperturbed energies, $E^0(A) - E^0(X)$ and $e_\pm = (a/2)\langle L\rangle S_\pm - B\langle L\rangle N_\pm$ consists of the two terms corresponding to the two types of the interactions. Equation (1) explains some of the anomalies semiquantitatively, provided that the $\tilde{A}$ state is located as low as 1000 cm^{-1}.

Reference

1) T. Ishiwata, K. Kawaguchi, E. Hirota, and I. Tanaka, IMS Ann. Rev., 29 (1982).

Table I. Centrifugal Distortion Constants and Coriolis Coupling Constant of the NO_3 Radical in $\tilde{X}^2A_2'$

	Calc.[a]		Obs.	
F_{34}(md) =	0.0	−0.2	ν_3	G.S.
D_N (MHz)	0.040	0.039	−0.14	1.25
D_{NK} (MHz)	−0.074	−0.072	−2.88	−2.75
ζ_3	0.7206	0.6733	0.1956	

a. $\nu_1 = 1060$, $\nu_2 = 831$, $\nu_2 = 1480$, and $\nu_4 = 380$ cm^{-1} were used.

II-A-6 Doppler-Limited Dye Laser Excitation Spectroscopy of the HSO Radical: the $\tilde{A}^2A'(001) - \tilde{X}^2A''(000)$ Band

Koichi TSUKIYAMA[1], Shuji SAITO, Tetsuo SUZUKI, Ikuzo TANAKA *(Tokyo Inst. Tech. and IMS)*, **and Eizi HIROTA**

To explore the vibrational dependencies of the molecular constants of HSO in the $\tilde{A}^2A'$ state, the earlier measurements[2,3] have been extended to the (001) − (000) band. As in the earlier studies, HSO was generated by the reaction of O_2 discharge products (about 20 mTorr) with H_2S (about 90 mTorr). The spectrum was scanned in the region of 15034 to 15136 cm^{-1}, and 685 lines were assigned to transitions of $K' - K''$ up to 4 − 3. The least-squares analysis yielded upper-state molecular constants listed in Table I with $\sigma_{fit} = 0.0039$ cm^{-1}. Table I also shows the vibrational changes of molecular constants, $A(v_3 = 3) - A(v_3 = 2)$ and $A(v_3 = 2) - A(v_3 = 1)$, etc. As is seen, most molecular constants vary smoothly with ν_3, and the constants obtained by an extrapolation to $\nu_3 = -1/2$ may give a more consistent set of molecular parameters (e.g. force field) than that calculated previously.[4]

References

1) IMS Graduate Student 1981—1983 from Tokyo Inst. Tech.
2) M. Kakimoto, S. Saito, and E. Hirota, *J. Mol. Spectrosc.*, **80**, 334 (1980).
3) K. Tsukiyama, S. Saito, T. Suzuki, I. Tanaka, and E. Hirota, IMS Ann. Rev., 31 (1981).
4) N. Ohashi, M. Kakimoto, S. Saito, and E. Hirota, *J. Mol. Spectrosc.*, **84**, 204 (1980).

Table I. Molecular Constants of HSO in the $\tilde{A}^2A''$ State (MHz)

Constant	(001)[a]	(003) − (002)	(002) − (001)
A	288 668(22)	1696.	1498.
B	17 131.3(23)	−98.9	−97.7
C	16 064.2(24)	−131.0	−131.1
Δ_N	0.040 4(14)	0.0042	0.0037
Δ_{NK}	1.784(83)	0.950	0.584
Δ_K	23.4(15)	20.7	−4.2
δ_N	0.003 2(14)	0.001 17	0.000 7
δ_K	1.7(10)	1.13	1.15
ϵ_{aa}	15 510(165)	1198.	1146.
ϵ_{bb}	72(15)	4.	11.
ϵ_{cc}	−358(16)	1.	5.
ν_0 (cm^{-1})	15 090.6531(24)	692.4875	699.8846

a. Values in parentheses denote 2.5σ and apply to the last digits of the constants.

II-A-7 Coriolis Interaction between the (020) $K_a = 2$ and (100) $K_a = 1$ Levels of HNO in the $\tilde{A}^1A''$ State

Kojiro TAKAGI *(Toyama Univ.)*, **Shuji SAITO, Tetsuo SUZUKI, and Eizi HIROTA**

As briefly mentioned previously,[1] we have shown by MODR (microwave optical double resonance) that the (020) $K_a = 2$ and (100) $K_a = 1$ levels of HNO in $\tilde{A}^1A''$ are Coriolis coupled with each other. To obtain further information, the laser excitation

spectrum was recorded in the region 15 960 to 16 060 cm^{-1}, which included the $^rQ_1(J)$ and $^rR_1(J)$ transitions for (020) $K_a = 2$ and the $^rR_0(J)$ and $^rQ_0(J)$ transitions for (100) $K_a = 1$. Using these data the term values were calculated up to $J = 17$ for the two series of levels. The two series were found to be closest to each other at $J = 13$ and 14, and intervibrational state transitions involving these levels have been observed by an MODR technique and employed to detail the level structure.

Reference

1) E. Hirota and S. Saito, IMS Ann. Rev., 131 (1982).

II-A-8 Far-Infrared Laser Magnetic Resonance Spectroscopy of the PH and PD Radicals in the $X^3\Sigma^-$ State

Nobukimi OHASHI *(Kanazawa Univ.)*, **Kentarou KAWAGUCHI, and Eizi HIROTA**

A previous measurement[1] of the far-infrared laser magnetic resonance (LMR) spectra of PD in $X^3\Sigma^-$ v = 0 has been extended to include the transitions of $N = 2 \leftarrow 1$ up to $7 \leftarrow 6$, using six far-infrared laser lines. The $N = 3 \leftarrow 2$ transition in $\nu = 1$ was also detected with the 392.1 μm laser line. These data, combined with those of mid-infrared LMR by Uehara and Hakuta[2], were subjected to the least-squares analysis. The observation by Davies et al.[3] of the PH far-infrared LMR spectrum has also been extended using five new laser lines, and all the observed data were least-squares analyzed by adding the two centrifugal distortion terms in H and γ_D to the Hamiltonian; the latter term was found to remove the discrepancy mentioned in Ref. 3. All the molecular constants thus obtained are listed in Table I.

The hyperfine parameter α_P of PD, which is often referred to as the Fermi contact term, allows to estimate the s character to be 0.98%. The second hyperfine parameter β_P gives the unpaired electron spin density on the P atom to be 86.6%. Using the results on both PD and PH, the Born-Oppenheimer equilibrium bond length and the potential constants up to the fourth order were derived: r_e^{BO} = 1.42140(22) Å, ω_e (PH) = 2366.79(16) cm^{-1}, a_1 = −2.3797(18), and a_2 = 3.461(14).

References

1) N. Ohashi, K. Kawaguchi, and E. Hirota, IMS Ann. Rev., 31 (1982).
2) H. Uehara and K. Hakuta, *J. Chem. Phys.*, **74**, 4326 (1981).
3) P. B. Davies, D. K. Russell, D. R. Smith, and B. A. Thrush, *Can. J. Phys.*, **57**, 522 (1979).

Table I. Molecular Constants of PD and PH in $X^3\Sigma^{-a}$

Constant	PD		PH
	$\nu = 0$	$\nu = 1$	$\nu = 0$
B	4.362 8675(77)	4.269 248(65)	8.412 524(21)
$D \times 10^3$	0.118 03(24)	[0.1154]^b	0.443 67(77)
$H \times 10^8$			2.56(77)
λ	2.208 48(57)	2.209 5(10)	2.209 93(24)
γ	−0.039 900(52)	−0.038 82(21)	−0.076 894(24)
$\gamma_D \times 10^5$	0.323(67)	[0.33]^b	0.130 8(70)
α_P	0.004 330(39)	0.004 66(40)	0.004 254(77)
β_P	−0.005 312(32)	−0.004 79(69)	−0.005 255(96)
α_H			−0.001 603(53)
β_H			0.000 181(65)
$g_S + g_l$	2.007 22(51)	2.005 2(11)	2.006 83(39)
$\Delta g'$	−0.004 31(93)	[−0.004 3]^b	0.003 9(10)
g_r	0.000 43(13)	[0.000 43]^b	0.000 77(17)
ν_0		1653.28491(51)	

a. Values in parentheses denote 3σ and apply to the last digits of the constants. The unit is cm^{-1}, except for the g factors.
b. Assumed.

II-A-9 Far-Infrared Laser Magnetic Resonance Detection and Microwave Spectroscopy of the PO Radical

Kentarou KAWAGUCHI, Shuji SAITO, and Eizi HIROTA

[*J. Chem. Phys.*, **79**, 629 (1983)]

Although more than 40 papers have already been published on emission and absorption spectra of the PO radical in the ultraviolet and visible regions, very few studies have been reported on the vibrational and rotational spectra. Many attempts to detect PO using microwave and gas-phase electron-paramagnetic-resonance (EPR) spectroscopy have failed presumably because the efficiency of the radical production was too low. We could have observed the spectra of PO by far-infrared

LMR spectroscopy, where we employed the reaction of red phosphorus with microwave discharge products of an O_2 (30 mTorr) and H_2 (350 mTorr) mixture. We have confirmed that hydrogen atoms are indispensable in generating PO. We suspect that $H + P \rightarrow PH$, $PH + O \rightarrow PO + H$ are the most probable route for generating PO.

The far-infrared LMR spectra were combined with microwave spectra observed subsequently to yield molecular constants listed in Table I, where the data obtained from optical spectroscopy are also given for comparison. The sign of the Λ doubling constant of Verma and Singhal[1] was corrected to be positive. A comparison of the hyperfine coupling constants of PO and NO shows that both the orbital and spin averages of $1/r^3$ are larger in PO than in NO by 15 to 18%, indicating the back donation (i.e. the contribution of $X^- = O^+$, X = P or N) to be smaller in PO than in NO.

Reference

1) R. D. Verma and S. R. Singhal, Can. J. Phys., **53**, 411 (1975).

Table I. Molecular Constants of the PO Radical in the $X^2\Pi_r$ State[a]

Constant	Present	Verma-Singhal[b]	Rao[c]
B_0	21 899.4915(33)	21 916.6(27)	21 894
D_0	0.031 120(42)	0.039 3(45)	
A_1^{eff}	3.102 6(30)	3.1(22)	
p_0	188.01(51)	−210	219
q_{eff}	−0.57(29)		
$a + (b + c)/2$	472.27(36)		
$a - (b + c)/2$	660.04(12)		
b	227.5(64)		
d	751.169(90)		
a	566.16(19)[d]		
c	−415.3(64)[d]		
A_0 (cm^{-1})	[224.01][e]	224.01	224.03

a. In MHz except for A_0. Values in parentheses denote 3σ and apply to the last digits of the constants.
b. Ref. 1).
c. K. S. Rao, *Can. J. Phys.*, **36**, 1526 (1958).
d. Derived constants.
e. Fixed.

II-A-10 Far-Infrared Laser Magnetic Resonance Spectroscopy of the PO_2 Radical

Kentarou KAWAGUCHI, Nobukimi OHASHI *(Kanazawa Univ.)*, **and Eizi HIROTA**

In the course of studying the PD radical (II-A-8) by far-infrared laser magnetic resonance (LMR), we observed additional resonances when we employed the reaction of red phosphorus with microwave discharge products of D_2O rather than D_2. The spectrum increased intensity when D_2O was replaced by a mixture of O_2 and H_2. It is interesting to note that hydrogen is also indispensable, as in the case of PO (II-A-9).

The LMR spectrum was observed on 17 laser lines; Figures 1-a and 1-b show two examples obtained using the CH_2F_2 256 μm and CH_3OH 251.1 μm laser lines as sources, respectively. The spectrum is similar to that of NO_2 and shows large splittings due to the ^{31}P hyperfine interaction. These observations, combined with chemical evidences mentioned above, suggest the observed spectrum to be assigned to the PO_2 radical. We have subsequently observed the microwave spectrum, and all these data are being analyzed.

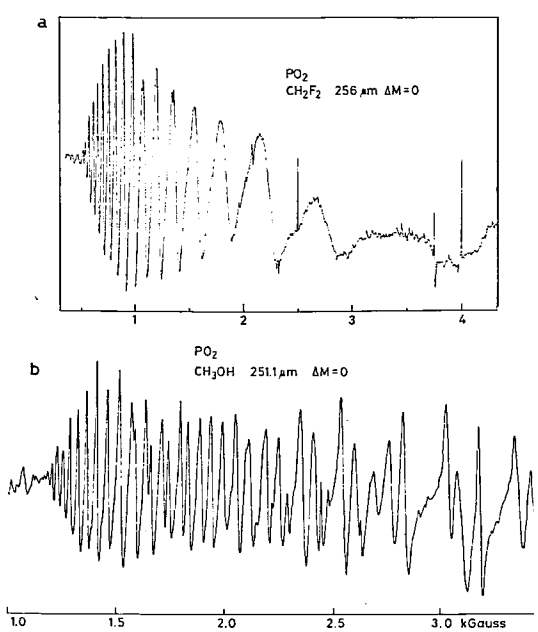

Figure 1.
a) Far-infrared LMR spectrum of PO_2 recorded using the CH_2F_2 256 μm laser line as a source. The polarization of the laser line was chosen such that $\Delta M = 0$ selection rule is satisfied.
b) Far-infrared LMR spectrum of PO_2 recorded using the CH_3OH 251.1 μm laser line as a source. The selection rule chosen is $\Delta M = 0$.

II-A-11 Difference Frequency Laser Spectroscopy of the ν_1 Band of the HO_2 Radical

Chikashi YAMADA, Yasuki ENDO, and Eizi HIROTA

[*J. Chem. Phys.*, **78**, 4379 (1983)]

After we took the spectrum of the HO_2 ν_1 band,[1] the ground-state molecular constants have been subsequently much improved by Charo and De Lucia.[2] This result has allowed us to fit the observed spectrum much more satisfactorily. The HO_2 radical was generated directly in a cell by a dc discharge in a mixture of allyl alcohol and oxygen. Zeeman modulation was employed, and apparent shifts in the observed line frequencies caused by Zeeman modulation were carefully corrected for by simulation of the line shape. About 280 lines were thus observed and analyzed to yield molecular constants in the $\nu_1 = 1$ state, as listed in Table I, where the ground-state constants were fixed to those of Ref. 2). the band origin is 22 cm^{-1} higher than the value previously obtained by a matrix isolation study. After making corrections for minor effects, the equilibrium rotational constants of HO_2 were calculated to be A_e = 619 568(30) MHz, B_e = 33 664.8(85) MHz, and C_e = 31 944.2(86) MHz, which gave the inertia defect to be −0.0071(57) uÅ^2.

References

1) C. Yamada and Y. Endo, IMS Ann. Rev., 48 (1980).
2) A. Charo and F. C. De Lucia, *J. Mol. Spectrosc.*, **94**, 426 (1982).

II-A-12 The Microwave Spectrum of the Fluoromethyl Radical, CH_2F

Yasuki ENDO, Chikashi YAMADA, Shuji SAITO, and Eizi HIROTA

[*J. Chem. Phys.*, **79**, 1605 (1983)]

Our previous measurements[1] have been extended so as to include the a-type R-branch transitions of $N = 1 \leftarrow 0$, $2 \leftarrow 1$, and $3 \leftarrow 2$ for the ground vibrational state and of $N = 2 \leftarrow 1$ and $3 \leftarrow 2$ for the first excited state of the out-of-plane bending mode (ν_4). All of these transitions were found to be split into fine and hyperfine components, and the hyperfine structure observed for the ground state is consistent with electronic symmetry of B_1 and with odd parity with respect to the reflection on the "molecular plane". A relative intensity measurement shows that the $\nu_4 = 1$ state with even parity is located 300 (30) cm^{-1} above the ground state. These observations suggest that the CH_2F molecule is essentially planar, although the presence of a small hump at the planar configuration cannot be excluded.

Reference

1) Y. Endo, S. Saito, and E. Hirota, Ann. Rev., 24 (1982).

II-A-13 The Microwave Spectrum of an Unstable Molecule, HPO

Shuji SAITO, Yasuki ENDO, and Eizi HIROTA

Table I. Molecular Constants of HO_2 in the $\nu_1 = 1$ State[a]

A	587 118.0(20)	Spin-rotation coupling constants	
B	33 649.0(12)	ϵ_{aa}	−46 678.0(51)
C	31 725.5(11)	ϵ_{bb}	−432.0(18)
		ϵ_{cc}	26.2(19)
Δ_N	0.119 98(66)		
Δ_{NK}	3.325(30)	Δ_{NK}^S	−5.22(57)
Δ_K	118.3(30)	Δ_K^S	52.0(13)
δ_N	0.005 52(19)		
δ_K	2.40(59)		
ν_0 ($\nu_1 = 1 \leftarrow$ G.S.)		3436.195 13(41) cm^{-1}	

a. Values in parentheses denote one standard error and apply to the last digits of the constans. The unit is MHz, except for ν_0. Sextic centrifugal distortion constants and δ_K^S were fixed to the ground-state values of Ref. 2).

The singlet-triplet transition is often difficult to observe for simple molecules. However, if a molecule contains a heavy element, the large spin-orbit interaction associated with it may make the singlet-triplet transition probability large enough for its observation. The lowest triplet state of HNO has not been located precisely, but it may be possible for HPO to observe the direct transition from the singlet ground state to the lowest triplet state because of the large spin-orbit mixing due to phosphorus. The HPO molecule is also interesting because it may be a good candidate for the P-containing interstellar molecule.

The present study reports the microwave spectrum of HPO generated by the reaction of PH_3 with microwave discharge products of a H_2/O_2 mixture. The a-type R branch transitions of $J = 1 \leftarrow 0$ up to $4 \leftarrow 3$ have been observed. The least-squares analysis yielded the rotational constants and centrifugal distortion constants of high precision, as listed in Table I. Some of the high-K lines were found to be split by the nuclear spin rotation interaction, and the aa component of the coupling constant was determined to be 1.12(37) MHz. This large constant is ascribed to the large A rotational constant, the large P nuclear magnetic moment, and the presence of a low-lying excited electronic state of A″ symmetry (the $\tilde{A}$ state).

Table I. Molecular Constants of HPO in the Ground Vibronic State (MHz)[a]

A	265 307(253)
B	21 074.689(34)
C	19 464.478(34)
Δ_J	0.024 54(49)
Δ_{JK}	0.889 8(168)
Δ_K	[29.1][b]
δ_J	0.002 04(65)
δ_K	[0.0][b]
C_{aa}	1.12(37)
C_{bb}	0.078(238)
C_{cc}	0.021(237)

a. Values in parentheses denote 2.5σ and apply to the last digits of the constants.
b. Fixed.

II-A-14 The Microwave Spectrum of the $N^{35}Cl$ Radical in the $X^3\Sigma^-$ State

Chikashi YAMADA, Yasuki ENDO, and Eizi HIROTA

[*J. Chem. Phys.*, **79**, 4159 (1983)]

The microwave spectrum of the $N^{35}Cl$ radical in the ground vibronic state has been observed by using a source frequency modulation spectrometer with a 3.5-m long free space absorption cell. The NCl radical was generated directly in the cell by a dc discharge in a mixture of N_2 and Cl_2 flowing through the cell. The electric-dipole allowed rotational transitions of N up to $4 \leftarrow 3$, each being resolved into a few spin components, were observed in the frequency region 41.5 to 155 GHz. Each transition was found to consist of many hyperfine components. To analyze the observed spectrum, the matrix elements of magnetic hyperfine and electric quadrupole hyperfine Hamiltonians were derived for a diatomic molecule in the triplet state of which both nuclei have non-zero spins. The rotational, spin-spin interaciton, and spin-rotation interaction constants were determined to be B = 19 383.4655(42) MHz, λ = 56 390.850(16) MHz, and γ = −208.6306(96) MHz, with 3σ in parentheses. The hyperfine parameters were obtained as follows (in MHz): b = 22.774(29), c = −57.764(36), eQq = −63.13(18) for Cl and b = 44.011(33), c = −63.159(51), eQq = 1.842(96) for N. The spin density of the unpaired electrons was estimated to be 76% and 22%, respectively, on N and Cl from the observed c constants.

II-A-15 The Microwave Spectrum of the FeO Free Radical

Yasuki ENDO, Shuji SAITO, and Eizi HIROTA

Because both Fe and O are abundant in the universe, FeO is a molecule of interest in astrophysics and space science. The gas-phase spectra of FeO in the visible have long been known as the orange band, but it is quite recently that the definite assignment was made for them. Cheung et al.[1] have established that the ground electronic state of FeO is $^5\Delta_i$ and have obtained precise ground-state constants from laser induced fluorescence spectra and near-infrared Fourier transform emission spectra.

The present study is aimed at the observation of the microwave spectrum of FeO to facilitate its radioastronomical observation in interstellar space. The radical was generated directly in a 1-m long absorption cell by a dc discharge in a mixture of ferrocene and O_2 with the partial pressures of 5 and 10 − 15 mTorr, respectively. The $J = 5 \leftarrow 4$ and $6 \leftarrow 5$ transitions were observed for $\Omega = 4$, 3, and 2. Figure 1 shows the $J = 6 \leftarrow 5$, $\Omega = 4$ transition. From the observed spectrum the rotational constant and the centrifugal distortion constant for the spin-spin interaction were determined to be $B_0 = 15\,493.736(30)$ MHz and $\lambda_D = -0.1611(67)$ MHz, respectively, with 2.5σ in parentheses, whereas the other constants were either fixed to, or obtained to agree within experimental uncertainties with, those of Ref. 1.

Reference

1) A. S-C. Cheung, R. M. Gordon, and A. J. Merer, J. Mol. Spectrosc., **87**, 289 (1981); A. S-C. Cheung, N. Lee, A. M. Lyyra, A. J. Merer, and A. W. Taylor, J. Mol. Spectrosc., **95**, 213 (1982).

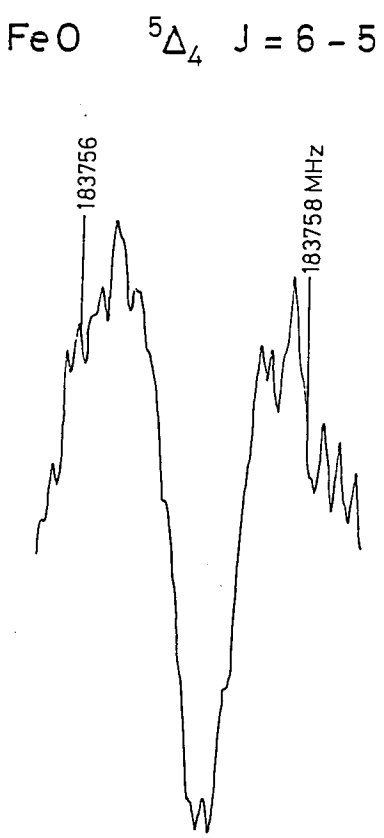

Figure 1. The $J = 6 \leftarrow 5$ $\Omega = 4$ transition of FeO. The spectrum was obtained by integrating 200 scans with the repetition rate of 5 Hz and the PSD time constant of 1 msec

II-A-16 The ν_2 Band of the FO_2 Radical Investigated by Infrared Diode Laser Spectroscopy

Chikashi YAMADA and Eizi HIROTA

In contrast with HO_2, very little has been known about its halogen derivatives. For FO_2 the vibrational spectra have been observed only in low temperature matrices, whereas no gas phase spectra have been reported. The present study has successfully employed infrared tunable diode lasers in observing the ν_1 (O-O stretching) and ν_2 (F-O stretching) bands of the FO_2 radical. The radical was generated in an absorption cell by the reaction of O_2 (10 ~ 18 Torr) with microwave discharge products of a F_2(5%)/He mixture (1 ~ 2 Torr).

The ν_2 band has so far been analyzed. Only a-type lines have been identified, and the observed spectrum, when least-squares analyzed, yielded the molecular constants listed in Table I. The spin-rotation splitting was analyzed using a symmetric-top expression. Only two of the three rotational constants supply independent information on the structure, and several sets of structural parameters are calculated from the observed A and B constants, as listed in Table II, and are compared with those of F_2O and F_2O_2. Table III compares the ϵ_{aa} constants of three F-containing molecules scaled by A. It is interesting that they are not much different from one another.

Table I. Molecular Constants of FO_2 Radical[a]

	$\nu_2 = 1$	$\nu_2 = 0$
A	78 245(420)	78 515(420)
B	9 953.9(12)	10 013.3(12)
C	8 781.7(15)	8 854.8(13)
Δ_N	[0][b]	0.0159(48)
Δ_{NK}	[0][b]	−0.116(13)
Δ_K	[0][b]	−0.080 0(45)
ν_0	579.318 39(29)	0.0
ϵ_{aa}	−821(49)	−822(48)
$\epsilon_{bb} + \epsilon_{cc}$	16(29)	5.4(29)

a. In MHz, except for ν_0 which is given in cm^{-1}. Values in parentheses denote 2.5σ and apply to the last digits of the constants.
b. Fixed.

Table II. Molecular Structure of the FO_2 Radical

FO_2	I	II	III	F_2O_2	F_2O
F-O (Å)	1.875	1.704	1.492	1.575	1.4053
O-O (Å)	1.012	1.160	1.370	1.217	—
FOO (Å)	100	109	114	109.5	103.067

Table III. Spin-Rotation Interaction Constants of F-containing Molecules

	ϵ_{aa} (MHz)	A (MHz)	$\lvert\epsilon_{aa}/A\rvert$
FSO	−339.543	38 698.	0.008 77
FCO	1822.	191 200.	0.009 53
FO_2	−845.	78 538.	0.010 76

II-A-17 Infrared Diode Laser Spectroscopy of the BrO Radical

James E. BUTLER *(NRL and IMS)*, **Kentarou KAWAGUCHI, and Eizi HIROTA**

A recent microwave study on the BrO radical[1] gave an estimate for the fundamental vibrational frequency in the ground electronic state to be about 725 cm^{-1}, in contradiction with 772 cm^{-1} obtained from electronic spectroscopy. Barnett et al.[2] have reinvestigated the $A^2\Pi_i - X^2\Pi_i$ absorption spectrum of $^{81}Br^{16}O$ and have arrived at $\Delta G_{1/2}''$ of 722.1 ± 1.1 cm^{-1}, supporting the microwave result. The present study was initiated to directly observe the $v = 1 \leftarrow 0$ vibration-rotation band of BrO by infrared tunable diode laser spectroscopy and to remove all ambiguities concerning the vibrational frequency.

The BrO radical was generated directly in a multiple-reflection absorption cell by a glow discharge in a Br_2/O_2 mixture. So far 5P, 7Q, and 11R and 2P, 7Q, and 11R branch transitions were observed, respectively, for $^{81}Br^{16}O$ and $^{79}Br^{16}O$, both in the $X^2\Pi_{3/2}$ state. These observed spectral lines were least-squares fit to an effective Hamiltonian to obtain the band origins and refined $v = 1$ rotaional parameters of the $^2\Pi_{3/2}$ state. The results are ν_0 = 721.9282(6) cm^{-1} and 723.4151(5) cm^{-1}, respectively, for $^{81}Br^{16}O$ and $^{79}Br^{16}O$, which are in good agreement with the values of Refs. 1 and 2.

References

1) E. A. Cohen, H. M. Pickett, and M. Geller, *J. Mol. Spectrosc.*, **87**, 459 (1981).
2) M. Barnett, E. A. Cohen, and D. A. Ramsay, *Can. J. Phys.*, **59**, 1908 (1981).

II-A-18 Infrared Diode Laser Spectroscopy of the PO Radical

James E. BUTLER *(NRL and IMS)*, **Kentarou KAWAGUCHI, and Eizi HIROTA**

[*J. Mol. Spectrosc.*, **101**, 161 (1983)]

The pure rotational spectrum of the PO radical in the ground vibronic state has recently been observed and analyzed to yield accurate molecular constants (II-A-9). The present study was carried out to obtain the accurate equilibrium values of the molecular constants through the observation of high-resolution vibration-rotation spectra by infrared tunable diode laser spectroscopy. No gas-phase infrared spectra have been previously reported.

The PO radicals were produced by the reaction of the microwave discharge products of a $H_2/He/O_2$ mixture with solid red phosphorus, as described in II-A-9. Only R-branch lines of the $v = 1 \leftarrow 0$ band were observed for both $^2\Pi_{3/2}$ and $^2\Pi_{1/2}$ in the region between 1226 and 1254 cm^{-1}. Seven and ten transitions observed for $^2\Pi_{3/2}$ and $^2\Pi_{1/2}$, respectively, were least-squares analyzed to obtain $v = 1$ constants, where the ground-state constants were fixed to those of II-A-9. The band origin and the equilibrium constants thus obtained are listed in Table I.

Table I. Molecular Constants of PO in $X^2\Pi_r$[a]

B_e	0.733 2273(18) cm^{-1}	ν_0	1220.249 01(43) cm^{-1}
α_e	0.005 4777(36) cm^{-1}	A'-A''	0.163 54(78) cm^{-1}
r_e	1.476 370(15) Å		

a. Values in parentheses denote 3σ and apply to the last digits of the constants.

II-A-19 Infrared Diode Laser Spectroscopy of the FO Radical

A. R. W. McKELLAR *(NRC and IMS)*, **Chikashi YAMADA, and Eizi HIROTA**

[*J. Mol. Spectrosc.*, **97**, 425 (1983)]

The FO radical has recently been detected for the first time in the gas phase by infrared LMR spectroscopy,[1] and the small dipole moment of it,

as determined from the Stark effect of the LMR spectra, has explained why many attempts to detect FO by microwave and EPR have failed. The present study was motivated by the fact that only the $^2\Pi_{3/2}$ state had been observed by LMR, and an attempt was made to observe vibration-rotation spectra of FO in the $^2\Pi_{1/2}$ state. Although it was not possible to detect any $^2\Pi_{1/2}$ lines, 14 transitions of $^2\Pi_{3/2}$ were observed and used to improve the molecular constants as follows: ν_0 = 1033.4829(5) cm^{-1}, B_0 = 1.05285(9) cm^{-1}, B_1 = 1.03933(8) cm^{-1}, $D_0 = 4.4(4) \times 10^{-6}$ cm^{-1}, and $D_1 = 4.4(3) \times 10^{-6}$ cm^{-1} with 3σ in parentheses.

Reference

1) A. R. W. McKellar, *Can. J. Phys.*, **57**, 2106 (1979).

II-A-20 Detection of the ν_2 Bands of CD_2 and CH_2 by Infrared Diode Laser Spectroscopy

A. R. W. McKELLAR *(NRC and IMS)*, **Chikashi YAMADA, and Eizi HIROTA**

[*J. Chem. Phys.*, **79**, 1220 (1983)]

The laser magnetic resonance (LMR) spectroscopic study of methylene, the simplest carbene, has recently been much advanced[1]; the pure rotational and the ν_2 vibrational and rotational spectra have been observed and analyzed to characterize this important free radical in the triplet ground $\tilde{X}^3B_1$ state. In order to get more information, isotopic species of methylene are being investigated as well. The present study is devoted to the ν_2 band of CD_2. Because this band is located outside the wavelength range where LMR can be applied, the infrared tunable diode laser is used as a source. The methylene molecules were generated by the reaction of fluorine atoms with ketene. The CD_2 transitions observed are of the form $N_{0,N} \leftarrow N_{1,N-1}$ with N = 3 to 7, and two transitions of CH_2 were also observed around 892 cm^{-1}. Analysis of CD_2 spectrum yields the ν_2 band origin ν_0 = 752.3748(16) cm^{-1} as well as the rotational constant $(B + C)/2$ = 3.93057(18) cm^{-1} and the spin-spin interaction parameter D = 0.78844(62) cm^{-1} in the ν_2 = 1 state.

References

1) T. J. Sears, P. R. Bunker, and A. R. W. McKellar, *J. Chem. Phys.*, **75**, 4731 (1981); **77**, 5363 (1982); T. J. Sears, P. R. Bunker, A. R. W. Mckellar, K. M. Evenson, D. A. Jennings, and J. M. Brown, *J. Chem. Phys.*, **77**, 5348 (1982); A. R. W. McKellar and T. J. Sears, *Can. J. Phys.*, **61**, 480 (1983); P. R. Bunker, T. J. Sears, A. R. W. McKellar, K. M. Evenson, and F. J. Lovas, *J. Chem. Phys.*, in press.

II-A-21 Zeeman and Stark Effects of the HCF $\tilde{A}^1A''(000)$ — $\tilde{X}^1A'(000)$ Band

R. J. BUTCHER *(Univ. of Cambridge and IMS)*, **Shuji SAITO, and Eizi HIROTA**

The excited electronic state like the $\tilde{A}^1A''$ state of HCF may be perturbed by highly excited vibrational states associated with the ground electronic state (referred to as the electronic Coriolis interaction) and/or by vibrational states in the manifold of the lowest triplet state, $\tilde{a}^3A''$ (referred to as the singlet-triplet, or S-T interaction).[1] In order to clarify the nature of the perturbations observed for the HCF $\tilde{A}^1A''(000)$ state,[2] the Zeeman effect has been measured for a number of rotational transitions in the $\tilde{A}^1A''(000) - \tilde{X}^1A'(000)$ band, with both Doppler-limited and sub-Doppler resolution.

Most of the transitions with K' = 1, 2, 3, and J' = 1 ~ 7 show linear Zeeman effects that fit well with an expression $g_{eff}\beta\,[K^2/(J+1)]B$ *with* g_{eff} = 0.015. These Zeeman effects can be explained by the electronic Coriolis interaction with $g_{eff} = g_l \langle X | L_a | A \rangle$. On the other hand, a few perturbed lines such as $^rQ_0(J)$ with J = 6, 10, and 13 show much larger Zeeman effects, which are ascribed to the S-T mixing.

A preliminary value 0.63 D was obtained for the a component of the upper-state dipole moment through the sub-Doppler observation of the Stark effect of the $^rR_1(1)$ transition. Unfortunately, deposit of reaction products on the surface of the Stark electrodes has precluded more detailed observation of the Stark effects.

References

1) E. Hirota, *Faraday Discuss.*, **71**, 87 (1981).
2) M. Kakimoto, S. Saito, and E. Hirota, *J. Mol. Spectrosc.*, **88**, 300 (1981).

II-A-22 Far-Infrared Laser Magnetic Resonance Spectroscopy of the AsH Radical in the $X^3\Sigma^-$ State

Kentarou KAWAGUCHI and Eizi HIROTA

As an extension of the measurements on PH and PD (II-A-8), the AsH radical was investigated by far-infrared LMR spectroscopy. The radical was generated by the reaction of metallic arsenic with microwave discharge products of a H_2/O_2 mixture with the partial pressures of 160 mTorr and 10 mTorr, respectively, for H_2 and O_2. Using five laser lines, the $N, J = 1,2 \leftarrow 0,1$, $2,3 \leftarrow 1,2$ $3,4 \leftarrow 2,3$, $3,3 \leftarrow 2,2$, and $4,5 \leftarrow 3,4$ transitions were observed, each being split into hyperfine components due to both the As ($I = 3/2$) and H ($I = 1/2$) nuclei. The least-squares analysis of the observed spectrum led to molecular constants listed in Table I. The hyperfine coupling constants which were also obtained are compared with those of NH and PH in Table II. The α constant, which is equal to $b + c/3$, gives an estimate for the s character on M to be 1.1%, 0.96%, and −0.08% for M = N, P, and As. On the other hand, the β constant equal to $c/3$ is converted to the spin density on M: 82%, 86%, and 95% for the three elements. The unpaired electrons in AsH seem to occupy the orbitals that are very close to the $4p_\pi$ orbital.

Table I. Molecular Constants of the AsH Radical in the $X^3\Sigma^-$ State[a]

B	215 877.07(24)	$g_S + g_l$	2.015 91(11)
λ	1 763 474(60)	$\Delta g'$	[−0.019 51][b]
γ	−8 111.8(63)	g_r	0.000 663(81)
D	9.829(11)		

a. In MHz, exept for the g factors. Values in parentheses denote 3σ and apply to the last digits of the constants.
b. Fixed to $\gamma/2B$.

Table II. Hyperfine Coupling Constants of the NH, PH, and AsH in $X^3\Sigma^-$[a]

M	N[b]	P[c]	As
α_M	20.0(18)	127.5(23)	−11.6(15)
β_M	−22.8(30)	−157.5(29)	−159.3(13)
α_H	−70.6(30)	−48.1(16)	−49.68(66)
β_H	29.6(48)	5.4(19)	4.27(60)
$eQq(M)$	—	—	−99.5(75)

a. See footnote a of Table I.
b. F. D. Wayne and H. E. Radford, *Mol. Phys.*, **32**, 1407 (1976).
c. II-A-8.

II-A-23 The Infrared Diode Laser Spectrum of the SCl Radical

Chikashi YAMADA, James E. BUTLER *(NRL and IMS)*, Kentarou KAWAGUCHI, Hideto KANAMORI, and Eizi HIROTA

Very little has been known of the SCl radical. Willner[1] has observed an infrared absorption band at 574.2 cm^{-1} by photolyzing SCl_2 trapped in a Ne matrix, which was assigned to the $\nu = 1 \leftarrow 0$ transition of $^{32}S^{35}Cl$, based on the observation of similar bands at 566.9 and 565.5 cm^{-1}, assigned, respectively, to $^{32}S^{37}Cl$ and $^{34}S^{35}Cl$.

In the present study the fundamental band of SCl in the $X^2\Pi_{3/2}$ state was observed by diode laser spectroscopy. The SCl radical was generated in a cell by a discharge in either S_2Cl_2 or SCl_2 diluted with He. Zeeman modulation was successfully applied to low-J lines. Although high-J lines have too small Zeeman coefficients to be modulated, they were observed even in Zeeman-modulation arrangement. This observation was ascribed to the fact that electrical discharge in the cell was affected by the magnetic field, causing the generation of the radical to be modulated.

Six Q and twenty-two P and R lines have been assigned to $^{32}S^{35}Cl$ in $^2\Pi_{3/2}$. The least-squares analysis of these lines gave $\nu_0 = 574.61270(81)$, $B'' = 0.257\,907(45)$, $B' = 0.256\,345(42)$, $D'' = 0.229(48) \times 10^{-6}$, and $D' = 0.226(42) \times 10^{-6}$, all in cm^{-1} with 3σ in parentheses, where B and D are the effective constants for the $^2\Pi_{3/2}$ state.

Reference

1) H. Willner, *Spectrochim. Acta* **37A**, 405 (1981).

II-A-24 Microwave Spectroscopy of the PF Radical

Shuji SAITO, Yasuki ENDO, and Eizi HIROTA

The PF radical has previously been investigated by optical spectroscopy.[1,2] There have been reported neither infrared nor microwave spec-

troscopic investigations. The present study was aimed at obtaining precise mlecular constants, in particular hyperfine coupling constants, through the observation of rotational spectra by microwave spectroscopy.

The PF radical was generated directly in a 3.5-m long free space cell by a dc discharge in a PH_3/CF_4 mixture. The rotational transitions with $N = 1 \leftarrow 0$ up to $5 \leftarrow 4$ have been observed and assigned. Each transition is split into fine and hyperfine components, and the observed lines, 50 in total, were subjected to a least-squares analysis to yield the molecular constants including the rotational, spin-spin, spin-rotation, and hyperfine coupling constants. The hyperfine constants, two each for the P and F nuclei, give estimates for the s character and spin density to be 0.67 and 65.5 for P and 0.22 and 28.5 for F, respectively.

References

1) A. E. Douglas and M. Frackowiak, *Can. J. Phys.*, **40**, 832 (1962).
2) R. Colin, J. Devillers, and F. Prevot, *J. Mol. Spectrosc.*, **44**, 230 (1972).

II-A-25 Microwave Spectroscopy of the GeF Radical

Mitsutoshi TANIMOTO *(Sagami Chem. Res. Center)*, **Shuji SAITO, Yasuki ENDO, and Eizi HIROTA**

As an extension of our previous studies[1] on SiF and SiCl, the GeF radical was investigated by microwave spectroscopy. Martin and Merer[2] have observed and analyzed the bands of GeF to obtain molecular constants including the rotational constant and the Λ-doubling constant in the $X^2\Pi$ state.

The GeF radical was generated directly in a free space absorption cell by a dc glow discharge in GeF_4. Because the spin-orbit coupling constant A is as large as 935 cm^{-1}, the spectrum of the $^2\Pi_{3/2}$ state was too weak to be observed and that of the $^2\Pi_{1/2}$ state did not show Zeeman effects which were useful in discriminating GeF spectral lines from among those of other species. However, the short lifetime of the radical allowed us to distinguish GeF lines from others. Six rotational transitions $J = 7/2 \leftarrow 5/2$ up to $17/2 \leftarrow 15/2$ have been observed for three isotopic species, ^{70}GeF, ^{72}GeF, and ^{74}GeF, and have provided effective molecular constants for $^2\Pi_{1/2}$; A_J, γ, q, p^*, and q^* were fixed to zero. The present result agrees well with that of Ref. 2.

References

1) M. Tanimoto, S. Saito, Y. Endo, and E. Hirota, *IMS Ann. Rev.*, 30 (1982).
2) R. W. Martin and A. J. Merer, *Can. J. Phys.*, **51**, 125 (1973); **52**, 1458 (1974).

II-A-26 Infrared Diode Laser Spectroscopy of the Coriolis-Coupled ν_2/ν_3 Bands of DO_2

Hiromichi UEHARA *(Sagami Chem. Res. Center)*,[1] **Kentarou KAWAGUCHI, and Eizi HIROTA**

McKellar[2] has investigated the ν_2 band of DO_2 by mid-infrared laser magnetic resonance (LMR) spectroscopy. He has noticed the ν_2 state to be perturbed by the Coriolis interaction with ν_3, although no resonances have been identified for ν_3. The present study aimed at obtaining a more detailed information on the ν_3 state as well as the Coriolis interaction between the two states through the observation of the vibration-rotation spectra in both ν_2 and ν_3 using infrared diode lasers as sources.

The DO_2 radical was generated by the reaction of deuterated allyl alcohol with microwave discharge products of oxygen. We have assigned 46 and 19 transitions for the ν_2 and ν_3 bands, respectively. These data were augmented with McKellar's LMR data extrapolated to zero-field frequencies, 39 transitions in total, to yield molecular parameters listed in Table I, where McKellar's results are included for comparison.

References

1) Present address: Department of Chemistry, Faculty of Science, Jyosai University, Keyaki-dai 1-1, Sakado, Saitama 350-02.
2) A. R. W. McKellar, *J. Chem. Phys.*, **71**, 81 (1979); *Faraday Discuss.*, **71**, 63 (1981).

Table I. Molecular Constants of DO_2 in the ν_2 and ν_3 States[a]

Constant	Present ν_2	Present ν_3	Ref. 2 ν_2	Ref. 2 ν_3
ν_0	1020.160 8(16)	1121.471 7(13)	1020.161 5(2)	1121.35(3)
ζ_{23}^C	0.6837(9)		0.68029(96)	
Z_1	0.0025(20)			
A	11.431 52(9)	11.176 6(4)	11.431 885(42)	
B	1.056 89(7)	1.046 08(27)	1.056 796(68)	$\bar{B}$ = 0.995 1(18)
C	0.955 912(62)	0.948 46(27)	0.955 891(67)	
$10^3\Delta_K$	1.619 4(32)	0.925(63)	1.639 4(21)	
$10^5\Delta_{NK}$	8.37(10)	11.5(10)	8.83(23)	
$10^6\Delta_N$	4.20(22)	0.4(11)	4.43(73)	
$10^5\delta_K$	[5.17][b]	67.7(135)	[5.17][b]	
$10^6\delta_N$	3.10(59)	4.1(9)	5.2(15)	
ϵ_{aa}	−0.948 23(49)	−0.948 2(24)	−0.946 74(21)	−0.897 0(59)
$10^2\epsilon_{bb}$	−1.441(31)	−1.260(36)	−1.399(30)	
$10^4\epsilon_{cc}$	4.7(23)	[2.03][b]	3.2(29)	
$10^4\Delta_K^S$	3.90(27)	14.3(46)	2.71(16)	

a. Values in parentheses denote 1σ and apply to the last digits of the constants.
b. Fixed.

II-A-27 Electric Dipole Moments of the H_2CS Molecule in the $\tilde{A}^1A_2$ $v = 0$ and $\tilde{a}^3A_2$ $\nu_3 = 1$ States

Tetsuo SUZUKI, Shuji SAITO, and Eizi HIROTA

In order to obtain information on the $\tilde{a}$ state complementary to that described in II-A-3, the electric dipole moment of H_2CS was measured using the MODR method. The Stark effect was also measured on the $\tilde{A}$ state for comparison.

The H_2CS molecule was generated by pyrolyzing $(CH_2)_3S$. A ring dye laser (SP 380 A) was employed with rhodamine 6G or DCM dyes to pump electronic transitions; the output power ranged from 200 to 300 mW. The MODR cell used was made of an X-band waveguide with a Stark electrode inside, to which the rf voltage was fed superimposed with a dc field; an output power up to 10W was obtained from a VHF oscillator combined with a solid-state amplifier. The Stark effect was measured for K-doubling transitions with $K = 2$, and was analyzed by taking into account only the Stark effect between the K-type doublets. An example of the observed Stark effect is shown in Figure 1. The measured dipole moments are listed below:

$\tilde{A}^1A_2$ $v = 0$

$3_{21} - 3_{22}$	0.826(6) D	
$4_{22} - 4_{23}$	0.848(7) D	
$5_{23} - 5_{24}$	0.851(5) D	

$\tilde{a}^3A_2$ $\nu_3 = 1$

$J = 4 - 4$	$5_{23} - 5_{24}$	0.547(22) D
$J = 5 - 5$	$6_{24} - 6_{25}$	0.548(9) D

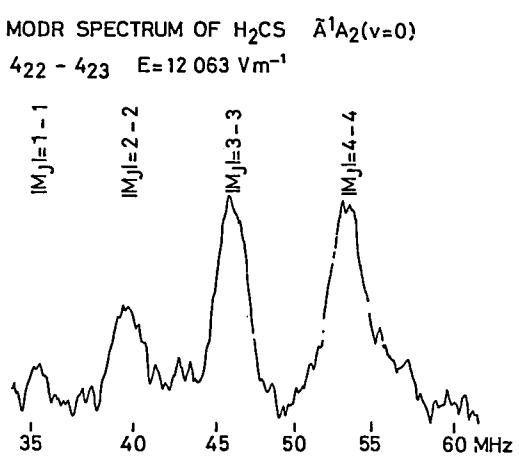

Figure 1. Stark effect of the $4_{22} - 4_{23}$ transition of H_2CS in the $\tilde{A}^1A_2$ $v = 0$ state, observed by MODR.

The values in parentheses denote 1σ deviations and apply to the last digits of the dipole moments.

II-A-28 Third-Order Anharmonic Potential Constants and Equilibrium Structure of HCO

Eizi HIROTA

Because of its importance in various fields, the formyl radical has been the subject of a number of spectroscopic studies. The present study deals with the determination of the equilibrium structure (r_e) and of the harmonic (F_{ij}) as well as anharmonic (F_{ijk}) potential constants of the radical. The method employed is a slight extension of the one previously described:[1] a computer program was written which computes r_e, F_{ij}, and F_{ijk} from all the observed spectroscopic data available by the least-squares method. As in our previous studies[1,2] all ten F_{ijk}'s cannot be determined because of the correlation among parameters. However, the "diagonal" terms F_{iii} were determined, independent of the model chosen: $F_{111} = -28.8 \pm 6.0$ md/Å^2, $F_{222} = -93 \pm 30$ md/Å^2, and $F_{333} = -0.631 \pm 0.055$ mdÅ, where the coordinates 1, 2, and 3 correspond to δr(H-C), δr(C=O),and $\delta\theta$(HCO). Tables I and II list the structure parameters and the harmonic force field, respectively, with those of previous studies.

Table I. Molecular Structure of the Formyl Radical

Parameter	Present r_e	Brown and Ramsay[a] r_0	Ogilvie[b] r_0
r(H-C) (Å)	1.118 2(50)	1.125(5)	1.151 4 (H-C) 1.147 4 (D-C)
r(C=O) (Å)	1.175 6(20)	1.175(1)	1.177 08
θ(HCO) (O)	124.26(30)	124.95(25)	123.01

a. J. M. Brown and D. A. Ramsay, *Can. J. Phys.*, **53**, 2232 (1975).
b. J. F. Ogilvie, *J. Mol. Struct.*, **31**, 407 (1976).

Table II. Harmonic Force Field of the Formyl Radical

Force constant	Present	Milligan and Jacox[a]	Dixon[b]
F_{11} (md/Å)	3.485(25)	3.42	3.47(7)
F_{12} (md/Å)	0.730(40)	0.79	0.54(12)
F_{13} (md)	0.012(75)	0.36	[0.0][c]
F_{22} (md/Å)	14.474(80)	14.24	14.19(28)
F_{23} (md)	0.346(95)	0.20	[0.0][c]
F_{33} (mdÅ)	0.6856(50)	0.77	0.76(2)

a. D. E. Milligan and M. E. Jacox, *J. Chem. Phys.*, **51**, 227 (1969).
b. R. N. Dixon, *J. Mol. Spectrosc.*, **30**, 248 (1969).
c. Fixed.

References

1) E. Hirota and Y. Endo, *IMS Ann. Rev.*, 41 (1981).
2) E. Hirota, *IMS Ann. Rev.*, 29 (1982).

II-A-29 Microwave Spectroscopy of Boron Chloride (BCl). The Chlorine Nuclear Quadrupole Coupling Constant

Yasuki ENDO, Shuji SAITO, and Eizi HIROTA
[*Bull. Chem. Soc. Jpn.*, **56**, 3410 (1983)]

The rotational transitions of $J = 2 \leftarrow 1$, $3 \leftarrow 2$, and $4 \leftarrow 3$ have been observed for $^{11}B^{35}Cl$ in the millimeter wave region. The BCl molecule was directly generated in a 3.7-m long free space absorption cell by a dc glow discharge in BCl_3. Each rotational transition was found to be split by

Table I. Molecular Constants of BCl (MHz)[a]

Constant	Present $^{11}B^{35}Cl$	Present $^{11}B^{37}Cl$	Ref. 1[b] $^{11}B^{35}Cl$	Ref. 1[b] $^{11}B^{37}Cl$
B_0	20 413.9422(91)	20 150.562(18)	20 412.40(93)	20 148.99
D_0	0.054 10(35)	0.052 87(79)	0.055 1(16)	0.053 68
eQq(Cl)	−16.737(11)	−13.191[c]		
eQq(B)	−3.70[d]	−3.70[d]		

a. Values in parentheses denote 2.5σ and apply to the last digits of the constants.
b. Calculated from the Dunham coefficients reported.
c. Calculated from eQq (^{35}Cl).
d. Determined by simulation.

the nuclear quadrupole interactions of Cl, and in some cases, of B. The least-squares analysis of the observed spectrum yielded molecular constasnts in the ground vibronic state, as listed in Table I. The present B_0 values are larger than the recent results of Maki et al.[1] using infrared diode laser spectroscopy by four times their standard errors. The observed value of the chlorine nuclear quadrupole coupling constant is in conformity with that predicted from the data on other diatomic molecules each consisting of a second-row element and a chlorine atom (see II-A-14). A better fit is obtained by allowing back donation of 0.12 π-electrons from Cl to B, in other words, by making the 2π orbital (HOMO) to receive 3% contributions from the B $2p_\pi$ orbital.

Reference

1) A. G. Maki, F. J. Lovas, and R. D. Suenram, *J. Mol. Spectrosc.*, **91**, 424 (1982).

II—B Development of New Instruments and New Experimental Methods for High Resolution Spectroscopy

The scope of research is limited by the techniques and the capabilities of the instruments available to the researcher. This is particularly true for the primary research interest of this Department, namely, the spectroscopic investigations of simple molecules, radicals, and ions. The high precision with which we determine molecular parameters often unravels new aspects of molecular properties which have previously escaped experimental observation. The deversity of molecular systems which we can detect and analyze is often limited by the sensitivity of the particular spectrometer. Thus it is imperative for us to improve continuously the levels of performance of our research facilities and to develop equipments of radically new conceptual designs. The rewards of these efforts will include not only the detailed knowledge of the molecules under investigation, but also some contributions to related fields. However, various types of technical problems will need to be solved to attain these goals. In this sense the collaboration of the Equipment Development Center on joint research programs will be indispensable. The new instruments developed in this program promise to open new research areas in the field of molecular science.

II-B-1 Extension of the Wavelength Region for a cw Dye Laser Spectrometer

Tetsuo SUZUKI, Shuji SAITO, and Eizi HIROTA

One of the most serious limitations of the cw dye laser is that it normally oscillates only in the narrow wavelength region of 540 to 625 nm using rhodamine dyes. Recent developments in the synthetic techniques have produced a few dyes that allow the cw dye laser to oscillate outside the region mentioned above, e.g. DCM can be used down to 14 700 cm^{-1} (680 nm) and Coumarin 535 up to 19 600 cm^{-1} (510 nm). If a UV pumping source such as a Kr^+ laser line is available, then Coumarin 460 may be used in the 450 ~ 480 nm region.

An attempt has been made to extend the wavelength region more drastically, namely by means of harmonic and sum-frequency generation. An ADA crystal of 10 × 10 × 30 mm 45°Z cut was used to double the output of the dye laser, and the absorption spectrum of H_2CO was observed around 33 900 cm^{-1}. Also sum-frequency light generation was tried by mixing the outputs of an Ar^+ laser and a cw dye laser in a KDP crystal 45°Z 72°Y′ cut to 15 × 15 × 30 mm dimensions.

II-B-2 Data Processing System for Dye Laser Excitation Spectroscopy

Tetsuo SUZUKI, Shuji SAITO, and Eizi HIROTA

The cw dye laser excitation spectrum ususally consists of quite a large number of rotational lines, and it takes long time to determine the wavenumber of each line manually. The present study aimed at developing a microcomputer system which records the observed excitation spectra of both the sample and the iodine gas used as a wavenumber standard

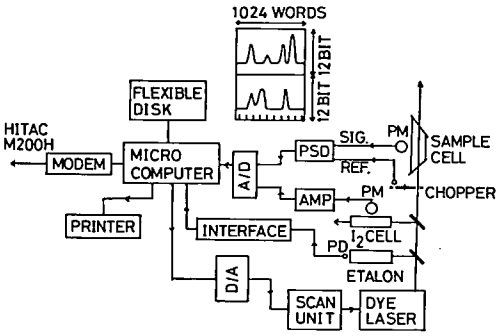

Figure 1. Blockdiagram of a data sampling system for a cw dye laser spectrometer.

and reference markers derived from an etalon. These data are then sent to the IMS Computer Center for further processing, e.g. locating the absorption peak, the determination of its wavenumber, the drawing of the observed spectrum, and so on.

Figure 1 shows the blockdiagram of the system. The microcomputer used is a SORD M243, which generates ramp signals to scan the dye laser and receives the excitation spectra after it is A/D converted. One scan covers 30 GHz, which is allocated to 1024 points with 30 MHz intervals, and the signals are stored with 12 bits resolution. Because the marker is 15 MHz wide, it is shaped to an appropriate waveform. The data are temporarily stored on floppy disks, and are then transferred to the IMS Computer Center after completion of the experiment.

II-B-3 Data Processing System for an Infrared Diode Laser Spectrometer

Hideto KANAMORI, Kentarou KAWAGUCHI, Chikashi YAMADA, and Eizi HIROTA

The data acquisition procedure most widely employed for infrared diode laser spectroscopy consists of recording sample spectra simultaneously with those of an appropriate reference molecule used as a standard and also with fringes generated by an etalon of good stability; fringes are used as markers for interpolation. It is a tedious step to determine the wavenumber of each absorption line. In the present study a minicomputer system was developed which allows us to read out line wavenumbers more precisely and more rapidly than

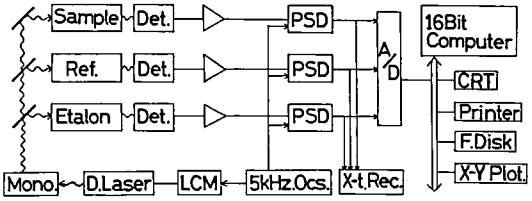

Figure 1. Blockdiagram of a data processing system for an infrared diode laser spectrometer.

by hand.

Figure 1 shows a block diagram of the system in the case of source-frequency modulation. Three kinds of signals, the sample and reference spectra and fringes, are A/D converted to 12 bit data and are sent to a minicomputer SORD M343. The memory of the computer is divided into three groups of 6000 words each to which the three signals are allocated. A CRO scope displays the spectra in real time for monitoring. The computer averages and smoothes the signals to improve the S/N ratio and determines the peaks of reference lines, fringes, and sample spectral lines while monitoring on the CRO scope, and then displays the sample spectrum thus processed on an X-Y plotter, where the abscissa is already converted to the unit of cm^{-1}. The software is written mainly in BASIC, but assembly language is used in some part to decrease execution time.

II-B-4 Infrared Diode Laser Spectroscopic System for Transient Molecules Generated by an Excimer Laser

James E. BUTLER *(NRL and IMS)*, Kentarou KAWAGUCHI, Hideto KANAMORI, Chikashi YAMADA, and Eizi HIROTA

In II-A transient molecules have been generated by electrical discharge or discharge induced chemical reactions; the method has proved extremely efficient in producing simple short-lived molecules. However, it would be difficult or even impossible by this method to generate transient molecules with more complicated structure, because the discharge will dissociate precursors as well as transients into even smaller fragments. Photolysis is more attractive than discharge in this respect, and recent development of high-power pulse lasers makes

photolysis more promising.

An excimer laser was introduced in the infrared diode laser spectroscopic system which has been employed in various experiments described in II-A. The excimer laser delivers about 100 mJ per pulse (8-16 ns duration) at 193 nm (ArF) or 249 nm (KrF), which corresponds to about 10^{17} photons. The repetition rate is about 100 Hz. A two-channel boxcar integrator was employed to observe the absorption signal; one channel (B) collected the signal (or noise) before the excimer laser was fired and the other (A) recorded the signal right after the excimer laser pulse irradiated the cell, and the A − B output was displayed. We have so far observed spectra of CH_3 (CH_3I, $(CH_3)_2CO$), CS (CS_2), and SO (SO_2) with precursors in parentheses.

II—C High Resolution Spectroscopy of Molecules of Fundamental Importance

The needs for high quality spectroscopic data has recently been increasing, especially for fundamental molecules. Perhaps such spectroscopic data have been accumulated in the past because of interest in precise molecular structure determination. However, research activities in other related fields such as reaction kinetics, environmental sciences, plasma chemistry and physics, and astronomy have recently been advanced such that precise specroscopic data are indispensable as a means of monitoring molecules. Spectroscopic data which are available are not necessarily good enough and must often be replaced by new data that meet the necessary requirements. Such spectroscopic data on chemically stable molecules of fundamental importance will be presented in this section.

II-C-1 Micorwave Spectrum and Internal Rotation of 2-Butyne-1,1,1-d_3 *(Dimethylacetylene)*, $CH_3C \equiv CCD_3$

Jun NAKAGAWA *(Hiroshima Univ.)*, **Michiro HAYASHI** *(Hiroshima Univ.)*, **Yasuki ENDO, Shuji SAITO, and Eizi HIROTA**

Dimethylacetylene has attracted much attention, because it is a typical example of molecules executing free (or nearly free) internal rotation. In principle, the perpendicular vibration-rotation band reflects the effects of internal rotation, but, in practice, is too complicated to be analyzed. Actually only an upper limit of the barrier height

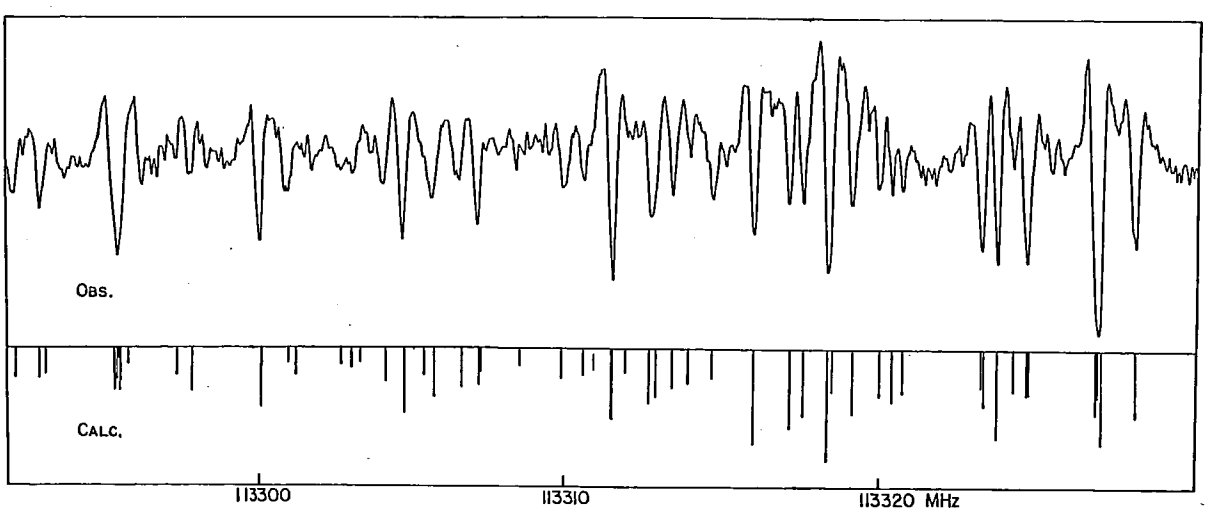

Figure 1. The observed $J = 19 \leftarrow 18$ transition of $CH_3C \equiv CCD_3$. The calculated transitions are indicated by sticks below the observed spectrum.

was determined by high resolution infrared spectroscopy.

In the present study, we have observed the microwave spectra of the $CH_3C \equiv CCD_3$ molecule, using a source-frequency modulation spectrometer. Eight rotational transitions have been recorded, of which four, $J = 15 \leftarrow 14$, $19 \leftarrow 18$, $23 \leftarrow 22$, and $26 \leftarrow 25$, have been measured precisely. Figure 1 shows the $19 \leftarrow 18$ transition.

The observed transition frequencies have been assigned and least-squares analyzed with the aid of the Kirchhoff-Lide formulation[1] to yield B = 2982.498(1) MHz, a few centrifugal distortion constants, and s (reduced barrier height) = 0.326(10). From this s value and the assumed moment of inertia, the barrier height was determined to be 5.84(18) cm^{-1}.

Reference

1) W. H. Kirchhoff and D. R. Lide, Jr., *J. Chem. Phys.*, **43**, 2203 (1965).

II-C-2 Microwave Spectroscopy of Deuterated Silanes

Keiichi OHNO *(Hiroshima Univ.)*, **Hiroatsu MATSUURA** *(Hiroshima Univ.)*, **Yasuki ENDO, Shuji SAITO, and Eizi HIROTA**

Because silane is a spherical-top molecule with T_d symmetry, it shows only weak absorptions in the microwave region which are due to a small dipole moment induced by centrifugal distortion. In the present study we have investigated deuterated species of silane by microwave spectroscopy, which are expected to have isotope-induced dipole moments large enough for the observation of rotational spectra.

The spectrometer used is a source-frequency modulation spectrometer with a free-space absorption cell held at about 100 K. As shown in Table I, the $J = 1 \leftarrow 0$ transition has been observed for the two symmetric-top species, SiH_3D and $SiHD_3$, and the B_0 constants derived therefrom are compared with those obtained from vibration-rotation bands; the precision has been two orders of magnitude improved. For the dideuterated species SiH_2D_2, more than ten transitions have been observed, including the $1_{11} \leftarrow 0_{00}$ transition listed in Table I, and are being analyzed.

Table I. Observed Rotational Transitions and Rotational Constants of Deuterated Silanes (in MHz)

	$^{28}SiH_3D$	$^{29}SiH_3D$	$^{30}SiH_3D$
ν ($J = 1 \leftarrow 0$)	125 885.320	125 855.326	125 827.111
B_0 (MW)	62 942.660	62 927.663	62 913.556
B_0 (IR)[a]	62 941.8	62 935.	63 109.
	$^{28}SiHD_3$	$^{29}SiHD_3$	$^{30}SiHD_3$
ν ($J = 1 \leftarrow 0$)	106 573.101	106 554.380	106 536.737
B_0 (MW)	53 286.551	53 277.190	53 286.369
B_0 (IR)[b]	53 287.58	53 275.58	53 264.28
	$^{28}SiH_2D_2$	$^{29}SiH_2D_2$	$^{30}SiH_2D_2$
ν ($1_{11} \leftarrow 0_{00}$)	119 070.708	119 036.154	119 003.741

a. Wm. B. Olson and R. W. Lovejoy, *J. Mol. Spectrosc.*, **66**, 314 (1977).
b. C. Frommer, R. W. Lovejoy, R. L. Sams, and Wm. B. Olson, *J. Mol. Spectrosc.*, **89**, 261 (1981).

II-C-3 Analysis of the High-resolution Infrared Spectrum of Methane-d_2 in the 2000 ~ 2400 cm^{-1} Region

Mitsuru AKIYAMA *(Tokai Univ. and IMS)* **and Eizi HIROTA**

In a previous study[1] the two C-D stretching bands of CH_2D_2, ν_2 and ν_8, were analyzed by taking into account the Coriolis interaction between them. However, five combination or overtone states are expected to lie near the $\nu_2 = 1$ and the $\nu_8 = 1$ states, as listed in Table I, and interactions of ν_2 and ν_8 with these states need to be analyzed in detail to derive molecular constants of ν_2 and ν_8 free of perturbations.

The high-resolution infrared spectrum of CH_2D_2 in the region between 1800 and 2400 cm^{-1} measured by Guelachvili with the resolution of 0.006 cm^{-1} was used in the present study, about 7200 lines being recorded. First, $\nu_4 + \nu_9$ was added to the ν_2/ν_8 manifold, by taking into consideration the Fermi interaction between ν_8 and $\nu_4 + \nu_9$, and later the a-type Coriolis interaction between $\nu_7 + \nu_9$ and $\nu_4 + \nu_9$ was added. It is interesting to note that the $\nu_4 + \nu_9$ band is as strong as the two fundamental bands, ν_2 and ν_8, or even stronger than ν_2. For the low-frequency side, it was straightforward to assign the $2\nu_4$ band, but the $2\nu_7$ and $\nu_4 + \nu_7$ bands were found to be heavily overlapped with each other and also

with ν_2 and were extremely difficult to assign. However, we have recently succeeded in making a partial assignment for the $2\nu_7$ band, which will give us a clue to completely assign all the bands.

Reference

1) M. Akiyama, T. Nakagawa, and K. Kuchitsu, *J. Mol. Spectrosc.*, **64**, 109 (1977).

Table I. Vibrational States of CH_2D_2 in the 2050 ~ 2350 cm^{-1} Region

State		Approximate energy (cm^{-1})	Interaction
$2\nu_4$	(A_1)	2054	
$\nu_4 + \nu_7$	(B_1)	~ 2124	a-type Coriolis
$2\nu_7$	(A_1)	2146	a-type Coriolis
ν_2	(A_1)	2203	Fermi
ν_8	(B_2)	2235	c-type Coriolis
$\nu_4 + \nu_9$	(B_2)	2286	Fermi
$\nu_7 + \nu_9$	(A_2)	~ 2327	a-type Coriolis

II-C-4 Stark Modulation Infrared Diode Laser Spectroscopy of the $\nu_6 + \nu_8$ Band of Diacetylene

Keiji MATSUMURA *(Seinan Gakuin Univ.)*, **Kentarou KAWAGUCHI, Eizi HIROTA, and Takehiko TANAKA** *(Kyushu Univ.)*

The non-polar molecule in an excited vibrational state may exhibit Stark effects if another vibrational state to which the transition is allowed comes close; the Stark effect is not due to the permanent dipole moment, but to the vibrational transition moment. The present study utilizes this fact to locate two infrared inactive bands, $2\nu_6$ (Σ_g^+) and $2\nu_8$ (Σ_g^+), through the observation of the Stark effect of the infrared active band, $\nu_6 + \nu_8$ (Σ_u^+).

Table I lists the rotational lines of the $\nu_6 + \nu_8$ band that show Stark effects. The Stark coefficients given in the Table were calculated from the ratios of intensities observed by Stark and source modulations. It was concluded from these observations that the $2\nu_6$ $J = 0$ level is located between $J = 0$ and 1 of $\nu_6 + \nu_8$ and the $2\nu_8$ $J = 54$ and 55 levels lie between $J = 55$ and 56 of $\nu_6 + \nu_8$. From the observed Stark coefficients the vibrational energy difference was calculated to be $E\,[2\nu_6\,(\Sigma_g^+)] - E\,[\nu_6 + \nu_8\,(\Sigma_u^+)] = 0.250(12)$ cm^{-1} and $E\,[2\nu_8\,(\Sigma_g^+)] - E\,[\nu_6 + \nu_8\,(\Sigma_u^+)] = 16.290(14)$ cm^{-1}.

Table I. Stark Effects Observed for the $\nu_6 + \nu_8(\Sigma_u^+)$ Band of Diacetylene

Rotational Transition		Stark Coefficient	State responsible for the Stark effect
P(1)	$J' = 0$	−0.1892	$2\nu_6$ (Σ_g^+)
P(2)	1	+1.0[a]	
P(3)	2	+0.0806	
R(53)	$J' = 54$	−0.0758	$2\nu_8$ (Σ_g^+)
R(54)	55	−0.5354	
R(55)	56	+1.0[a]	
P(57)	56		
P(58)	57	+0.2588	

a. Normalized to 1.0.

II—D Raman Spectroscopy of Macromolecules and Molecular Aggregates.

Raman spectroscopy reveals molecular vibrations. Since the vibrational frequencies are sensitive to a stereostructure as well as a potential function of a molecule, analysis of Raman spectra provides detailed structural information of a molecule. One of our projects is to apply the technique for elucidating the solvation mechanism of surfactant which may depend upon concentrations. It is practically to develope a highly sensitive detection system which allows us to observe the vibrational spectrum of surfactant in a molecular solvation. Our second project is to apply resonance Raman spectroscopy to the problem of structure-function relationship of macromolecules. In resonance Raman scattering there appear only the vibrational spectra of chromophores which are relatively simple and therefore allows detailed analysis. Since the chromophore of an enzyme generally serve as a catalytic site, resonance Raman spectroscopy brings about substantially important structural informatin of the enzyme. We are particularly interested in an activation mechanism of molecular oxygen by an iron porphyrin. The third project aims to observe the vibrational

spectrum of their reaction intermediates. A new detection system to obtain the time resolved Raman spectra is under construction for this purpose.

II-D-1 Raman Spectroscopic Studies of Submillimolar Surfactant Solutions; Concentration Dependence of the C-H Stretching Raman Lines.

Keiji KAMOGAWA, Kazuo TAJIMA *(Tokyo Metropolitan Univ.)*, **Kazuo HAYAKAWA, and Teizo KITAGAWA**

C-H stretching Raman spectra of very dilute surfactant solutions and their concentration difference spectra were obtained with the aid of a highly sensitive OMA detection system. By effective subtraction of the water background, profiles of the C-H spectra could be revealed even for the 0.5 mM solution, although so far the concentrations examined were mostly above 100 mM. Upon dilution in the concentration region slightly higher than the CMC, appreciable high frequency shifts of the 2860- and 2900-cm^{-1} bands were elucidated in the difference spectra in addition to an intensity rise around 2950 cm^{-1}. The intensity rise around 2950 cm^{-1} appeared to be coupled with the upward shift of the 2860-cm^{-1} band irrespective of the length of the hydrocarbon chain. These features seem to be general characteristics of surfactants upon the change from the micellar to molecular solvation, and presumably caused by a change of the intermolecular vibrational coupling but not by a simple change of surrounding polarity.

II-D-2 PO_2^- Symmetric-Stretching Raman Line and Molecular Aggregation States of Barium Dialkyl Phosphates

Hirofumi OKABAYASHI *(Nagoya Inst. Tech.)*, **Tadayoshi YOSHIDA** *(Nagoya Inst. Tech.)*, **Teruki IKEDA** *(JASCO Ltd.)*, **Hiroatsu MATSUURA** *(Hiroshima Univ.)*, **and Teizo KITAGAWA**

[*J. Am. Chem. Soc.* **104**, 5399 (1982)]

Raman spectra of barium dialkyl phosphate with various chain lengths were investigated. Dipentyl phosphate (DPP) was found to form a liquid crystal stable at room temperature. Calorimetric measurements of the DPP liquid crystal exhibited a phase transition at 60°C with $\Delta H = 1.7$ kcal/mol. The PO_2^- symmetric-stretching Raman line of DPP was observed at 1106 cm^{-1} for the crystal, and at 1075 cm^{-1} for an aqueous solution. For the liquid crystal two lines were observed at 1096 and 1075 cm^{-1}. The relative intensities of these lines changed sharply at the temperature of the phase transition but were essentially constant below and above the transition point. On the other hand, the intensity of the diester OPO symmetric stretching Raman line as well as that of the accordion vibration was hardly altered by the phase transition. This suggested little structural change in the phosphoalkyl group upon the phase transition and the coexistence of two types of aggregation structures having different $Ba^{2+} \cdots PO_2^-$ interaction modes in liquid crystal. The PO_2^- symmetric-stretching modes of dibutyl phosphate were observed at 1090 and 1068 cm^{-1}, and their relative intensities changed significantly upon micellization. It was concluded that the cation-phosphate interaction mode is important for investigation of the aggregation structure of dialkylphosphates and is characterized by the PO_2^- symmetric-stretching Raman lines.

II-D-3 Resonance Raman Spectra of the Reaction Intermediates of Horseradish Peroxidase Catalysis.

Junji TERAOKA, Takashi OGURA, and Teizo KITAGAWA

[*J. Am. Chem. Soc.*, **104**, 7354 (1982)]

Resonance Raman spectra of the reaction intermediates of horseradish peroxidase (HRP) were measured successfully through stabilization of them at cryogenic temperatures. The ν_4 lines of compound **I** and compound **II** were observed at 1359 and 1381 cm^{-1}, respectively. Upon raising temperature of the compound **I** sample the 1359-cm^{-1} line diminished and the 1381-cm^{-1} line grew first, then the latter gradually shifted to a lower frequency, and finally returned to the frequency of the native ferric enzyme (1376 cm^{-1}). Since the ν_4 line primarily involve the $C_\alpha N$ stretching vibration,

the frequency shift of ν_4 in compound **I** is consistent with the high spin-density at pyrrole nitrogen of the porphyrin π cation radical, in agreement with the results of recent NMR, ENDOR, and theoretical studies of compound **I**. Both compound **I** and compound **II** exhibited a new Raman line at 1131 cm^{-1}, which was absent in the resting ferric state. This line showed no isotopic frequency shift upon preparation of the sample with ^2H_2O and $^2H_2O_2$. The Fe-histidine stretching frequency was significantly altered during the reaction cycle, suggesting considerable involvement of the fifth ligand of iron in the stabilization of the intermediates having higher oxidation states.

II-D-4 Distinct Heme-Substrate Interactions of Lactoperoxidase Probed by Resonance Raman Spectroscopy: Difference between Animal and Plant Peroxidases

Teizo KITAGAWA, Shinji HASHIMOTO, Junji TERAOKA, Shingo NAKAMURA *(Hirosaki Univ.)*, **Hisa YAJIMA** *(Chiba Univ.)*, **and Toichiro HOSOYA** *(Chiba Univ.)*

[*Biochemistry,* **22**, 2788 (1983)]

Resonance Raman scattering from cow milk lactoperoxidase (LPO) and its complexes with various electron donors and inhibitors was investigated. The Raman spectrum of LPO is strikingly close to that of hog intestinal peroxidase but distinctly different from that of horseradish peroxidase (HRP). The ν_{10} frequency suggested the six-coordinate high-spin structure of heme for native LPO in contrast with the five coordinate high-spin structure for HRP. For the ν_{10} band, benzhydroxamic acid caused a frequency shift with HRP but not with LPO. Guiacol, *o*-toluidine, and histidine brought about a frequency shift of the ν_4 mode for LPO but not for HRP. The frequency shift was restored upon removal of the substrate or inhibitor by dialysis. The down shift of the ν_4 frequency is considered to represent an appreciable donation of electrons from the substrate or inhibitor to the porphyrin LUMO and thus their direct interaction with the heme group. From the relative intensity of the shifted and unshifted ν_4 lines, the dissociation constant was determined to be K_d = 52 mM for guaiacol and 87 mM for histidine at pH 7.4. The binding of histidine was relatively retarded in the presence of sulfate anion (K_d = 150 mM for 0.53 M sulfate present), and imidazole alone yielded no frequency shift, indicating the binding of the carboxyl group of histidine to the protein cationic site on one hand and a weak charge-transfer interaction between the imidazole group and the heme group on the other.

II-D-5 Resonance Raman Study of Plant Tissue Peroxidases: Common Characteristics in Iron Coordination Environments

Junji TERAOKA, Dominique JOB *(CNRS France)*, **Yuhei MORITA** *(Kyoto Univ.)*, **and Teizo KITAGAWA**

[*Biochim. Biophys. Acta,* **747**, 10 (1983)]

Resonance Raman spectra of isozymes 2, 3, 9, 15, and 16 of Japaneseradish peroxidase and isozymes 1, 3, and 7 of turnip peroxidase were measured and compared with those of horseradish peroxidase. All the resting isozymes gave the ν_{10} band around 1629-1631 cm^{-1}, indicating the five coordinate high-spin structure. The reduced form of all these isozymes gave the iron-histidine stretching Raman line at distinctly higher frequencies in comparison with those of hemoglobin and exhibited a clear pH-dependent frequency shift at neutral pH in accord with the results for horseradish peroxidase. Therefore, we conclude that the presence of strong hydrogen bonding of the proximal histidine and a small structural change of the proximal histidine upon a pH change at neutral region without breakage of the hydrogen bond are the common characteristics of plant peroxidases which contrast with those of oxygen carrier hemoproteins.

II-D-6 Resonance Raman Studies of Hemoglobin M: Evidence for Iron-Tyrosine Charge-Transfer Interactions in the Abnormal Subunits of Hb M Boston and Hb M Iwate.

Kiyoshi NAGAI *(Nara Med. Univ.)*, **Tadashi KAGIMOTO** *(Kumamoto Univ.)*, **Akira HAYASHI** *(Osaka Univ.)*, **Fumito TAKETA**

(Med. Coll. Wisconsin), **and Teizo KITAGAWA**

[*Biochemistry*, **22**, 1305 (1983)]

Resonance Raman spectra have been obtained for Hb M Boston, Hb M Iwate, and Hb M Milwaukee. The abnormal α subunits of Hb M Boston and Hb M Iwate exhibited the porphyrin ν_{10} band at 1628 and 1627 cm^{-1} respectively, which indicates that the ferric α hemes are five-coordinated in both Hb M Boston and Hb M Iwate. In addition to the porphyrin bands, four extra polarized lines were observed at 1607, 1506, 1278, and 603 cm^{-1} for the α abnormal subunit of Hb M Boston and at 1605, 1506, 1310, and 589 cm^{-1} for that of Hb M Iwate. By comparison with the vibrational spectra of Fe-tyrosine proteins and Fe-phenolate complexes, the 1605-1607 and 1506 cm^{-1} lines were assigned to the phenolate ring vibrations of the heme-coordinated tyrosine, and 1278-cm^{-1} line of Hb M Boston and 1310-cm^{-1} line of Hb M Iwate were assigned to the phenolate CO stretching mode. We propose that the 603-cm^{-1} line of Hb M Boston and the 589-cm^{-1} line of Hb M Iwate arise from the Fe-O (tyrosine) stretching mode. Intensities of these lines were relatively enhanced upon excitation around 475-520 nm, suggesting the presence of a charge-transfer interaction between Fe and Tyr. The dissimilarity of the Fe-O and phenolate CO stretching frequencies between Hb M Boston and Hb M Iwate, despite the similarity of frequencies of their porphyrin and phenolate ring modes, may indicate an appreciable difference of heme-phenolate bonding angles between Hb M Boston and Hb M Iwate. Hb M Milwaukee showed no anomaly in the Raman spectra.

II-D-7 Resonance Raman Study of an aa_3-Type Cytochrome Oxidase of Thermophilic Bacterium PS3.

Takashi OGURA, Nobuhito SONE *(Jichi Med. School)*, **Kunio TAGAWA** *(Osaka Univ.)*, **and Teizo KITAGAWA**

Resonance Raman spectra of an aa_3-type cytochrome oxidase of thermophilic bacterium PS3, known to have simpler subunit compositions than the mitochondrial one but very similar enzymatic properties, were investigated under various conditions and compared with those of mitochondrial enzymes. Intensity dependencies of the two marker lines of reduced cytochrome a_3 at 1667 and 213 cm^{-1} upon the incubation temperature were different. The former was almost parallel to the oxidase activity whereas the latter was rather close to the proton pumping activity with regard to the dependence upon the incubation temperatures. The 213-cm^{-1} line disappeared upon binding of carbon-monoxide, upon raising pH above 9.2, or after incubating above 55°C, similar to the Fe(II)-histidine stretching Raman lines of deoxyHb, deoxyMb, and ferroHRP, and was accordingly presumed to arise from the Fe-histidine stretching mode of ferrous high-spin a_3-heme. The pH dependence of this line was also distinct from that of the 1667-cm^{-1} line, which arise from the peripheral CH = O stretching mode of the a_3-heme. The Raman line at 1611 cm^{-1}, which was recently claimed to probe the proton pump activity, remained unaltered after incubation at 60°C for 20 min despite the reduced proton pump activity to one third. This was unfavorable to the proposed mechanism. The frequencies of these Raman lines and others as well were the same between the intact membrane and isolated enzyme. The oxidase of the present preparation was apparently autoreduced in the presence of 100-mM, but not 2-mM, cyanide, although the cytochrome oxidase activity was completely lost even for the latter.

I-D-8 Subunit Assembly Dependent Photoreduction of Heme of Giant Hemoglobin Probed by Resonance Raman Spectroscopy.

Teizo KITAGAWA, Sosuke CHIHARA *(Osaka Univ.)*, **Kenzo Fushitani** *(Osaka Univ.)*, **and Hideki MORIMOTO** *(Osaka univ.)*

Resonance Raman spectra of a giant hemoglobin and its subunit assembly dependence were investigated. The intact Hb ($M_r = 3 \times 10^6$) and the 1/12 subunit ($M_r = 2.4 \times 10^5$) were extensively photoreduced by laser illumination at 441.6 nm but little at 488.0 nm or longer wavelengths. The photoreduction was prohibited for the 26,000 assembly and separated chains with $M_r = 14{,}000 -$

18,000, although the deoxy forms of all the four species exhibited the Fe-histidine stretching mode at the frequency of the usual tetramer deoxyHb with the high-affinity quaternary structure (219-221 cm^{-1}). The photoreduction of native metHb was also retarded upon raising pH. It is, therefore, likely that a photo-excited electron is transferred from the protein moiety to the heme under the specific conformation of the protein.

II-D-9 Iron-Histidine Stretching Raman Line of the aa_3-Type Cytochrome Oxidases

Takashi OGURA, Koyu HON-NAMI *(Mitsubishi-Kasei Inst Life Sci.)*, **Tairo OSHIMA,** *(Mitsubishi-Kasei Inst. Life Sci.)*, **Shinya YOSHIKAWA** *(Konan Univ.)*, **and Teizo KITAGAWA**

The Fe-histidine stretching Raman line of the high-spin a_3 heme of the aa_3-type cytochrome oxidases was assigned for mammalian, yeast, and bacterial enzymes in the reduced state. The isotope replacement of the heme iron of the bacterial enzyme was worked out by cultivating a thermophilic bacterium in a ^{56}Fe- or ^{54}Fe- enriched synthetic medium. The Raman line of the reduced bacterial cytochrome oxidase at 211 cm^{-1} exhibited an upward frequency shift by 2 cm^{-1} upon the ^{54}Fe substitution while other lines remained unshifted. This Raman line disappeared upon binding of cyanide to the sixth coordination position. Upon raising pH, the 211-cm^{-1} line lost intensity without any frequency shift. All these features, which are consistent with the characteristics of the Fe-histidine stretching Raman lines of ferroHRP, deoxyHb and deoxyMb, strongly suggest that the 211-cm^{-1} line of the bacterial cytochrome oxidase arises primarily from the Fe-histidine stretching mode of the high-spin a_3 heme. The Raman spectral patterns of beef heart and yeast cytochrome oxidases were somewhat different from that of bacterial one. However, the Raman lines of the beef heart enzyme at 214 cm^{-1} and the yeast enzyme at 220 cm^{-1} disappeared upon binding of cyanide and diminished upon raising pH similar to the 211-cm^{-1} line of the bacterial enzyme. Accordingly, these two lines are also considered to involve mainly the Fe-histidine stretching vibration of the five coordinate ferrous high-spin a_3 heme.

II—E Structures of Liquids and Noncrystalline Solids

The structures of liquids and noncrystalline solids still remain to be determined. Since the majority of chemical reactions takes place in the liquid state and amorphous solids exhibit interesting and useful properties such as conductivity and catalytic activity, it is necessary to understand their structures from molecular viewpoint.

The study of local structure of binary solution by the use of light scattering has been continued. X-ray diffraction and Raman spectroscopy helped to understand further the shapes and sizes of aggregates formed in solution. The understanding of dynamic behavior of solute has improved by the use of NMR relaxation time in the past year.

An effort to construct a reliable in-laboratory EXAFS facility is almost over, which is described in detail at special research projects section. Now the local structure change around the metal atom during synthesis procedures of supported catalysts are being studied by EXAFS technique.

II-E-1 X-Ray Diffraction Study of Mixing States in the Carbon Tetrachloride Solutions of Methanol and Pentane

Masami TANAKA *(Tokyo Metropolitan Univ.)*, **Keiko NISHIKAWA** *(Gakushuin Univ.)*, **Kazuyuki TOHJI, and Tsunetake FUJIYAMA**

[*Bull. Chem. Soc. Jpn.*, **56**, 1273 (1983)]

A simple method has been proposed for estimating the state of mixing in a binary solution directly from the radial distribution function. The method has been applied to the estimation of the size of the cluster or aggregate in a binary solution of methanol and carbon tetrachloride. Pure liquid

carbon tetrachloride and a binary solution of pentane and carbon tetrachloride have also been studied as reference systems. The number of methanol molecules which form a cluster in the solution at the volume ratio of 8.5 (CCl_4) : 1.5 (CH_3OH) has been estimated to be about 18, which is in good agreement with an estimate by light scattering.

II-E-2 On the Effect of the Finite Size of the Solvent Molecule in Dielectric Friction Theory

Shi-aki HYODO *(Tokyo Metropolitan Univ.)*, **Unpei NAGASHIMA** *(Hokkaido Univ.)*, **and Tsunetake FUJIYAMA**

[*Bull. Chem. Soc. Jpn.*, **56**, 1041 (1983)]

By considering the charge distribution function around the ion , the effect of the finite size of the solvent molecule can be introduced in the homogeneous dielectric continuum model. A vey simple and useful model is presented. The results of this model are compared quantitatively with the experimental Walden products of some simple cations in water, methanol, ethanol, acetone, and acetonitrile solutions, and found to be satisfactory.

II-E-3 Catalyst Preparation procedure Probed by EXAFS Spectroscopy I. Nickel on Silica

Kazuyuki TOHJI, Yasuo UDAGAWA, Shuji TANABE *(Toyohashi Univ. of Tech.)*, **and Akifumi UENO** *(Toyohashi Univ. of Tech.)*

[*Chem. Lett.*, 1983, 1089]

[*J. Amer. Chem. Soc.*, in press]

Environments of Ni atoms were probed by extended X-ray absorption fine structure (EXAFS) at every elementary step of Ni/SiO_2 catalyst preparation by two different methods. Combining the structural information obtained at atomic level by EXAFS with the observation of bulk by electron microscope, detailed reaction procedures leading to different products have been revealed. The reason why metal particle size distribution differs by the preparation procedure employed is ascribed to whether homogeneous dispersion of small metal oxide cluster is realized or not before reduction.

II-E-4 A Study of Orientational Pair Correlation of Pyridine and 2, 4-Dimethylpyridine in Water by depolarized Rayleigh Scattering and NMR Spectra

Nobuyuki ITO *(Tokyo Metropolitan Univ.)* **and Tadashi KATO**

[*J. Phys. Chem.*, in press]

The depolarized Rayleigh relaxation times and spin-lattice relaxation times of carbon-13 NMR for 2,4-dimethylpyridine(DP)-water and pyridine(PY)-water systems have been studied as a function of concentration and temperature. The concentration dependences of the mean-square concentration fluctuation for these systems were also measured at various temperatures. The concentration fluctuation indicates that the solute molecules associate with each other at low concentration. The effect of the pair correlation on molecular orientational motion was derived from these relaxation times. The results show that solute molecules not only gather together but also align their orientation at low concentration. Since no pair correlation was observed for the neat liquid, it can be concluded that water molecules play essentially important role for the aggregation of solutes.

II-E-5 Kirkwood-Buff Parameters and Correlation Length in Aqueous Solutions of n-Alkoxyethanols

Tadashi KATO

[*J. Phys. Chem.*, in press]

Mean-square concentration fluctuations for an aqueous solution of 2-ethoxyethanol(EE) were obtained by a Rayleigh-Brillouin scattering measurement. The concentration dependence of the Kirkwood-Buff parameters, G_{11}, G_{22}, and G_{12}, was determined for the binary solutions of EE-Water at 21°C and 2-butoxyethanol (BE)-water at 21°C and

42°C by using data on the concentration fluctuation, the isothermal compressibility and the partial molar volumes. The absolute values of G_{ij} for the BE system are about two orders of magnitude larger than those for the EE system. The correlation length of the local concentration for the BE system was roughly estimated from an analysis of G_{ij}.

RESEARCH ACTIVITIES III
Department of Electronic Structure

III—A Photochemical Formation and Reactions of Vibrationally Highly Excited ("Hot") Molecules and Radicals

Vibrationally highly excited ("hot") molecules and radicals were found to be efficiently formed by electronic excitation. For example a quantum yield close to unity was found with an excitation of benzene to its second excited singlet state. The "hot" benzene molecules thus produced have internal energy of 624 kJ/mol, which is equivalent to 3390 K in vibrational temperature. Phenyl halides give "hot" phenyl radical with an internal energy more than 150 kJ/mol and benzyl chloride gives "hot" benzyl radical with high efficiency. Ethylene derivatives likewise give "hot" allyl-type radicals. Collisional energy relaxation of "hot" molecules and radicals was studied in detail. Energy-dependent energy transfer was proposed to explain the wavelength dependent and non-exponential relaxation of hot molecules. Importance of the "hot" intermediate was pointed out in the mechanism of "photochemical" reactions.

III-A-1 Laser Flash Photolysis of Benzene. VIII. Formation of Hot Benzene from the S_2 State and its Collisional Deactivation

Nobuaki NAKASHIMA and Keitaro YOSHIHARA

[*J. Chem. Phys.*, **79**, 2727 (1983)]

In Figure 1 time-resolved absorption spectra of gaseous benzene are shown in the time range from 0 to 4 μs with an ArF laser (193 nm) as an excitation source, which pumps the S_2 state. The absorption strength in the transient spectrum observed immediately after excitation with a 10 ns pulse decreases monotonically from 210 to 290 nm. This spectrum is postulated to be due to $B^{**}(S_0)$ (a hot benzene with internal energy of 624 kJ/mol). The transient spectrum can be simulated as part of the $S_3(^1E_{1u}) \leftarrow S_0$ transition at 3390 K on the basis of a modified Sulzer-Wieland model. The agreement between calculated and observed molar extinction coefficients of $B^{**}(S_0)$ indicates that the yield of internal conversion from S_2 to $B^{**}(S_0)$ is close to unity. Deactivation processes have been detected from $B^{**}(S_0)$ to a thermal equilibrium state in inert gas baths. The time profile of absorption intensity due to collisional deactivation is non-exponential and depends upon observing wavelength, being faster at longer wavelength. The deactivation processes are explained in terms of a simple energy transfer model, which assumes that the removal energy per collision depends on the internal energy

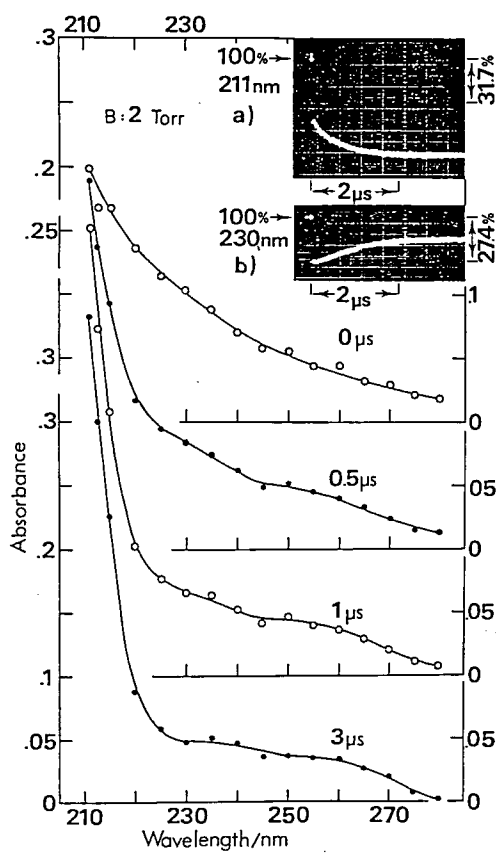

Figure 1. Time-resolved absorption spectra of benzene at a pressure of 2 Torr. Inserted Photos. typical oscilloscope traces at: (a) 211 nm, (b) 230 nm.

of the hot molecule. Internal conversion from S_2 to $B^{**}(S_0)$ is suggested to be the initial step in the photochemical reactions of gaseous benzene. The absorption spectrum and collisional deactivation processes following excitation with a KrF laser (248 nm) have been analysed in the same way.

III-A-2 Formation of Hot Hexafluorobenzene in the 193 nm Photolysis

Teijiro ICHIMURA*, Yuji MORI* *(*Tokyo Inst. Tech)*, **Nobuaki NAKASHIMA, and Keitaro YOSHIHARA**

Time-resolved absorption spectra of hexafluorobenzene (HFB) vapor have been observed with an ArF laser (193 nm) excitation. The absorption spectrum observed at the time "t = 0" (Figure 1) is postulated to be due to $HFB^{\dagger}$ (S_0) (a hot hexafluorobenzene with the internal energy of 639 kJ/mol). The transient spectrum can be simulated as part of the $S_3(^1E_{1u}) \leftarrow S_0$ transition at 3050 K.

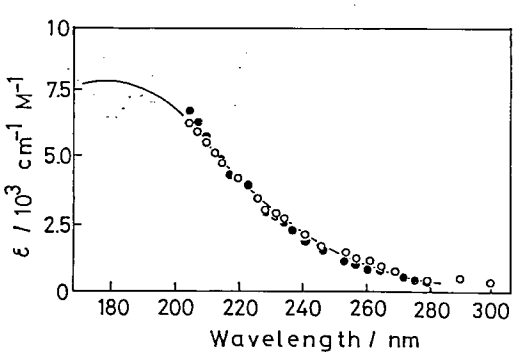

Figure 1. Calculated absorption spectra of "hot" HFB on the basis of the Sulzer-Wieland model at 3050 K (——) and observed transient absorbances at "t = 0".

III-A-3 Nanosecond Laser Photolysis of Phenyl Halide at 193 nm in the Gas Phase: Formation of Hot Radical and its Reaction.

Noriaki IKEDA, Nobuaki NAKASHIMA, and Keitaro YOSHIHARA

Phenyl halides have been photolyzed with an ArF (193 nm) excimer laser. The absorption spectrum immediately after excitation (0 ns) gave a structureless absorption, of which intensities decreased monotonically with increasing wave-

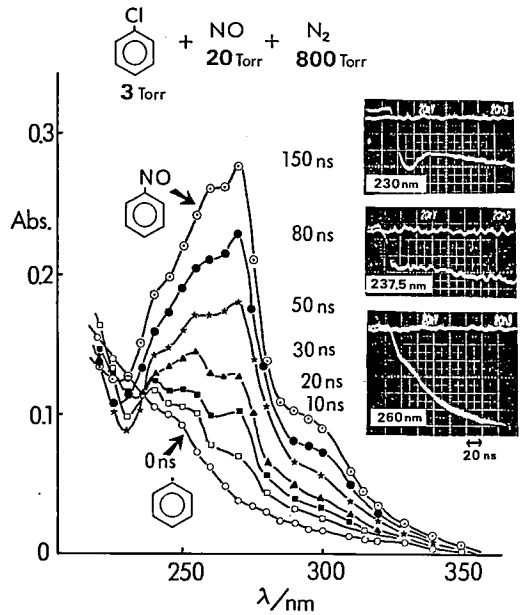

Figure 1. Time-resolved absorption spectra of the chlorobenzene 3 Torr + nitric oxide 20 Torr + nitrogen 300 Torr system by laser photolysis (193 nm). Typical oscillograms of transient absorption at 260, 237.5 and 230 nm were inserted.

length. In the presence of nitric oxide as a scavenger, strong absorption of nitrobenzene was observed as shown in Figure 1. This demonstrates that the "t = 0 ns" absorption is due to a vibrationallly highly excited (hot) phenyl radical. The relaxation of this species shows both pressure dependence and wavelength dependence, as a hot molecule usually does. The internal energy of hot phenyl radical is estimated to be 165.2 kJ mol^{-1}, and 1370 K in vibrational temperature. The absorption spectrum of phenyl-oxygen adduct has also been detected.

III-A-4 Photodissociation of Benzyl Chloride at 193 nm in the Gas Phase: the Absorption Spectra of Hot and Relaxed Benzyl Radical

Noriaki IKEDA, Nobuaki NAKASHIMA, and Keitaro YOSHIHARA

Benzyl chloride in the gas phase has been photolyzed with an ArF (193 nm) excimer laser. Time-resoleved absorption spectra have shown that benzyl raical is formed by dissociation. The broad absorption spectrum obtained immediately after excitation was gradually sharpened as shown in

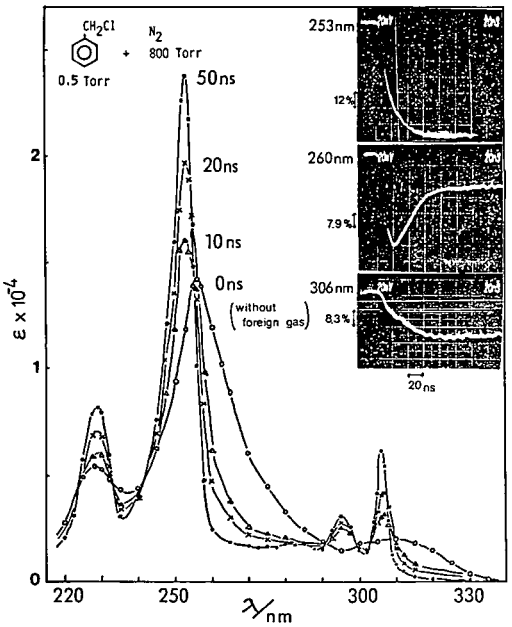

Figure 1. Time-resoleved absorption spectra of benzyl radical formed by laser photolysis (193 nm) of benzyl chloride 0.5 Torr + nitrogen 800 Torr system. The spectrum at 0 ns is taken without foreign gas. Typical oscillograms of the transient absorption at 253, 260, and 306 nm are inserted.

Figure 1. This dynamical behavior can be explained in terms of collisional relaxation of highly excited vibrational state in the ground electronic state, hot benzyl radical. The vibrational temperature has been estimated by simulation of absorption spectra with a modified Sulzer-Wieland model. It seems that the intramolecular vibrational redistribution of benzyl radical formed by photodissociation should be achieved within the duration of excitation pulse. The extinction coefficient of each band (229, 253, 306 nm) of relaxed benzyl radical has also been determined.

III-A-5 Direct Masurement of Formation Rates of Allyl-type Radicals from Ethylene Derivatives

Nobuaki NAKAHSHIMA, Nobuo SHIMO, Noriaki IKEDA, and Keitaro YOSHIHARA

Formation rates of allyl-type radicals have been measured under collision free conditions with excitation by an ArF (193 nm) laser. Absorption spectra of allyl-type and methyl radicals are observed in nanosecond time-resolved spectra as

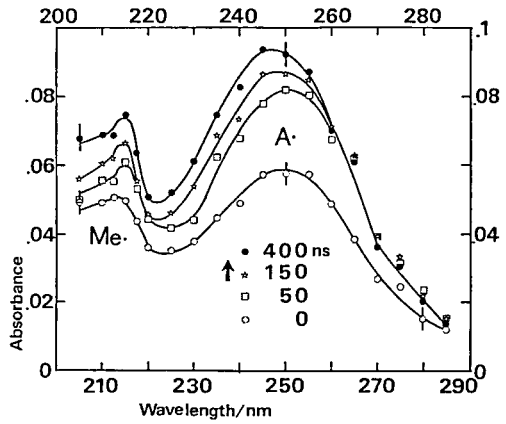

Figure 1. Time-resolved absorption spectra of 2,3,3-trimethyl-1-butene at 0.435 Torr. The peak around 250 nm (A•) is due to absorption of a "hot" allyl-type radical and around 215 nm (Me•) to a "hot" methyl radical.

shown in Figure 1. Rise curves of those spectra give formation rates of allyl-type radicals: 4×10^7 s^{-1} from 2,3,3-trimethyl-1-butene, 2×10^7 s^{-1} from 2,3-dimethyl-2-pentene, and 1.6×10^7 s^{-1} from tetramethylethylene. Hot molecules produced after internal conversion are postulated to be the initial intermediates for the dissociation, because yields of these radicals are suppressed by foreign gases. Yield of allyl-type radicals are reduced by nitrogen. A rate constant of 8×10^5 s^{-1} $Torr^{-1}$ has been obtained for the case of 2,3,3-trimethyl-1-butene. The formation rates should be explained in terms of specific rate constants in the thermal reaction.

III-A-6 ArF Laser Flash Photolysis of Ethylene Derivatives: Substituents Dependence of Allyl Radical Formation

Nobuo SHIMO, Nobuaki NAKASHIMA, Noriaki IKEDA, and Keitaro YOSHIHARA

Various ethylene derivatives were photolyzed with an ArF(193 nm) excimer laser. Time-resolved transient absorption specra showed that allyl radical ($\lambda_{max.}$ = 223 nm) was formed by dissociation of β position to the double bond. The broad absorption spectrum, obtained immediately after excitation, was gradually sharpened by collisional relaxation. The relative yield of relaxed allyl radical formation was decreased as substituents became larger in an order as H, CH_3, C_2H_5 > n-C_3H_7, i-C_3H_7, n-C_4H_9 >

$$CH_2{=}CH\text{-}CH_2{-}X \xrightarrow{193\ nm} CH_2{=}CH\text{-}CH_2\cdot + X\cdot$$

X	Molecule	Pressure[a)]/ Torr	Absorbance[b)]	Relative Yield[c)]
H	Propylene	38.0	0.329	1.00
CH_3	Butene-1	16.2	0.325	0.98
C_2H_5	Pentene-1	12.6	0.301	0.91
n-C_3H_7	n-Hexene-1	12.4	0.077	0.23
i-C_3H_7	i-Hexene-1	11.9	0.074	0.22
n-C_4H_9	n-Heptene-1	7.6	0.076	0.23
n-C_5H_{11}	n-Octene-1	8.7	0.031	0.09
$CH_2CH{=}CH_2$	1,5-Hexadiene	4.8	0.577	0.88(1.75)
Cl	Allylchloride	4.5	0.323	0.98
NH_2	Allylamine	3.4	0.166	0.50
OH	Allylalcohol	5.8	0.075	0.23

a) Absorbance at 193 nm is adjusted.
b) The absorbance of relaxed allyl radical ($\lambda_{max.}$ = 223 nm)
c) The absorbance of propylene excitation is taken for 1.00.

n-C_5H_{11}, as shown in Table 1. In the case of the photolysis of 1-butene, the main process was dissociation to CH_3. and C_3H_5 (allyl), which were coupled to form ethane and 1,5-hexadiene, respectively, and these compounds were detected by final product analysis.

III—B Radiationless Processes in Large Molecules—Channel Three in Benzene

Fluorescence quantum yields and lifetimes together with excitation and emission spectra have been measured following excitation of benzene and perdeuterated benzene vapour under collision free conditions. Excitation was made above the channel three threshold with a recently developed high power, picosecond, narrow bandwidth laser continuously tunable from 214 to 252 nm. The dramatic channel three effect was indeed observed in both quantum yields and lifetimes and three orders of magnitude change was found upon excitation at all vibrational levels. Single vibronic level fluorescences were observed and a pronounced line broadning was found above the channel three threshold. The principal cause of the channel three was discussed.

III-B-1 Laser Flash Photolysis of Benzene. VII. Fluorescence Decay in the Channel 3 Region

Yoshihiro TAKAGI, Minoru SUMITANI, Nobuaki NAKASHIMA, Desmond V. O'CONNOR, and Keitaro YOSHIHARA

[*J. Chem. Phys.*, 77, 6337 (1982)]

The benzene vbronic level $7_0^1 16_1^1 1_0^2$ (0_2^1), which lies about 2000 cm^{-1} above the channel 3 threshold, was selectively pumped with tunable UV laser radiation. The resulting single vibronic level fluorescence was

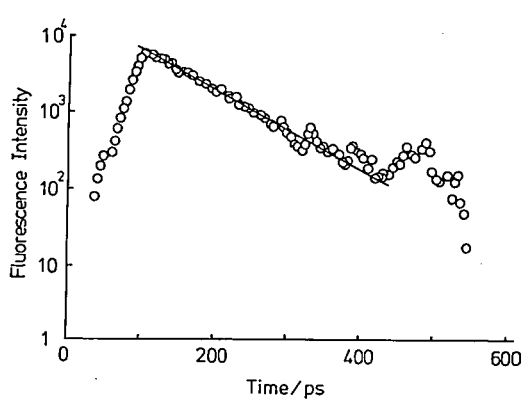

Figure 1. Fluorescence decay of benzene excited at 233.4 nm. Streak camera detection. Benzene pressure 85 Torr. (OOO) observed data averaged over 30 laser shots (———) single exponential fit to observed data τ = 42 ± 10 ps.

exponential with a lifetime of 42 ± 10 ps as shown in Figure 1. A small amount of fluorescence from the thermalized S_1 level was also detected.

III-B-2 Fluorescence Quantum Yields of S_1 Benzene in the Channel 3 Region

Minoru SUMITANI, Desmond V. O'CONNOR, Yoshihiro TAKAGI, Nobuaki NAKASHIMA, Keiji KAMOGAWA, Yasuo UDAGAWA, and Keitaro YOSHIHARA

[*Chem. Phys. Lett.*, 97, 508 (1983)]

Fluorescence quantum yields from isolated benzene molecules have been measured following excitation into the channel 3 region. The particular transition excited always plays a role in determining the yield but a gross excitation energy effect becomes stronger at higher excess energies as shown in Figure 1.

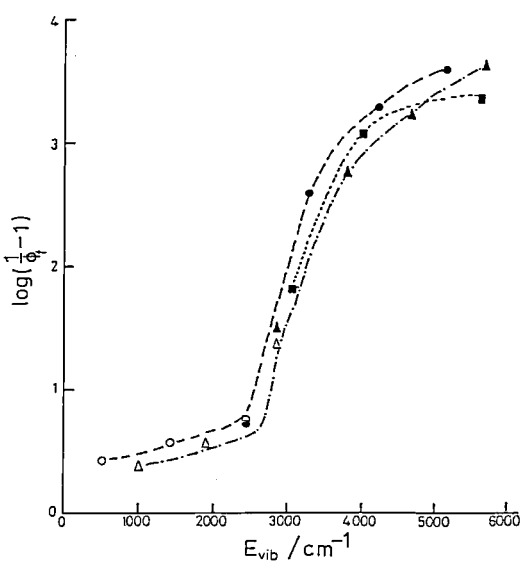

Figure 1. Plots of log $(1/\phi_f - 1)$ vs E_{vib} for the transitions $6_0^1 1_0^n$ (circles), $6_1^2 1_0^n$ (triangles) and $7_0^1 1_0^n$ (squares). Filled symbols are data taken from Spears and Rice (ref [1]). The lines delineate members of the same series and have no further significance.

Reference

1) K.G. Spears and S.A. Rice, *J. Chem. Phys.*, 55, 5561 (1971).

III-B-3 Fluorescence Spectra from Highly Excited Vibrational Levels in Benzene

Desmond V. O'CONNOR, Minoru SUMITANI, Yoshihiro TAKAGI, Nobuaki NAKASHIMA, Keiji KAMOGAWA, Yasuo UDAGAWA, and Keitaro YOSHIHARA

[*J. Phys. Chem.*, in press]

Fluorescence spectra resulting from excitation of short wavelength absorption bands in benzene have been measured under collision-free condition. Spectra resulting from excitation of $6^1 1^{n+2}$ and $7^1 1^n$ (n = 0, 1, 2, 3) are shown in Figure 1 (a) and (b), respectively. Good signal to noise ratios were achieved by the use of high sample pressures in conjunction with early gated time-resolved spectra. Most of the measured spectra, even those from levels well above the channel 3 threshold, are characteristic of the level(s) initially excited. The relevance of the spectra to the elucidation of the channel 3 mechanism is discussed.

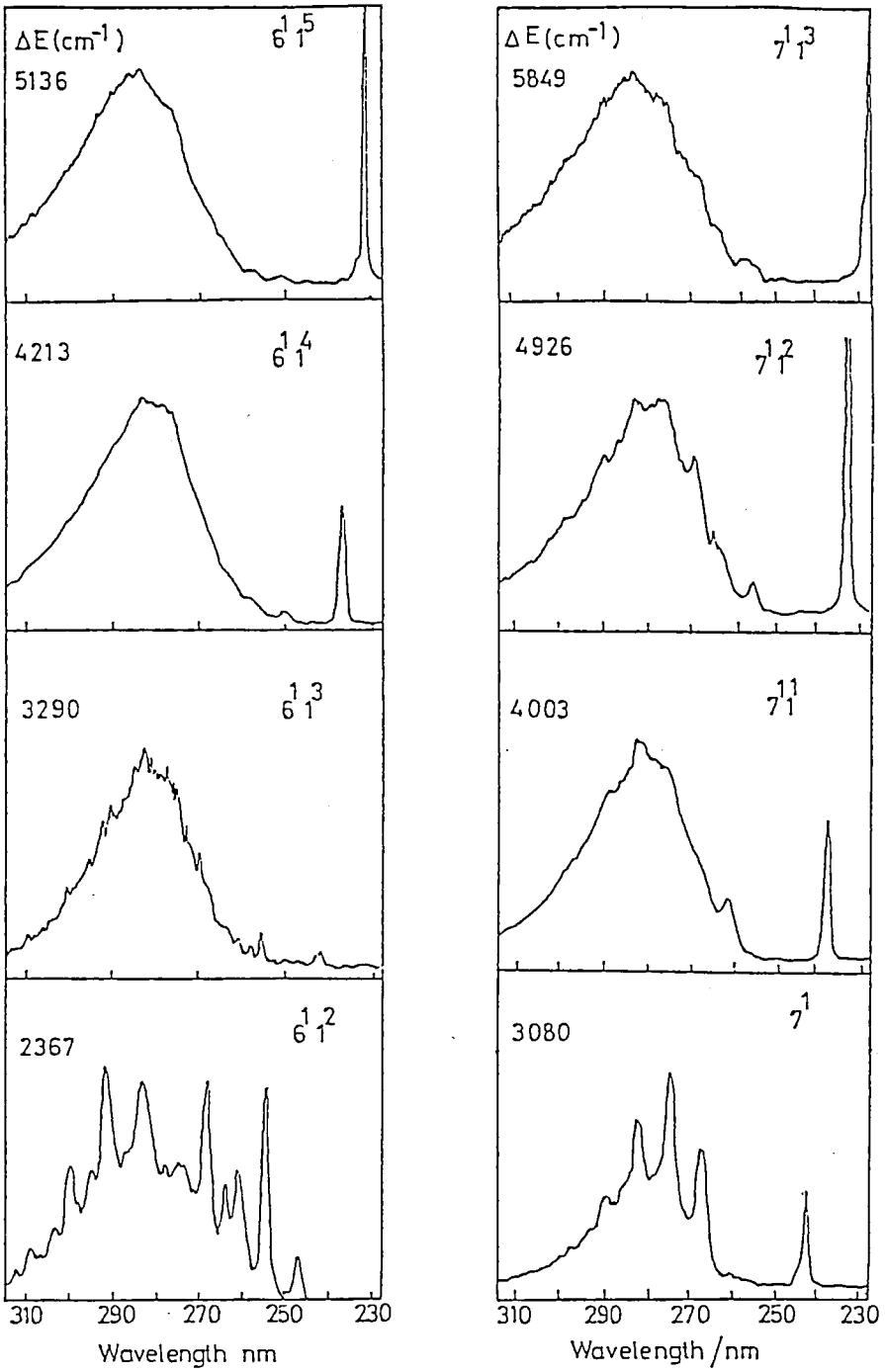

Figure 1. Spectra resulting from excitation of $6^1 1^{n+2}$ (a) and of $7^1 1^n$ (b) for n = 0, 1, 2, and 3. Gated spectra except $6^1 1^2$ and 7^1. ΔE is an excess vibrational energy.

III-B-4 Channel Three Decay in Benzene; A Fluorescence Investigation

Minoru SUMITANI, Desmond V. O'CONNOR, Yoshihiro TAKAGI, Nobuaki NAKASHIMA, and Keitaro YOSHIHARA

Fluorescence quantum yields and decay times together with excitation and emission spectra have been measured following excitation of benzene vapor above the channel three threshold. The excitation source was a recently developed high power, picosecond, narrow bandwidth laser con-

tinuously tunable from 214 nm to 252 nm. The characteristic channel three effect was present in both quantum yields and lifetimes and was observed for all vibrational levels investigated as summerized in Table 1. We propose that absorption linebroadening, which affects only certain series of transitions is not directly related to channel three decay. For similar reasons we discount intramolecular vibrational redistribution as the principal cause of channel three. Instead we propose a mechanism based on the presence of secondary minima on the S_1 potential surface.

Table I. Quantum yields, decay times and charactic features of fluorescence spectra

transition	λ, nm	Level	ΔE, cm^{-1}	Fluoresc. spect.	ϕ_f			τ_f, ns		
								(b)		(c)
				(a)	(b)	(c)		τ_1	τ_2	τ
$6_0^1 1_0^2$	247.1	$6^1 1^2$	2367	s	1.8×10^{-1}	0.17 [1, 2]		47		55 [1], 53 [2]
$6_0^1 11_0^2 1_0^1$	246.5	$6^1 11^2 1^1$	2470	s	1.4×10^{-1}	0.14 [2]		33		
$6_0^1 16_1^1 1_0^2$	248.1	$6^1 16^1 1^2$	2610	s	(e)	0.08 [1], 0.10 [2]		30		42 [1], 28 [5]
$6_0^1 10_0^2 1_0^1$	245.7	$6^1 10^2 1^1$	2614	s	1.0×10^{-1}	0.06 [1], 0.07 [2]		27		42 [1]
$6_0^1 16_2^2 1_0^2$	249.1	$6^1 16^2 1^2$	2853	s	6.3×10^{-2}	0.04 [2]		44		
$6_0^1 17_0^2 1_0^1$	244.0	$6^1 17^2 1^1$	2856	sb	1.4×10^{-2}	< 0.005 [2]		13	2.8	
$6_1^2 1_0^2$	247.7	$6^2 1^2$	2888	s	4.6×10^{-2}	0.03 [1], 0.05 [2]		40		47 [1]
7_0^1	242.8	7^1	3080	s	1.6×10^{-2}	< 0.01 [2], 0.04 [3]		18	4.0	19 [6]
$6_0^1 1_0^3$	241.7	$6^1 1^3$	3290	s	2.5×10^{-3}	< 0.005 [2]		0.7	2.9	7 [6]
$6_0^1 16_1^1 1_0^3$	242.6	$6^1 16^1 1^3$	3533	(d)	1.4×10^{-3}			0.8	3.4	
$6_0^1 10_0^2 1_0^2$	240.2	$6^1 10^2 1^2$	3537	b	1.3×10^{-3}	1.1×10^{-3} [4]		0.15	1.0	
$6_0^1 2_0^1$	239.6	$6^1 2^1$	3651	sb	9.7×10^{-4}			0.075	0.5	
$6_1^2 1_0^3$	242.2	$6^2 1^3$	3811	sb	1.8×10^{-3}			0.7	3.7	
$7_0^1 1_0^1$	237.5	$7^1 1^1$	4003	s	9.0×10^{-4}	6.3×10^{-4} [4]		0.13		
$6_0^1 1_0^4$	236.4	$6^1 1^4$	4213	sb	5.7×10^{-4}			0.09		
$6_1^2 1_0^4$	236.9	$6^2 1^4$	4734	b	6.1×10^{-4}			0.057		
$7_0^1 1_0^2$	232.4	$7^1 1^2$	4926	s	4.7×10^{-4}	3.6×10^{-4} [4]		0.080		
$6_0^1 1_0^5$	231.4	$6^1 1^5$	5136	b	2.8×10^{-4}			0.023		
$6_1^2 1_0^5$	231.9	$6^2 1^5$	5657	(d)	2.5×10^{-4}	3.6×10^{-4} [4]		(d)		
$7_0^1 1_0^3$	227.6	$7^1 1^3$	5851	sb	(d)			0.026		

(a) S: structrure, sb: broad with some structure, b: broad with little structure
(b) this work
(c) literature [reference number n square brackets]
(d) not measured
(e) reference level for quantum yield calculation. ϕ_f assumed = 0.10

References

1) K. G. Spears and S. A. Rice, *J. Chem. Phys.*, **55**, 5561 (1971).
2) W. R. Ware, A. M. Garcia, C. S. Parmenter, M. D. Schuh and K. Y. Tang, *Chem. Phys.*, **17** 377 (1976).
3) A. E. W. Knight, C. S. Parmenter, and M. W. Schuyler, *J. Am. Chem. Soc.*, **97** 2005 (1975).
4) I. Yamazaki, T. Murao, t. Yamanaka and K. Yoshihara, *Farad. Disc. Chem. Soc.*, **75** 23 (1983).
5) W. Hack and W. Langel, *Nouvo Chim. Soc. Ital.*, **638**, 207 (1981)
6) L. Wünsch, H. J. Neusser and E. W. Schlag, *Chem. Phys. Lett.*, **32** 210 (1975).

III-B-5 Assignment of the E absorption Transitions in C_6D_6 by Means of Isolated-Molecule Fluorescence Spectra

Yoshihiro TAKAGI, Minoru SUMITANI, Desmond V. O'CONNOR, Nobuaki NAKASHIMA, Keiji KAMOGAWA, Yasuo UDAGAWA, and Keitaro YOSHIHARA

[*Chem. Phys. Lett.*, **99**, 445 (1983)]

Fluorescence spectra following narrow bandwidth excitation of C_6D_6 have been observed and their structure analysed. Excitation of the E_1^0 absorption band gives rise to fluorescence that cannot originate in a level with ν_8 excited. One of the obtained single-vibronic level fluorescence is shown in Figure 1.

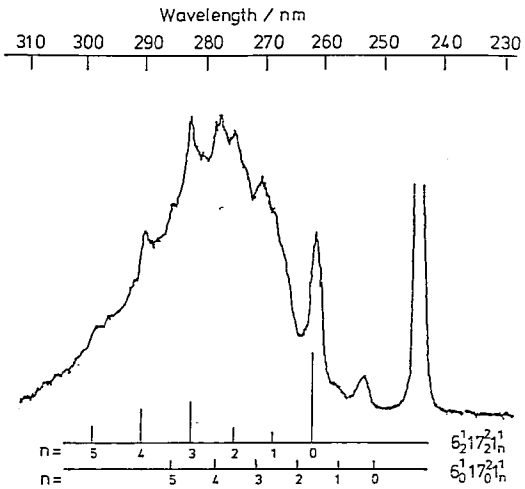

Figure 1. Fluorescence spectrum resulting from excitation of the $6_0^1 17_0^2 1_0^1$ transition at 244.8 nm. The height of the vertical bars on the line representing the $6_2 17_2 1_n$ fluorescence progression corresponds to the expected intensity for the members of every $1^1 \rightarrow 1_n$ progression. The scattered light signal at the excitaiton wavelength has not been drawn in fully. Sample presssure 90 mTorr. Ungated spectrum.

III—C Dynamic Behavior of Excited States

Optical excitation of molecules to electronic excited states causes a variety of dynamical behavior, depending on electronic structures and environments, such as energy transfer, proton transfer, chemical reaction, radiationless transition, ionization and others. Most of these proceses fall into the picosecond time scale. In this section energy transfer of submonolayer dye on single crystals and of dyes in micelles, photoionization and photoreduction in solution, solvent-solute interaction, solvent effect on nonradiative relaxation, and decomposition reaction in the gas phase are investigated either with combination of a mode-locked Nd: YAG laser and a streak camera or with that of a synchronously pumped picosecond dye laser and a time-correlated photon counting system.

III-C-1 Picosecond Fluorescence Measurement of Submono- and Monolayer of Adsorbed Rhodamine B on a Single Crystal of Naphthalene and on Glass

Klaus KEMNITZ, Toshiro MURAO, Iwao YAMAZAKI, Nobuaki NAKASHIMA, and Keitaro YOSHIHARA

[*Chem. Phys. Lett.*, **101**, 337 (1983)]

Fluorescence quenching of adsorbed rhodamine B (RhB) due to energy transfer from fluorescing monomer and dimer to nonfluorescing aggregate species was observed and explained with Förster-type energy transfer. The fluorescence lifetime of adsorbed RhB decreased with increasing coverage. The fluorescence of rhodamine B dimer could be detected at 300 K and two types of adsorbed monomer were found to exist at ambient temperature, as it was elucidated from measurements at very low coverage.

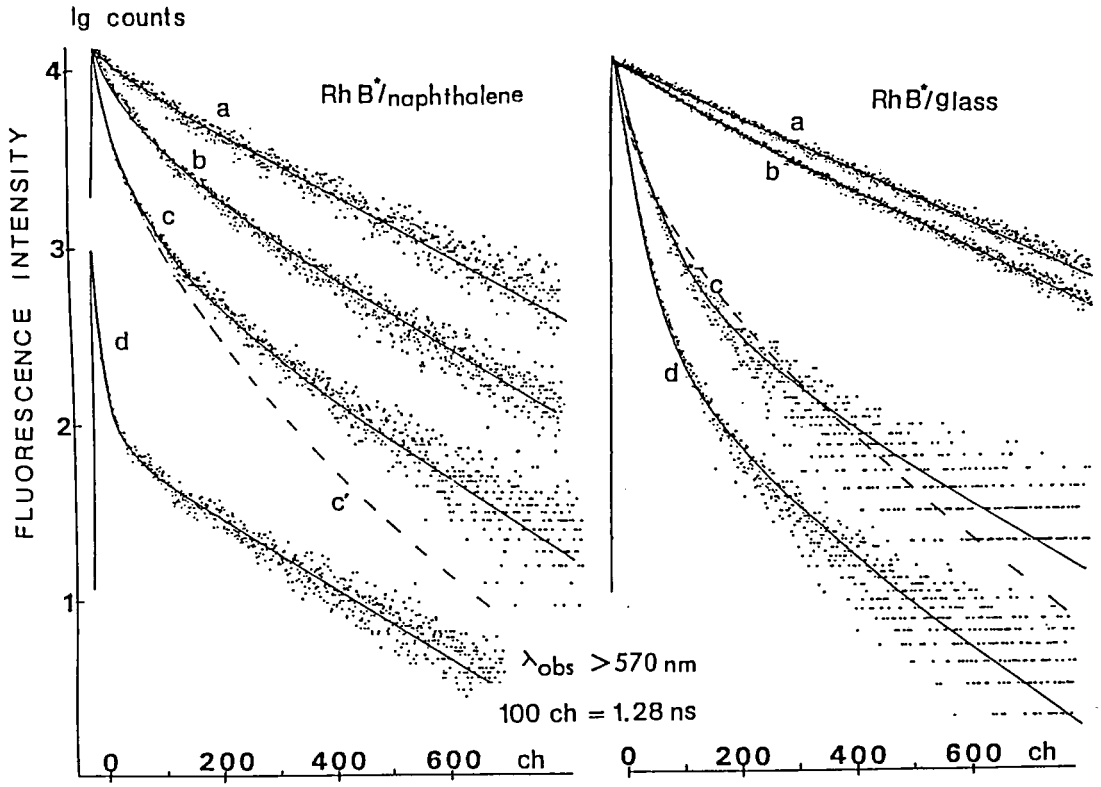

Figure 1. Coverage dependent fluorescence decay on naphthalene and glass at 300 K; λ_{ex} = 550 nm
naphthalene: $\theta \sim$ 0.01, 0.1, 1, > 1 (from a to d)
glass: $\theta \sim$ 0.007, 0.07, 0.65, 1 (from a to d)

III-C-2 Interaction of Cationic Dye and Anionic Detergent above and below the Critical Micelle Concentration as Revealed by Fluorescence Characteristics

Hiroyasu SATO, Masahiro KAWASAKI, Kazuo KASATANI *(Mie Univ.)*, **Nobuaki NAKASHIMA, and Keitaro YOSHIHARA**

[*Bull. Chem. Soc. Jpn.*, in press]

The interaction of 3, 3′-diethylthiacarbocyanine iodide (DTC), a cationic dye, with sodium dodecylsulfate (SDS), an anionic detergent, was studied as a funciton of the concentration of SDS ([SDS]) above and below the critical micelle concentration (cmc). The [SDS]-dependent fluorescence spectra, quantum yield and decay measurements revealed the deaggregation of the dye above the cmc and the formation of the dye-SDS aggregate below the cmc. Some of the fluorescence decay characteristics of the dye with different SDS concentratin are shown in Figure 1.

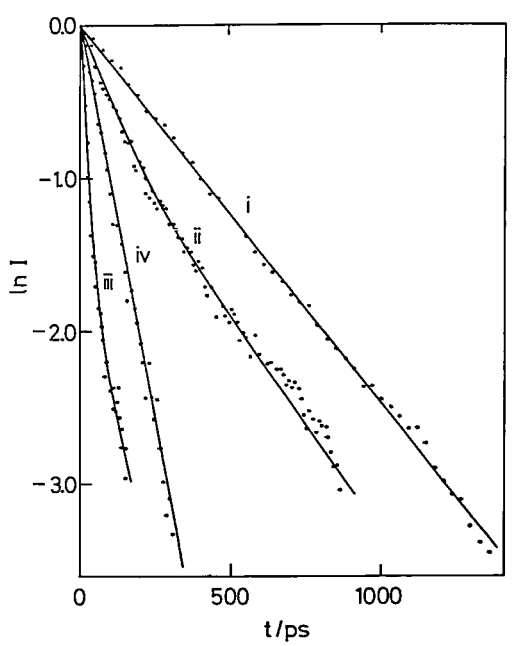

Figure 1. Fluorescence decay curves of DTC-SDS solutions. (a) [DTC] = 5.0×10^{-1}M, (i) [SDS] = 1.0×10^{-2}M, (ii) 8.0×10^{-3}M, (iii) 5.0×10^{-3}M, (iv) 0 M;

III-C-3 Photoreduction of Polyhalogenated Anthraquinones by Direct Electron Transfer from Alcohol

Haruo INOUE, Kenji IKEDA, Hayao MIHARA, Mitsuhiko HIDA *(Tokyo Metropolitan Univ.)*, **Nobuaki NAKASHIMA, and Keitaro YOSHIHARA**

[*Chem. Phys. Lett.*, **95**, 60 (1983)]

Polyhalogenated anthraquinones such as perfluoro-anthraquinone, 1,2,3,4-tetrafluoroanthraquinone, and 1,2,3,4-tetrachloroanthraquinone are photoreduced in ethanol via direct elecron transfer from ethanol. A dramatic switch-over from hydrogen-atom abstraction to electron transfer is induced by mixing of $\pi\pi$ with $n\pi^*$ states in their T_1 state and the enhanced electron-accepting character of polyhalogenated anthraquinones. Some of the important characters of these molecules are summerized in Table I.

Table I. The relative $n\pi^*$ character and the electron accepting character in the lowest excited triplet states of the anthraquinones.

Anthraquinones	$k_q/k_q(AQ)$ (Relative $n\pi^*$ character) in CCl_4	in CH_3CN	$E_{1/2}^*$ vs SCE[a] Volt	$\Delta E_{1/2}^*$[b] kJ/mol	Type of reaction in ethanol
AQ	1.0	1.0	1.78	0	H. A.[c]
F_4AQ	0.58	0.92	1.90	−11.6	E. T.[d]
F_8AQ	0.64	0.75	2.00	−21.2	E. T.
Cl_4AQ	0	0	< 1.70	> + 7.7	E. T.

a) Estimated reduction potential of the lowest excited triplet state of the anthraquinones.
b) $\Delta E_{1/2}^* = E_{1/2}^*(AQ) - E_{1/2}^*$ in kJ unit.
c) H. A. : Hydrogen abstraction
d) E. T. : Electron transfer

III-C-4 Photoionization Mechanism of TMPD in Acetonitrile

Shigemasa NAKAMURA, Nobuaki KANAMARU, Sawako NOHARA, Hiroki NAKAMURA, Yasuyoshi SAITO, Jiro TANAKA *(Nagoya Univ.)*, **Minoru SUMITANI, Nobuaki NAKASHIMA, and Keitaro YOSHIHARA**

Photoionization mechanism of TMPD in acetonitrile solution was investigated by fluorescence lifetime, picosecond and nanosecond laser photolysis and photocurrent measurements. The temperature dependence of fluorescence lifetime was interpreted by thermally activated mono-photonic ionizatin or ion-pair formation mechanism from $S_{1,0}$ excited level. As shown in Figure 1 picosecond laser photolysis clearly showed that a direct ionization from higher S_1 levels took place before relaxation into the $S_{1,0}$ level. The relative yields of triplet, ion-pair and cation formation were estimated from analysis of transient spectra and photocurrent.

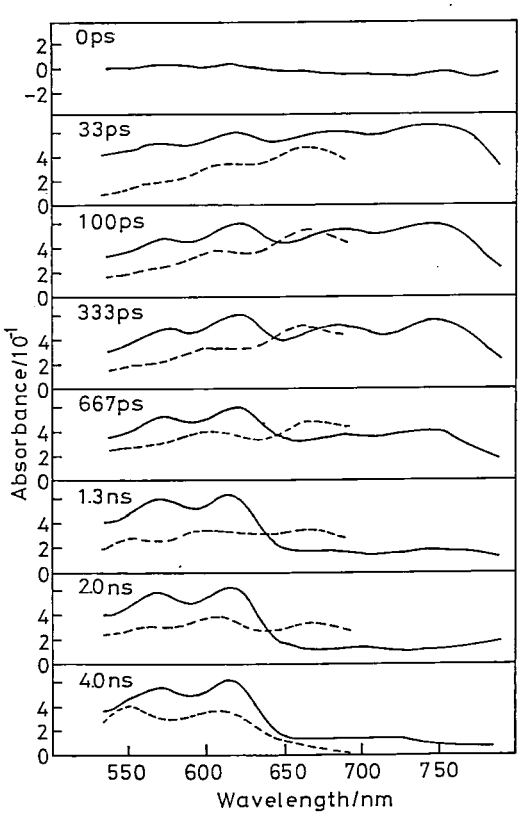

Figure 1. Transient spectra of photolyzed TMPD measured with MCPD system in acetonitrile (——) and in n-hexane (– – –) solutions.

III-C-5 Picosecond Dynamic Stokes Shift of α-Naphthylamine

Tadashi OKAMURA *(Tokyo Zokei Univ.)*, **Minoru SUMITANI, and Keitaro YOSHIHARA**

[*Chem. Phys. Lett.*, **94**, 339 (1983)]

The time-resolved fluorescence Stokes shift of α-naphthylamine in polar solvents has been measured at room temperature using a mode-locked Nd: YAG laser and a streak camera. Fluorescence spectra show a red-shift with an exponential rise time of 52 ps in isopropanol at 295 K as shown in Figure 1. The rate of the relaxation process involved in the Stokes shift appears to be dependent on the extent of the change in dipole moment of the solute upon excitation.

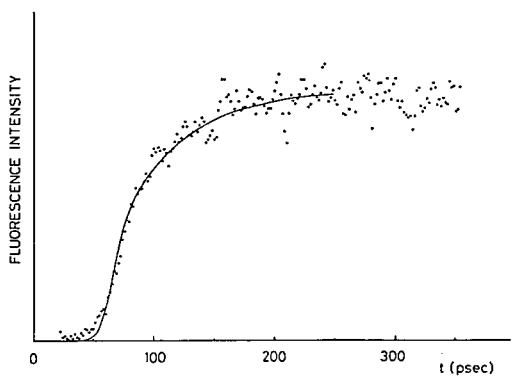

Figure 1. Fluorescence profile of α-naphthylamine in isopropanol at 460 nm. Observed values are represented by dots, and the solid line is a calculated profile according to a relaxation time of 52 ps. Fluorescence was detected through a short-cut filter (Toshiba UV-46).

III-C-6 Solvent Effects on the Nonradiative Relaxation Processes of the Lowest Excited Singlet States of Meso-substituted Bromoanthracenes

Kumao HAMANOUE, Toshiharu HIDAKA, Toshihiro HAKAYAMA, Hiroshi TERANISHI *(Kyoto Inst. Tech.)*, **Minoru SUMITANI, and Keitaro YOSHIHARA**

[*Bull. Chem. Soc. Jpn.*, **56**, 1851 (1983)]

From the measurements of the fluorescence lifetimes and the 0-1 emission maxima in solutions, it is concluded that the solvent dependence of the nonradiative transition rates of the lowest excited singlet states of 9-bromoanthracene and 9,10-dibromoanthracene is due to the different extent to which the lowest excited singlet and adjacent higher excited triplet states are stabilized by solvents. Fluorescence decay curve of 9-bromoanthracene in acetonitril is shown in Figure 1.

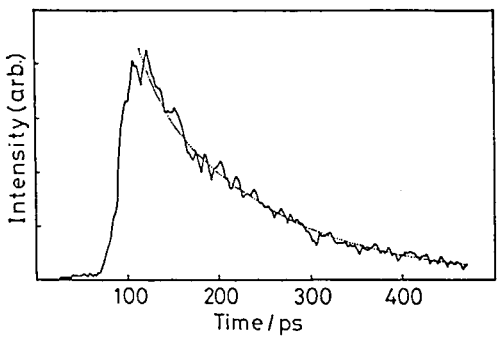

Figure 1. Fluorescence decay curves of 9-bromoanthracene in acetonitrile at 296 K. —; Observed curve by a streak camera, ...; simulated curve based on a single exponential decay with $k = 6.25 \times 10^9 s^{-1}$.

III-C-7 Decomposition Rate of Benzyl Chloride Excited at 266 nm in the Vapor Phase

Tei-ichiro ICHIMURA, Yuji MORI *(Tokyo Inst. Tech.)*, **Minoru SUMITANI, and Keitaro YOSHIHARA**

[*J. Chem. Phys.*, in press]

Picosecond laser photolysis of benzyl chloride vapor has been examined by monitoring the transient absorption time porfile of benzyl radicals formed in the 266 nm photodecomposition. The rise time (6 ns) of benzyl radical absorption shown in Figure 1 was attributed to the decomposition rate of benzyl chloride molecules excited at 266 nm under collision free conditions.

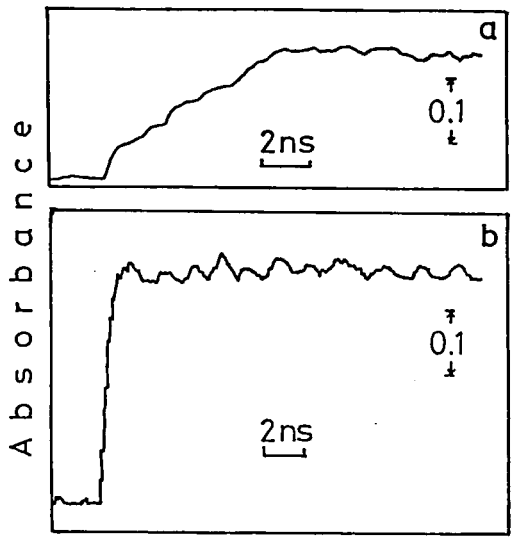

Figure 1. Time-resolved absorption of benzyl radicals in the 266 nm laser photolysis of benzyl chloride. (a) time evolution of the benzyl radical absorption $\log_{10} [I_0/(I_b - I_f)]$ where I_f was normalized for the laser light intensity and I_b was normalized to I_0 at the initial four data points before the laser excites benzyl chloride. (b) rise of the benzyl radical absorption in n-Hexane observed at 315 nm after the photolysis of benzyl chloride. Sample pressure was 0.5 Torr.

III—D Solar Energy Conversion by Using Photocatalytic Effects of Semiconductors and Dyes —Decomposition of Water and Hydrogen Evolution—

Essential roles are played by semiconductors and dyes in the photocatalytic effects to which a particular attention has been paid in connection to the direct conversion of solar energy to chemical energy. One of the most important applications is the water splitting reaction. Photocatalytic reactions of water with various organic compounds are also interesting not only from the view point of hydrogen production but also from that of the application to organic synthesis. In order to elucidate the mechanism of these photocatalytic reactions, we need detailed knowledges on the electronic structures of adsorbed molecules, the fundamental processes of photoinduced electron transfer at the semiconductor-liquid interface and catalysis on the surface. Work on the following topics is in progress with the purpose of clarifying the photocatalytic effects of semiconductors and dyes from the view point of solar energy conversion.

III-D-1 Mechanism of Hydrogen Production from Water with Fluorescein Derivatives as Photocatalysts

Kazuhito HASHIMOTO, Tomoji KAWAI, and Tadayoshi SAKATA

The efficient photocatalytic hydrogen production systems could be constructed by using halogenated fluorescein derivatives in the presence of a reduction catalyst such as Pt/TiO_2 and various reducing agents. These are stable and efficient in the high pH region.[1] The quantum yields of hydrogen production for erythrosin as a sensitizer are 12% and 0.15% with triethanolamine (TEOA) and ethanol, respectively. The components of these systems are very similar to those of dye-sensitized semiconductor system,[2] which is composed of a dye, a Pt/TiO_2 and a reducing agent, but the reaction mechanisms are quite different each other. The existence of a semiconductor is indispensable for the latter system although colloidal Pt and Pt/SiO_2 serve as reduction catalysts for the present system. We measured the transient absorption spectrum and the time behavior of the intermediate species (Figure 1), and confirmed the reaction processes of the hydrogen production as follows. The excited dyes are photo-reduced to stable semi-reduced radicals with a life time of more than ten seconds, so that these dyes can serve as both photosensitizers and electron relays. The radical formed in the bulk solution diffuses to the surface of the catalyst initiating in the electron transfer in the hydrogen production system. These processes are very similar to those of a photogalvanic cell, so that

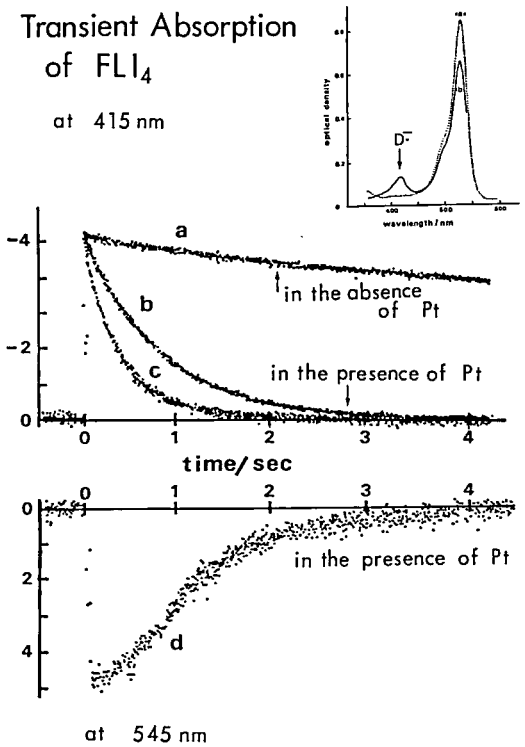

Figure 1. Transient absorption of erythrosin (FII_4) in the presence of TEOA.
(a), (b), (c): semi-reduced dye, (d): original ground state dye

we call this a photogalvanic type hydrogen production system.

References

1) K. Hashimoto, T. Kawai and T. Sakata, *Chem. Lett.*, 709 (1983).
2) K. Hashimoto. T. Kawai and T. Sakata. *Nouv. J. Chim.*, **7**, 249 (1983).

III-D-2 Photoelectrochemical Cell Composed of Fluorescein Derivatives

Kazuhito HASHIMOTO, Tomoji KAWAI, and Tadayoshi SAKATA

Halogenated fluorescein derivatives are reduced to stable semi-reduced dyes under visible light illumination in the presence of various kinds of reducing agents. By making use of a high reducing power of the semi-reduced radicals, relatively efficient photoelectrochemical cells could be constructed in the high pH region. The cells are composed of the dyes and TEOA as sensitizers and a reducing agent, respectively. The open voltage and the quantum yield of the current for the cell

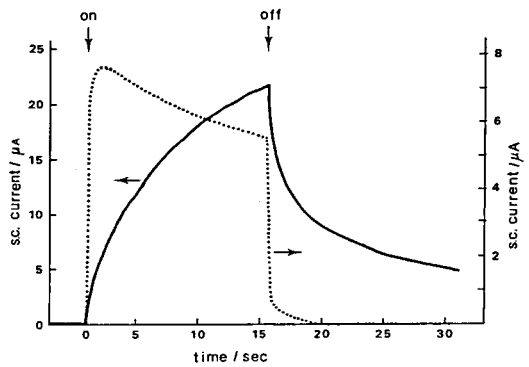

Figure 1. Time response of photocurrent by irradiation.
solid curve : <ZnO |Eosin-Y, TEOA| Pt>
dotted curve : <ZnO |Rose bengal, EDTA| Pt>

used eosin Y as a sensitizer are about 1V and 21%, respectively. These cells show the behaviors of photogalvanic type cell as follows. (1) A Pt plate as well as semiconductor also serves as a light electrode. (2) The time response of the photocurrent is very slow. The solid curve in Figure 1 shows the change of photocurrent with irradiation. The current arises and decays very slowly with the on-off of the light, taking about several minutes to become constant. This behavior agrees with that for the typical photogalvanic cell with an irreversible reducing agent. On the other hand, the cell composed of rose bengal and EDTA as a sensitizer and a reducing agent, respectively, shows the very fast photo-response behavior (dotted curve). This clealy indicates that the hydrogen production system composed of rose bengal, Pt/TiO_2 and EDTA is based on the dye-sensitization effect of semiconductor and its reaction mechanism is quite different from that of the system composed of a halogenated fluorescein derivatives, Pt/TiO_2 and TEOA.

III-D-3 Photocatalytic Reactions of Aliphatic Hydrocarbons with Water

Kazuhito HASHIMOTO, Tomoji KAWAI, and Tadayoshi SAKATA

When aqueous solutions of linear saturated hydrocarbons were irradiated in the presence of Pt/TiO_2 photocatalyst, CO_2 and H_2 were produced from an early stage of irradiation (Figure 1). The

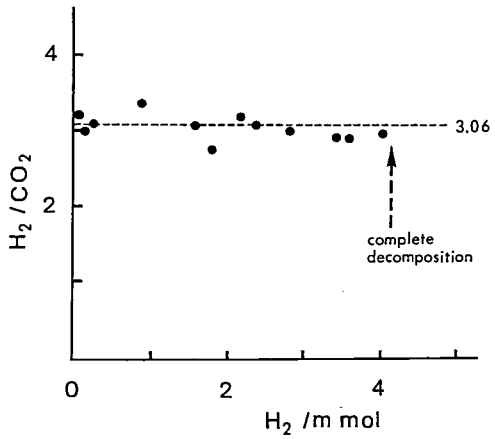

Figure 1. Ratio of H_2 to CO_2 produced during the complete decomposition of n-hexadecane ($C_{16}H_{34}$).
Neutral aq. soln., light source: 1 kW Xe lamp, photocatalyst: Pt/TiO_2, total irradiation time: ~700 hrs.

ratio of CO_2 to H_2 was constant during the irradiation. In order to elucidate the mechanism of the above phenomenon, the photocatalytic oxidation of the hydrocarbons in water were studied in the presence of silver ion as an electron acceptor. The products both in gas and liquid phase were analysed. Alcohols, aldehydes and carboxylic acids were detected. These products were much more reactive than aliphatic hydrocarbons. Thus once an aliphatic hydrocarbon is oxidized to an alcohol, this might be oxidized to an aldehyde and a carboxylic acid successively. CO_2 was produced through photo-Kolbe reaction of the produced carboxylic acids. The above consideration explains well the results of the product analysis and the result of the complete decomposition of n-hexadecane.

III-D-4 Photocatalytic Oxidation of Benzene in Water

Kazuhito HASHIMOTO, Tomoji KAWAI, and Tadayoshi SAKATA

Benzene is easily oxidized to CO_2 with the near UV light irradiation in the presence of TiO_2 powder by the photocatalytic reaction with water, although benzene itself is known to be very stable against near UV light. CO_2 is produced from an early stage of irradiation. We carried out product analysis for several aromatic compounds in the presence of silver ion. For example, biphenyl (3.0 μmol), phenol

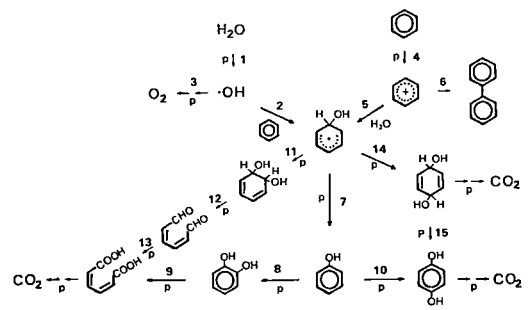

Figure 1. Reaction scheme of photocatalytic oxidation of benzene in water.

(21 μmol), catecohol (1.0 μmol), hydroquinone (13 μmol) and muconic acid (1.0 μmol) were detected for the decomposition of benzene after 1 mmol of silver ion was consumed. We also measured the CO_2 and O_2 production rates by using several semiconductor powders as photocatalysts. The relative reactivities of the reactants could be also determined from the rates of oxygen production which is in competition with oxidation of the reactants. Based on these results, the oxidation process of benzene is presented as follows. First hydroxycyclohexadienyl radical is formed by both the addition of OH radical to benzene ring and the direct oxidation of benzene by photogenerated holes. This radical is oxidized to phenol, muconic acid or hydroquinone by the photogenerated holes directly as is shown in Figure 1. It is considered that CO_2 production occurs mainly by way of muconic acid through the path 11-12-13 in Figure 1, resulting in photo-Kolbe type decomposition of the acid. The reactivities of the intermediate products are much more larger than that of benzene, so that these reactions proceed successively.

III-D-5 The Valence Band Position of Anatase TiO_2

Tadayoshi SAKATA, Tomoji KAWAI, and Kazuhito HASHIMOTO

[*J. Phys. Chem.*, in press]

The energy structure of anatase is not clear, because of the difficulty of preparing an anatase electrode. As shown in Equation 1, the valence band of rutile is located deep and the photo-

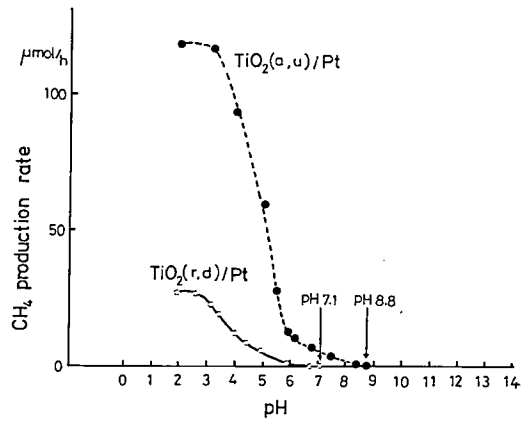

Figure 1. Dependence of methane production rate on pH for the photocatalytic decomposition of acetic acid in aqueous medium.
30 ml of a water-acetic acid mixture (6 : 1 in volume) with 300 mg of TiO_2/Pt was irradiated with a 500W Xe lamp. The pH of the mixture, which was controlled by adding NaOH or H_2SO_4, hardly changed after each experimental run (1 hour irradiation).

generated holes in the valence band has an enough power to oxidize CH_3COO^-.

$$U_{vb} = +2.79 - kT/e \cdot [pH] \quad V \text{ vs NHE} \qquad (1)$$

However, the oxidation power of the photogenerated holes decreases with increasing pH, since the valence band is shifted in the negative direction according to Equation (1). Therefore, at high pH, the oxidation of CH_3COO^- becomes difficult and the oxidation of OH^- ($OH^- + p \rightarrow \cdot OH$) begins to overwhelm that of CH_3COO^-, since the valence band of TiO_2 is located deeply enough to oxidize OH^- even under alkaline conditions. Figure 1 shows the dependence of CH_4 production rate on pH. As seen in this figure, CH_4 is not produced above pH 8.8 for anatase and pH 7.1 for rutile. The pH value above which methane formation is prevented, relates presumably to the critical potential of the oxidation of CH_3COO^-. When the pH value of 7.1 for rutile is used in Eq. (1), 2.37 V vs NHE is obtained as the potential of the valence band. If direct oxidation by the photogenerated hole in the valence band is assumed, this potential is thought to be equal to the critical potential of the oxidation of CH_3COO^- on the rutile surface in aqueous medium. If the critical potential of the oxidation of CH_3COO^- on the anatase surface is the same with that on the rutile surface, the valence band must be located at 2.37 V vs NHE at pH 8.8. Since the valence band edge of rutile at pH 8.8 is estimated to be located at 2.27 V vs NHE from Equation (1), the valence band of anatase is located more deeply by 0.1eV than that of rutile, which explains well the difference in the photocatalytic activity between them.

III-D-6 Difference in Photocatalytic Activity between Rutile and Anatase TiO_2

Tadayoshi SAKATA, Tomoji KAWAI, and Kazuhito HASHIMOTO

Remarkable differences were observed in the photocatalytic activities between rutile and anatase TiO_2. Table 1 shows the results. The photocatalytic activity of anatase for CH_4 production form acetic acid is very high compared with that of rutile as was already reported by Krauetler and Bard. Besides the photocatalytic activity, difference was also observed in the ratio of H_2 to CH_4: For rutile the ratio is 1.0 and for anatase 0.2 at pH 2.1. On the other hand, the same photocatalysts behaved differently for the hydrogen production from ethanol-water mixture. The rutile showed a higher activity in this case. One of the possible explanations to this interesting result might be that this difference in the photocatalytic activity is brought about by the difference in the energy structure. From the pH dependence of CH_4 production from acetic acid, the valence band of anatase was estimated to be located deeper by 0.1 eV than that of rutile, which is critical to the oxidation of acetic acid because of the large positive oxidation potential (2.05 ~ 2.7 V vs NHE). On the other hand, the oxidation of ethanol is very easier than acetic acid. ethanol is decomposed efficiently by CdS/Pt photocatalyst, although the valence band of CdS is located more negatively than that of TiO_2 (rutile) in aqueous medium. Therefore the rate of hydrogen production from an ethanol-water mixture is limited by the reduction rate of water (H_3O^+) on Pt on the semiconductors. This result seems to indicate the possibility of increasing the selectivity in reaction by choosing an appropriate semiconductor photocatalyst.

Table I. Difference in photocatalytic activity between rutile and anatase.[a)]

Reactant	photocatalyst[d)]	H_2 production rate (μmol/h)	CH_4 production rate (μmol/h)
CH_3COOH[b)]	TiO_2 (r, d)/Pt	19	18
	TiO_2 (a, u)/Pt	23	119
C_2H_5OH[c)]	TiO_2 (r, d)/Pt	1410	—
	TiO_2 (a, u)/Pt	456	—

a) A 500W Xe lamp was used as a light source.
b) CH_3COOH: 6 ml, H_2O: 30 ml
c) C_2H_5OH: 15 ml, H_2O: 15 ml
d) photocatalyst: 300 mg
r = rutile, a = anatase, d = doped, u = undoped

III-D-7 Application of Photocatalytic Reaction to Organic Synthesis

Tadayoshi SAKATA, Tomoji KAWAI, and Kazuhito HASHIMOTO

[*J. Phys. Chem.*, in press]

Photocatalysis on semiconductor surface is essentially a redox reaction. Accordigly, not only H_2 production from water but also the application of photocatalysis to CO_2 and N_2 fixation has been investigated. Futhermore, a variety of photocatalytic reactions with organic substances has been developed. We carried out photocatalytic reactions of several organic acids in aqueous medium in the presence of a strong electron acceptor such as Ag^+. For the photocatalytic reaction of acetic acid, glycol acid, propionic acid and succinic acid were formed. Their formation can be reasonably explained by the reaction of ·OH and ·CH_3 (Figure 1 (a)). From the analogous reactions, two isomeric radicals, ·CH_2CH_2COOH and $CH_3\dot{C}HCOOH$, are expected to be formed for the photocatalytic reactions of C_2H_5COOH (Figure 1 (b)). Acturally, both compounds were detected in the aqueous medium. These reactions are interesting from the view point of organic synthesis because the number of carbon is increased in the products compared with that in the starting material. Formation of succinic acid from fumaric acid was also succeeeded in by the hydrogen addition to the unsaturated bond with powdered semiconductor photocatalyst (Figure 1 (c)).

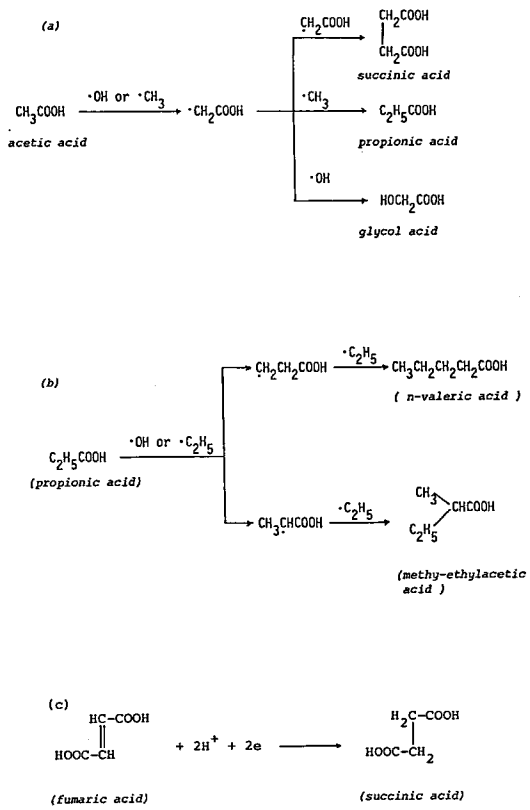

Figure 1. Several examples of photocatalytic reaction products which are interesting from a view point of organic synthesis.
a) Formation of succinic acid, propionic acid and glycol acid by the photocatalytic reaction of acetic acid.
b) Formation of n-valeric acid and methyl-ethylacetic acid by the photocatalytic reaciton of propionic acid.
c) Hydrogen addition fumaric to acid by the photocatalytic process.

III-D-8 The Catalytic Role of RuO_2 on n-Type Semiconductor for Photocatalytic Oxygen Evolution

Tadayoshi SAKATA and Kazuhito HASHIMOTO

RuO_2 is well known as a good oxidation catalyst for O_2 evolution because of the particularly low over voltage. In recent years RuO_2 on particulate TiO_2 (or CdS) has often been used for photocatalytic water splitting. In these systems RuO_2 has been considered to play as an oxidation catalyst. However, RuO_2 can work also as a good catalyst for hydrogen evolution. In order to elucidate the catalytic role of RuO_2 on n-type semiconductors, we measured the photoelectrochemical behavior of a single crystal TiO_2 (or CdS) by depositing a small amount RuO_2, together with the dependence of

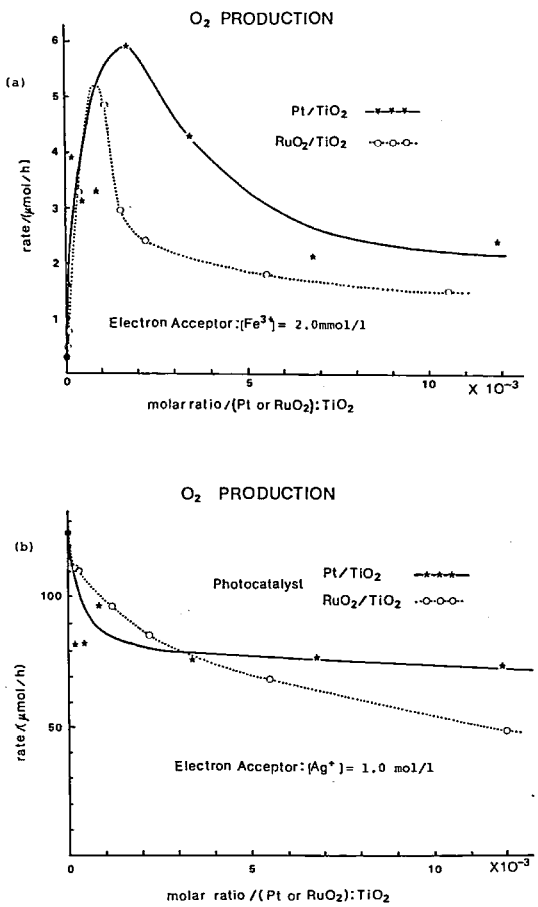

Figure 1. Dependence of the oxygen production rate on the molar ratio of RuO_2 (or Pt) to TiO_2

catalytic activity on the concentration of RuO_2 deposited on particulate TiO_2. For hydrogen evolution reaction, we had gotten a conclusion that RuO_2 functions as reduction catalyst under irradiation[1].

Figure 1 shows the dependence of oxygen evolution rate on the molar ratio of RuO_2 (or Pt) to TiO_2 (powdered system). For Ag^+ system, both RuO_2 and Pt on TiO_2 supress oxygen evolution as shown in this Figure. For Fe^{3+} system, the oxygen evolution rate is much smaller than that in the Ag^+ system. And Pt on TiO_2 has a better effect than RuO_2. The voltage of RuO_2 and Pt on a TiO_2 single crystal electrode was shifted in the negative direction in the presence of Fe^{3+} (or Ag^+) under irradiation. From these results, RuO_2 was concluded to be a reduction site even for oxygen evolution reaction in the presence of a strong electron aceptor such as Fe^{3+} and Ag^+. The maximum of the oxygen evolution rate, which was observed in the presence of Fe^{3+}, was interpreted by a rectifying action of the metal/semiconductor junction.

Reference

1) T. Sakata, T. Kawai and K. Hashimoto, *Denki kagaku*, **51**, 79 (1983)

III-D-9 Analysis of the Transient Response of a Semiconductor-Electrolyte Circuit to a Short Light Pulse: Application to CdSe Eelctrodes

Ronald H. Wilson *(G. E. and IMS)*, **Tadayoshi SAKATA, Tomoji KAWAI, and Kazuhito HASHIMOTO**

The photo transient response of a circuit with a semiconductor-electrolyte interface has been investigated in a number of previous reports. The experimental results have suggested that such measurements can provide important information about the rate constants for the various charge

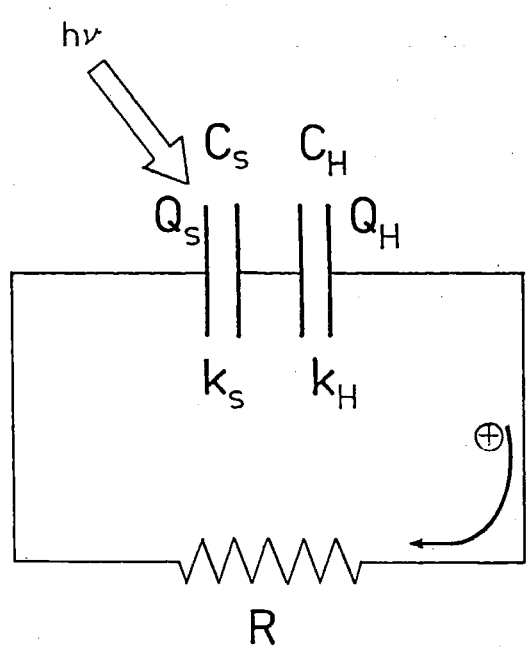

Figure 1. The model circuit used for the analysis.
Here, Q_s and C_s are the charge and capacitance at the depletion region of the semiconductor. Q_H and C_H are the charge and capacitance at the Helmholtz layer, respecively. k_s and K_H are the rate constant of the recombination and charge transfer, respectively. R is the total resistance of the circuit.

transfer processes involved. Here a model is developed and applied to experimental measurements using an n-type CdSe electrode. Figure 1 shows the model circuit used for the analysis. The fundamental equations which describe the transient behavior of the photocurrent are as follows.

$$Q_s/C_s + Q_H/C_H = iR \quad (1)$$
$$dQ_s/dt = -i - k_s (Q_s - Q_H) \quad (2)$$
$$dQ_H/dt = -i + k_H (Q_s - Q_H) \quad (3)$$

Using these equations and the initial conditions, we could obtain the solution in an analytical form. The model treats the system as a simple RC circuit with the depletion layer cpacitance and resistance internal and external to the cell. A short light pulse creates minority carriers in the semiconductor which rapidly move across the depletion region to change the potential across the depletion capacitance in a process faster than other processes in the circuit. Charge transfers across the Helmholtz capacitance, recombination of the photoexcited carriers or charge redistribution through the external circuit then occur with their own rates. Information available in the resulting external signal depends on the relative values of these rates and the relative size of the depletion and Helmholz capacitance. This model was found to explain well the photo transient response of the semiconductor electrode.

III—E Dynamical Processes in Electronically and/or Vibrationally Excited Molecules

III-E-1 Vibrational Randomization and Predissociation of Benzene Dimer

Iwao NISHIYAMA and Ichiro HANAZAKI

The predissociation of a vibrationally excited van der Waals molecule is one of current interests, since the rate is a direct measure of the intramolecular vibrational energy flow. We studied the infrared photodissociation of a benzene dimer by the combined use of a supersonic molecular beam and a CO_2 TEA laser. An absolute dissociation yield was determined by measuring the attenuation of parent beam intensity. Dissociation spectra were obtained by plotting the yield as a function of excitation wavelength (shown in Figure 1). The profile is well approximated by a single Lorentzian suggesting that the line shape is homogeneous. Additionally, a significant line broadening was observed as the laser fluecce was increased. The uncertainty-lifetime is evaluated to be 3.3 ps from the line width measured at a low laser fluence. The time should be responsible for the intramolecular energy randomization into the low-frequency mode of a benzene dimer. On the other hand, the predissociation-lifetime was estimated to be ca. 300 ns from the analysis of saturation broadening of the line shape on the basis of the rate equation. These observations suggest that the vibrational randomization occurs as the first step of energy flow and then predissociation follows slowly.

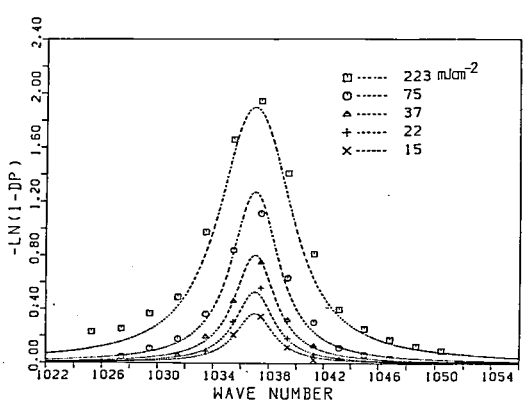

Figure 1. The dissociation spectra of benzene dimer as a function of laser fluence. In this figure, observed dissociation yields, **D**, are transformed to −ln (1-**D**), since the latter is proportional to absorption cross section. The broken lines are the calculation based on the rate equation.

III-E-2 Translational Energy Distribution of Benzene Produced by the Infreared-photo-dissociation of Benzene Dimer

Iwao NISHIYAMA and Ichiro HANAZAKI

Distribution of energy released among the fragments carries and important information for the understanding of molecular dissociation dynamics. In order to investigate the mechanism of vibrational predissociation of benzene dimer, time-of-flight spectra of the fragment (benzene monomer) were measured and analyzed to give a translational energy distribution. A typical spectrum observed near the direction of the parent molecular beam is shown in Figure 1. Translational energy distribution in a center-of-mass system was obtained by simulation analyses of the spectrum. As shown in Figure 1, satisfactory fit was obtained by using a Boltzmann function having an average energy of ca. 1 kJ/mol. The results indicate that the energy distribution has a maximum near the zero energy, only a small part of excess energy is released in the translational excitation. Namely, formation of the benzene monomer in vibrationally and/or rotationally excited states was strongly suggested,. This fact implies that the predissociation occurs through a vibrationally randomized state rather than through a direct coupling between the initially excited state and a dissociation continuum.

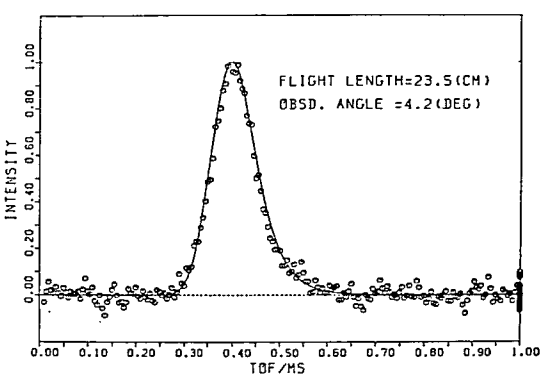

Figure 1. Time-of-flight spectrum of benzene monomer produced by the IR photodissociation of benzene dimer. The solid line is a calculated one assuming a Boltzmann type function.

III-E-3 The S_1, $^1A_2$ (n, π^*) state of Acetone in Supersonic Nozzle Beam

Masaaki BABA and Ichiro HANAZAKI

[*Chem. Phys. Letters,* in press]

In IMS Annual Review (1982), we reported the first observation of well resolved vibronic structure for the S_1, $^1A_2$ (n, π^*) state of acetone using a pulsed supersonic nozzle beam. In this report, we present improved spectra of $(CH_3)_2CO$ and $(CD_3)_2CO$ together with assignments of lower vibronic bands (Figure 1). The origins of the S_1 states of $(CH_3)_2CO$ and $(CD_3)_2CO$ are located at 30435 and 30431 cm^{-1}, respectively. Active vibrational modes are the CH_3 internal rotation (ν_{rot}) and the CO out-of-plane wagging (ν_{23}). Barrier hights to methyl internal rotation are 736 and 716 cm^{-1} for $(CH_3)_2CO$ and $(CD_3)_2CO$, respectively. These are much higher than those of the ground state, which is consistent with acetaldehyde.[1] We observed a

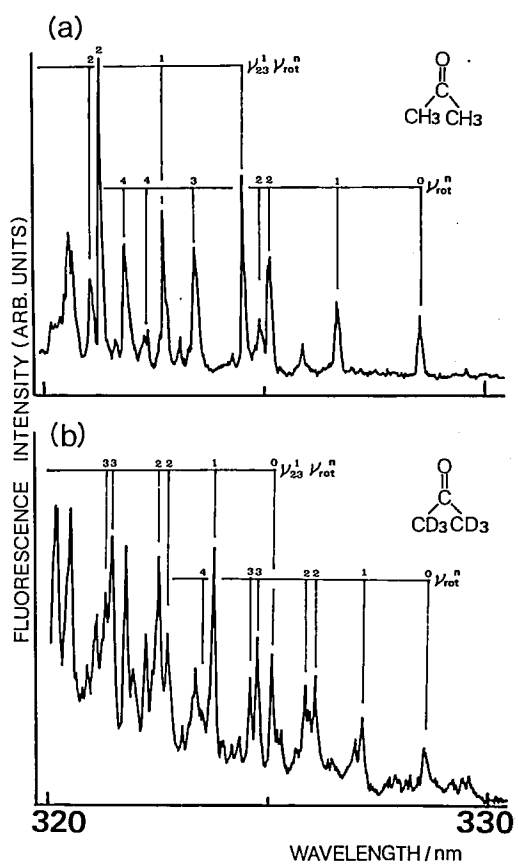

Figure 1. Fluorescence excitation spectra of (a) $(CH_3)_2CO$ and (b) $(CD_3)_2CO$ in Ar supersonic jet. The stagnation pressure is 4 atm and the temperature of nozzle is 50°C.

doublet for the v′ = 2 level with the splitting of about 20 cm^{-1}, which is presumably due to the interaction between two methyl rotors. The CO wagging (ν_{23}) fundamental frequencies of $(CH_3)_2CO$ and $(CD_3)_2CO$ are 373 and 327 cm^{-1}, respectively, which are rather close to the ground state values. The splitting of the origin band due to the double minimum potential has not been observed. It suggests that the barrier hight to CO out-of-plane wagging is much higher than that of formaldehyde or acetaldehyde.

Reference

1) M. Noble, E. C. Apel and E. K. C. Lee, *J. Chem. Phys.*, **78**, 2219 (1983)

III-E-4 Intensity of Local Mode Transition

Ichiro HANAZAKI

The concept of local mode has successfully been applied to the C-H stretching overtones in various organic molecules. We have made a series of measurements on methyl-substituted aromatic hydrocarbons and acetyl compounds.[1] We have concluded that the splitting of the methyl C-H stretching overtone is common for molecules with a plane of symmetry and ascribed to the inequivalent orientational sites of the C-H bond with respect to the molecular plane. In the course of this work, the light absorption probability of the local mode transition was shown to need more detailed investigation; *e.g.*, the relative intensities of the split components and the change of overtone intensity upon substitution of polar groups (*e.g.*, C = O, $-OC_nH_{n+1}$, *etc.*).

For the purpose of understanding the local mode intensity, we have chosen the bond dipole function

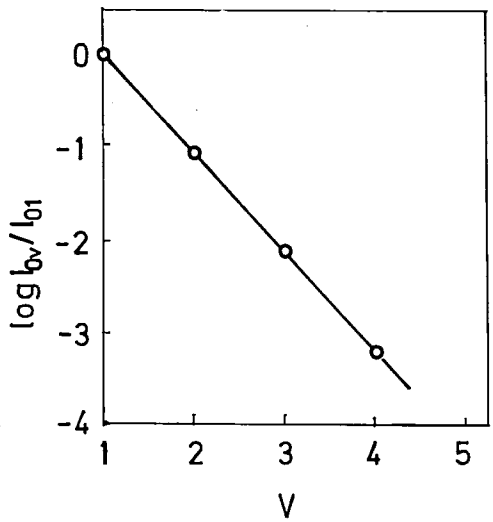

Figure 1. Relative intensity of the C-H stretching overtones of CH_2Br_2 (pure liquid). Solid curve is the calculated result with r* = 0.3 Å.

of the form;

$$\mu \sim r\exp(-r/r^*)$$

and gave a theoretical basis to this type of dipole function. Fitting of the function to the overtone intensities of CH_2Br_2 gave a satisfactory agreement with a parameter value of $r^* \approx 0.3$ Å, a reasonable value from the theoretical point of view (Figure 1).

In order to analyse relative intensities of split components, it seems to be necessary to take accounts of the interaction of two C-H local modes into the dipole function. This extension is now being developed on the same theoretica basis as above.

Reference

1) R. Nakagaki and I. Hanazaki, *Chem. Phys. Letters*, **83**, 512 (1981); Chem. Phys., **72** 93 (1982); *J. Phys. Chem.*, **86**, 1501 (1982).

III—F Study on Photochemical Processes Related to Planetary Space Chemistry

III-F-1 Photodetachment of Surface Molecules from Ice

Nobuyuki NISHI and Tohru OKUYAMA

Saturn's rings and some icy objects in space are surrounded by clouds of atomic hydrogen. Carlson suggested that the UV photosputtering mechanism is a probable explanation for the observed Lyman α grow.[1]. By using a ultra-high vacuum chamber equipped with a quadrupole mass spectrometer and a VUV laser at 193 nm, we have found that edge

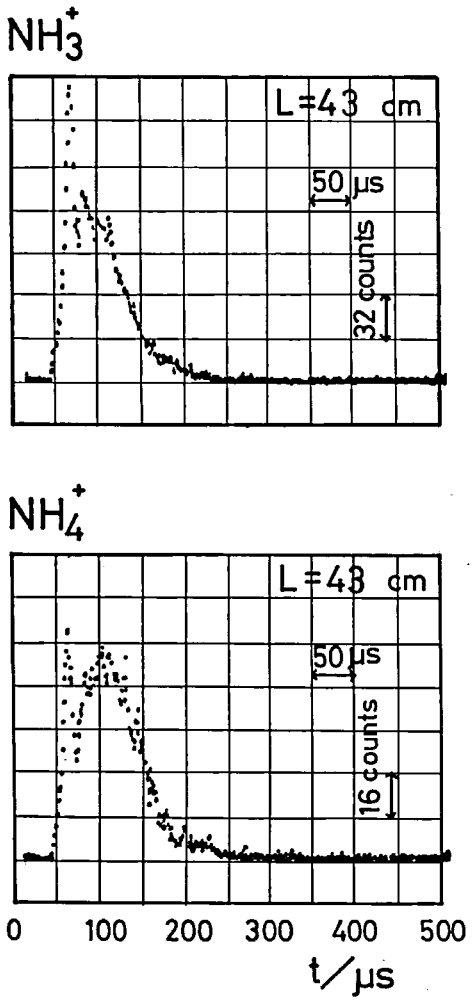

Figure 1. Time-of-flight spectra of NH_3^+ and NH_4^+ ejected from an NH_3 + H_2O (1 : 4) solid surface upon the irradiation of focused 193 nm laser (~1 J/cm^2).

molecules on ice surface are ejected upon the electronical excitation of surface and near surface molecules. Intermolecular interaction between the pair of an edge molecule and the inside molecule changes when one of the pair molecules is excited electronically. Upon the excitation, the overlap of the electron clouds of the pair molecules increases and the force due to electronical exchange repulsion interaction acts on the two molecules ejecting the edge molecule into the vacuum. Under the weak laser condition (0.1 ~ 10 mJ/cm^2), any ionic species was not detected in an NH_3 + H_2O (1 : 4) ice. By increasing the laser intensity (> 500 mJ/cm^2), the detachment of ions was observed at mass numbers 17 and 18. These ions are assigned to NH_3^+ and NH_4^+ respectively, by considering the ion-molecular reactions in the NH_3 + H_2O system. Figure 1 shows the time-of-flight spectra of the two ions. The peak energy of the main component is ~1 eV and the other component has a peak at ~4 eV. The most probable force acting on the cation must be Coulombic repulsion by another positively charged particle. The detachement yield of the ionic species was found to be about 10^{-7} of the yield of the detachment of neutral molecules at a laser fluence of 1 J/cm^2.

Reference

1) R. W. Carson, Nature 283, 461 (1980)

III-F-2 Formation of Heterocyclic Compounds Induced by UV Light Irradiation on Low Temperature Solids Containing Ammonia and Acetonitrile

Tohru OKUYAMA, Hisanori SHINOHARA, and Nobuyuki NISHI

VUV light from a 193 nm laser (20 mJ/cm^2, 10 ns) or a low pressure Hg lamp (185 nm) was irradiated on the solid containing NH_3 and CH_3CN at 77 ~ 130 K. Mass numbers and kinetic energies of the particles, ejected from the surface by the photon impact at 193 nm, were analyzed by a high resolution quadrupole mass spectrometer. Reaction products were identified by mass spectrometry (MS) and micro bore (1 mm) high performance liquid chromatography (HPLC). The following two different reactions between NH_3 and CH_3CN were identified as primary reactions in the solid.

$$NH_3 + CH_3CN \xrightarrow{h\nu} H_2NCH_2CN + H_2 \quad (1)$$

$$\xrightarrow{h\nu} CH_3C(=NH)NH_2 \quad (2)$$

Reaction (1) is a bimolecular condensation reaction and (2) an addition reaction of NH_3 to CH_3CN. The products determined by MS and HPLC were HCN, CH_3NH_2, $(HCN)_2$, $CH_3C(=NH)NH_2$, $(HCN)_4$, etc. Two isomers of $(HCN)_4$, diaminomaleonitrile (DAMN) and 4-amino-imidazole-5-carbonitrile (AICN) were detected, which are key precursores in the prebiotic syntheses of purins, amino acids, and peptides. Especially, AICN, which

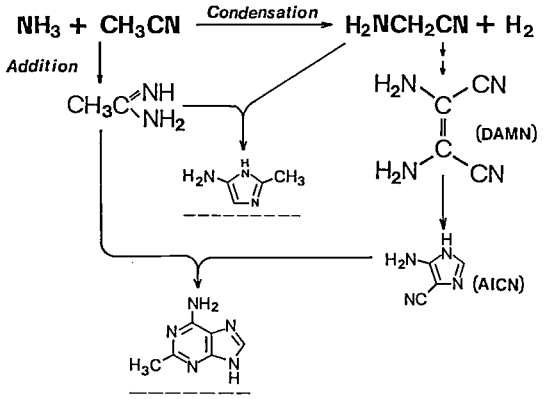

Figure 1. The scheme of the formation of heterocyclics by UV light induced reactions in the solid containing ammonia and acetonitrile (1 : 4).

is a five membered heterocyclic compound, has been known as a significant intermediate in the prebiotic synthesis of adenine[1]. The HPLC data indicated the presence of other heterocyclics, e.g., adenine derivatives. Figure 1 shows a scheme of the syntheses of heterocyclics in the solid.

Reference

1) J. P. Ferris and L. E. Orgel, *J. Amer. Chem. Soc.*, **88**, 1074 (1966).

III-F-3 Photochemistry of Solid Acetylene

Tohru OKUYAMA and Nobuyuki NISHI

Photochemistry of acetylene solid is particularly interesting in relation to the reactions on comet surface. A pulsed UV laser (193 nm) was irradiated on the pure acetylene solid at 110 K. Analysis of the primary products by GC-MS and laser photo-sputtering at 248 nm showed the formation of vinylacetylene, diacetylene and ethylene molecules. This observation is consistent with the gas phase reactions of C_2H_2 reported by Okabe.[1] The primary reaction processes may by explained by the following equations.

$$C_2H_2 \xrightarrow{h\nu} C_2H_2^* \longrightarrow C_2H_2^{**} \quad (1)$$

$$C_2H_2^{**} + C_2H_2 \longrightarrow HC{\equiv}C\text{-}CH{=}CH_2 \quad (2)$$

$$HC{\equiv}C\text{-}CH{=}CH_2^* + C_2H_2 \longrightarrow H\text{-}C{\equiv}C\text{-}C{\equiv}C\text{-}H + H_2C{=}CH_2. \quad (3)$$

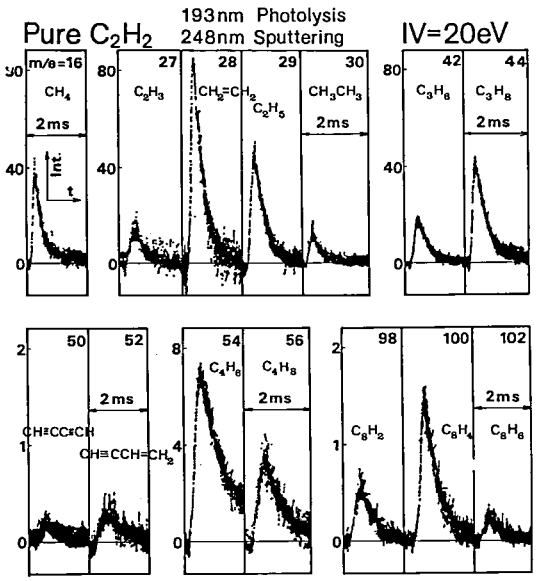

Figure 1. Time-of-flight spectra of photoproducts sputtered from the solid acetylene surface. Before the sputtering at 248 nm, 1×10^5 shots of weak laser pulse (193 nm, < 10 mJ/cm^2) were irradiated on the solid at 110K.
flight length = 16 cm.

The fluorescence lifetime of C_2H_2 in Ne matrix is reported to be 80 ± 5 nsec,[2] which is long enough to allow excitation energy transfer between acetylene molecules in the solid. The nature of $C_2H_2^{**}$ is not known but it must be the same as the metastable acetylene in gas phase.[1] Since the lowest excited state energy of vinylacetylene or diacetylene is lower than that of acetylene, excitation energy may be trapped in these molecules. Thus the reactions at the traps could occur very efficiently. Long exposure effects were investigated by the laser sputtering on the irradiated solid. After the irradiation of 1×10^5 shots of 193 nm laser pulses, the products were sputtered by 248 nm laser photons and detected by a quadrupole mass spectrometer (Figure 1). The product distribution was quite similar that obtained for the mercury lamp photolysis of C_2H_2 solids at 77-110 K. As well as polyacetylene compounds, saturated or nearly saturated hydrocarbons were formed in the solid.

References

1) H. Okabe. *J. Chem. Phys.*, **78**, 1312 (1983).
2) L. E. Brus, *J. Mol. Spectrosc.*, **75**, 245 (1979).

III-F-4 Detection of Hot-Hydrogen Atoms from UV laser Photodissociation of Ammonia at 193 nm

Hisanori SHINOHARA, Nobuyuki NISHI, and Akiyoshi MATSUZAKI* *(The Institute of Space and Astronautical Science*)*

Ammonia is abundant in the interstellar space and in the Giant Planets. Quantitative data for NH_3 photodissociation processes are indispensable for a better understanding of their photochemistry in these environments. The present investigations are concerned with the mechanism of the photo-

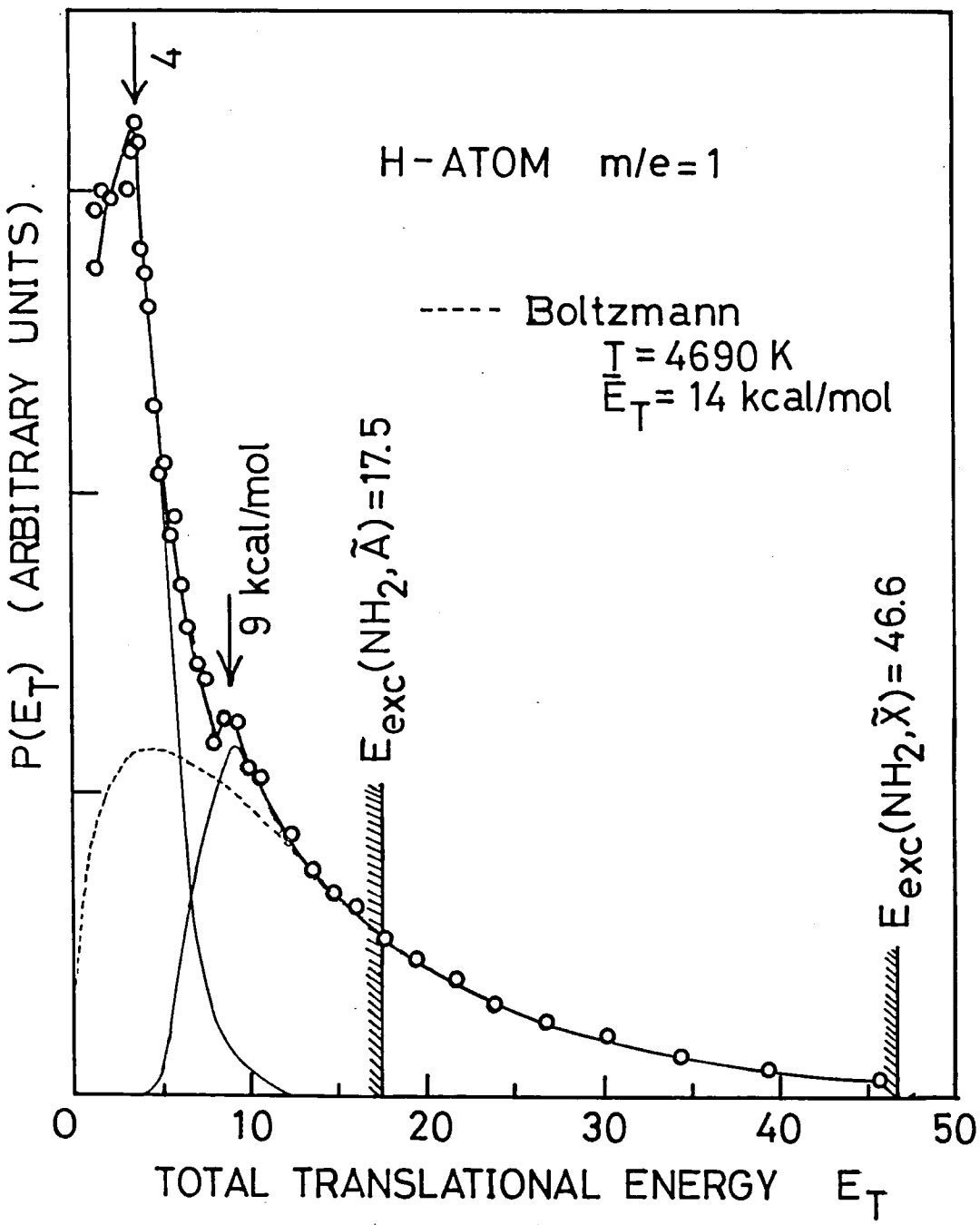

Figure 1. The distribution of total translational energy, P (E_T). Open circle plot originates from the laboratory TOF spectrum of H atom photofragments. The values of E_{exc} = 46.6 kcal/mol for NH_2 ($\tilde{X}$) and E_{exc} = 17.5 kcal/mol for NH_2 ($\tilde{A}$) are indicated by vertical lines. A Boltzmann distribution with a characteristic temperature of 4690 K is also indicated by a broken line for a comparison.

dissociation of ammonia in its first absorption band at 193 nm.

The total translational energy distribution of the following photodissociation process was determined by analysing the observed time-of-flight (TOF) spectrum of recoiling photofragments:

$$NH_3\ (\tilde{X}^1A_1') + h\nu\ (193\ \text{nm}) \longrightarrow NH_3^*\ (\tilde{A}^1A_2'',\ v = 6) \longrightarrow H + NH_2\ (\tilde{X}^2B_1,\ \tilde{A}^2A_1).$$

Both the TOF spectrum and the total translational energy distribution show bimodal distributions (Figure 1), suggesting two distinct photodissociation pathways. From the measurements of angular distribution of the H fragments it can be concluded that a sharp distribution peaked at 4 kcal/mol corresponds to the dissociation process of generating NH_2 ($\tilde{A}^2A_1$) radical, whereas a broad one ranging from 5 to 40 kcal/mol stems from the ground state of NH_2. Since the sharp distribution gives approximately $\sin^2\theta$ angular distribution, the excited state photodissociation process has a relatively short ($\lesssim$ 1 ps) predissociation lifetime.

III—G Photodissociation and Multiphoton Ionization Dynamics of Molecular Beams Initiated by UV Excimer Lasers

III-G-1 Photodissociation of Molecular Beams of Alkyl and Alkyne Halides

Masahiro KAWASAKI,* Kazuo KASATANI,* Hiroyasu SATO* *(Mi'e Univ.*)*, **Hisanori SHINOHARA, and Nobuyuki NISHI**

Molecular beams of halogenated hydrocarbons containing chloro and bromo atoms were photodissociated by an excimer laser at 193 nm. The molecules are HCCBr, $HCCCH_2Br$, C_2H_5Br, $HCCCH_2Cl$, C_2H_5Cl and C_3H_7Cl. The time-of-flight distributions of photofragments were measured to study primary processes and dissociation dynamics. Atomic mechanism (RX → R + X) is due to the direct excitation to the C-X repulsive state, while molecular elimination (RX → R′ + HX) is attributed to the indirect process: dissociation of the hot ground state molecule. The TOF distribution in Figure 1 is shown for C_2H_5Cl. HCl fragments have a slow and broad distribution, while Cl photofragments have a fast and narrow distribution. The difference between alkyne and alkyl halides is that the former has the larger quantum yield in the molecular elimination. It is attributed to involvement of triplet states in the photodissociation processes.

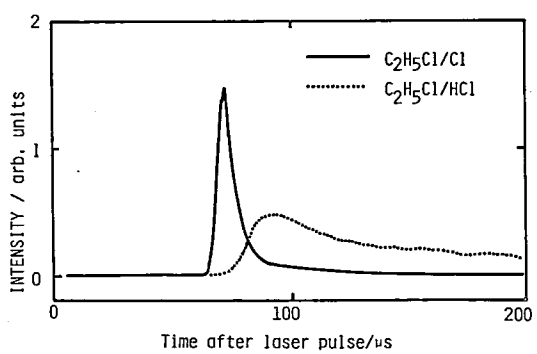

Figure 1. Time-of-flight distribution Cl and HCl in the photolysis of C_2H_5Cl at 193 nm.

III-G-2 Photofragmentation Dynamics of Cl_2SO at 193 nm

Masahiro KAWASAKI,* Kazuo KASATANI,* Hiroyasu SATO* *(Mi'e Univ.)*, **Hisanori SHINOHARA, and Nobuyuki NISHI**

Photofragment spectroscopy of Cl_2SO at a wavelength of 193 nm shows evidence for two decomposition pathways: (a) Cl + ClSO and (b) Cl_2 + SO. The TOF spectra of Cl, ClSO and SO were observed as signals of m/e = 35 (Cl^+) and 48 (SO^+) in a mass spectrometer detector as shown in Figure 1. From the Cl TOF signals, the maximum and averaged translational energies are 420 and 300 kJ/mol, respectively. Although the Cl-S bond

dissociation energy has not yet been known for process (a), the upper limit is estimated to be 200 kJ/mol from an equation, $D_0 = h\nu - (E_T)_{max.}$. This value is in good agreement with that estimated from similar compounds. An impulsive spectator model is consistent with $\overline{E_T}$ measured in precess (a). The results imply vibrationally excited CSCl fragment. For process (b) the translational energy distribution is statistical. It implies that dissociation must proceed through ground vibrationally excited parent molecules like formaldehyde photodissociation.

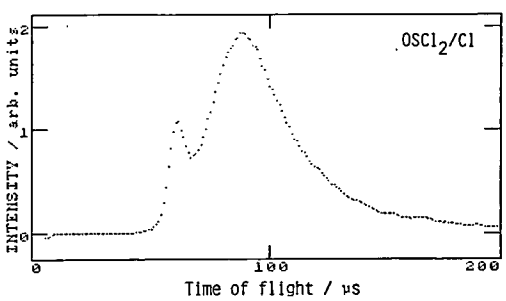

Figure 1. Time of flight distribution for m/e = 35 (Cl^+) in the photolysis of Cl_2SO at 193 nm.

III-G-3 Multiphoton-Ionization and Fragmentations of Acetone and Cyclic Ketones: Effects of One-photon Dissociation

Masaaki BABA, Hisanori SHINOHARA, Nobuyuki NISHI, and Noboru HIROTA *(Kyoto Univ. and IMS)*

[*Chemical Physics*, in press]

Resonantly enhanced MPI mass spectra of acetone and cyclic ketones have been investigated by using two exciting wavelengths (248 and 193 nm) which select the resonant intermediate states: $^1(n, \pi^*)$ or $^1(n, 3s)$ state. Because of the laser duration (~10 ns) longer than the dissociation period at the intermediate state (≤ 1 ns), MPI mass spectra of smaller ketones contain fragment ion peaks originated in the secondary photoionization of photofragments containing carbonyl group. The rate equations were solved for the ionization processes involving four parent-molecule states and four fragment states. The population of parent and fragment ions are expressed as functions of absorption cross sections, lifetimes, duration of laser pulse and laser power. The laser power dependence of parent and fragment signal intensities showed that the overall processes have the same bottle-neck in the first pumping stage. Population leakage due to the photodissociation from the intermediate state makes the signal intensity less sensitive to the increment of photon density. As the molecular size becomes larger, however, generation of fragment ions through the direct two-photon excitation becomes more important.

III-G-4 Multiphoton-Ionization Mass Spectroscopy of 2,4-hexadiyne at 248 and 193 nm: Wavelength Dependence on H atom Detachment

Yoshiya TAKENOSHITA *(Kitakyushu Univ.)*, **Hisanori SHINOHARA, and Nobuyuki NISHI**

Benzene is one of the most extensively studied molecules with multiphoton-ionization (MPI) mass spectroscopy. A most remarkable finding of this

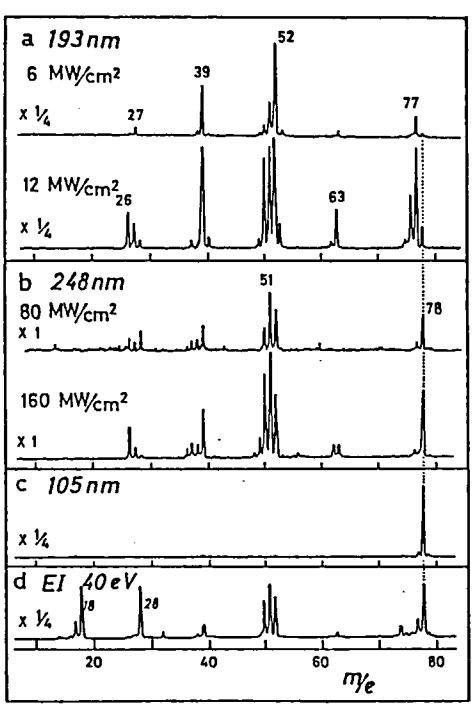

Figure 1. Multiphoton-ionization mass spectra of 2,4-hexadiyne at 248 and 193 nm (a, b). Spectra c and d are photoionization at 105 nm from Ar resonance lamp and the conventional 40 eV electron impact ionization, respectively.

molecule by the method is that extensive fragmentations occur during the MPI processes. We have obtained the MPI mass spectra of 2,4-hexadiyne, a benzene isomer.

Figure 1 presents typical MPI mass spectra of the molecule at 248 and 193 nm. For comparison a 40 eV electron impact mass spectrum as well as a vacuum UV photoionization spectrum at 105 nm are included in the figure. Ion intensities observed at 193 nm were fifty times as strong as those at 248 nm, which reflects the absorption cross sections of C_6H_6 at the both wavelengths. Overall spectral patterns of the MPI mass spectra of 2,4-hexadiyne are relatively similar to those of benzene. One of the striking features of the spectra, which is absent in the corresponding benzene spectra, is that the parent ion at m/e = 78 is either absent or very weak at the 193 nm MPI.

The measurement of fragmentation branching ratios for various isomers of $C_6H_6^+$ was done by Baer et al.[1] According to their study the statistical theory calculations are consistent with the assumption that this common precursor has the benzene structure. It is highly probable that H atom loss from $C_6H_6^+$ occurs at the so-called "metastable range" of the electronically excited $C_6H_6^+$.

Reference

1) T. Baer, G. D. Willet, D. Smith, and J. S. Phillips, *J. Chem. Phys.*, **70**, 4076 (1979).

III—H Formation and Properties of Hydrogen-Bonded Molecular Clusters Both in Supersonic Nozzle Beams and Inert-Gas Matrices at Low Temperatures

III-H-1 Infrared Spectra of Cryodeposited Thin Film of Ammonia: Temperature Dependence on Solid NH_3 Phases

Teruhiko NISHIYA *(Kyoto Univ.)*, **Noboru HIROTA** *(Kyoto Univ. and IMS)*, **Hisanori SHINOHARA, and Nobuyuki NISHI**

Ammonia, in its condensed states, is a major constituent of the clouds of the Jovian planets. The 8.5 ~ 11.5 μm spectral region of the Saturn's IR spectrum coincides with a similar feature in laboratory spectra of solid ammonia. There has been, however, an apparent contradiction that exists between laboratory spectra for solid NH_3 and actual observations for the upper cloud of Saturn at the 3.0 μm region.

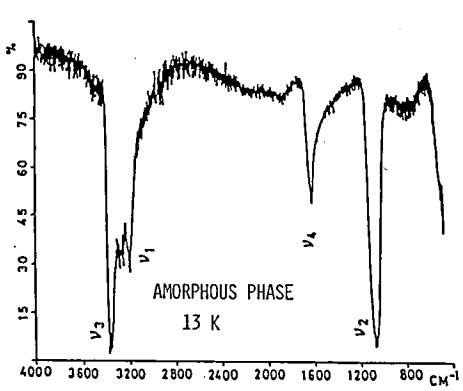

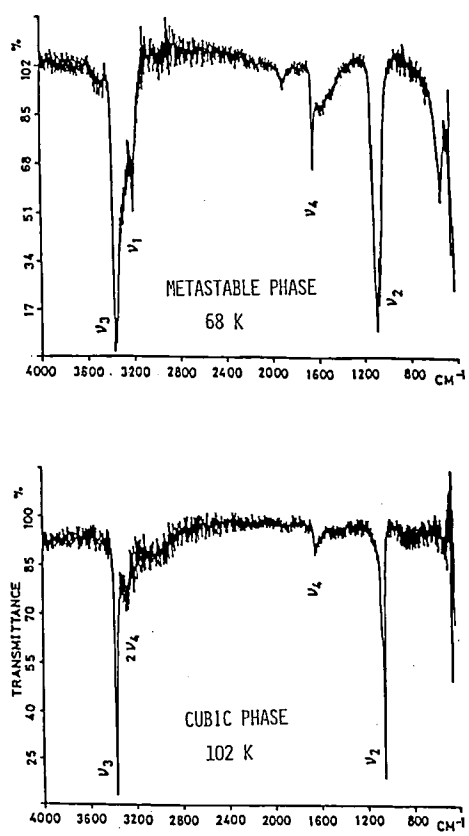

Figure 1. IR spectra of thin films of three different solid NH_3 phases (~50 μm thick) deposited on CsI substrate. Low frequency oscillations in baseline are due to interference fringes of the thin films.

Solid NH_3 can be produced in several different polycrystalline phases, depending upon deposition temperature and deposition rate. Figure 1 illustrates IR spectra of cryodeposited thin film of NH_3 obtained at three different deposition temperatures. Amorphous, metastable (mixed-polycrystalline), and cubic phases of NH_3 thin film were obtained at the temperatures of 13, 68, and 102 K, respectively. The spectrum of the cubic phase exhibits sharp and well-defined absorptions at 1057 (ν_2) and 3375 cm^{-1} (ν_3). The absorptions originating from ν_1 and ν_4 are much less prominent. The metastable phase shows broader character of the absorptions at 1060, 1078, and 1101 cm^{-1} in place of the single strong absorption at 1057 cm^{-1}. Above 120 K we could not obtain thin film spectra probably because of depositon difficulties on the substrate. In addition to these two phases, an amorphous phase of NH_3 has been observed at 13 K, a temperature never achieved by any of other investigators.

III-H-2 Infrared Spectra of Ammonia Clusters Trapped in an Argon Matrix at 16 K: Deposition from Pulsed Nozzle Beam

Teruhiko NISHIYA *(Kyoto Univ.)*, **Noboru HIROTA** *(Kyoto Univ. and IMS)*, **Hisanori SHINOHARA, and Nobuyuki NISHI**

Recently hydrogen-bonded molecular clusters in supersonic molecular beams have been the subject of many investigations. The matrix-isolated IR spectra of the complexes, on the other hand, provide complementary information on bonding and structure in the clusters.

Preparation of matrix-isolated ammonia clusters at low temperatures (12 ~ 20 K) can be achieved by deposition from pulsed supersonic beams. The pulsed matrix isolation has advantages over the conventional slow deposition when it comes to preparing clustered species. Figure 1 depicts the FTIR matrix spectrum of ammonia clusters of

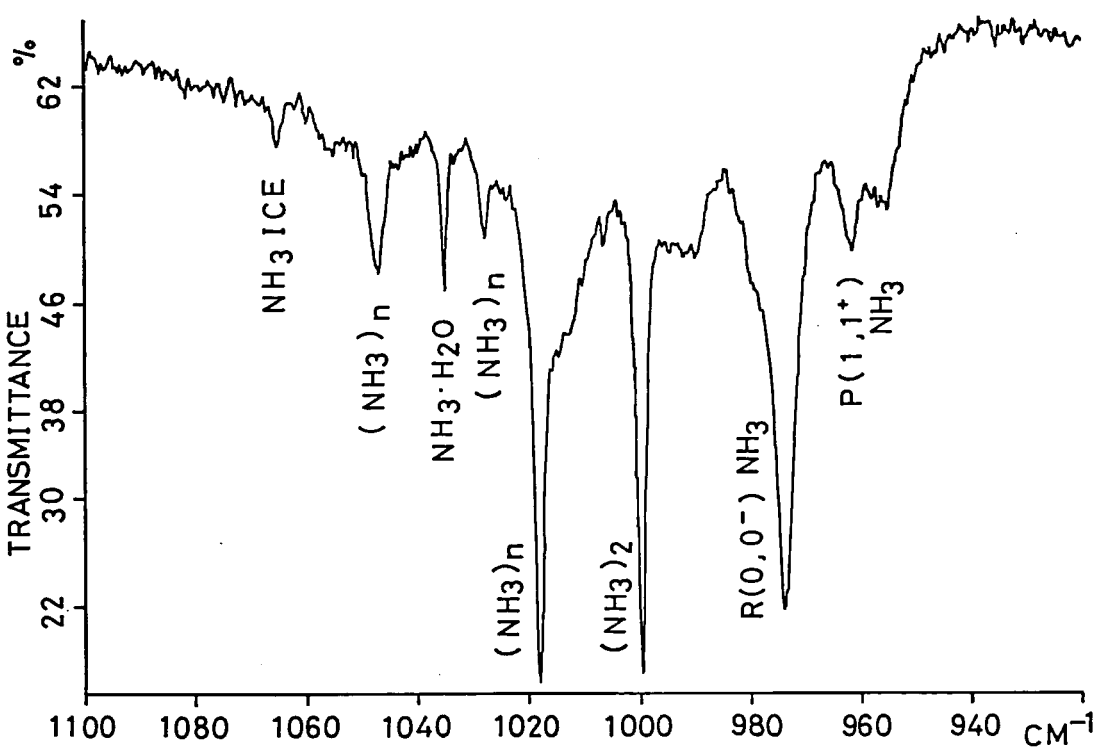

Figure 1. Infrared spectrum of ammonia and ammonia clusters (Ar : NH_3 = 230 : 1). Final deposite thikness is approximately 50 μm.

various sizes in their ν_2 regions. Absorptions due to the aggregates became strong when the concentration of ammonia was increased. When the sample was allowed to warm to higher temperatures (~30 K), the absorptions due to the clusters became more prominent, whereas the NH_3 absorption diminished in intensity. One of the striking features of the specrtrum is that the cluster absorptions are not only quite strong but more importantly very sharp (2 ~ 4 cm^{-1}). The absorption at 1000 cm^{-1} is assigned to $(NH_3)_2$. Although at the present stage of our investigation we are not able to unambigiously identify the cluster signal at 1018 cm^{-1}, we think that the band stems from a relatively small cluster such as trimer or tetramer.

III-H-3 Two-Photon-Ionization Mass Spectroscopy of Ammonia Clusters in a Pulsed Supersonic Nozzle Beam

Hisanori SHINOHARA

[*J. Chem. Phyis.*, **79**, 1732 (1983)]

Two-photon-ionization (TPI) with an ArF excimer laser at 193 nm, when combined with a mass spectrometer, is found to be a very sensitive and selective method for detecting ammonia clusters. Ammonia cluster distributions in the pulsed beam expansion have been measured via the TPI by varying the delay time between the pulsed beam and the laser firing (Figure 1). It can be regarded that the TPI mass spectra present "cross-sectional" distributions of the clusters perpendicular to the beam axis where various sizes of the ammonia cluster are distributed inhomogeniously. The cross-sectional cluster distribution in the pulsed beam can be obtained because of the fact that the two-photon-ionization period (i.e., within the laser pulse width ~10 ns) is too short for the molecular beam to proceed to the forward direction. An electron impact mass specrum, on the other hand, represents an "overall" cluster distribution, where ionization of the clusters is performed during the sampling time of the boxcar integrator used (~500 μs).

Seeding effects on the ammonia cluster distribution with He, Ne, Ar, and Kr carrier gases are also examined. The distribution shifts toward high mass region with increasing the mass of the seeding gases. The TPI spectroscopy with mass-spectroscopic detection is a method of considerable potential for further cluster-works.

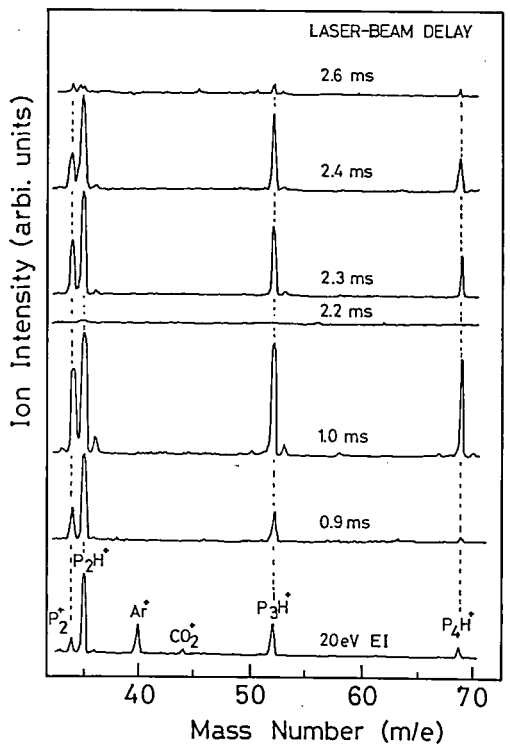

Figure 1. Variations of two-photon-ionization mass specrtra of ammonia clusters with the laser-beam delay time. Small peaks appeared next to the main one in the spectra stem from ammonia-water binary clusters owing to trace amount of residual water in the gas inlet system. Electron impact mass spectrum (40 eV) is also included for a comparison. Note that residual gases such as Ar and CO_2 which appeared in the EI specrum are completely absent in the TPI spectra.

III-H-4 Photoionization of Ammonia Clusters by Vacuum UV Photons

Hisanori SHINOHARA, Nobuyuki NISHI, and Nobuaki WASHIDA* *(National Institute for Environmental Studies*)*

Recently it has been shown[1,2] that two-photon-ionization (TPI) mass spectroscopy with a pulsed molecular beam is an excellent technique for detecting ammonia and the related clusters. In the present work photoionizations of ammonia clusters by argon, krypton, and xenon resonance lines are investigated. The results provide us information

about proton-transfer and related internal ion-molecule reactions in the clusters.

Figure 1 shows photoionization mass spectra of ammonia clusters by using three different vacuum UV photons (10.03, 10.64, and 11.83 eV). As in the TPI as well as in the electron impact ionization, the observed cluster ions were mostly protonated clusters with a general formula, $H^+(NH_3)_{n-1}$. The cluster ions fragment rapidly with the loss of an NH_2 radical:

$$(NH_3)_n + h\nu \longrightarrow (NH_3)_n^+ + e^-$$
$$\longrightarrow H^+(NH_3)_{n-1} + NH_2 + e^-.$$

In contrast to the two-photon and electron impact ionizations, parent cluster ions, $(NH_3)_n^+$, were also observed with the amount of less than 10% relative to the corresponding protonated clusters. Unimolecular decay processes for the $(NH_3)_n^+$ molecular ions were too fast to be observed at the rather long smapling times characteristic of the apparatus. The results are explained and discussed in terms of the two ionization channels leading to $H^+(NH_3)_{n-1}^+ + NH_2$ and to $(NH_3)_n^+$ formation.

References

1) H. Shinohara and N. Nishi, *Chem. Phys. Lett.*, **87**, 561 (1982).
2) H. Shinohara, *J. Chem. Phys.*, **79**, 1732 (1983).

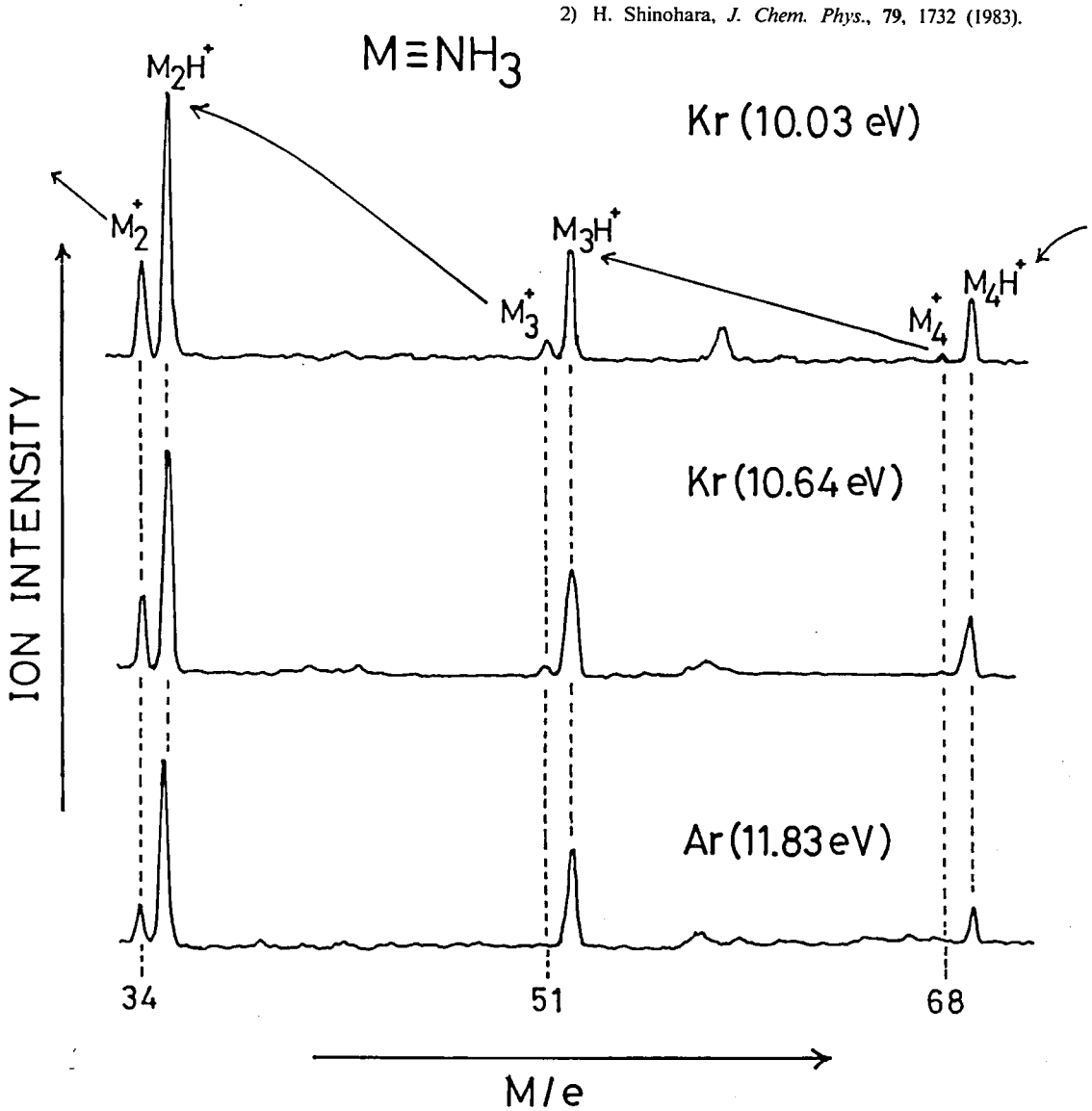

Figure 1. Vacuum UV photoionization mass spectra of ammonia clusters produced in a pulsed supersonic nozzle beam. Argon (11.83 eV), and krypton (10.64, 10.03 eV) resonance lines were used for the ionizations. Nozzle stagnation pressure was 740 ~ 760 Torr of neat ammonia.

III—I Proton Transfer in Excited states of Salycilaldehyde

III-I-1 Investigation of the Dynamic Processes of the Excited States of o-Hydroxybenazaldehyde and o-Hydroxyacetophenone by Emission and Picosecond Spectroscopy

Shin-ichi NAGAOKA *(Kyoto Univ.)*, **Noboru HIROTA** *(Kyoto Univ. and IMS)*, **Minoru SUMITANI, and Keitaro YOSHIHARA**

[*J. Am. Chem. Soc.*, **105**, 4220 (1983)]

We have investigated the structures and dynamic processes of the excited states of o-hydroxybenzaldehyde (OHBA) and o-hydroxyacetophenone (OHAP) by means of emission and picosecond spectroscopy. It is shown that the main species existing in non-polar solvents are intramolecularly hydrogen bonded closed conformers from which proton or hydrogen transfer takes place. The Stokes shifted fluorescences originate from the transfered forms which are likely to be the enol tautomers. The main species in alcohols are intermolecularly hydrogen bonded open conformers which phosphoresce at low temperatures, but fluorescing species also exist. OHBA in ethanol and methanol shows two different fluorescences with different decay times. It is suggested that one arises from the closed conformer of the enol form of OHBA, and the other is due to the strongly solvated open conformer. At 77 K in non-polar solvents the closed conformer of OHBA is converted to the open conformer by UV irradiation changing the fluorescence into the phosphorescence. The fluorescence decay rate constants are temperature dependent and are given as the sums of the radiative and nonradiative decay rate constants. From the picosecond measurements and the quantum yields of fluorescence we have estimated the rates of the transfer and the nonradiative decay rates of the closed conformers of OHBA and OHAP in non-polar solvents at 77 K.

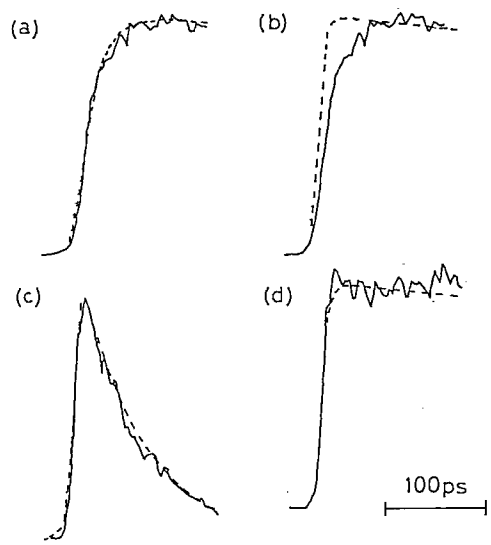

Figure 1. The fluorescence rise and decay curves. For each figure the solid lines are the observed ones obtained after averaging and the broken ones are the simulated ones. The curves shown here were obtained with the excitation at 266 nm but similar results were obtained with the 355 nm excitation in all cases.
(a) OHBA in D/MCH at 77 K simulated with an equation in the text. $k_t + k_d = 5.0 \times 10^{10}$ s^{-1}.
(b) OHBA in D/MCH at 77 K simulated with a different equation in the text.
(c) OHBA in D/MCH at room temperature simulated with equation (6).
(d) Dibromoanthracene in CH at room temperature simulated with equation (6).

It is concluded that the proton or hydrogen transfers are relatively slow and the nonradiative decays are dominant in the decay processes of the excited states of the closed conformers of OHBA and OHAP in non-polar solvents. The fluorescence rise and decay curves are shown in Figure 1. The slow transfer rates were attributed to the $^1n\pi^*$ characters of the S_1 states.

III—J Studies on Electronic Structure, Energy Transfer, Dissociation and Recombination of Small Molecules

III-J-1 Effects of External Magnetic Field on Laser-iduced Fluorescence of NaK

Hajime KATO *(Kobe Univ. and IMS)*, **Masaaki BABA, and Ichiro HANAZAKI**

Each line of the fluorescence to the $^3\Sigma^+$ state following the excitation $^1\Pi(v' = 12, J' = 14) \leftarrow {}^1\Sigma^+$ $(v'' = 0, J'' = 14)$ is found to split into three lines when an external magnetic field is applied. The changes of the intensity and the energy splitting are measured as a function of the field strength. Formulae for the intensities of the Zeeman lines of the resonance fluorescence to a $^3\Sigma^+$ state following the Q excitation $^1\Pi$ (v, J M) $\leftarrow {}^1\Sigma^+$ (v^o, J M) are presented. From the observed Zeeman splitting and the theoretical calculation, the contamination of lower triplet state a $^3\Sigma^+$ by a singlet perturber X $^1\Sigma^+$ is shown to be negligible. The intensity assymetry between three lines split by the Zeeman effect is observed, and it is explained by the M dependent excitation to the Zeman components of the D $^1\Pi$ states.

III-J-2 Laser-induced Fluorescence of the NaCs Molecule

Kyoko ONOMICHI *(Kobe Univ.)* **and Hajime KATO** *(Kobe Univ. and IMS)*

[*Bull. Chem. Soc. Jpn.*, **56**, 2577 (1983)]

Laser-induced fluorescence of NaCs is observed when a mixture of sodium and cesium is irradiated by the 5782 Å laser line. The specroscopic constants of the ground state $X^1\Sigma^+$ have been determined and the potential energy curve was calculated by the RKR method. The excited state was identified as $D^1\Pi$, and the potential curve was estimated from the analysis of the fluorescence intensities.

RESEARCH ACTIVITIES IV
Department of Molecular Assemblies

IV—A Photoelectron Spectroscopy of Organic Solids in Vacuum Ultraviolet Region

Vacuum ultraviolet photoelectron spectra were measured on various types of organic solids; aromatic solids, organic polymers, phthalocyanines, and donating components of organic metals.

IV-A-1 UV Photoelectron Spectroscopy of Photoconducting Polymers

Yasuhiko SHIROTA *(Osaka Univ. and IMS)*, **Yasuyo MATSUMOTO** *(Osaka Univ.)*, **Hiroshi MIKAWA** *(Osaka Univ.)*, **Kazuhiko SEKI, and Hiroo INOKUCHI**

As an extention of a previous study of uv photoelectron spectroscopy of 1:1 alternating copolymers,[1] uv photoelectron spectra of several photoconducting polymers in thin films have been measured to determine their threshold ionization potentials (I_s^{th}). The polymers studied include poly (N-vinylcarbazole) (PVCz), poly (3-bromo-N-vinylcarbazole) (PBrVCz), poly (3,6-dibromo-N-vinylcarbazole) (PDBrVCz), poly (2-methyl-N-vinylindole) (PMVI), poly (1,3-diphenyl-5-p-vinylphenyl-2-pyrazoline) (PVTPP), poly (1,3-diphenyl-5-p-methacryloylaminophenyl-2-pyrazoline) (PMTPP), poly (2-phenyl-5-p-methacryloylaminophenyl-1,3-oxazole) (5-PMPPO), and poly (5-phenyl-2-p-methacryloylaminophenyl-1,3-oxazole) (2-PMPPO). Table I summarizes the values of I_s^{th} determined for these polymers. The results show that the polymers containing a pendant 1,3,5-triphenyl-2-pyrazoline group possess the lowest I_s^{th} values among the polymers studied and that PBrVCz, PMVI, 5-PMPPO, and 2-PMPPO have similar I_s^{th} values. The results provide valuable information for understanding their photoconductivities and for designing photoreceptors for use in electrophotography.

Table I. Threshold ionization potentials (I_s^{th}) of polymers (in eV)[a]

Polymer	I_s^{th}
PVCz	5.8_5
PBrVCz	6.0_3
PDBrVCz	6.1_3
PMVI	6.0_2
PVTPP	5.5_3
PMTPP	5.5_6
5-PMPPO	6.0_3
2-PMPPO	5.9_6

a. The I_s^{th} values were obtained from the spectra taken at incident photon energies of 6.89, 7.75, and 9.18 eV.

Reference

1) Y. Shirota, Y. Matsumoto, H. Mikawa, K. Seki, and H. Inokuchi, *IMS Ann. Rev.*, 64 (1982); *Chem. Phys. Lett.*, 97, 57 (1983).

IV-A-2 Ultraviolet Photoelectron Spectra of α- and β-Polymorphs of Copper Phthalocyanine

CHEN Shang Xian *(Inst. Chem., Acad. Sinica, China and IMS)*, **Kazuhiko SEKI, Hiroo INOKUCHI, SHI Zurong,* and QIAN Renyuan*** *(*Inst. Chem., Acad. Sinica, china)*

[*Bull Chem. Soc. Jpn.* **56**, 2565 (1983)]

The ultraviolet photoelectron spectra have been measured for α- and β-forms of copper phthalocyanine at 183°C, to investigate the correlation of photoemissive behavior with crystal structure. Their threshold ionization potentials were 4.8_8 and 4.6_2 eV, with polarization energy of 1.2_7 and 1.5_3 eV, respectively. This difference could not be explained by calculation with point charge − point dipole approximation, but calculation with distributed charge on the cation and distributed induced dipoles on the nearest neighbor two molecules gave semi-quantative agreement with the experimental findings.

IV-A-3 Ionization Potentials and Polarization Energies of Tetraselenafulvalene (TSF) Derivatives

Naoki SATO, Gunzi SAITO, and Hiroo INOKUCHI

[*Chem. Phys.*, **76**, 79 (1983)]

Gaseous and solid-state ionization potentials of several derivatives of tetraselenafulvalene (TSF) and tetrathiafulvalene (TTF) have been determined from ultraviolet photoelectron spectroscopy. The first ionization potentials of the molecules in the gaseous state are appraised in terms of their molecular structures and the substitution effects. The characteristics in the electronic structure of these molecules as donors forming conductive salts with various acceptors are discussed.

The polarization energies, obtained as the difference of the threshold ionization potentials for both states of these compounds, ~1.4 eV, were found to be slightly smaller than the nearly constant value for polycyclic aromatic hydrocarbons, ~1.7 eV. As the value of the polarization energy is determined mainly by the molecular polarizability and by the molecular packing density in the solid, the molecular polarizabilities of these compounds were estimated from the observed polarization energies, using a simplified relation, as listed in Table I. Such values are also useful in characterizing electronic states of the solids containing them.

Table I. Molecular Polarizabilities Calculated from the Observed Polarization Energies

Compound	$\bar{\alpha}/10^{-30}m^3$	ρ/Mgm^{-3}
TSF	24.5	2.76
TMTSF	30.7	2.34_9
	30.7	crystal data
HMTSF	32.6	2.29_1
TTF	16.5	crystal data
TMTTF	21.0	1.48
HMTTF	27.5	1.62
BEDTTTF	37.9	1.72
	36.8	crystal data
TTMTTF	39.4	1.56_5

IV-A-4 Ultraviolet Photoelectron Spectroscopy of Fluorosubstituted Polyethylenes

CHEN Shang Xian *(Inst. Chem., Acad. Sinica, China and IMS)*, **Kazuhiko SEKI, Hiroo INOKUCHI, Nobuo UENO,* and Kazuyuki SUGITA*** *(*Chiba Univ.)*

[*Polymer J.*, in press]

HeI, NeI, and ArI ultraviolet photoelectron spectra were measured for multi-substituted polyethylenes: poly(vinylidene fluoride)(PVdF), poly (trifluoroethylene)(PTrFE), and poly(tetrafluoroethylene)(PTFE) to determine their photoemission threshold energies. The obtained thresholds are listed in Table I with the values for polyethylene (PE)[1] and poly(vinyl fluoride)(PVF)[2]. The values of F-substituted polymers are larger than that of PE. This is consistent with the high electronegativity of fluorine. The threshold energies correspond to the ionization from the orbitals formed by the σ_{CH} bonds for PVF, PVdF, PTrFE, while the band formed by F···F interaction determines the threshold for PTFE. The similar values for all the four F-containing polymers indicate that the F···F interaction is large enough to lower the threshold energy of PTFE to those of the σ_{CH} orbitals.

Table I. Observed threshold ionization potentials I_s^{th} of fluorosubstitued polyethylenes

Compound	I_s^{th}/eV
polyethylene (PE)	8.5
poly(vinyl fluoride) (PVF)	9.2
poly(vinylidene fluoride) (PVdF)	9.2
poly(trifluoroethylene) (PTrFE)	9.2
poly(tetrafluoroethylene) (PTFE)	9.0

References

1) M. Fujihira and H. Inokuchi, *Chem. Phys. Lett.* **17**, 554 (1972).
2) Chen S.X., K. Seki, H. Inokuchi, S. Hashimoto, N. Ueno, and K. Sugita, to be published.

IV—B Electric- and Photo-conduction in Organic Solids

Among a many organic semiconductors, tetrabenzo [*de,hi,op,st*] pentacene (TBPA) has a very peculiar electrical behavior; high conduction ($\sim 10^5$ Ωcm) in air, abrupt change of its conduction as a function of pressure and intrinsic photoconductive character. The photoconduction of TBPA and tetrabenzo [*a,cd,j,lm*] perylene has been observed with an ultra-high vacuum photoconduction apparatus.

IV—C Energy Transfer in Cytochrome c_3 and Hydrogenase

Since the complete analysis of molecular structure of cytochrome c_3 has been succeeded (1981), the electron transfer mechanism in cytochrome c_3 and also the enzymatic activity of hydrogenase are studied by magnetic resonance, electrochemical analysis and also A.C. conductivity measurement.

IV-C-1 Magnetic Resonance Study of Hydrogenase and Cytochrome c_3

Keisaku KIMURA, Hiroo INOKUCHI, Tatsuhiko YAGI *(Shizuoka Univ.)*, **Shinsuke NAKAJIMA** *(Yokohama Nat. Univ.)*, **and Katsumi NIKI** *(Yokohama Nat. Univ.)*

Hydrogenase is an enzyme for hydrogen cleavage reaction and cytochrome c_3 is a native electron acceptor in this reaction. The active center of hydrogenase was reported to be an iron-sulfur cluster as found in ferredoxin. However the essential component in hydrogenase has not yet been settled. A nickel atom and also a zinc atom have recently been detected as a component of hydrogenase.[1] Therefore we examined an active center of hydrogenase of Desulfovibrio vulgaris.

The X-band ESR spectra of the hydrogenase preparation were recorded at temperatures ranging from 4.2K to 42K at 1 mW microwave power and at microwave powers from 10 μW to 100 mW at 17K. The spectrum line shape was analysed by computer simulation. The model of the cluster was constructed from the analysis.

^{1}H-NMR measurement of cytochrome c_3 was studied at 400 MHz. The temperature dependence, redox titration, and pH titration classified the methyl protons of four hemes. The electron transfer rate was also elucidated.

Reference

1) H-J. Krüger, B.H. Huynh, P.O. Ljungdahl, A.V. Xavier, D.V. DerVartanian, I. Moura, H.D. Peck, Jr, M. Teixeira, J.J.G. Moura, and J. LeGAll, *J. Biol. Chem.*, **257**, 14620 (1982).

IV—D Physics and Chemistry of Graphite and its Intercalates

For analysis of electron transfer from alkali metal guest to graphite host, the catalytic activity for hydrogen dissociation and/or chemisorption and the enhancement of superconduction by introduction of hydrogen on the graphite-alkali metal intercalation compounds are being studied.

IV-D-1 Chemisorption of Hydrogen in Graphite-Alkali Metal Intercalation Compounds

Toshiaki ENOKI, Mizuka SANO *(Kumamoto Univ.)* **and Hiroo INOKUCHI**

[*J. Chem. Phys.*, **78**, 2017 (1983)]

The hydrogen chemisorption mechanism in the graphite-alkali metal intercalation compounds have been investigated by means of ESR and electrical resistivity under hydrogen atmosphere. (See section **VI-J**)

IV-D-2 Responsible Layer for Superconductivity in the First Stage Potassium Graphite Intercalation Compound

Mototada KOBAYASHI, Tsuyoshi MURAO,* and Ikuji TSUJIKAWA* *(*Kyoto Univ.)*

[*J. Phys. Soc. Jpn.*, **52**, 1890 (1983)]

The superconductivity in the first stage potassium graphite intercalation compound is discussed in connection with the electron transfer rate from potassium atom to graphite layers. From this discussion together with the experimental result that transition temperature T_c depends little on the K atom concentration above a critical concentration, we conclude that the superconductivity takes place mainly on the graphite layer. The mechanism to increase three dimensional character with decreasing K atom concentration is also discussed.

IV-D-3 Sulfur-Bridged Polycyclic Aromatic Compounds

Hideo AKAMATU, Hiroo INOKUCHI, and Minoru KINOSHITA *(Inst. Solid State Physics, Univ. Tokyo)*

[*Carbon.*, **21**, 337 (1983)]

When polycyclic aromatic hydrocarbons are heat-treated with an excess amount of sulfur in evacuated closed tubing, they react with sulfur, liberating hydrogen sulfide; after removing free sulfur, dark-colored compounds in the form of an amorphous solid are obtained. These compounds possess semiconductive properties; the electrical resistivity is greatly reduced from that of the original hydrocarbons. The ESR absorption of these compounds is characterized by the large g-value, which is due to sulfur-centered unpaired electrons.

We assume the polycyclic aromatic nuclei crosslink with each other through the sulfur-bridges, which are good electron transport paths, and yield the aromaticity of the molecule. The sulfur-bridged polycyclic aromatic hydrocarbons can be considered as the structural model of chars and cokes. The ESR studies of violanthrene-sulfur compound were carried out during the heat-treatment up to 1000°C. This work was carried out at the Department of Chemistry, University of Tokyo.

IV—E Organic Metals

Electrical, magnetic, optical, and structural properties of solid charge transfer (CT) complexes including organic metals and organic superconductors are being studied in order to clarify electronic interactions, spin correlations, and dimensionality in these materials.

Our continued interest in the requirements for an organic metal has been extended to the complexes of tellurium π-donor.

Our molecular designing to enhance metallic character of the organic CT complexes by increasing polarizability, conduction band width, and dimensionality and also by decreasing on-site Coulomb repulsion has been focused on synthetic modification of tetrethiafulvalene (**TTF (1)**). For that purpose, we have employed alkylthio substituted TTFs, one of which is bis(ethylenedithiolo)-tetrathiafulvalene (**BEDT-TTF (2)**). A number of new BEDT-TTF complexes with a variety of anions have been prepared and their extraordinal properties are investigated.

The preparation of the first organic superconductor (TMTSF (3))$_2PF_6$ and the first ambient pressure organic superconductor $(TMTSF)_2ClO_4$ have reinstilled interest in the search for a dream; high T_c superconductors. A variety of measurements has been done on the superconductor $(TMTSF)_2ClO_4$ to elucidate the electronic structures, electronic and spin correlations, and superconductivity.

Preparation of new compounds is a vital force to develope the study of organic metals. Diaminopyrene and benzidine type new π-donors were prepared and the electrical conductivities of their complexes with TCNQs were investigated. Some weak π-acceptors of TCNQ family are needed to investigate the requirements for an

organic metal concerning to the degree of CT. Furthermore, strong π-acceptors which are capable of forming quasi two-dimensional organic metals are very effective in the design of new type organic superconductors composed of anion radicals.

Polyacetylene is a well known organic polymer which becomes organic metal after doping. An inorganic polymer $(SN)_x$ is a metal and shows superconductivity at very low temperatures. We have studied poly (carbon diselenide) in the hope that this polymer is a new synthetic metal.

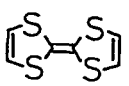

1 TTF

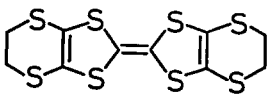

2 BEDT-TTF

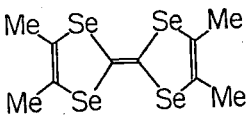

3 TMTSF

IV-E-1 Organic Conductors: Electrical Properties of HMTTeF (Hexamethylenetetratellurafulvalene) Complexes

Gunzi SAITO, Toshiaki ENOKI, Hiroo INOKUCHI, Hiroaki KUMAGAI,* and Jiro TANAKA** *(*Nagoya Univ. and IMS, **Nagoya Univ.)*

[*Chem. Lett.*, **1983** 503]

One of the most effective ways to suppress the Peierls transition in low-dimensional organic metals, thiafulvalene or thianaphthacene complexes has been the enhancement of the intermolecular interaction by replacement of sulfur with selenium atoms.[1] Taking into account the van der Waals radius of charcogenide atoms (S:1.80, Se:1.90, Te:2.06Å), it is more promising to use tellurium π-donors in order to obtain a complex with strong

Table I. Electrical Properties of HMTTeF Complexes

π-Acceptor	E_A(eV)	Color	Ratio	ρ_{RT}(Ωcm)	ϵ_a(eV)
TCNQs					
1. F_4	3.15	dark blue	1 : 1	3.3	0.034
2. F	2.92	dark blue	1 : 1	2.7	<0.001
3. TCNQ	2.83	dark blue	1 : 1	0.14	0.0030
4. 2,5-dimethyl	2.74	green	2 : 1	0.22	0.0024
5. 2,5-dimethoxy	2.56	blue	1 : 2	1.7×10^9	0.30
p-quinones					
2,3-dibromo-5,6-dicyano	3.00	black	1 : 1	4.9×10^2	0.079
2,3-dichloro-5,6-dicyano	2.99	black	1 : 1	8.3×10	0.046
2-bromo-5,6-dicyano	2.88	black	~1 : 2	1.6×10^4	0.045
2-chloro-5,6-dicyano	2.87	black	2 : 3	2.3×10^3	0.092
2,3-dicyano	2.76	brown	2 : 3	2.7×10^5	0.23
2,3-dicyano-1,4-naphthoquinone	2.64	brown	1 : 1	1.2×10^2	0.071
others					
9-dicyanomethylene-2,4,5,7-tetranitrofluorene	2.69	black	3 : 2	4.1×10^2	0.080
9-dicyanomethylene-2,4,7-trinitrofluorene	2.52	black	1 : 1	3.7×10^{11}	0.50
tetracyanoethylene	2.76	dull green	~1 : 1	1.4×10^3	0.069
2,4-bisdicyanomethylene-1,3-dithietan	2.04	dark brown	1 : 1	3.0×10^8	0.49
TTF·TCNQ		black	1 : 1	0.19	0.0053

E_A: electron affinity, Ratio: donor: acceptor

intermolecular interaction. In addition to this, using tellurium analogues will increase the conduction band width and polarizability, and hence an enhancement of metallic character is expected.

Several CT complexes of HMTTeF **(4)**[2] with TCNQs, p-quinones, and other π-acceptors were prepared and electrical resistivities were measured with compaction samples. In general, 1 : 1 HMTTeF complexes with strong π-acceptors having E_A>2.60 eV show relatively high conductivity and low activation energy (Table I) suggesting partial CT is playing an important role in the conduction. Single crystals of TCNQ and 2,5-dimethyl-TCNQ complexes show metallic temperature dependence (σ_{RT} = 1400 and 1800 $\Omega^{-1}cm^{-1}$, respectively).

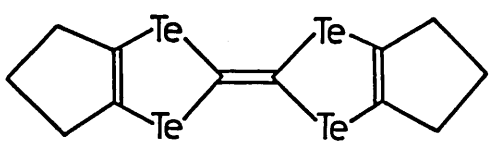

4 HMTTeF

References

1) T.E. Phillips, T.J. Kistenmacher, A.N. Bloch, and D.O. Cowan, *J.C.S. Chem. Commun.*, **1976**, 334, J.R. Cooper, M. Weger, D. Jerome, D. Lefur, K. Bechgaard, A.N. Bloch, and D.O. Cowan, *Solid State Commun.*, **19**, 749 (1976).
2) F. Wudl and E. Aharon-Shalom, *J. Am. Chem. Soc.*, **104**, 1154 (1982).

IV-E-2 Crystal Structure of a New Type of Two-Dimensional Organic Metal, (BEDT-TTF)$_2$ClO$_4$(C$_2$H$_3$Cl$_3$)$_{0.5}$

Hayao KOBAYASHI,* Akiko KOBAYASHI, Yukiyoshi SASAKI,** Gunzi SAITO, Toshiaki ENOKI, and Hiroo INOKUCHI** *(*Toho Univ., **Univ. of Tokyo)*

[*J. Am. Chem. Soc.*, **105**, 297 (1983)]

The crystals of the perchlorate salt of BEDT-TTF were grown by electrocrystallization method. The single crystal resistivity along the elongated direction ($\rho_{\parallel}$), which is close to the a axis in the (010) plane, decreases monotonically from the room-temperature value (3.8×10^{-2} Ωcm) to the minimum at 16K (1.0×10^{-3} Ωcm). Metallic conduction is retained even at the lowest

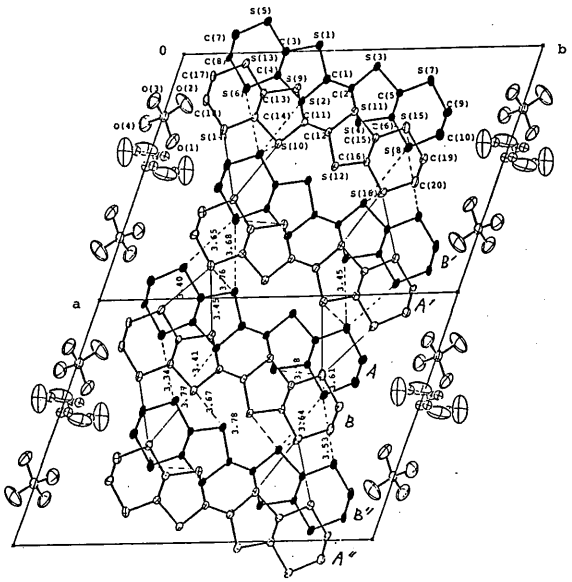

Figure 1. Crystal structure viewed along c* axis. Molecule A and B indicate two crystallographically independent BEDT-TTF molecules. The coordinates of the center of molecule A are (0.10, 0.48, −0.26) and those of molecule B are (0.34, 0.43, 0.21). Molecules A' and A" (B' and B") are the molecules related to A (B) by symmetry operations. The symmetry operations are A (x, y, z), B (x, y, z), A' (−x, 1−y, −z), B' (−x, 1−y, −z), A" (1−x, 1−y, −z), and B" (1−x, 1−y, −z). Molecules A, B', and B" are approximately on the same plane at z = 0.25.

measured temperature (1.4K, 1.5×10^{-3} Ωcm). The anisotropy of the resistivity is very small in the a-c plane ($\rho_{\parallel}/\rho_{\perp}$ = 0.4 ~ 0.9), but the room-temperature resistivity parallel to the b* direction is 10^2 ~ 10^3 times bigger.[1]

We report on the structure of this new type of organic metal where the planar molecules are not stacked face-to-face but are arranged side-by-side to form a two-dimensional system. The two-dimensionality of the structure originates from short intermolecular contacts between the sulfur atoms of the donor molecules (Figure 1). The crystal structure of (BEDT-TTF)$_2$ClO$_4$ (C$_2$H$_3$Cl$_3$)$_{0.5}$ suggests a way to introduce a two-dimensional interaction in the organic conductors, which will be effective in the design new organic systems. The crystal data (room temperature) are as follows: triclinic; space group $P\bar{1}$; a = 12.966, b = 18.620, c = 7.740Å, α = 79.32, β = 104.80, γ = 110.85°; V = 1684Å^3; z = 2.

Reference

1) G. Saito, T. Enoki, K. Toriumi, and H. Inokuchi, *Solid State Commun.*, **42**, 557 (1982).

IV-E-3 X-Ray Evidence for a Structural Phase Transition in the Organic Two-Dimensional Conductor $(BEDT\text{-}TTF)_2ClO_4(C_2H_3Cl_3)_{0.5}$

Seiichi KAGOSHIMA*, J.P. POUGET, Gunzi SAITO, and Hiroo INOKUCHI** *(*Univ. of Tokyo, **Univ. Paris-Sud)*

[*Solid State Commun.*, **45**, 1001 (1983)]

By x-ray diffuse scattering experiments, the formation of the superstructure with the periodicity 2a × b × 2c was found below about 200K in the organic two-dimensional conductor $(BEDT\text{-}TTF)_2ClO_4(C_2H_3Cl_3)_{0.5}$. Figure 1 shows a typical x-ray patterns taken at 20K and 200K. With the crystal orientation chosen, these x-ray patterns contain mostly the a* and c* reciprocal directions. At 20K strong satellite spots are observed on the center of each "unit cell" formed by the a*-c* array of main Bragg spots. This result means that the superstructure is characterized by wave vector components of 0.5a* and 0.5c* in the a*-c* plane.

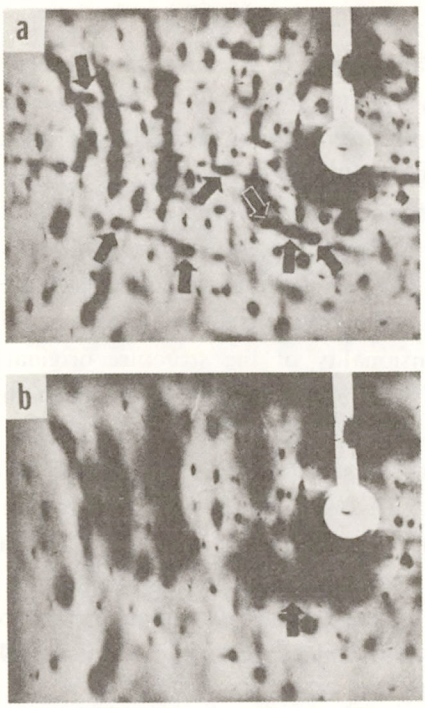

Figure 1. Typical x-ray scattering patterns from $(BEDT\text{-}TTF)_2ClO_4(C_2H_3Cl_3)_{0.5}$ at (a) 20K and (b) 200K. The a* axis is nearly horizontal and the c* axis is vertical. Arrows indicate some of satellite spots.

With other orientation of the sample in the experimental setup, we found that the component of the wave vector along the b*-axis is 0. Thus the periodicity of the superstructure is 2a × b × 2c. The intensity of satellite reflections decreases with increasing temperature and becomes hardly detectable above the diffuse background at 200K. From the above results and the structural analysis performed at room temperature,[1] the origin of the superstructure is considered to be an orientational order-disorder transition of the molecule $C_2H_3Cl_3$ (1,1,2-trichloroethane). The electrical anomaly observed near 180K in the complex[2] may be associated with this transition.

References

1) H. Kobayashi, A. Kobayashi, Y. Sasaki, G. Saito, T. Enoki, and H. Inokuchi, *J. Am. Chem. Soc.*, **105**, 297 (1983).
2) G. Saito, T. Enoki, and H. Inokuchi, *Chem. Lett.*, **1982**, 1345.

IV-E-4 Two-Dimensional Band Structure of an Organic Metal, $(BEDT\text{-}TTF)_2ClO_4(C_2H_3Cl_3)_{0.5}$

Takehiko MORI,* Akiko KOBAYASHI,* Yukiyoshi SASAKI,* Hayao KOBAYASHI, Gunzi SAITO, and Hiroo INOKUCHI** *(*Univ. of Tokyo, **Toho Univ.)*

[*Chem. Lett.*, **1982**, 1963]

The intermolecular overlap integrals and the band structure of $(BEDT\text{-}TTF)_2ClO_4(C_2H_3Cl_3)_{0.5}$ were calculated using semiempirical molecular orbital calculation. The overlap integral (Table I) in $(BEDT\text{-}TTF)_2ClO_4$ is considerably smaller than those of TTF·TCNQ[1] and $(TMTSF)_2X$,[2] and the

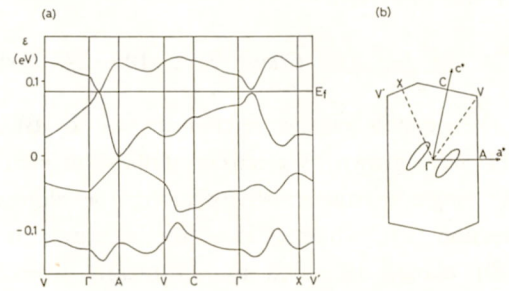

Figure 1. Energy Band Structure of $(BEDT\text{-}TTF)_2ClO_4$.

ratio of the longitudinal and the transverse overlap integrals decreases in the order; TTF·TCNQ> $(TMTSF)_2X$>$(BEDT\text{-}TTF)_2ClO_4$ indicating the increased dimensionality in the BEDT-TTF complex. The energy band structure (Figure 1) is completely different from those of other one-dimensional organic metals and strongly indicates that $(BEDT\text{-}TTF)_2ClO_4$ is a new-type multi-dimensional organic semimetal.

References

1) S. Shitzkovky, M. Weger, and H. Gutfreund, *J. Phys.* (Paris), **39**, 711 (1978), A.A. Bright, A.F. Garito, and A.J. Heeger, *Phys. Rev.*, **B10**, 1328 (1974).
2) T. Mori, A. Kobayashi, Y. Sasaki, and H. Kobayashi, *Chem. Lett.*, **1982**, 1923.

Table I. Overlap integrals

		S_{max}	$S_{\parallel}/S_{\perp}$
TTF·TCNQ	TCNQ	20×10^{-3}	~100
	TTF	9×10^{-3}	
$(TMTSF)_2X$		36×10^{-3}	~10
$(BEDT\text{-}TTF)_2ClO_4$		6×10^{-3}	0.1~0.3

IV-E-5 Crystal Structure of α-$(BEDT\text{-}TTF)_2PF_6$

Hayao KOBAYASHI,* Reizo KATO, Takehiko MORI,** Akiko KOBAYASHI,** Yukiyoshi SASAKI,** Gunzi SAITO, and Hiroo INOKUCHI** *(*Toho Univ., **Univ. of Tokyo)*

[*Chem. Lett.*, **1983**, 759]

The crystal of α-$(BEDT\text{-}TTF)_2PF_6$ belongs to triclinic system. The close intermolecular contacts along the c axis (Figure 1) suggests the strong tendency for the side-by-side arrangement of BEDT-TTF molecules. The possible origin of this transverse array of BEDT-TTF molecules may be as follows:

(1) Since the atoms of the ethylene groups are not on the molecular plane, intermolecular steric repulsion makes the usual face-to-face overlapping unstable.

(2) The face-to-face overlapping may not be necessarily required for the intermolecular interaction in the complexes of π-donor with charcogen atoms because the mixing of the $p\pi$ and $d\pi$ atomic

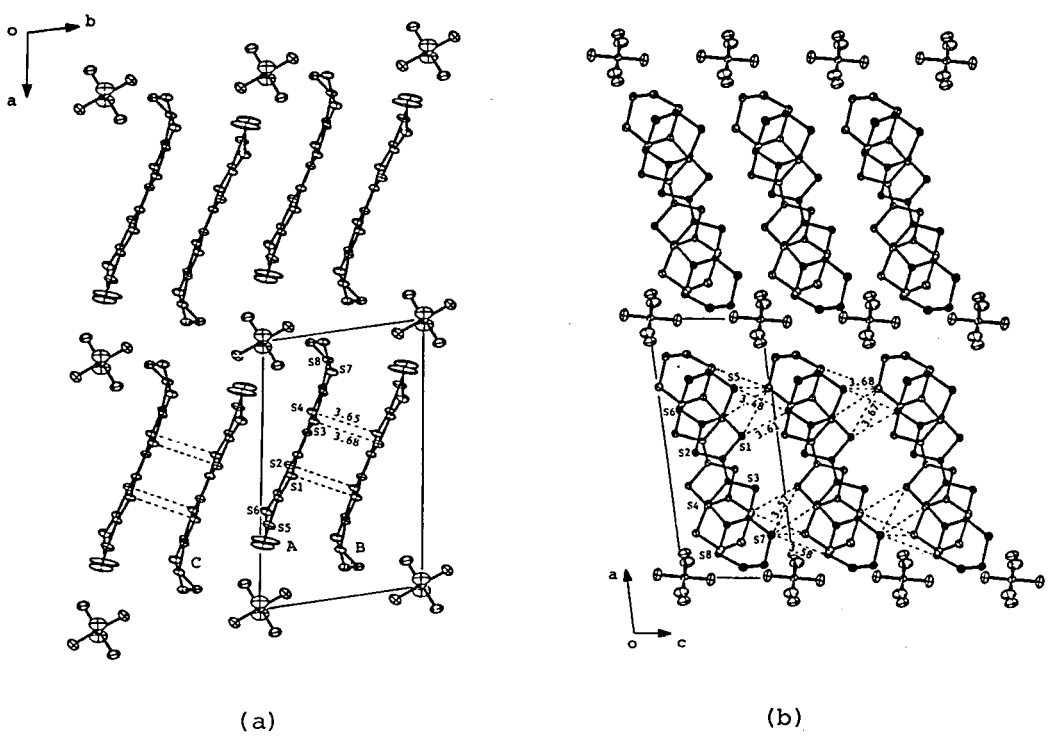

Figure 1. (a) Crystal structure viewed along the c* axis. The molecules A and B are related by the symmetry operation (1-x, 1-y, 1-z). (b) Crystal structure viewed along the b* axis.

orbitals can be expected. The side-by-side arrangement is not so unfavorable for $d\pi$-$d\pi$ interaction. (3) Since every sulfur atom in the six-membered rings of BEDT-TTF has two short S ··· S contacts, the sulfur atom seems to play an important role for the formation of the transverse arrangement. It might possible that the σ(or n) orbitals interact with the unoccupied molecular orbital of the adjacent molecule through sulfur atoms.

The electrical resistivity measurements show this complex is a semiconductor with a small band gap of about 0.1 eV.

IV-E-6 Transverse Conduction and Metal-Insulator Transition in β-(BEDT-TTF)$_2$PF$_6$

Hayao KOBAYASHI,* Takehiko MORI, Reizo KATO,** Akiko KOBAYASHI,** Yukiyoshi SASAKI,** Gunzi SAITO, and Hiroo INOKUCHI** *(*Toho Univ., **Univ. of Tokyo)*

[*Chem. Lett.* **1983**, 581]

In the organic metals hitherto known, the one-dimensional metallic properties are originated mainly from the intermolecular $p\pi$-$p\pi$ interaction along the stack. In other words, the $p\pi$ orbitals of the HOMO break the isolated state of the molecules. However, the crystal structure and the anisotropy of the electrical resistivity of β-(BEDT-TTF)$_2$PF$_6$ suggest that the organic compounds can be metallic in the absence of the column structure. In this crystal the small intermolecular overlapping and no intermolecular short contact along the a axis indicate a very weak interaction within the stack. On the other hand, each BEDT-TTF molecule has four intermolecular short S···S contacts (3.440 ~ 3.519Å vs. van der Waals contact 3.60Å) along the c axis. The temperature dependence of the electrical resistivity (Figure 1) shows metal-insulator transition at around 297K. The anisotropy above this temperature is $\rho_c : \rho_a : \rho_b = 1 : 50 : 10^4$, and this indicates that β-(BEDT-TTF)$_2$PF$_6$ is the first organic metal whose transverse conductivity is much higher than the parallel conductivity.

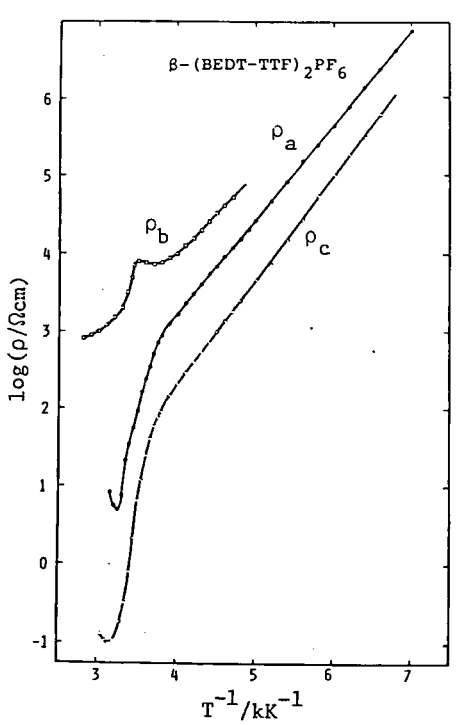

Figure 1. Electrical resistivities of β-(BEDT-TTF)$_2$PF$_6$ along the a, b, and c axis.

IV-E-7 Tunneling Spectroscopic Study on the Superconductivity of (TMTSF)$_2$ClO$_4$ Crystals

Yusei MARUYAMA,* Reiko HIROSE, Gunzi SAITO, and Hiroo INOKUCHI** *(*Ochanomizu Univ. and IMS, **Ochanomizu Univ.)*

[*Solid State Commun.*, **47**, 273 (1983)]

We observed the energy gap spectra for (TMTSF)$_2$ClO$_4$-Al$_2$O$_3$-Au junctions at 1.5K by measuring their tunneling current characteristics. Figure 1 shows typical temperature dependence of dI/dV curves. The curves observed above 20K are just flat in this voltage range. Below 4.2K, however, remarkable change in the curvature of the curves appears, which may directly indicate the change, or reduction, of electron state densities in the energy region around the Fermi level of (TMTSF)$_2$ClO$_4$ crystal. This fact means the existence of the superconducting fluctuation in this substance below 4.2K.

At the lowest temperature measured (1.5K), a narrow flat portion can be recognized around the zero-bias voltage, which may be the indication of the appearance of superconducting gap, that is zero

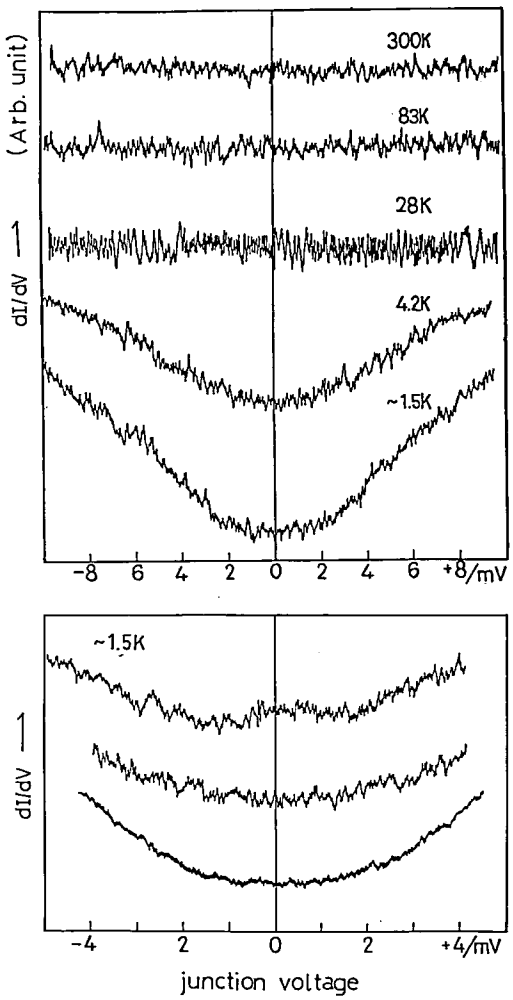

Figure 1. Temperature dependence of dI/dV characteristics. In the lower figure, dI/dV curves of three different stages of cells are presented.

state-density region, even at 1.5K. The width of the flat portion is 1.5 − 2 meV which corresponds to 2 − 6K as T_c, superconducting transition temperature. These values are about 1/4 of those reported by French group (8 meV).[1)]

Reference

1) A. Fournel, C. More, G. Roger, J.P. Sorbier, J.M. Delrieu, D. Jerome, M. Ribault, and K. Bechgaard, *J. Phys. Lett.*, **42**, L-445 (1981)

IV-E-8 Precise Determination of Critical Field Anisotropy in $(TMTSF)_2ClO_4$

Kokichi OSHIMA,* Hiroshi BANDO,* Hayao KOBAYASHI, and Gunzi SAITO** *(*Univ. of Tokyo, **Toho Univ.)*

[*J. Magnetism and Magnetic Materials,* **31-34,** 1147 (1983)]

The superconducting transition field of $(TMTSF)_2ClO_4$ was studied in the basal plane by the microwave (9 GHz) technique at liquid ^3He temperature. The result indicates a sharp superconducting transition in the magnetic field in contrast with that so far reported. The distribution of the critical field in the crystal was observed and related to the crystal twinning effect (Figure 1).

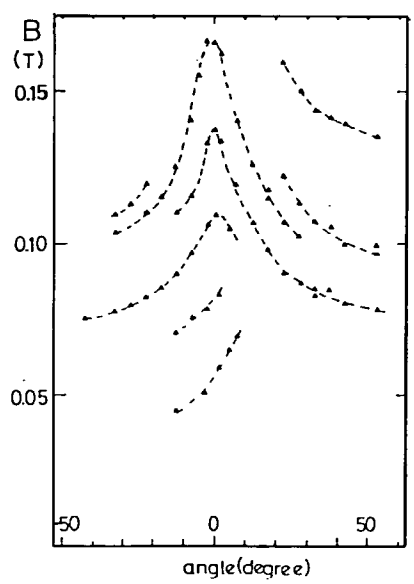

Figure 1. Angular dependence of the critical field in the b-c plane. Angle 0 corresponds to nearly the b axis. Dashed curves are guides.

IV-E-9 Anomalous Longitudinal Magnetoresistance in $(TMTSF)_2ClO_4$

Keizo MURATA,* Takashi UKACHI,* Hiroyuki ANZAI,* Koji KAJIMURA,* Takehiko ISHIGURO* and Gunzi SAITO *(*Electrotechnical Laboratory)*

[*J. Magnetism and Magnetic Materials,* **31-34**, 1145 (1983)]

Negative longitudinal magnetoresistance was observed in the nonmetallic state of $(TMTSF)_2ClO_4$, which showed no resistance jumps during the cooling process (Figure 1). This is explained by the assumption of the spin density wave gap which is suppressed by a magnetic field. Below the superconducting temperature, anomalous enhancement of resistivity was observed around 10 kOe.

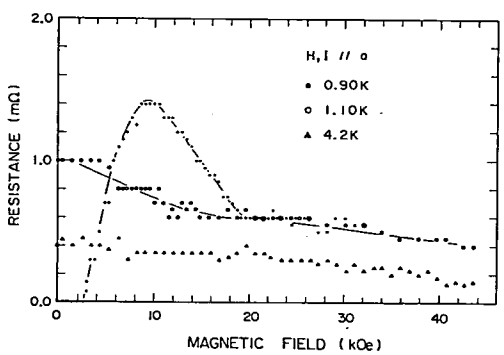

Figure 1. Longitudinal magnetoresistance at three temperatures. At 0.9K, the measuring current was 0.5 mA. The lines are guides to the eye.

IV-E-10 Superconducting Transition of Organic Metal $(TMTSF)_2ClO_4$: Effects of Thermally Induced Microcracks

Keizo MURATA,* Koji KAJIMURA,* Hiroshi TOKUMOTO,* Takashi UKACHI,* Madoka TOKUMOTO,* Hiroyuki ANZAI,* Takehiko ISHIGURO,* and Gunzi SAITO *(*Electrotechnical Laboratory)*

[*Proc. Int. Cryog. Mater. Cong.*, 434 (1982), K. Tachikawa, A.F. Clark ed., Butterworth, Guildford, UK]

The shape of the resistive transition of $(TMTSF)_2ClO_4$ has been sample dependent. We

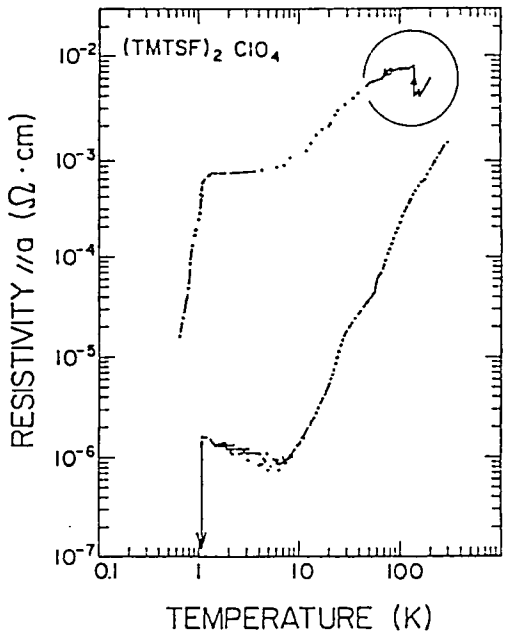

Figure 1. Two typical examples of the overall behavior of the resistivity vs. temperature relation of $(TMTSF)_2ClO_4$ with and without the resistance jumps. In the circle, one arrow indicates the resistance jump, and the other, the cooling process. The arrow near 1K shows the transition to zero-resistance state.

show that the transition behaviors are closely related to the occurrence of the resistance jumps, i.e. thermally induced microcracks, which reduce apparent resistance ratio R(300K)/R(near T_c). The broading in the resistive transition is considered to be either due to the distribution in the strength of Josephson coupling between the domains separated by microcrack barriers or due to the distribution in the transition temperature of the domains (Figure 1).

IV-E-11 Kink Deformation of $(TMTSF)_2ClO_4$ Single Crystal and Its Influence on Electrical Resistivity

Takehiko ISHIGURO,* Takashi UKACHI,* Katsuo KATO,* Keizo MURATA,* Koji KAJIMURA,* Madoka TOKUMOTO,* Hiroshi TOKUMOTO,* Hiroyuki ANZAI,* and Gunzi SAITO *(*Electrotechnical Laboratory, **National Institute for Research in Inorganic Materials)*

[*J. Phys. Soc. Jpn.*, **52**, 1585 (1983)]

Mechanical kinks are formed in a needle crystal

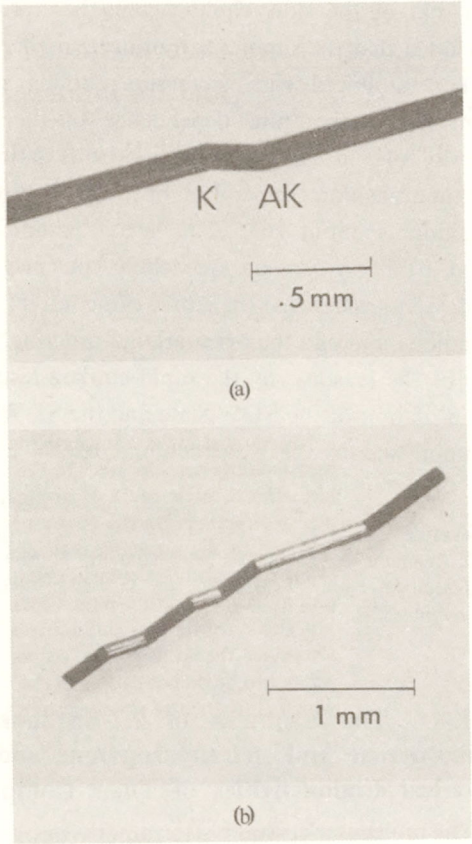

Figure 1. (a) A pair of kink (denoted with **K**) and antikink (**AK**) formed in $(TMTSF)_2ClO_4$ needle crystal.
(b) Three pairs of kink and antikink formed in a crystal. The sample was illuminated so that deformed part lying between kink and antikink (shining by reflecting light) and the undeformed part were discriminated.

of $(TMTSF)_2ClO_4$ by applying stresses. The kink which has definite angle of 18.4° accompanies antikink with the same angle in the opposite direction (Figure 1). By the X-ray precession photograph, we show that the kink is ascribed to the mechanical twinning with the boundary on the (210) plane. The electrical resistivity measurements in a deformed part lying between the kink and antikink and in a region including the kink were carried out, but they did not show substantial difference compared with those in an undeformed part. However, the kink which accompanies distortion in a molecular stack is considered to be one of causes of the resistance jump (stepwise increase in resistance), which is frequently observed during cooling.

IV-E-12 Spin-Density-Wave and Superconducting States in Thermally Quenched $(TMTSF)_2ClO_4$

Koji KAJIMURA,* Hiroshi TOKUMOTO,* Madoka TOKUMOTO,* Keizo MURATA,* Takashi UKACHI,* Hiroyuki ANZAI,* Takehiko ISHIGURO,* and Gunzi SAITO *(*Electrotechnical Laboratory)*

[*Solid State Commun.*, **44**, 1573 (1982)]

Successive transitions from metal to the spin-density-wave (SDW) state and the three-dimensional superconducting state were found in $(TMTSF)_2ClO_4$ when the high-temperature disordered state above 25K is frozen at low temperatures by thermal quenching (Figure 1). The SDW state was suppressed after the sample was warmed above 25K and cooled slowly. The appearance of the SDW and the three-dimensional superconducting state in the quenched state is interpreted in terms of the

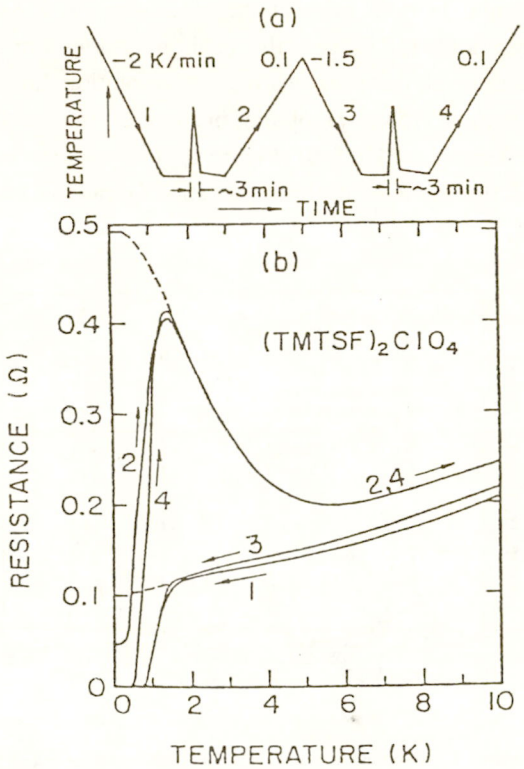

Figure 1. (a) Schematic diagram of thermal quenching and annealing. The rates of temperature variation are indicated along lines.
(b) Resistance vs. temperature for the thermal quenching and annealing. Labels corresponds to those in (a).

decrease in interchain distance or the reduction of the coherence between columns, both of which could result from the thermally quenched random occupancy of two possible configurations of ClO_4 anions.

IV-E-13 Quenching Effect on the Anion Ordering in $(TMTSF)_2ClO_4$ ··· An X-Ray Study ···

Seiichi KAGOSHIMA,* Takashi YASUNAGA,* Takehiko ISHIGURO, Hiroyuki ANZAI,** and Gunzi SAITO** *(*Univ. of Tokyo, **Electrotechnical Laboratory)*

[*Solid State Commun.*, **46**, 867 (1983)]

It is found directly by an x-ray diffuse scattering study that the orientational ordering of ClO_4 anions is suppressed when the organic superconductor $(TMTSF)_2ClO_4$ is quenched from higher temperature to 15K. In the present study, the sample is cooled from 30K to 15K after annealing at 30K for 30min. In both cases of the cooling speed, 15K/40 min and 15K/9 sec, the peak intensities are the same and the peak widths are resolution limited. Then, at 15K, we obtain profiles of the satellite reflection at (4 0.5 0) (Figure 1). The peak intensity of the satellite of the rapid cooling case is lower than that of the slow cooling case, therefore it is concluded that the suppression of ordering becomes more pronounced with increasing cooling speed. From the temperature dependence of the peak intensity of the satellite reflection, it is estimated that the transition temperature of the order-disorder transition is about 26K. The lattice parameter is found to be frozen on quenching, on the other hand, we consider that the lattice can contract when the anions undergo the orientational ordering. That may be the reason why the rapid cooling results in the formation of the SDW state and the SDW state is suppressed in the slow cooling case.[1]

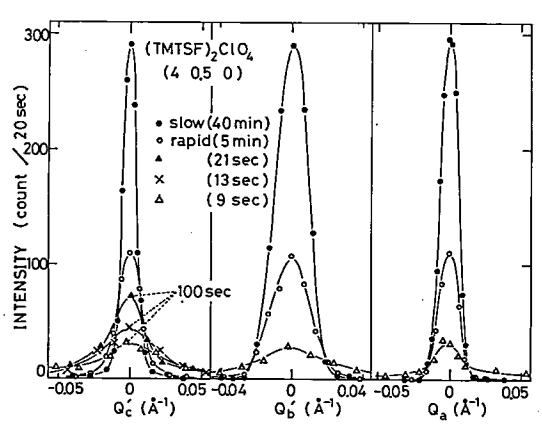

Figure 1. Profiles of the satellite reflection at (4 0.5 0) measured at 15K after a slow cooling and rapid coolings from 30K. Times spent to cool down the samples are shown in brackets. Widths of peaks in the slow cooling case are resolution limited. Note that the measurement time was 100 sec in the cases of rapid cooling with speeds of 15K/21 sec, 15K/13 sec, and 15K/9 sec. Q_a is parallel to the a* axis but Q_b, and Q_c are nearly parallel to the b* and c* axis, respectively.

Reference

1) K. Kajimura, H. Tokumoto, M. Tokumoto, K. Murata, T. Ukachi, H. Anzai, T. Ishiguro, and G. Saito, *Solid State Commun.*, **44**, 1573 (1982)

IV-E-14 The Synthesis of 2,7-Bis(dimethylamino)pyrene and -tetrahydropyrene and the Electrical Conductivities of Their Complexes

Naomi UEDA,* Bunji NATSUME, Kazumi YANAGIUCHI,* Yoshiteru SAKATA,* Toshiaki ENOKI, Gunzi SAITO, Hiroo INOKUCHI, and Soichi MISUMI* *(*Osaka Univ.)*

[*Bull. Chem. Soc. Jpn.*, **56**, 775 (1983)]

New π-donors containing a pyrene or a tetrahydropyrene ring were synthesized by means of a unique transannular reaction of the corresponding [2,2]metacyclophane derivatives. The CT complexes of these donors with a series of TCNQ derivatives different in electron affinity were prepared, and their electrical conductivities on single crystals were measured. The highest conductivity (0.36 $\Omega^{-1}cm^{-1}$) was that of the tetrahydropyrene derivative-TCNQ complex. It was reconfirmed that the partial CT from a donor to an acceptor is very important for high conductivity. (See section **VI-K**)

IV-E-15 Synthesis of Cyclobutane-fused Tetracyanoquinodimethanes

Shunro YAMAGUCHI,* Hitoshi TATEMITSU,* Yoshiteru SAKATA,* Toshiaki ENOKI, and Soichi MISUMI* *(*Osaka Univ.)*

[*J. Chem. Soc., Chem. Commun.*, **1982** 1065]

The preparation of the title π-acceptors from the corresponding cyclohexane-1,4-diones and the electrical conductivities of their CT complexes with TTF are described. (See section **VI-K**)

IV-E-16 New Wurster-Type Acceptors Isoelectronic with 2,6-Anthraquinone

Masakatsu NAKATSUKA,* Kazuhiro NAKASUJI,* Ichiro MURATA,* Iwao WATANABE,* Gunzi SAITO, Toshiaki ENOKI, and Hiroo INOKUCHI *(*Osaka Univ.)*

[*Chem. Lett.*, **1983**, 905]

It is worth exploring new strong acceptors which contain charcogenide atoms in pursuit of organic metals where anion radicals of the acceptors play the essential role in the conduction. An enhanced intermolecular interaction may be expected in their complexes due to charcogenide···charcogenide and/or charcogenide···other hetero atom atomic contacts.

We have synthesized the new Wurster-type acceptors, 3,7-dihalo-2H,6H-benzo[1,2-b:4,5-b'] dithiophene-2,6-diones (**5a, 5b**), which have C_{2h} molecular symmetry with two sulfur atoms. The cyclic voltammograms yield electron affinities of 2.43 eV and 2.41 eV, in excellent agreement with those estimated from the solution CT bands of their pyrene complexes, 2.41 eV and 2.39 eV for 5a and 5b, respectively [using E_A (p-chloranil) = 2.48 eV].

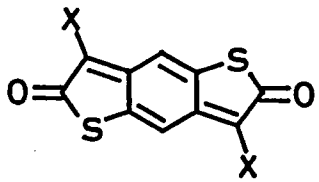

5

a, X = Br
b, X = Cl

The room temperature compaction resistivity of the 2:1 complex of tetrathiatetracene was 26 Ωcm.

IV-E-17 Poly (Carbon Diselenide) ; A Metallic Polymer?

Hayao KOBAYASHI,* Takehiko MORI, Reizo KATO,** Akiko KOBAYASHI,** Yukiyoshi SASAKI,** Gunzi SAITO, and Hiroo INOKUCHI** *(*Toho Univ., **Univ. of Tokyo)*

[*Chem. Lett.*, **1983**, 1407]

We have prepared poly(carbon diselenide) as black solid from pure CSe_2. The compaction sample of our poly(carbon diselenide) was 10^4 – 10^5 times more conductive than the Okamoto and Wojciechowski's sample[1] (6×10^{-2} Ωcm vs. 10^3 Ωcm). The activation energy for the conduction of the compaction sample was very small down to about 30K and the thermoelectric power is as small as those of normal metals. Our poly(carbon diselenide) gave a sharp powder X-ray diffraction pattern, while the Okamoto and Wojciechowski's sample is amorphous. These facts suggeset that the solid poly(carbon diselenide) can be a metallic polymer barring crystal imperfection.

Reference

1) Y. Okamoto and P.S. Wojciechowski, *J. Chem. Soc., Chem. Commun.*, **1982**, 386.

IV—F Studies of Ion-Molecule Reactions by a Threshold Electron-Secondary Ion Coincidence (TESICO) Technique

The knowledge of the microscopic reaction cross sections for evolution of a system in a single reactant quantum state (translational, rotational, vibrational, and electronic) to a single product quantum state is essential for a complete understanding of a chemical reaction. Ion-molecule reactions are particularly suited

for studying such microscopic cross sections since ions can readily be prepared in various internal states in the initial ionization processes, such as photoionization, and the emitted photoelectrons provide information on the distribution among these states.

In this project, we study state-selected ion-molecule reactions by the use of a photoionization technique which utilizes the threshold photoelectron-secondary ion coincidence. The technique allows direct determination of $\sigma(i, v)$, i.e. the reaction cross section as a function of the internal and collisional energies of reactants. The selection of electronic, vibrational, rotational, and fine-structure states are possible by this technique.

IV-F-1 State Selected Charge-Transfer Reactions: $NO^+(a^3\Sigma^+,v\ ;\ b^3\Pi,v) + H_2 \rightarrow H_2^+ + NO$ and $H_2^+(X^2\Sigma_g^+,v) + NO \rightarrow NO^+ + H_2$

Kenichiro TANAKA, Tatsuhisa KATO, and Inosuke KOYANO

As a part of our continuing TESICO studies[1] of state selected ion-molecule reactions, we have determined the relative charge-transfer cross sections for individual vibrational states of reactant ions $NO^+(a^3\Sigma^+)$, $NO^+(b^3\Pi)$, and $H_2^+(X^2\Sigma_g^+)$ in the reactions

$$NO^+(a^3\Sigma^+,b^3\Pi) + H_2 \rightarrow H_2^+ + NO \qquad (1)$$
$$H_2^+(X^2\Sigma_g^+) + NO \rightarrow NO^+ + H_2. \qquad (2)$$

Vibrational states studied for the above three reactions are $v = 0 - 5$, $v = 0$ and 1, and $v = 0 - 6$, respectively. Experimental results for Reaction (1) obtained at a collision energy of 0.8 eV are shown in Figure 1.

In Reaction (1), the $a^3\Sigma^+$ state has been found to exhibit comparatively low reactivity and have cross sections which are almost independent of the vibrational state in the range $v = 0 - 5$. When we go from $v = 5$ of $a^3\Sigma^+$ to $v = 0$ of $b^3\Pi$, however, the cross section increases sharply by a factor of four, subsequently followed by a slight decrease at $v = 1$ of $b^3\Pi$. The cross section for Reaction (2) has also been found to be almost independent of vibrational quantum number in the range studied.

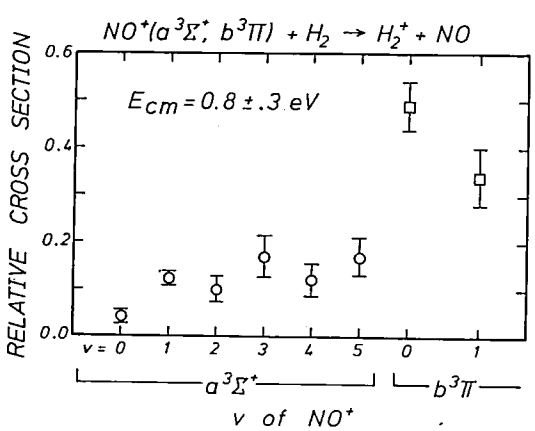

Figure 1. State selected cross sections for Reaction (1).

The vibrational-state independence of the $NO^+(a^3\Sigma^+)$ and $H_2^+(X^2\Sigma_g^+)$ cross sections, especially the lack of the expected resonant enhancement at $v = 2$ in both cases, shows that these reactions are governed by some factor(s) other than the energy defect and the Frank-Condon factors. This indicates that the charge transfer in these systems takes place via some intimate interaction between the reactants, rather than by an electron jump mechanism at relatively large intermolecular distances.

Reference

1) I. Koyano and K. Tanaka, *J. Chem. Phys.*, **72**, 4858 (1980).

IV-F-2 State Selected Charge-Transfer Reactions: $O_2^+(X^2\Pi_g,\ v\ ;\ a^4\Pi_u,\ v) + Ar \rightarrow Ar^+ + O_2$ and $Ar^+\ (^2P_{3/2},^2P_{1/2}) + O_2 \rightarrow O_2^+ + Ar$

Tatsuhisa KATO, Kenichiro TANAKA, and Inosuke KOYANO

We have investigated the vibronic-state selected charge transfer reactions

$$O_2^+(X^2\Pi_g,v;a^4\Pi_u,v) + Ar \rightarrow Ar^+ + O_2 \qquad (1)$$

and the spin-orbit state selected charge-transfer reactions

$$Ar^+(^2P_{3/2},\ ^2P_{1/2}) + O_2 \rightarrow O_2^+ + Ar \qquad (2)$$

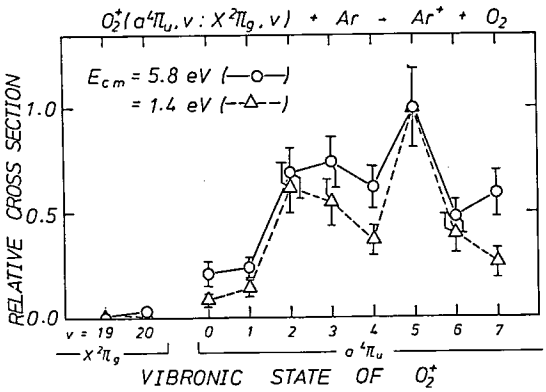

Figure 1. State selected cross sections for Reaction (1).

using the threshold electron-secondary ion coincidence (TESICO) technique.[1]

Experimental relative cross sections for Reaction (1) obtained at two different collision energies (1.4 and 5.8 eV) are summarized in Figure 1. As can be seen, the cross section is extremely small for the v = 19 and 20 states of $X^2\Pi_g$ in spite of the fact that Reaction (1) is exoergic for v = 19 and above. On the other hand, the cross section has significant values at v = 0 of the $a^4\Pi_u$ state and above, and shows an interesting variation as the vibrational quantum number is increased in the $a^4\Pi_u$ state. These salient feature are almost explained in terms of the energy resonance and Franck-Condon factors between the reactant and product states.

In contrast to the results for Reaction (1), no significant difference was observed in the cross section of Reaction (2) between the two spin-orbit states, the ratios of the J = 3/2 and J = 1/2 cross sections being essentially unity at both collision energies studied (1.4 and 5.8 eV). These results suggest that Reaction (2) dose not occur by a simple electron jump mechanism to form $O_2^+(a^4\Pi_u)$, but proceeds via some complex state(s), to form $O_2^+(X^2\Pi_g)$.

Reference

1) I. Koyano and K. Tanaka, *J. Chem. Phys.*, **72**, 4858 (1980).

IV-F-3 Vibrational-State Selected Study of the Reaction of $O_2^+(v)$ with CH_4

Kenichiro TANAKA, Tatsuhisa KATO, and Inosuke KOYANO

We have applied the TESICO technique[1] to the vibrational-state selection of the O_2^+ ions in the reactions

$$O_2^+ (v) + CH_4 \rightarrow CH_3O_2^+ + H \quad (1a)$$
$$\rightarrow CH_3^+ + HO_2 \quad (1b)$$
$$\rightarrow CH_4^+ + O_2. \quad (1c)$$

The reaction $O_2^+ + CH_4$ has been investigated extensively from the viewpoint of the kinetic energy dependence of its overall rate constant, but very few studies have been performed from the viewpoint of the internal (vibrational) energy dependence.

In the present study, relative cross sections for the three vibrational states of the O_2^+ ions (v = 0 – 2) have been separately determined for each of reactions (1a) – (1c). In Figure 1, experimental results obtained at the average collision energy of 0.2 eV are summarized. In the reaction with O_2^+ (v = 0), $CH_3O_2^+$ is the dominant product ion (>60%),

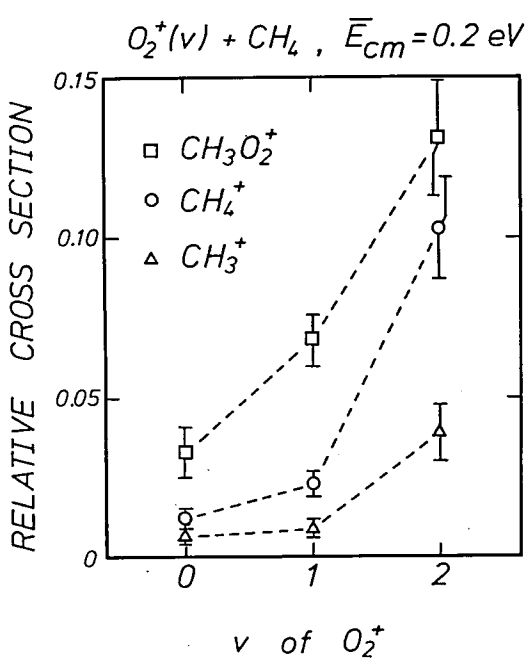

Figure 1. State selected cross sections of reactions (1a) – (1c) for the vibrational states of the O_2^+ ion, obtained at the average collision energy of 0.2 eV.

as has been established previously. With $v = 1$, the cross sections for both reactions (1a) and (1c) increase by a factor of about two. While the sum of the $v = 1$ vibrational energy (0.23 eV) and the average translational energy (0.2 eV) overcomes the endoergicity of reaction (1b), the cross section for this reaction still remains small for $v = 1$. With $v = 2$, however, the cross section for this reaction increase significantly, as well as those for the other two reactions. The increase is most conspicuous for reaction (1c).

Reference

1) I. Koyano and K. Tanaka, *J. Chem. Phys.*, **72**, 4858 (1980).

IV-F-4 Vibrational-State Selected Reaction Cross Sections for $C_2H_2^+(v) + D_2$.

Kenji HONMA *(Univ. of Tokyo)*, **Tatsuhisa KATO, Kenichiro TANAKA, and Inosuke KOYANO**

Relative cross sections of the reaction of acetylene ion with deuterium molecule have been determined for individual vibrational states ($v = 0 - 2$ of the C-C stretching mode) of the $C_2H_2^+$ ion. This reaction system has the following four product channels, two of which (channels (3) and (4)) are endothermic for the vibrational ground states of the reactants.

$$C_2H_2^+(v) + D_2 \rightarrow C_2HD^+ + HD \quad (1)$$
$$\rightarrow C_2D_2^+ + H_2 \quad (2)$$
$$\rightarrow C_2H_2D^+ + D \quad (3)$$
$$\rightarrow C_2HD_2^+ + H \quad (4)$$

The results are summarized in Figure 1. As can be seen from the figure, the cross section of channel (4) (σ_{29} in the figure) increases with increasing vibrational quantum number at low collision energies, and becomes independent of the vibrational quantum number at higher collision energies. The cross section of channel (1) shows sharp contrast with that of channel (4); it decreases with increasing vibrational quantum number at low collision energy. The large cross section of this H-D exchange channel indicates that the reaction proceeds via a complex mechanism. At high

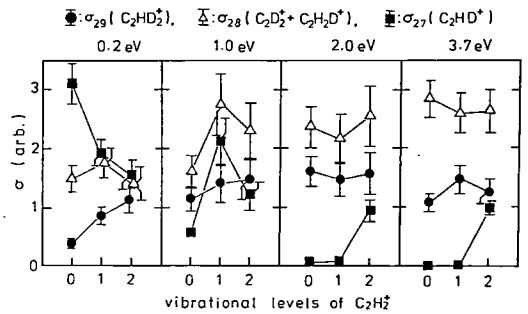

Figure 1. State selected cross sections of Reactions (1) - (4) for the vibrational states of the $C_2H_2^+$ ion, obtained at the collision energies of 0.2 eV, 1.0 eV, 2.0 eV, and 3.7 eV.

collision energies (2.0 and 3.7 eV), channel (1) has very small cross sections for $v = 0$ and 1. Only for $v = 2$ this channel proceeds with significant probability. This behavior may imply that the complex mechanism changes to some direct one at collision energies around 1.0 eV.

IV-F-5 An *ab initio* Study of Potential Energy Surfaces for the Reaction $NO^+(a^3\Sigma^+) + Ar \rightarrow Ar^+ + NO$.

Tatsuhisa KATO, Kenichiro TANAKA, and Inosuke KOYANO

In order to understand the experimental results of our previous study[1] on the state selected charge transfer reactions

$$NO^+(a^3\Sigma^+,v;\ b^3\Pi,v) + Ar \rightarrow Ar^+ + NO \quad (1)$$
$$Ar^+(^2P_{3/2},\ ^2P_{1/2}) + NO \rightarrow NO^+ + Ar, \quad (2)$$

we have performed an *ab initio* calculation of partial potential energy surfaces of the triplet states of the $(Ar\text{-}NO)^+$ system.

A part of the results is shown in Figure 1 in which the calculated potential energies are plotted as a function of the Ar-NO distance at a fixed N-O distance of 1.2Å and for two angles of approach (0° and 90° with respect to the NO molecular axis, taking the N atom end as 0°). In the 0° approach, the strong interaction between the ($Ar^+ + NO$) and [NO^+ ($b^3\Pi$) + Ar] states at large internuclear separation stabilizes the ($Ar^+ + NO$) state, causing an (avoided) crossing with the [$NO^+(a^3\Sigma^+)$ + Ar]

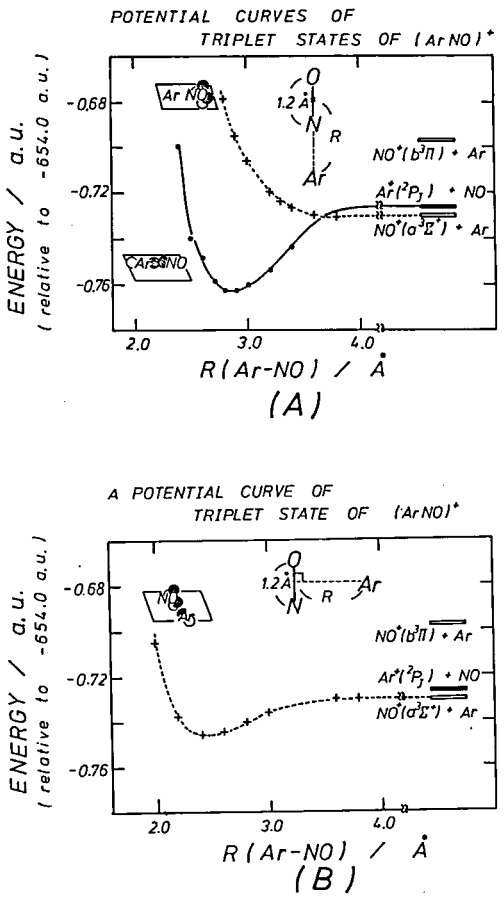

Figure 1. Potential energy surfaces of the triplet states of the $(Ar\text{-}NO)^+$ system. A: for the 0° approach, B: for the 90° approach.

state at a shorter distance. At this crossing a Landau-Zener type transition would occur, in which the properties of the system at infinite internuclear distance (energy defect and Franck-Condon factors) have nothing to do with the transition probability. In the 90° approach, on the other hand, the interaction between the close lying (Ar^+ + NO) and [$NO^+(a^3\Sigma^+)$ + Ar] states makes these states repel each other, causing a Steuckelberg-Demkov type transition between these states at comparatively large internuclear distances. In this case, the properties at infinite internuclear distance would still have relevance to the transition probability.

Reference

1) T. Kato, K. Tanaka, and I. Koyano, *J. Chem. Phys.*, **79**, No. 12 (1983); *IMS Ann. Rev.*, 1982, 72.

IV—G Photoionization Processes in Small Molecules

Inosuke KOYANO, Kenichiro TANAKA, and Tatsuhisa KATO

Two techniques have been generally used for the study of molecular photoionization processes, i.e., measurements of photoionization efficiency curves (PIEC) and photoelectron spectra (PES). While PIEC yields a wealth of information on the ionization processes and energy levels of ions and neutral molecules, difficulty is often encountered with this technique when autoionization obscures the step structure of the curve. In such a situation, we often resort to PES which provides precise locations of ionic states and transition probabilities of these states. However, ionic states that can be studied by the ordinary (constant wavelength) PES are largely limited to the states which combine with the ground state of the parent molecule with favorable Franck-Condon factors. Another type of photoelectron spectroscopy is the threshold electron spectroscopy (TES) which uses a variable wavelength light source and detects only the zero kinetic energy photoelectron (threshold electrons). In this method, ionic states which are not favored by direct ionization are often observed through autoionization.

In this project, we study photoionization processes in small molecules by simultaneous measurements of photoionization efficiency curves and threshold electron spectra. Furthermore, we find that the analysis of autoionizing transitions is often possible utilizing charge-transfer processes of the product ions.[1] This technique is also incorporated.

Reference

1) K. Tanaka, T. Kato, and I. Koyano, *IMS Ann. Rev.*, 1981, 100; *Chem. Phys. Lett.*, **97**, 562 (1983)

IV—H Spectroscopy and Chemical Dynamics Using Supersonic Nozzle Beams

The usefulness of supersonic nozzle beams has increasingly been recognized in both spectroscopy and chemical dynamics. The capability of cooling internal degrees of freedom of molecules and the possibility of producing various kinds of molecular clusters are important properties of the technique. In this project, we aim at high resolution absorption and Raman spectroscopy, dynamical studies of cluster reactions, and their combination, utilizing the above properties of supersonic nozzle beams.

IV-H-1 Characterization of Seeded Molecular Beams: Translational Nonequilibrium and Velocity Slip

Norio TAKAHASHI *(Kyoto Univ.)*, **Tomio MORIYA** *(Kyoto Univ.)*, **Koji TESHIMA** *(Kyoto Univ.)*, **Kenichiro TANAKA, Tatsuhisa KATO, and Inosuke KOYANO**

As a continuation of our previous studies on the characterization of molecular beams,[1] time-of-flight measurements of supersonic molecular beams of He seeded by 2% Ne, Ar, or Kr have been performed. Parallel temperature of the seeded molecule has been found to be always higher than that of the diluent and to increase with mass of the seeded molecule, whereas that of He (diluent) is almost independent of the nature of the seeded molecule. The mean velocity of the seeded molecule has been found to be always smaller than that of the diluent, and the difference between them (velocity slip) has been found to increase with mass of the seeded molecule and decrease with P_0d (P_0: source pressure, d: nozzle diameter).

These findings are nearly consistent with the numerical calculation based on the source flow expansion model of a binary gas mixture.[2] As a typical result, the parallel temperature and the final speed ratio for Kr and He, obtained from the time-of-flight measurements of the He supersonic beam seeded by 2% Kr, are shown in Figure 1, together with the results of the numerical calculation.

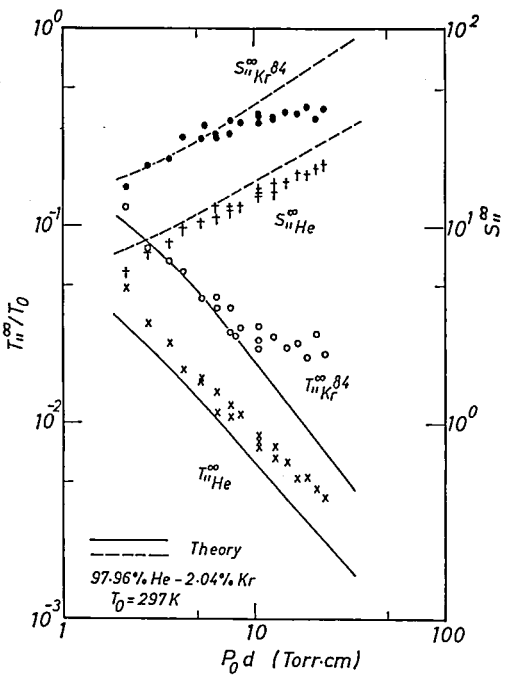

Figure 1. Parallel temperature ($T_{\parallel}^{\infty}$) and final speed ratio ($S_{\parallel}^{\infty}$) for Kr and He in the supersonic beam of He seeded by 2% Kr, as a function of P_0d.

References

1) K. Teshima, K. Tanaka, T. Kato, and I. Koyano, *IMS Ann. Rev.*, 75 (1982).
2) N. Takahashi and K. Teshima, *Memoirs of Faculty of Engineering*, Kyoto Univ. **45**, 79 (1983).

IV-I HeI Photoelectron Spectroscopic Studies of Gaseous Molecules

Molecular photoelectron spectroscopy with the 584 Å HeI resonance line is a useful and important technique to determine ionization potentials of valence electrons for organic and inorganic molecules in the gas phase. It seems to be an interesting subject to study correlations between ionization energies and other chemical properties for molecular systems.

IV-I-1 A Photoelectron Spectroscopic Study of A Series of Ferrocene Compounds

Takeko MATSUMURA *(Nara Univ. of Educ.)*, **Yoshio UMEZAWA** *(The Univ. of Tokyo)*, **Yohji ACHIBA, and Katsumi KIMURA**

In this project, measurements of HeI photoelectron spectra have been carried out for a series of ferrocene derivatives in the gas phase in order to study correlation between the electrochemical reversible oxidation potentials and the ionization potentials.

IV—J Studies of Ionization of Hydrogen Bonded Dimers by Photoelectron Spectroscopy

Photoelectron spectra of hydrogen-bonded dimers produced in a supersonic expansion are interesting from not only a geometrical point of view but also an electronic point of view. The first photoelectron band of the water dimer has been found to be very broad from our previous HeI photoelectron spectroscopic study, indicating that the adiabatic ionization potential is considerably smaller than the vertical ionization potential. This suggests that the equilibrium geometry of the water dimer cation considerably differs from that of the neutral water dimer because of proton transfer. In this project we have further extended our supersonic-beam photoelectron spectroscopic technique to other hydrogen-bonded dimers such as methanol dimer and formic-acid dimer. Ab initio calculations have also been carried out to study the equilibrium geometries and proton-transfer potential-energy surfaces of the water dimer cation in the two lowest electronic states. Ionization potential calculations have also been performed for various water clusters up to octamer to compare their ionization potentials with those available for ice.

IV-J-1 Photoelectron Spectroscopic Study of Simple Hydrogen-Bonded Dimers. I. Supersonic Nozzle Beam Photoelectron Spectrometer and The Formic Acid Dimer

Shinji TOMODA, Yohji ACHIBA, Katsunori NOMOTO, Kenji SATO, and Katsumi KIMURA

[*Chem. Phys.*, **74**, 113 (1983)]

In this paper we describe several characteristics of our supersonic nozzle beam photoelectron spectrometer recently constructed for studying hydrogen-bonded dimers in the gas phase by HeI (58.4 nm) radiation. Using this photoelectron apparatus, we have re-investigated the HeI photoelectron spectrum of the formic acid dimer $(HCOOH)_2$ which is well known as a fairly strong doubly hydrogen-bonded dimer. It was found that the $(HCOOH)_2$ spectrum deduced here from the spectrum of the monomer-dimer mixture considerably differs from that reported by Carnovale et al.[1] in the region beyond 16.5 eV. New spectrum assignments are given for four ionization bands beyond 16.5 eV. It is also indicated that the lower bound of the dissociation energy of $(HCOOH)_2^+$ is estimated to be 1.0 ± 0.1 eV on the basis of the experimental data. This value is considerably smaller than the value of 1.7 ± 0.2 eV recently reported for the water dimer cation $(H_2O)_2^+$.[2]

References

1) F. Carnovale, M.K. Livett, and J.B. Peel, *J. Chem. Phys.*, **71**, 255 (1979).
2) S. Tomoda, Y. Achiba, and K. Kimura, *Chem. Phys. Lett.*, **87**, 197 (1982).

IV-J-2 Photoelectron Spectroscopic Study of Simple Hydrogen-Bonded Dimers. II. The Methanol Dimer

Shinji TOMODA and Katsumi KIMURA

[*Chem. Phys.*, **74**, 121 (1983)]

HeI photoelectron spectra of a supersonic jet of methanol vapor have been obtained by using the temperature-controlled supersonic-nozzle-beam photoelectron spectrometer recently constructed in our laboratory.[1] A HeI photoelectron spectrum attributable to the methanol dimer $(CH_3OH)_2$ has been deduced by spectrum stripping from

monomer-dimer mixed spectra. The first ten vertical ionization energies and the first adiabatic ionization energy of $(CH_3OH)_2$ have been determined from the stripped spectrum. Ab initio SCF MO calculations of ionization energies have also been carried out for $(CH_3OH)_2$ on the basis of Koopmans' theorem. The lower bound of the dissociation energy of $(CH_3OH)_2^+$ has been estimated to be 1.2 ± 0.2 eV from the adiabatic ionization energies of the monomer and dimer. The equilibrium structure of $(CH_3OH)_2$ is also discussed.

Reference

1) S. Tomoda, Y. Achiba, K. Nomoto, K. Sato, and K. Kimura, *Chem. Phys.*, **74**, 121 (1983).

IV-J-3 A Photoelectron Spectroscopic Estimation of the Concentrations of Simple Hydrogen-Bonded Dimers Produced in the Temperature-controlled Supersonic Nozzle Beam

Shinji TOMODA and Katsumi KIMURA

[*Bull. Chem. Soc. Jpn.*, **56**, 1768 (1983)]

A photoelectron spectroscopic method is proposed to estimate the ratio of number densities between the monomer and the dimer produced in the supersonic jet. Approximate monomer-dimer ratios have been estimated for water, methanol and formic acid by assuming that the photoionization cross sections of the monomer and dimer are equal to each other. The results are given in Table I. The results show reasonable agreement under similar conditions to those available from mass spectrometric analyses of fragmentation patterns. A simple temperature-controlled supersonic nozzle beam source is described here, which enables us to produce hydrogen-bonded dimers in measurable amounts.

Table I. Approximate dimer concentrations estimated from the photoelectron measurements

	Estimated dimer/monomer ratio[a]	Stagnation Condition[b]	
		T(K)	P(Torr)
Water	0.06	335	390
Methanol	0.2	295 ~ 320	100 ~ 260
Formic acid	3	298	20 + 130 (He)

a. Probable errors depend on the validity of the assumptions.
b. An aperture of 0.1 mm in diameter is used for the nozzle.

IV-J-4 Ionization Energies of the Water Dimer and Clusters

Shinji TOMODA and Katsumi KIMURA

[*Ions and Molecules in Solution,* A Collection of Invited Papers Presented at the Session Lectures and Microsymposia during the VI ISSSSI, Eds. N. Tanaka, H. Ohtaki, and R. Tamamushi, Elsevier, Amsterdam, 1983, p.13]

Ionization energies recently determined for the water dimer from HeI (58.4 nm) photoelectron spectrum by Tomoda et al.[1] are compared with Koopmans' theorem ionization energies based on ab initio SCF MO calculations. Model calculations have been carried out for various water clusters up to the octamer. The calculated first vertical ionization energies of the pentamer and octamer show good agreement with available experimental data on ice. The relative stability of the pentamer and octamer is suggested on the basis of "hydrogen-bond strength per bond" evaluated from the total energies.

Reference

1) S. Tomoda, Y. Achiba, and K. Kimura, *Chem. Phys. Lett.*, **87**, 197 (1982).

IV-J-5 Electronic and Molecular Structure of the Water Dimer Cation. A Theoretical Study

Kenji SATO, Shinji TOMODA, Katsumi KIMURA, and Suehiro IWATA* *(*Keio Univ.)*

[*Chem. Phys. Lett.*, **95**, 579 (1983)]

Ab initio configuration-interaction calculations of the water dimer cation were performed with a basis set including polarization functions. The ground and first excited states are energetically close to each other and have $1^2A''$ and $1^2A'$ symmetries, with bent and linear H···O–H equilibrium geometries, respectively.

IV-J-6 Proton-transfer Potential-energy Surfaces of the Water Dimer Cation $(H_2O)_2^+$ in the $1^2A''$ and $1^2A'$ States

Shinji TOMODA and Katsumi KIMURA

[*Chem. Phys.*, in press]

Ab initio potential energy surface calculations have been carried out for the water dimer cation as well as the neutral dimer to clarify the essential features of ionization and the subsequent relaxation behavior. The potential energy surfaces of the dimer cation in a linear trans conformation have clearly indicated proton transfer with no activation energy barrier in both the ground ($1^2A''$) and the first excited ($1^2A'$) state. Potential energy surface of the ground state $(H_2O)_2^+$ is shown in **Figure 1.**

The following conclusions have been obtained for the $1^2A''$ and the $1^2A'$ ionic state. (1) The potential surface has only one minimum at which the geometry is regarded as a complex between an oxonium ion (H_3O^+) and a hydroxyl radical (OH). This geometry differs quite largely from that of the neutral dimer. (2) Proton transferring relaxation from the vertically ionized point to the potential minimum may easily occur with no activation energy. (3) The potential minimum is still far from the wide Frank-Condon region expected from the shallow potential minimum of the neutral dimer. (4) There exist two dissociation channels to H_3O^+ + OH and to H_2O^+ + H_2O. The former dissociation energy is much smaller than the latter. A semi-quantitative estimation is also given for the first photoelectron band width of the water dimer.[1]

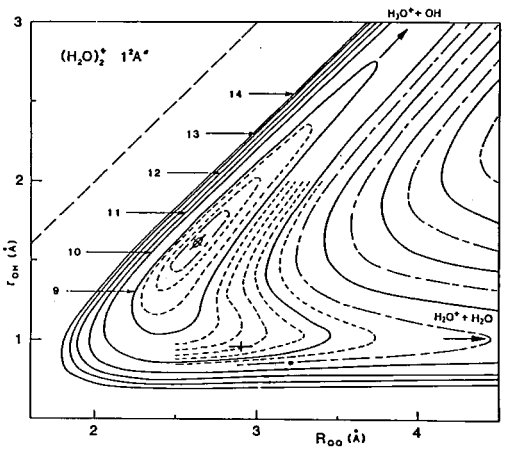

Figure 1. Potential-energy surface of the water dimer cation in the ground electronic ($1^2A''$) state. The solid, the dashed and the broken curves are drawn at intervals of 1, 0.5 and 0.2 eV, respectively. Values indicated by arrows are the potential energies measured from the H_2O + H_2O level. The cross (+) indicates the vertically ionized point and the cross with an ellipse indicates the $1^2A''$ potential energy minimum. Two dissociation channels are also indicated by arrows. The broken straight line defines the boundary of the R_{OO}-r_{OH} space.

Reference

1) S. Tomoda, Y. Achiba, and K. Kimura, *Chem. Phys. Lett.*, **87**, 197 (1982).

IV—K Developement of Multiphoton Ionization Photoelectron Spectroscopy and Its Application

Selective excitation and ionization of molecules by UV and visible lasers by means of multiphoton ionization technique seem to be very important from photo-physical and photo-chemical points of view. A combination of resonant multiphoton ionization with photoelectron spectroscopy has made it possible to study photoelectron spectra of the resonant excited states of atoms and molecules. In this project we have further extended the laser photoelectron technique which we have been developing to study various subjects: (1) multiphoton ionization of NO and NH_3 through Rydberg excited states; (2) ionization selectivity in multiphoton ionization of Xe and Kr; (3) autoionization processes of NO; (4) intramolecular relaxation processes at excited states of benzene and naphthalene; and (5) multiphoton ionization of atomic iron produced by decomposition of $Fe(CO)_5$ and ferrocence.

IV-K-1 A Photoelectron Spectroscopic Study of (3 + 1) Resonant Multiphoton Ionization of NO and NH_3

Yohji ACHIBA, Kenji SATO, Kosuke SHOBATAKE, and Katsumi KIMURA

[*J. Chem. Phys.*, **78**, 5474 (1983)]

In the present work, we have measured energy spectra and angular distributions of photoelectrons emitted by three-photon resonant four-photon ionization of **NO** and NH_3 in the gas phase. The following conclusions have been obtained: (1) Ionization of **NO** through the Rydberg **F** and **H** (**H'**) states at $v' = 0$ and 1 gives rise to the ground-state ion with $v = 0$ and 1, respectively, by a $\Delta v = 0$ transition; (2) Ionization of NH_3 through the Rydberg **C'** states with $v' = 0 - 5$ gives rise to the ground-state ion with $v = 0 - 5$, respectively, by $\Delta v = 0$ transitions; (3) Photoelectron angular distributions obtained for the (3 + 1) processes may well be interpreted in terms of cosine-square distributions. This fact strongly indicates that the ionization step takes place by one-photon direct ionization from the three-photon resonant states.

IV-K-2 Multiphoton Ionization Photoelectron Spectroscopic Study on Autoionization Processes of NO Molecule

Yohji ACHIBA, Kenji SATO, and Katsumi KIMURA

Autoionization processes resulting from a direct electronic coupling between neutral valence excited states and the ionization continuum have been studied for **NO** molecule by means of multiphoton ionization photoelectron spectroscopy. By selective excitation of the valence excited **B**, $^2\Pi$ state as a resonant intermediate, it was found that one additional photon absorption from the **B** state effectively produces the super-excited valence state lying above the ionization threshold and then the ionization transition takes place through an electronic coupling with the ionization continuum.

According to theoretical predictions, the valence excited states of **NO** have repulsive potentials above the ionization threshold. Thus, the autoionization may proceed in competition with a very fast dissociation process such as $\mathbf{NO^* \rightarrow N(^2D) + O(^3P)}$. The photoelectron branching ratio for such a case is expected to be governed by the Franck-Condon overlaps of the vibrational wave functions between the repulsive potential and the ground-state ion. This is indeed the case for the observed photoelectron spectrum shown in **Figure 1.**

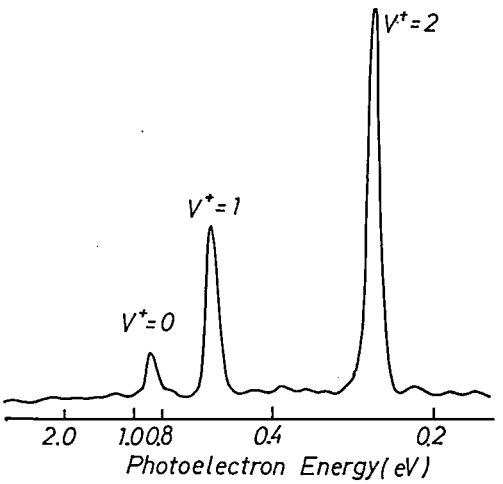

Figure 1. A multiphoton ionization photoelectron spectrum obtained by two-photon excitation at the **B**, $^2\Pi$, $v' = 9$ state of **NO** as an intermediate. The observed photoelectron kinetic energy clearly shows that the ionization transition is a three-photon process.

IV-K-3 A Photoelectron Spectroscopic Study of Ionization Selectivity in Resonantly Enhanced Multiphoton Ionization of Xe and Kr

Kenji SATO, Yohji ACHIBA, and Katsumi KIMURA

[*J. Chem. Phys.*, in press]

Photoelectron energy and angular distribution measurements were carried out for resonant multiphoton ionization (MPI) of Xe and Kr through some Rydberg excited states which have $^2P_{3/2}$ ionic core. From the (3 + 1) resonant MPI of Xe through the 5d [2 1/2]° J = 3 Rydberg state, it has been demonstrated that only the $^2P_{3/2}$ ionic state is produced. (See **Figure 1(b)**) Such selectivity, which can be explained in terms of removal of the Rydberg electron without relaxation of ionic core, has also been observed for the 5d [3 1/2]° J = 3 state of Xe and the 5s [1 1/2]° J = 1 state of Kr. For the 6s [1 1/2]° J = 1 state of Xe, however, both the $^2P_{1/2}$ and $^2P_{3/2}$ states are produced. This breakdown of the one-electron ionization picture may be due to the near resonance in the four-photon level.

Photoelectron angular distributions obtained here for the resonant MPI of Xe and Kr show obvious deviations from the cosine square dis-

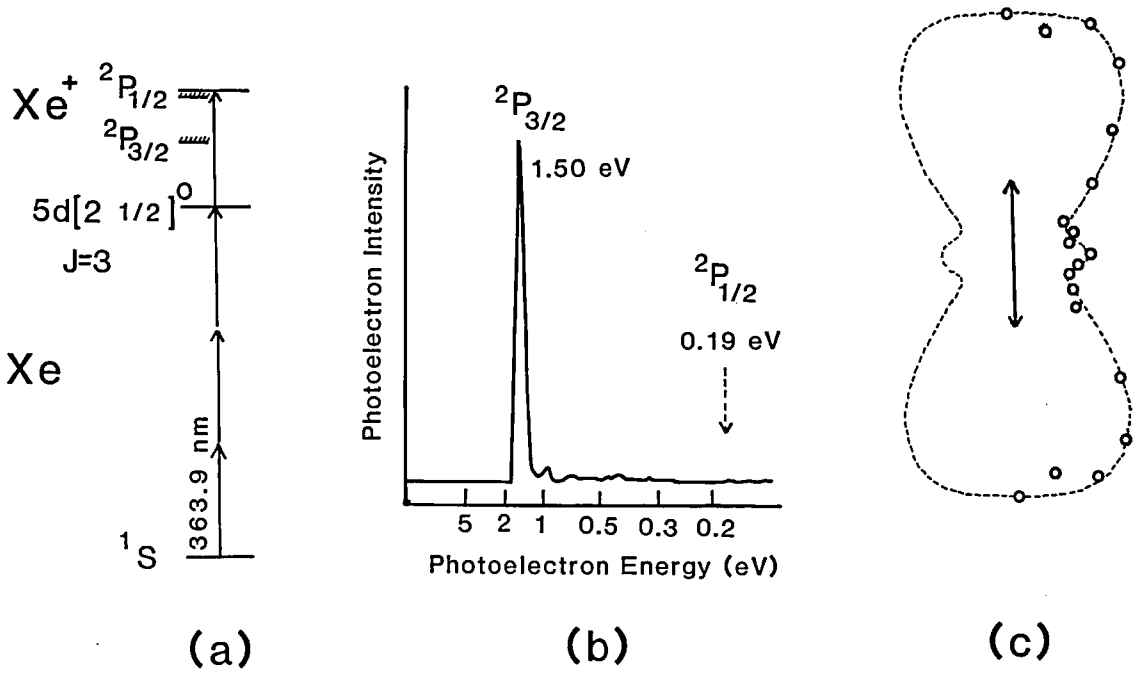

Figure 1. The (3 + 1) resonant MPI of Xe via the 5d [2 1/2]° J = 3 state. (a) Energy level diagram. (b) Photoelectron kinetic energy spectrum. (c) Photoelectron angular distribution. The dotted curve shows a least-squares fit: $0.303 - 0.943 \cos^2\theta + 3.40 \cos^4\theta - 0.587 \cos^6\theta - 1.18 \cos^8\theta$.

tribution, (See **Figure 1(c)**) reflecting the spatial alignment of the total electronic angular momentum in the resonant Rydberg states.

IV-K-4 Resonant Multiphoton Ionization Photoelectron Spectroscopic Study of Benzene. Evidences for Fast Intramolecular Vibrational Relaxation within the $^1E_{1u}$ State

Yohji ACHIBA, Kenji SATO, Kosuke SHOBATAKE, and Katsumi KIMURA

[*J. Chem. Phys.*, 79, 5213 (1983)]

Resonant multiphoton ionization photoelectron measurements were carried out for benzene under collision-free conditions in such a way that the benzene molecule is ionized by four photons through various two-photon allowed vibronic levels of the $^1E_{2u}$ excited state. As a result, single prominent, somewhat broad photoelectron bands were observed in the 0.14 − 0.36 eV region, arising from $\Delta v = 0$ ionization transitions. The prominent peak is shifted with increasing photon energy by $\mathbf{K} = h\nu_l - \mathbf{C}$, where **K** is the photoelectron energy, $h\nu_l$ the photon energy, and **C** a constant. This relationship strongly indicates that the third photon is resonant with a real intermediate excited state. Therefore, the overall ionization process is expressed by (2 + 1 + 1). It is concluded that fast intramolecular vibrational relaxation occurs at the third-photon states within the $^1E_{1u}$ ($\pi\pi^*$) state and subsequent ionization takes place from vibrationally relaxed levels. The relaxation within the $^1E_{1u}$ state is supported from the 0–0 energy which was evaluated here for the ionized states from the photoelectron data. It is also suggested that the lifetime of the vibrationally relaxed $^1E_{1u}$ states is the order of 10^{-11} − 10^{-12} s or longer.

IV-K-5 Multiphoton Ionization Photoelectron Spectroscopic Study on Intramolecular Relaxation Processes of Naphthalene

Atsunari HIRAYA *(Tohoku Univ. and IMS)*, **Yohji ACHIBA, Kenji SATO, Naohiko MIKAMI** *(Tohoku Univ. and IMS)*, **and Katsumi KIMURA**

Vibrationally resolved multiphoton ionization photoelectron spectra have been measured for various vibronic levels at the S_1 and S_2 of the jet cooled naphthalene. Measured photoelectron spectra provide new information about some vibrational frequencies of the molecular ion which have not been available from conventional vacuum UV photoelectron spectroscopy. Franck-Condon factors between the S_1 and the ground-state cation have also been determined for some vibrational modes.

On the basis of these experimental results obtained on the ionization process for each vibrational mode, the present photoelectron study also provides an insight into the dynamic properties of the excited state. The following conclusions have been derived. First, the intramolecular electronic relaxation from S_2 to S_1 is the faster process than the ionization, indicating that the relaxation rate is of order $\geq 10^{11}$ sec. Second, the intramolecular vibrational redistribution occuring at the energy level higher than 2200 cm^{-1} above the S_1 origin may be explained by the assumption that the redistribution populates all possible vibrational states with roughly equal probability.

IV-K-6 Multiphoton Dissociation of Ferrocene and Iron Pentacarbonyl. A Multiphoton Ionization Photoelectron Study.

Yatsuhisa NAGANO *(Osaka Univ.)*, **Yohji ACHIBA, Kenji SATO, and Katsumi KIMURA**

Multiphoton ionization (MPI) spectra obtained here for ferrocene and iron pentacarbonyl in the 360 − 460 nm laser wavelength region are both attributed to ionization of atomic iron generated by multiphoton dissociation of these compounds, although the both spectra largely differ from each other especially in intensity pattern, as shown in **Figure 1.** The present MPI photoelectron study has made it clear that this disagreement is due to the fact that the iron atoms generated from $Fe(CO)_5$ populate the excited states considerably higher than those from ferrocene. This fact may be explained by difference in the number of photons absorbed rather than the dissociation energy.

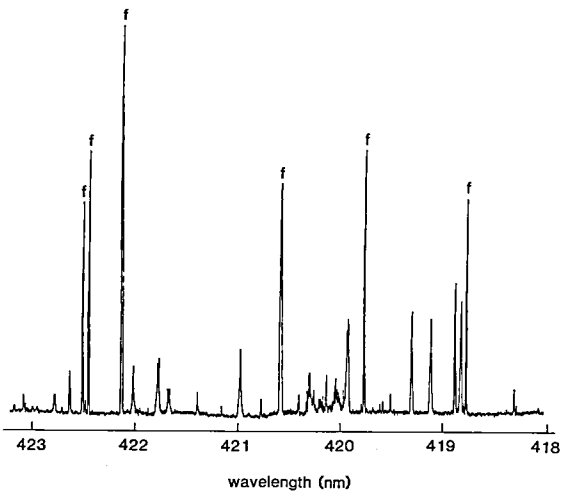

Figure 1. MPI ion current spectrum of iron pentacarbonyl. Only the lines marked with "f" appears in the MPI spectrum of ferrocene under the identical laser power conditions.

Previously, kinetic energies and angular distributions of photoelectrons emitted by (2 + 1) resonant MPI of atomic iron through two-photon resonant states e^7D and e^5D have been studied.[1]

Reference

1) Y. Nagano, Y. Achiba, K. Sato, and K. Kimura, *Chem. Phys. Lett.*, 93, 510 (1982).

IV—L Production, Characterization, and Spectroscopic Studies of Molecular Complexes and Clusters

There are several techniques to investigate the physics and chemistry of molecular complexes and clusters. One of the most powerful techniques for production of such weakly bound complexes is the supersonic expansion of a high pressure gas through a small nozzle hole, by which one can produce a very large number of exotic complexes. However, the characterization of these complexes is hard because of its weak bonding character.

In this project we adopt a couple of different approaches to determine the interaction potential between atoms and molecules. One approach is to apply a crossed molecular beams technique to the measurement of differential scattering cross sections. Another approach is to study the spectroscopy of van der Waals complexes and clusters. We plan to use both the Molecular Beam Chemistry Apparatus (MBC-I) and a color center infrared laser to investigate predissociation dynamics of vibrationally excited van der Waals molecules.

IV-L-1 Differential Cross Sections of NO Scattered from Ar at Thermal Collision Energies

Kosuke SHOBATAKE, Shigeru OHSHIMA, and Kiyohiko TABAYASHI

Van der Waals molecules (VDWM's) including a NO moiety present a good system for spectroscopic studies of VDWM's in the different electronic states.[1] It is important to determine the intermolecular potentials involving an NO molecule in the ground electronic state, since the VDWM's in the ground state are the starting complexes for their spectroscopic studies. Therefore, we have measured differential cross sections for non-reactive scattering of NO from Ar using the newly constructed crossed molecular beams apparatus mentioned in Research Activities IV-M-2. **Figure 1** shows the angular distribution of NO scattered from Ar at nominal collision energies E = 1.32 and 1.00 kcal/mole. For the production of NO and Ar beams we have used supersonic nozzle expansion technique. The mixture gas of 10% NO in Ar was expanded through a 50 micron nozzle of a variable temperature beam source. The Ar beam was produced through a 50 micron nozzle at a stagnation pressure of 3.0 atm. The source temperatures were 301K for Ar beam and 301K and 167K for NO beams. Figure 1 also shows the calculated angular distributions using the anisotropic potential determined from the integral scattering cross section measurement.[2] Data is being analyzed in order to obtain more accurate potential for NO-Ar system.

References

1) P.R.R. Langridge-Smith et al., *J. Chem. Phys.* **74**, 6513 (1981).
2) H.L. Schwartz, S. Stolte, and J. Reuss, *Chem. Phys.* **2**, 1 (1973).

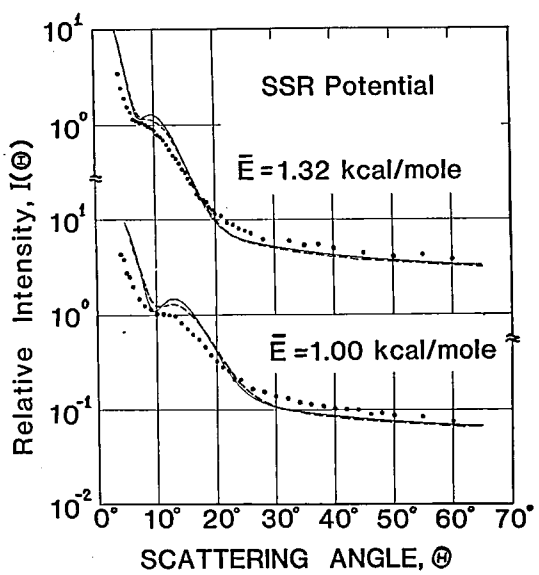

Figure 1. Angular distributions of NO scattered from Ar at nominal collision energies E = 1.32 and 1.00 kcal/mole. The solid curves are the calculated distributions for the spherically symmetric part of the potential determined by Scwartz et al.[2] The dashed curves are the calculated distributions using the infinite order sudden approximation for the NO-Ar anisotropic potential.[2]

IV—M Molecular Beam Studies of Reaction Dynamics Involving Chemically Reactive Atoms and Free Radicals

In this project we investigate the dynamics of chemical reactions involving reactive species such as N, B, C, CH, etc. using a crossed molecular beams technique. For the production of supersonic nozzle beams of these reactive species, especially for active nitrogen atoms, an arc-heated nozzle beam source has been used. Two molecular beam machines, MBC-I which applies the rotatable mass spectrometer detector and MBC-II with optical spectroscopic detection, are operational.

IV-M-1 Molecular Beam Chemiluminescence Studies Involving Active Nitrogen Atoms $N^*(^2D, ^2P)$. I. $N^*(^2D, ^2P) + HX \rightarrow NH(A^3\Pi) + X$ (X = I and Br)

Kiyohiko TABAYASHI, Shigeru OHSHIMA, and Kosuke SHOBATAKE

The title reactions have been studied using atomic nitrogen beams produced from the arc-heated nozzle source.[1] **Figure 1a** illustrates a typical chemiluminescence spectrum for the $NH(A^3\Pi, v', j')$ products from the reactions

$$N(^2P) + HI \rightarrow NH(A^3\Pi) + I(^2P_{3/2}) \qquad \Delta D_0^0 = 0.43\text{eV} \qquad (1)$$

$$N(^2D) + HI \rightarrow NH(A^3\Pi) + I(^2P_{3/2}) \qquad \Delta D_0^0 = -0.76\text{eV} \qquad (2)$$

run at a nominal collision energy $\overline{E} = 0.86$ eV. The stagnation temperature was controlled by changing the arc current and the magnet coil current. In Figure 1b the total NH(A–X) fluorecence intensity which is proportional to the product of the cross section of the chemiluminescence reaction σ_f and the N* flux intensity f_{N^*}, is plotted against the relative kinetic energy $\overline{E}$ for the above reactions, and

$$N(^2P) + HBr \rightarrow NH(A^3\Pi) + Br(^2P_{3/2}) \qquad \Delta D_0^0 = -0.27\text{eV}. \qquad (3)$$

Note that the fluorescence intensity I_f increases with the stagnation temperature and $\overline{E}$. The intensity ratios for v' = 1 relative to v' = 0 product were found to be 0.60 ± 0.12 for N* + HI and 0.40 ± 0.05 for $N(^2P)$ + HBr reaction over the collision energy range studied. The emission spectrum in **Figure 1a** was simulated using the best-fit rotational temperatures T_R's 4000 ± 250K for v' = 0 and 2000 + 250K for v' = 1 products. The observed v' = 1/v' = 0 intensity ratios for these reactions agree fairly well with the prior predictions, but cooler rotational

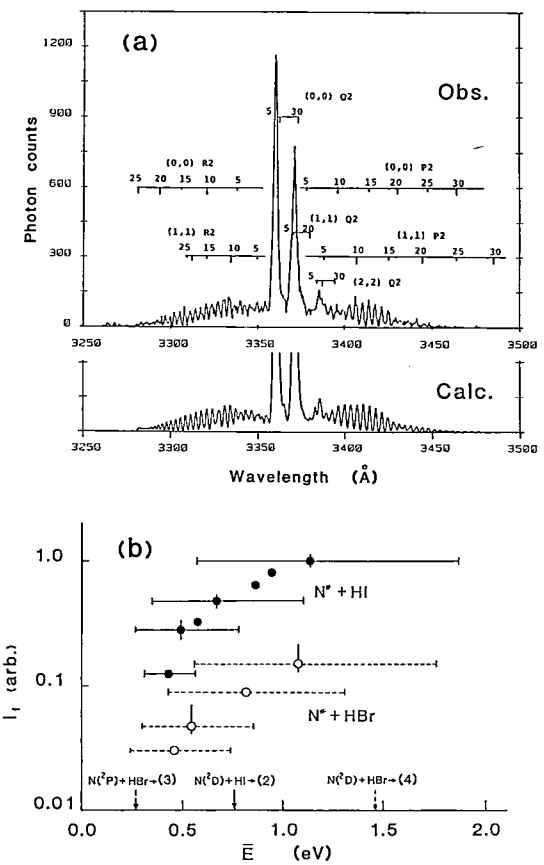

Figure 1. a) Chemiluminescence spectrum NH(X – A) from the reaction N* + HI at a nominal collision energy $\overline{E} = 0.86$ eV and computer simulated spectrum. b) Collision energy dependence of the chemiluminescence intensity for the reactions of metastable active nitrogen atoms with HI and HBr. The arrows indicate the onset of the reactions. Reaction (4) is the corresponding one to $N(^2D)$ + HBr.

distributions than the statiscal calculations were obtained.

Reference

1) K. Tabayashi and K. Shobatake, *IMS Ann. Rev.*, **1982**, 82.

IV-M-2 Construction of a Crossed Molecular Beams Apparatus with an Electron Bombardment Ionization Mass Spectrometer (MBC-I)

Kosuke SHOBATAKE, Shigeru OHSHIMA, Kiyohiko TABAYASHI, Manfred FAUBEL *(MPI fuer Stroemungsforschung and IMS),* **Toshio HORIGOME,* Mitsukazu SUZUI,* Nobuo MIZUTANI,* Hisashi YOSHIDA,* and Kazuo HAYAKAWA*** *(*Equipment Development Center)*

A crossed molecular beams apparatus with a rotatable mass spectrometer, nicknamed as Molecular Beam Chemistry Apparatus (MBC-I), has been constructed based on the design of Lee et al.[1] in order to study the dynamics of reactive as well as non-reactive scattering and photodissociation processes. **Figure 1** illustrates the top view of the apparatus, consisting of a main chamber (MC) with inside dimensions 107 × 106 × 58 cm, a diffferentially pumped primary beam source (BC1), a secondary beam source (BC2), and a rotatable mass spectrometer detector (DC1~3). The triply differentially pumped detector comprises an electron bombardment ionizer, an ENL quadrupole mass filter, and a Ceratron electron multiplier for ion detection. The buffer chamber (DC1) and the mass filter chamber (DC2) are pumped by Balzars turbomolecular pumps backed by a diffusion pump,

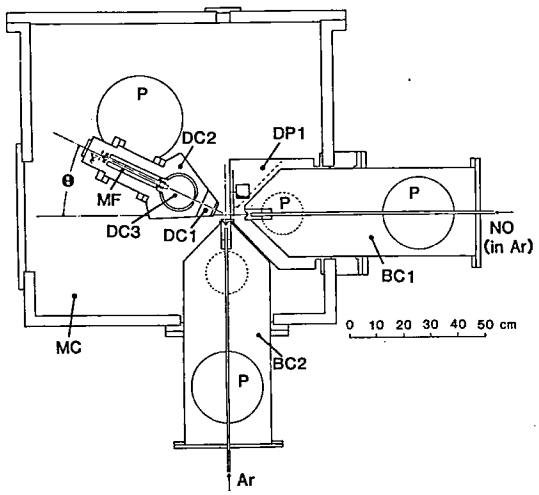

Figure 1. Top view of the Molecular Beam Chemistry Apparatus (MBC-I). P: Diffusion pump, MF: Mass filter. See the text for explanations.

and the innermost ionizer chamber (DC3) is evacuated by a liquid He cryopump. The detector chamber mounted on a rotatable platform rotates around the vertical axis (angular range 120°). The base pressure in DC1 and DC2 are 6×10^{-10} and 7×10^{-11} torr, respectively. The nominal distance between the collision center and the ionizer is 23.6 cm. A time-of-flight technique is applied to measure the velocity distributions of scattered species using a home-made multichannel scaler with a minimum channel width .5μs.

Reference

1) Y.T. Lee, et al. *Rev. Sci. Instrum.*, **40**, 1402 (1969).

RESEARCH ACTIVITIES V
Department of Applied Molecular Science

V—A Molecular Design of Bridged Aromatic Compounds and High-Spin Organic Compounds

Electronic interactions in the ground as well as excited states between the benzene rings in a fixed three dimensional molecular framework are the subject of our continued interest. As a chemical consequence of the excitonic interaction between the three benzene rings held at an angle of 120° to each other, triptycenes undergo photochemical bridging between the two benzene rings to give the monocentric diradical species, i.e., carbenes and nitrenes, due to one of the bridgehead atoms. A stereochemical effect on the spectroscopic and chemical properties of the nitrene triplets has been discolsed. The carbene chemistry has now been extended to molecular design of aromatic hydrocarbons in the ground quintet, septet, nonet and higher multiplet states.

V-A-1 Transient Absorption Spectra of the Excited States of Triptycene and 3-Acetyltriptycene

Tadashi SUGAWARA, Hiizu IWAMURA, Nobuaki NAKASHIMA,[1] Keitaro YOSHIHARA[1], and Hisaharu HAYASHI *(Inst. Phys. Chem. Res.)*

[*Chem. Phys. Lett.*, **101**, 303 (1983)]

In order to fully characterize the excited states of triptycenes, the $S_n \leftarrow S_1$ absorption spectrum of triptycene has been measured in cyclohexane solution by nanosecond laser spectroscopy using a KrF excimer laser.[2] The peak transient absorption spectra of triptycene and *o*-xylene are reproduced in Figure 1. The spectrum of triptycene extended out to 900 nm, showing a tremendous bathochromic shift and enhanced absorptivity compared with that of *o*-xylene. The peak at 650 nm ($\epsilon = 7 \times 10^3$ $M^{-1}cm^{-1}$) corresponds to the weak $^1E_{1u} \leftarrow {}^1B_{2u}$ transition (λ_{max} 620 ~ 700 nm) of benzene and *o*-xylene,[2] and may be assigned to the intramolecular excimer[3] between the benzenoid moieties of the triptycene molecule.

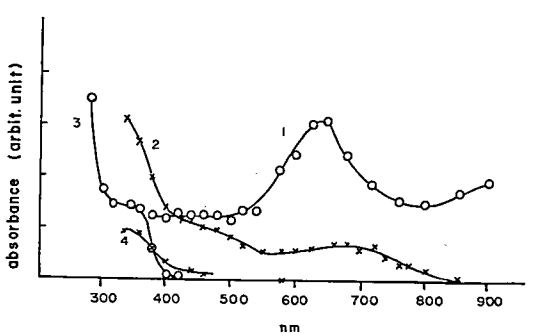

Figure 1. Time-resolved absorption spectra of triptyene (O) (5.3×10^{-4} M) and *o*-xylene (X) (1.6×10^{-3} M) in cyclohexane at 16.5°C.

1. Absorptions due to $S_n \leftarrow S_1$ transition of triptycene recorded at the peak of the time-trace.
2. Absorptions due to $S_n \leftarrow S_1$ transition of *o*-xylene recorded at the peak of the time-trace.
3. Absorptions due to the photoproduct of triptycene recorded 200 ns after the laser pulse.
4. Absorptions due to $T_n \leftarrow T_1$ transition of *o*-xylene recorded 200 ns after the laser pulse.

3-Acetyltriptycene showed a $T_n \leftarrow T_1$ absorption maximum at 550 nm which extended out to over 800 nm. A contribution of the CT character to the lowest triplet state of triptycene was estimated independently from the zerofield splitting parameter to be ca. 4%.

References

1) Department of Electronic Structure.
2) N. Nakashima, M. Sumitani, I. Ohmine, and K. Yoshihara, *J. Chem. Phys.*, **72**, 2226 (1980).
3) T. Sugawara and H. Iwamura, *IMS Ann. Rev.*, 110 (1981).

V-A-2 Contrasting ESR and UV Spectroscopic Properties and Reactivities between the Conformationally Fixed *o*-(9-Fluorenyl)phenylnitrenes at Cryogenic Temperatures

Shigeru MURATA, Tadashi SUGAWARA, and Hiizu IWAMURA

[*J. Am. Chem. Soc.*, **105**, 3723 (1983)]

Conformationally fixed *ap*- and *sp*-9-(2-azido-4, 6-dimethylphenyl)fluorenes (**4a** and **4b**, respectively) have been photolyzed in methylcyclohexane glass at 4.2K. Whereas **4a** gave the intense X,Y transition due to triplet nitrene **5a** at 6722 gauss, **4b** showed no signal under these conditions. 9-Deuterio derivative **4b'** of **4b** gave the signal at 6745 gauss. Photolysis of **4a** in an EPA matrix at 77K showed absorptions at 309 (due to **5a**) and 340 nm (due to azanorcaradiene **7**). No absorption due to **5b** was obtained. A broad absorption at 554 nm from the photolysis of **4b** was assigned to quinoid tautomer **6** which was converted to **8**. In both conformers, the high reactivities of the singlet nitrene are in competition with intersystem crossing to the triplet species. In **5a**, the geometrically favorable addition to the double bond of the fluorene ring is the competing path (Scheme 1). In **5b**, 1,4-migration of 9-H to give **6** is too fast to generate the triplet species. Retardation of the tunnelling effect of 9-H by replacement with deuterium enabled the conversion to triplet **5b** (Scheme 2). All the results are more than enough to corroborate the conformational theory of the slightly different behavior of the o-(9-fluorenyl)phenylnitrene intermediates **2** generated from 1-azatriptycene (**1**) and 9-(2-azidophenyl)-fluorene (**3**).[1]

Scheme 1.

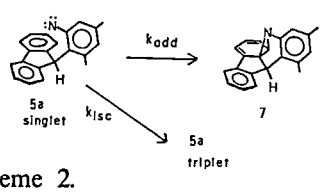

Scheme 2.

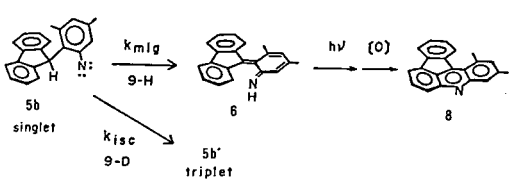

Reference

1) T. Sugawara and H. Iwamura, *J. Am. Chem. Soc.*, **102**, 7134 (1980).

V-A-3 Time-Resolved Absorption Spectroscopic Detection of 10,10-Dimethyl-10-silaanthracen-9(10H)-one Oxide

Tadashi SUGAWARA, Hiizu IWAMURA, Hisaharu HAYASHI *(Inst. Phys. Chem. Res.)*, **Akira SEKIGUCHI** *(Univ. of Tsukuba)*, **Wataru ANDO** *(Univ. of Tsukuba)*, **and Michael T.H. LIU** *(Univ. of Prince Edward Island)*

[*Chemistry Lett.*, 1261 (1983)]

Laser-photolysis studies have been carried out on a solution of 9-diazo-10,10-dimethyl-10-sila-9(10H)-anthracene (**1**) in cyclohexane. In degassed solutions, a series of UV abosorptions due to transient triplet carbene **2** (λ_{max} at 345 and 510 nm) and radical **3** (λ_{max} at 354 nm).[1] In aerated solutions, **2** was quenched with oxygen ($k_q = 2 \times 10^9 M^{-1}s^{-1}$) to give a characteristic absorption (λ_{max} at 425 nm) (Figure 1). The absorption due to **3** was not observable under these conditions. The solution became yellow after the experiment and formation of ketone **4** was indicated by its absorption spectrum (λ_{max} at 313 nm).[2] Addition of methanol (0.15M) accelerated the decay of the absorbance at 425 nm from 2.2×10^4 to $2.6 \times 10^4 s^{-1}$, suggesting the quenching of a carbonyl oxide with methanol to give an α-methoxy hydroperoxide. All these results support the assignment of the new species to carbonyl oxide **5**. Zwitterionic and diradical structures are proposed to carbonyl oxides. The observed absorption maximum resembles the ketyl radical (λ_{max} at 444 nm) rather than the conjugate acid (λ_{max} at 351 nm) of anthrone,[3] suggesting the diradical structure of **5**.

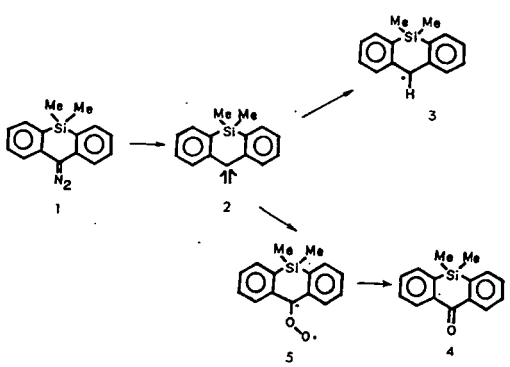

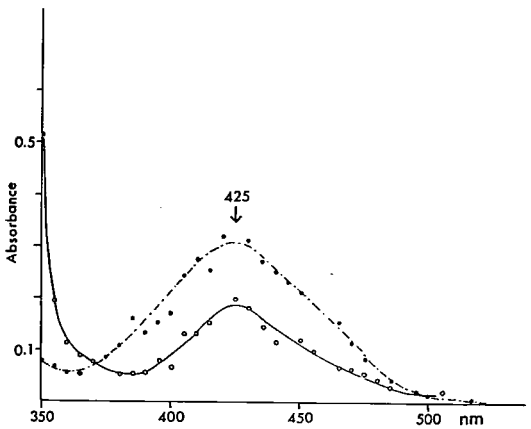

Figure 1. Absorption spectra of the transient product during the irradiation of **1** in non-degassed cyclohexane, recorded after 100 ns (–○–) and 2 μs (–●–).

References

1) T. Sugawara, H. Iwamura, H. Hayashi, A Sekiguchi, W. Ando, and M.T.H. Liu, *Chemistry Lett.*, 1257 (1983); *IMS Ann. Rev.*, 85 (1982).
2) A. Sekiguchi, W. Ando, T. Sugawara, H. Iwamura, and M.T.H. Liu, *Tetrahedron Lett.*, **23** 4095 (1982).
3) N. Kanamaru and S. Nagakura, *Bull. Chem. Soc. Jpn.*, **43**, 3443 (1970); R. Stewart, M.R. Granger, R.B. Moodie, and L. Muenster, *Can. J. Chem.*, **41**, 1065 (1963).

V-A-4 Design, Preparation, and ESR Detection of a Ground-State Nonet Hydrocarbon as a Model for One-Dimensional Organic Ferromagnets

Yoshio TEKI *(Osaka City Univ.)*, **Takeji TAKUI** *(Osaka City Univ.)*, **Koichi ITOH** *(Osaka City Univ.)*, **Hiizu IWAMURA, and Kazumasa KOBAYASHI**[1)]

[*J. Am. Chem. Soc.*, **105**, 3722 (1983)]

Tetrakis (diazo) compound **2** was synthesized via a series of standard reactions starting from the reaction of *m*-tolyl-magnesium bromide with isophthalonitrile (Scheme 1).[2)] UV irradiation of **2** oriented in single crystals of benzophenone at 4.2K

Scheme I

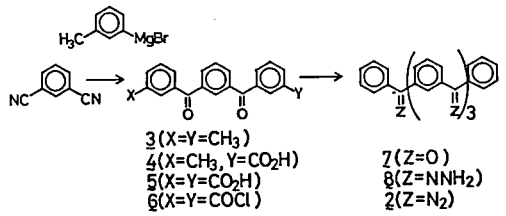

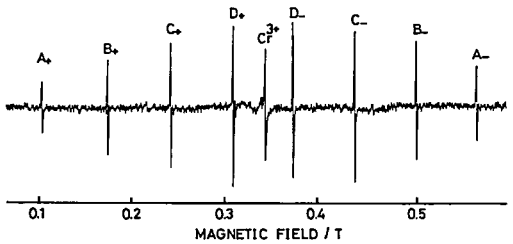

Figure 1. Electron spin resonance spectrum observed after the photolysis at 4.2K with the magnetic field along the direction 26° from the a axis in the ab plane of the host crystal. The microwave frequency is 9550.6 MHz. The central line is due to Cr^{3+} in MgO powder used as a reference substance.

gave the eight-line ESR spectrum (Figure 1) for *m*-phenylenebis((diphenylmethylen-3-yl)methylene) **1** which was analyzed by the spin Hamiltonian

$$\mathcal{H} = \beta g \mathrm{H} \cdot S + D[S_z^2 - \frac{1}{3} S(S+1)] + E(S_x^2 - S_y^2)$$

where $S = 4$, $g = 2.003$, $D = +0.0332$ cm^{-1} and $E = -0.0031$ cm^{-1}. The temperature dependence of the ESR signals in the range 1.8 ~ 150K confirmed **1** to be in the nonet ground state which is the highest spin multiplicity ever detected in organic compounds ($S = 3$) as well as inorganic compounds ($S = 7/2$).

References

1) IMS Graduate Student from Yamaguchi University for 1980.
2) K. Kobayashi and H. Iwamura, *IMS Ann. Rev.*, 86 (1982).

V—B Stereochemical Consequences of the Non-bonded Interactions in Overcrowded Molecules

Internal rotation around the two C-X bonds has been established to be perfectly correlated in bis(9-triptycyl)X molecules. An X-ray structural analysis has revealed that the molecule of bis(9-triptycyl) ether has the expected bevel gear shape. As a stereochemical consequence, new stereoisomers were generated in which the phase relationship of the labeled cogs was different. The new stereochemical concept has now been extended to a doubly geared molecule. These results suggest that transfer of information from one end of a molecule to the other end could take place in large molecules via cooperativity of the torsional motions of the chain.

V-B-1 Crystal and Molecular Structure of Bis-(9-triptycyl) Ether

Hiizu IWAMURA, Yuzo KAWADA *(Ibaraki Univ. and IMS)*, **Tasuku ITO, Koshiro TORIUMI, and Haruko ITO**

The crystal and molecular structure of a benzene solvate of the title compound, $Tp_2O{\cdot}2Bz$, has been determined; monoclinic, space group $P2_1/c$, a = 20.868(2), b = 10.405(1), c = 18.912(1) Å, β = 114.12(1)°, V = 3747.7(5) Å^3, Z = 4. Stereoview of the X-ray structure of Tp_2O is given in Figure 1. The molecule adopts a tightly meshed bevel gear structure in which there is an approximate symmetry plane formed by the ether linkage C-O-C. The two C-O bond lengths, 1.407(2) and 1.418(3) Å, are unequivalent but within the normal range of those of aliphatic ethers. The C-O-C valence angle is widened as much as 135.8(2)°, the highest angle ever reported for ethers, suggesting the presence of high non-bonded repulsive interaction between the two triptycyl units even in the gear meshed conformation.

The molecule of C_s symmetry is consistent with the previously reported ^{13}C NMR data taken by means of the CP-MAS technique for the powder sample.[1]

Reference

1) Y. Kawada and H. Iwamura, *J. Am. Chem. Soc.*, **105**, 1449 (1983).

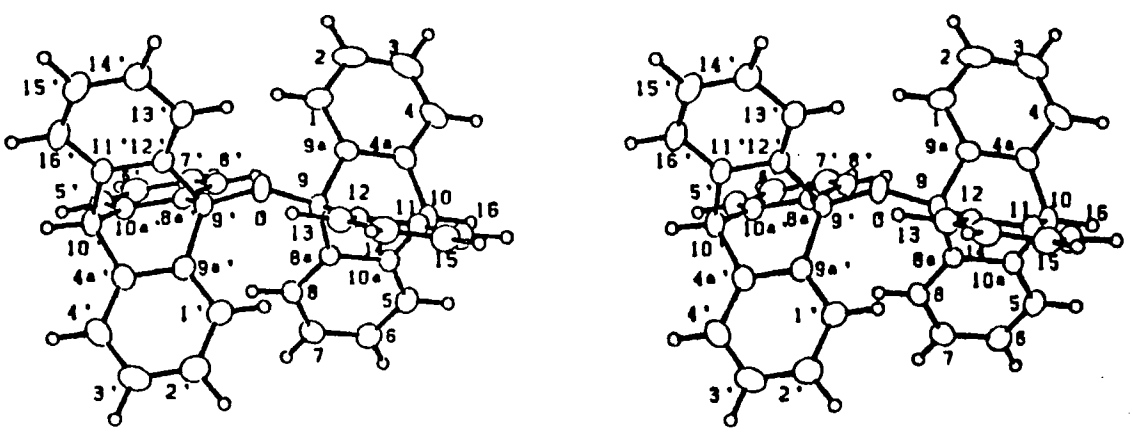

Figure 1. Stereoview of the X-ray structure of bis(9-triptycyl) ether (Tp_2O).

V-B-2 Molecular Structure of Bis(9-triptycyl) Ether by Molecular Mechanical Calculations

Hiizu IWAMURA, Yuzo KAWADA *(IMS and Ibaraki Univ.)*, **Eiji OSAWA** *(Hokkaido Univ.)*, **Teruyo FUJIYOSHI** *(Hokkaido Univ.)*, **and Carlos JAIME** *(Hokkaido Univ.)*

An empirical force field calculation has been carried out for bis(9-triptycyl) ether Tp_2O using the force field from Allinger's MM2 program.[1] The C-O-C angle in the energy minimized structure with C_s symmetry was 126.3°, an angle considerably smaller than the observed 135.8°.[2] The MM2 parametrization was improved by modifying the anharmonic term in the potential energy function due to C-O-C bending. On the modified MM2 energy surface, the C_2 conformation was also an energy minimum, but 0.24 kcal/mol higher in steric energy than the C_s conformation. Other structural features determined by the X-ray analysis were reasonably well reproduced.

About 70 points near the gearing coordinates have been calculated and smoothed to give the potential energy surface on which the dynamic gearing of the ether takes place rapidly. There is a very low unsymmetrical barrier of the height of only 0.93 kcal/mol between the two energy minima (Figure 1).

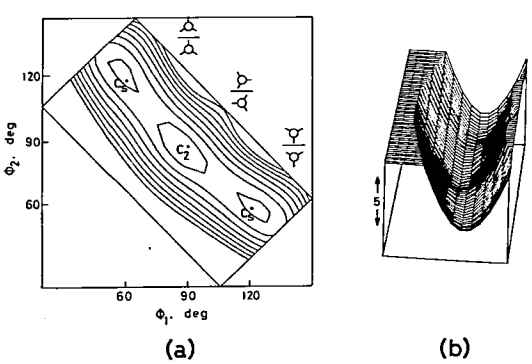

Figure 1. Partial torsional energy surface of Tp_2O: (a) contour map and (b) perspective view.

References

1) N.L. Allinger, *J. Am. Chem. Soc.*, **99**, 8127 (1977); N.L. Allinger and Y.H. Yuh, *QCPE*, **11**, 395 (1980).
2) The preceding paper.

V-B-3 Correlated Internal Rotation in Bis(2, 6-dichloro-9-triptycyl)methane. Separation, Optical Resolution and Identification of Five Possible Phase Isomers.

Yuzo KAWADA *(Ibaraki Univ. and IMS)*, **Hiizu IWAMURA, and Yoshio OKAMOTO** *(Osaka Univ.)*

[*Tetrahedron Lett.*, **24**, 5359 (1983)]

When internal rotation around the two adjacent C-C bonds is disrotatorily coupled, a new meso and a pair of dl (dl_1) isomers are produced from the *RS* isomer of bis(2,6-dichloro-9-triptycyl)methane (**1**). Three pairs of dl isomers (dl_2 ~dl_4) result from the *RR*/*SS* isomer.[1] The five possible phase isomers (one meso and four dl pairs) have now been separated by HPLC on a microsilica with 1% chloroform-hexane elution. Separation of the last two fractions was better effected by HPLC on a reversed-phase column with methanol-water (5 : 1) elution (Figure 1). Fractions 2 and 3 were unambiguously assigned to the meso and dl_1 isomers by the interconversion experiment and by their ^{13}C NMR spectra. Fraction 1 was tentatively

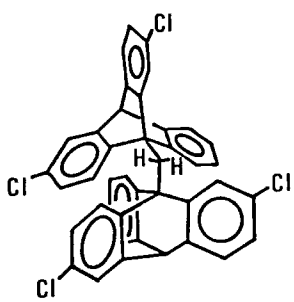

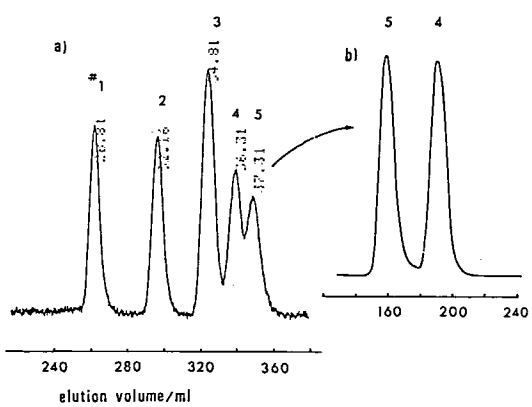

Figure 1. HPLC separation of the five diastereomers of **1**. (a) μPorasil (3/8 in. × 1 ft) and Develosil (10 × 250 mm) columns in series. (b) A 3/8 in × 1 ft μBondapak C_{18} column.

assigned to dl_2 based on the polarity consideration. Optical resolution of isomers $dl_2 \sim dl_4$ was found to be possible by HPLC using a column of silanized silica gel coated with chiral poly(triphenylmethyl methacrylate).

Reference

1) A. Guenzi, C.A. Johnson, F. Cozzi and K. Mislow, *J. Am. Chem. Soc.*, **105**, 1438 (1983). Y. Kawada and H. Iwamura, *ibid.*, **105**, 1449 (1983).

V-B-4 Recognition of the Phase Relationship between Remote Substituents in 9,10-Bis(3-chloro-9-triptycyloxy)triptycene Molecules Undergoing Rapid Internal Rotation

Noboru KOGA, Yuzo KAWADA *(Ibaraki Univ. and IMS)*, **and Hiizu IWAMURA**

[*J. Am. Chem. Soc.*, **105**, 5498 (1983)]

9,10-Bis(3-chloro-9-triptycyloxy)triptycene (**1**) was prepared by the thermal decomposition of bis(3-chloro-9-triptycyl) 9,10-triptycenebis(peroxycarboxylate) which in turn was obtained by the reactions of 9-bromo-3-chlorotriptycene with butyllithium, oxygen, and then with 9,10-triptycenedicarbonyl dichloride. As a result of strictly geared internal rotation at the two ether linkages in these molecules, new stereoisomers were born in which the phase relationship between the chloro-substituted benzene rings was different by 120°. The meso and racemic compounds were separated by HPLC on microsilica with a 4% CH_2Cl_2 in hexane elution and identified by means of their ^{13}C NMR spectra which revealed an interesting stereochemical effect; in the middle triptycene unit, one benzene ring (a) is diastereotopic to the other two (b and c). The rates of interconversion between the isomers were measured in diphenylmethane solutions to give the activation parameters for the gear slippage process as follows. $\Delta H^{\ddagger} = 42.1 \pm 1.3$ kcal/mol, $\Delta S^{\ddagger} = -3.2 \pm 2.3$ e.u., $E_a = 43.2 \pm 1.3$ kcal/mol, and $\log A = 12.8 \pm 0.5$. The data are in good agreement with those of bis(3-chloro-9-triptycyl) ether,[1] except that the frequency factor is twice larger in the double gear than in the single gear.

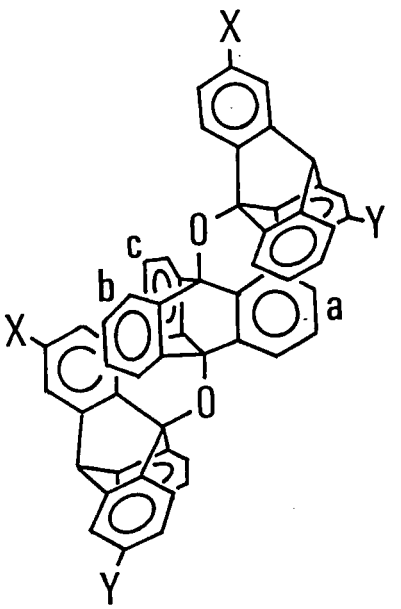

1 { meso (X = Cl, Y = H)
d(or l)(X = H, Y = Cl)

Reference

1) Y. Kawada and H. Iwamura, *J. Am. Chem. Soc.*, **105**, 1449 (1983).

V—C Structural and Mechanistic Studies by Means of NMR of the Less Common Nuclei

Structural and mechanistic studies with the aid of NMR of ^{17}O and ^{77}Se have been carried out on a Varian FT-80A and JEOL GX-400 spectrometers. The ^{17}O chemical shift data are instrumental in determining the preferred conformations of some sulfoxides. Stereochemistry of 9-selenoxanthene derivatives has been disclosed by the ^{77}Se chemical shift data.

V-C-1 The Conformations of Several 1-Phenylethyl and 1-Phenylpropyl Aryl Sulfoxides. Evidence for Attractive Aryl/Aryl Interaction

Keiji KOBAYASHI *(The Univ. of Tokyo)*, **Yoshio KODAMA** *(Meiji Seika Co.)*, **Motohiro NISHIO** *(Meiji Seika Co.)*, **Tadashi SUGAWARA**, and **Hiizu IWAMURA**

[*Bull. Chem. Soc. Jpn.*, **55**, 3560 (1982)]

The conformations of the diastereoisomers of 1-phenylalkyl aryl sulfoxides **1**, **2** and **3** have been studied by NMR spectroscopy, largely by means of the computer simulation of the lanthanoid-induced shifts. It has been suggested by the reliability factor analysis (Fig. 1) that the rotamer in which the aromatic group (Ar) is gauche to the phenyl (Ph) and anti to the alkyl (R) group is most populated in the conformational equilibria of (*RS*/*SR*)-**1**, **2**, **3**, and (*RR*/*SS*)-**3**. For (*RR*/*SS*)-**1** and **2**, the most important contributor has been suggested to have Ar flanked by Ph and R. The ^{17}O chemical shift data are interpreted in terms of the γ-gauche effect in these preferred conformations. The results are discussed in the light of the presence of attractive interactions between the relevant groups.

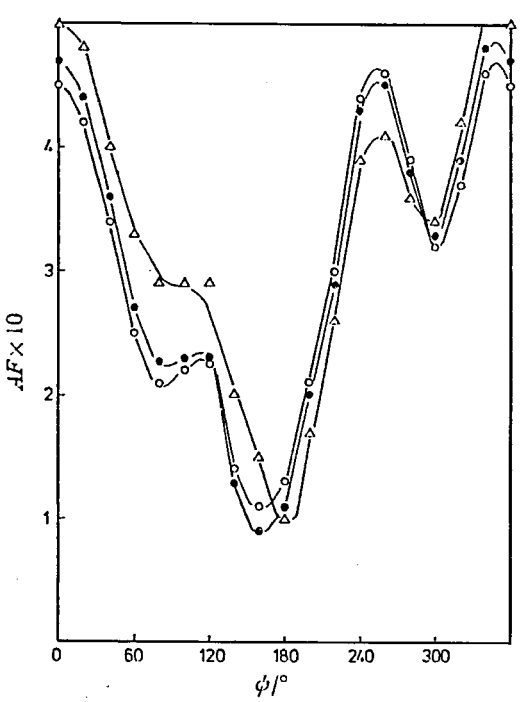

Figure 1. Plots of AF vs. the O/Ph dihedral angle (φ) for the sulfoxides with the (*RS*/*SR*) configuration. o-o-o (*RS*/*SR*)-1, •-•-• (*RS*/*SR*)-2 and Δ-Δ-Δ (*RS*/*SR*)-3.

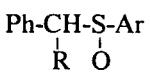

1: R = CH_3, Ar = C_6H_5
2: R = CH_3, Ar = C_6H_4–CH_3(*p*)
3: R = C_2H_5, Ar = C_6H_5

V-C-2 Selenium-77 NMR Studies of 9H-Selenoxanthenium Derivatives

Hideyuki TUKADA, **Hiizu IWAMURA**, and **Mikio HORI** *(Gifu Coll. Pharm.)*

Selenium compounds have lately attracted considerable attention due to their biological and synthetic importance, and some special uses (e.g. semi- and superconductor). In order to elucidate the structural features, we have studied ^{77}Se NMR of the title compounds. The results are summarized in Table 1. Selenium-77 chemical shifts are very sensitive to electronic structure, and move downfield from 250 ppm to 850 ppm (δ, from Me_2Se) in the order: R_2Se^+-alkyl > R_2Se^+-$^-CR'_2$ > R_2Se^+-$^-NR'$ > $R_2(R'O)Se$-Cl > $R_2(R'O)Se^+$, which is well understood by the electron-withdrawing ability of the attached groups. In Se^+-alkyl series, the α-substituent effects are in the same relationship to

Table I. ^{77}Se chemical shifts of 9H-selenoxanthenium perchlorates ($Y^- = ClO_4^-$).

R_1	R_2	R_3	chemical shift (ppm)[1]
Me	O		302.2
Ph	O		382.5
Me	H	H	339.0
Me	Me 3)	H	336.0
			332.0
Me	i-Pr 2)	H	346.1
Me	COPh 3)	H	361.5
			351.5
Me	Ph 3)	H	353.7
			340.9
Me	Mesityl 3)	H	319.0
			317.9
Et	H	H	385.3
n-Pr	H	H	372.2
i-Pr	H	H	427.9
Ph	H	H	422.2
Mesityl	i-Pr 2)	H	397.2
p-Tolyl	Ph 2)	H	638.1
$C^{COCO_2Et}_{CO_2Et}$	H	H	406.0
$C^{CHO}_{CO_2Me}$	Ph 2)	H	399.3
$C^{COCO_2Et}_{CO_2Et}$	Ph 2)	H	411.2
$-(CH_2)_2-$		H	275.6
$-(CH_2)_3-$		H	386.2
$-(CH_2)_2-$		Me	266.4
$-(CH_2)_2-$		Ph	264.1
$-O(CH_2)_2-$		Ph 4)	640.6
$-O(CH_2)_2-$		Me	835.3
$-O(CH_2)_2-$		Ph	813.7
-O-		Ph 4)	670.0

1) from $Se(CH_3)_2$ in $CDCl_3$.
2) trans, 3) a mixture of cis and trans.
3) not a perchlorate but with covalent Se-Y bond (Y = Cl).

the reported data of selenides and diselenides, and can be represented as $\delta(R_2Se^+\text{-}R) = -0.411\sigma + 339$ ppm, where σ is McFarlane's parametes of R for selenides. Even γ-substituents have large influences. Thus lowfield shift is observed as we go from = O to Ph and to Me (~H) in the R_2Se^+-Me derivatives and ethano-bridged compounds. Stereochemical differences also affect ^{77}Se chemical shifts and a cis/trans mixture of Se-alkyl-10-alkyl derivatives shows two peaks due to these isomers within $\Delta\delta =$ 4 ppm. In bridged compounds, obvious dependence on the length of the bridging chain is observed and is useful to stereochemical characterization.

V—D Zinc(II)-Tetraazacycloalkane Complexes

Chemical consequences of ligand macrocyclizations in tetraazacycloalkane complexes and their applications are the subject of our continued interest (see *IMS Ann. Rev.*, 115 (1979), 112 (1980), 124, 126 (1981), 93 (1982)). Previously we studied stabilization of high-oxidation states of metal ions by taking advantage of chemical characteristics arising from cyclic nature. Our studies along this line have now been extended to chemistry of one-dimensional M(II)-M(IV) mixed valence complexes (see V-F). In this study, we have investigated chemistry of Zn(II)-tetraazacycloalkane complexes. Certain Zn(II)-tetraazacycloalkane complexes take up CO_2 very easily under mild conditions.

V-D-1 Facile CO_2-uptake by Zn(II)-tetraazacycloalkane Complexes

Masako KATO and Tasuku ITO

Zn ([14]aneN$_4$) (ClO$_4$)$_2$ ([14]aneN$_4$ = 1, 4, 8, 11-tetraazacyclotetradecane) and Zn([15]aneN$_4$) (ClO$_4$)$_2$ ([15]aneN$_4$ = 1,4,8,12-tetraazacyclopentadecane) react with CO_2 easily and reversibly in methanol at room temperature to give monomethylcarbonato complexes, Zn(L)(O$_2$COCH$_3$)(ClO$_4$) (L = [14]aneN$_4$ (**1**), [15]aneN$_4$ (**2**)). The CO_2 uptake reactions proceed spontaneously in the air in the presence of bases such as NaOCH$_3$ and NEt$_3$, or below ca. 10°C. The structures of **1** and **2** have been determined by X-ray diffractometry (Figure 1). The monomethyl carbonate group plays a role of a bridging ligand, forming a linear chain structure which causes the easy isolation of the compounds. The reversible CO_2 uptake reaction has been studied by means of ^{1}H and ^{13}C NMR on a CDCl$_3$ solution of **2**. In the solution, the equilibrium between the O$_2$COCH$_3$ complex and the OCH$_3$ complex attains, accompanying absorption and desorption of CO_2. The equilibrium constant (K = [O$_2$COCH$_3$ complex] / [OCH$_3$ complex]) has been found to be 1.8 at 25°C. A decrease in temperature makes the equilibrium shift to increase the amount of O$_2$COCH$_3$ complex. The monomethylcarbonato ligand in **2** has been converted into dimethyl carbonate in a cyclic way by treating with FSO$_3$CH$_3$.

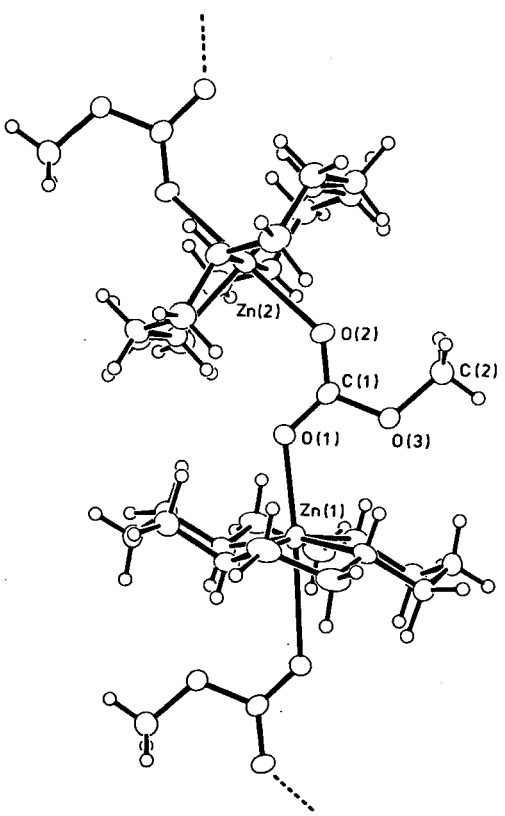

Figure 1. Structure of Zn([14]aneN$_4$)(O$_2$COCH$_3$)$^+$ in **1**

V-D-2 X-ray Structural and Ab Initio MO Studies on Molecular Stereochemistries of Six-coordinate Zn(II) Complexes of *trans*-ZnX$_2$N$_4$ Type. Flat Potential Surface with respect to Out-of-plane Displacement of Zn(II) from a Plane formed by In-plane Four Nitrogens

Tasuku ITO, Masako KATO, and Haruko ITO

Molecular structures of *trans*-bis (isothiocyanato) (1,4,8,11-tetraazacyclotetradecane and 1,4,8,12-tetraazacyclopentadecane)zinc(II) complexes, [Zn (NCS)$_2$(C$_{10}$H$_{24}$N$_4$)] (**1**) and [Zn(NCS)$_2$(C$_{11}$H$_{26}$N$_4$)] (**2**), have been determined by X-ray analyses. Crystal data are: for **1**, orthorhombic, space group $P2_1nb$, a = 14.502(2), b = 18.163(2), c = 6.552(1)Å, V = 1718.0(4)Å^3, Z = 4; for **2**, monoclinic, space group $P2_1/a$, a = 14.453(2), b = 14.436(1), c = 9.213(1)Å, β = 104.82(1)°, V = 1858.3(4)Å^3, Z = 4. In each compound, the Zn(II) ion takes an out-of-plane position and deviates from a plane defined

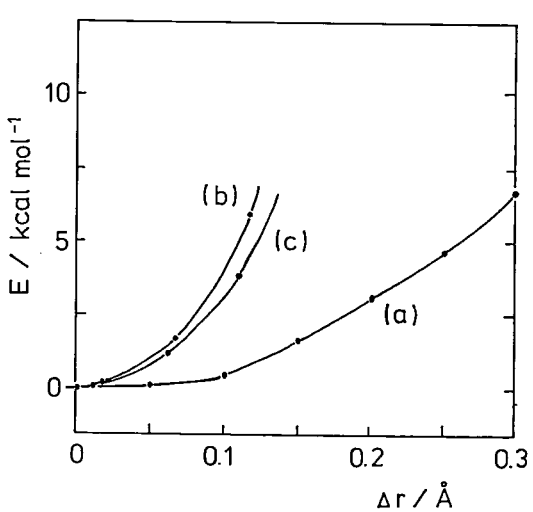

Figure 1. Potential energy surfaces of *trans*-[ZnCl$_2$(NH$_3$)$_4$] for displacements (Δr) of the Zn atom from the N$_4$ plane (a) and for lengthenings (Δr) of Zn-N (b) and Zn-Cl (c) bonds from the ideal distances in the in-plane structure.

by the four nitrogens of the macrocyclic ligand by 0.179Å on the average in **1** and 0.193Å in **2**. It has been found that the Zn-N(NCS) distance decreases as an in-plane Zn-N length (or cavity size of the ligand) increases. The observed negative correlation is substantially stronger than those for Ni(II) and Co(III) complexes and discloses the softness of a Zn(II) ion. Ab initio MO calculations for a model system, *trans*-$[ZnCl_2(NH_3)_4]$, have shown that the potential surface regarding the out-of-plane displacement is very flat (Figure 1).

V—E One-Dimensional M(II)-M(IV) Mixed Valence Complexes of Palladium and Nickel

One-dimensional M(II)-M(IV) mixed valence complexes of Pt and Pd have attracted much interest from the viewpoint of the chemistry and physics of low-dimensional compounds. In compounds of this class, square planar M(II) and elongated octahedral M(IV) are stacked alternately in the direction of the needle axis, constructing halogen-bridged linear chains of ···X-M(IV)-X···M(II)··· segments. They show characteristic properties such as metallic luster, remarkable dichroism, semiconducting nature, and so on. Such properties are affected by kinds of metals, bridged halogens, in-plane ligands, and counter ions. So far many studies on compounds of this class, mostly of Pt, have been reported from a variety of standpoints. In this study, we aimed at syntheses of new Pd and Ni complexes of this type. On going from Pt to Ni, it is expected that the electronic interaction between M(II) and M(IV) through a bridged halogen ion increases and thereby the electric conductivity would be enhanced, though it becomes more difficult to synthesize the compounds because of the instability of the M(IV) states. Such new Pd and Ni complexes have been successfully prepared using linear tetramines or tetraazacycloalkanes shown below as in-plane ligands. They have been characterized by means of X-ray structure analyses, electronic spectra, electric conductivities, X-ray photoelectron spectra, and EXAFS spectroscopy.

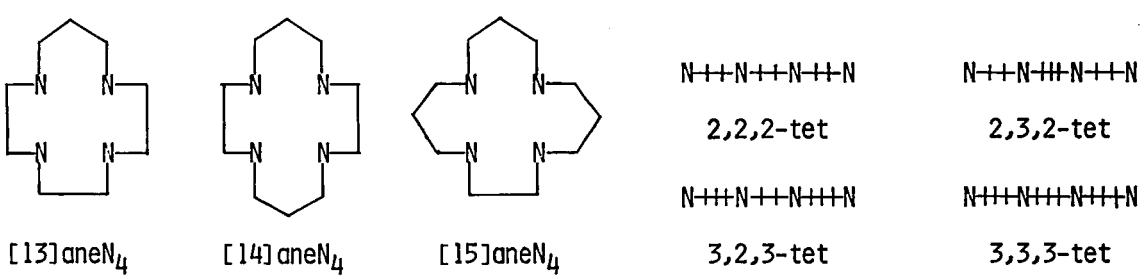

V-E-1 Syntheses, Electronic Spectra, Electric Conductivities, and X-Ray Photoelectron Spectra of One-Dimensional Pd(II)-Pd(IV) Mixed Valence Complexes with Linear Tetramines or Tetraazacycloalkanes

Masahiro YAMASHITA, Haruko ITO, Koshiro TORIUMI, and Tasuku ITO

[published partly in *Inorg. Chem.*, **22**, 1566 (1983)]

New Pd(II)-Pd(IV) mixed valence complexes $[Pd^{II}L]$ $[Pd^{II}X_2L]Y_4$ (L = [14]aneN$_4$, [15]aneN$_4$, 2,2,2-tet, 2,3,2-tet, 3,2,3-tet, 3,3,3-tet; X = Cl, Br; Y = ClO_4, BF_4, PF_6) have been prepared. Two route for the syntheses are shown in Scheme I.

Scheme I.

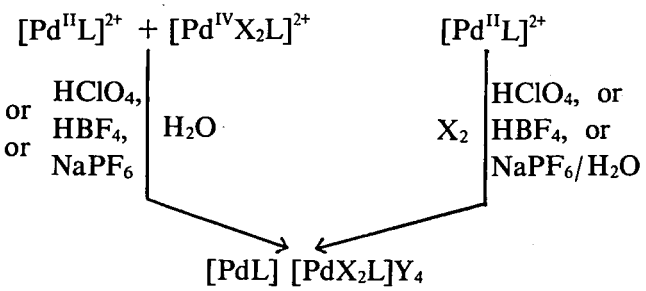

These compounds have been characterized by means of elemental analyses, electronic spectra (Nujol mull, $\tilde{\nu}_{max} \simeq 19 \times 10^3$ cm^{-1} for the Cl-bridged complexes and $\tilde{\nu}_{max} \simeq 12 \times 10^3$ cm^{-1} for the Br-bridged complexes), electric conductivities (pellet, $\sigma_{r.t.} \simeq 10^{-10} \Omega^{-1}$cm^{-1} for the Cl-bridged complexes and $\sigma_{r.t.} \simeq 10^{-7} \sim 10^{-8}$ Ω^{-1}cm^{-1} for the Br-bridged complexes), magnetic moments, XPS, and X-ray analyses of two complexes (Figure 1). All the data suggests that electronic interactions between Pd(II) and Pd(IV) in the Br-bridged complexes are stronger than those in the Cl-bridges complexes.

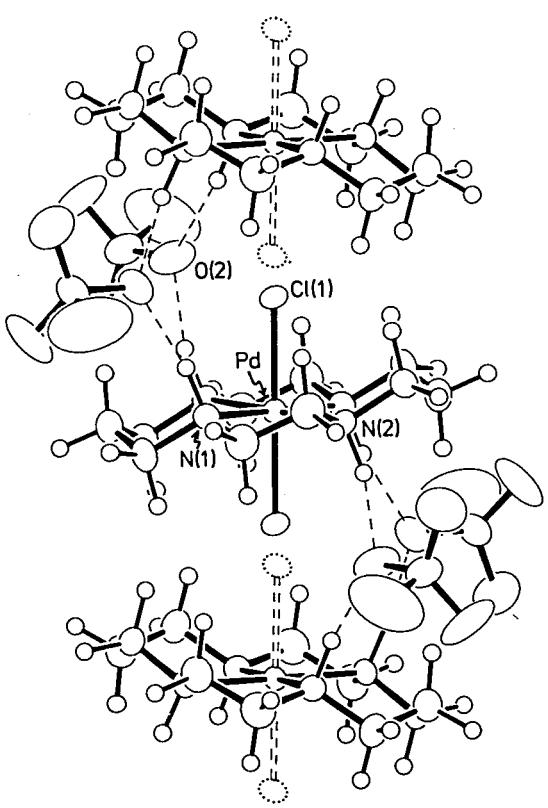

Figure 1. Portion of the infinite chain of $[Pd([14]aneN_4)][PdCl_2([14]aneN_4)](ClO_4)_4$ with surrounding ClO_4^- ions. Disordered perchlorate oxygens with minor occupancy factors are omitted for clarity. The dashed spheres and bonds represent the disordered positions of the Pd-Cl bonds. The dashed lines correspond to hydrogen bonds.

V-E-2 Structures of One-Dimensional Pd(II)-Pd(IV) Mixed Valence Complexes and Their Parent Pd(II) and Pd(IV) Complexes with 1,4,8,11-Tetraazacyclotetradecane

Masahiro YAMASHITA, Haruko ITO, Koshiro TORIUMI, and Tasuku ITO

[*Inorg. Chem.*, **22**, 1566 (1983)]

Crystal structures of Pd(II)-Pd(IV) mixed valence complexes, $[Pd^{II}([14]aneN_4)]$ $[Pd^{IV}Cl_2([14]aneN_4)]$ Y_4 (Y = ClO_4 (**1**) and PF_6 (**2**)), and those of discreate Pd(II) and Pd(IV) complexes, $[Pd^{II}([14]aneN_4)]$ $(ClO_4)_2$ (**3**) and $[Pd^{IV}Cl_2([14]aneN_4)]$ $(NO_3)_2 \cdot (HNO_3) \cdot (H_2O)$ (**4**), have been determined by X-ray diffractometry. Average molecular dimensions are compared in Table I. In the mixed valence complexes, **1** and **2**, the four-coordinate Pd(II) and six-coordinate Pd(IV), both of which have a 2+ charge, are stacked alternately in the direction of the needle axis, constructing linear chains of ···Cl-Pd(IV)-Cl···Pd(II) ··· segments (see V-E-1. Figure 1). In the chain structures **1** and **2**, the molecular dimensions within the $[Pd([14]aneN_4)]$ moiety of Pd(II) and Pd(IV) units are crystallographically the same. This observation is rationalized when bond distances and angles of the mixed valence complexes are compared with those of the parent discrete complexes (Table I). The Pd^{IV}-Cl distances in the chain structures are slightly longer than that of the complex **4**, indicating an electronic interaction along the chain.

Table I. Average Bond Distances (Å) and Angles (deg)[a]

compd	1	2	3	4
Pd^{IV}-Cl	2.320(3)	2.310(3)		2.303(1)
Pd^{II}···Cl	3.219(3)	3.514(3)		
Pd-N	2.055(3)	2.049(7)	2.051(5)	2.062(1)
Cl-Pd-N	86.7(2)	87.0(2)[b]		88.41(3)
	89.4(2)	90.1(2)[c]		
N-Pd-N(5*)	84.9(2)	85.0(3)	83.1(3)	84.72(4)
Pd-N-C(5*)	106.7(6)	106.9(5)	108.1(4)	106.82(8)
Pd-N-C(6*)	115.6(5)	116.4(5)	115.6(4)	115.64(7)

[a]Abbreviation: 5*, five-membered ring; 6*, six-membered ring. [b]Cl(1)-Pd-N(1). [c]Cl(1)-Pd-N(2).

V-E-3 Syntheses, Electronic Spectra, Electric Conductivities, and X-ray Photoelectron Spectra of Ni(II)-Ni(IV) Mixed Valence Complexes with Linear Tetramines or Tetra-azacycloalkanes

Masahiro YAMASHITA and Tasuku ITO

One-dimensional Ni(II)-Ni(IV) mixed valence complexes, $[Ni^{II}L]\ [Ni^{IV}X_2L]\ (ClO_4)_4$ (L = [13]aneN$_4$, [14]aneN$_4$, [15]aneN$_4$, 2,3,2-tet, 3,2,3-tet; X = Cl, Br), have been synthesized by the two methods shown in Scheme.

(i) L = 2,3,2-tet, 3,2,3-tet

$$NiCl_2 + L \xrightarrow[\text{abs. MeOH}]{Cl_2} [Ni^{III}Cl_2L]Cl$$

$$\xrightarrow[70\%\ HClO_4]{} [Ni^{II}L]\ [Ni^{IV}Cl_2L]\ (ClO_4)_4$$

(ii) L = [13]aneN$_4$, [14]aneN$_4$, [15]aneN$_4$

$$[NiL]\ (ClO_4)_2 \xrightarrow[70\%\ HClO_4]{Br_2}$$

$$[Ni^{II}L]\ [Ni^{IV}Br_2L]\ (ClO_4)_4$$

The authenticity for Ni(II)-Ni(IV) mixed valence states suggested by the elemental analyses, diamagnetism, electronic spectra, and electric conductivities, were directly evidenced by the X-ray photoelectron spectra (Table I). The electric conductivities (pellet) at room temperature are on the order of $10^{-6}\ \Omega^{-1}cm^{-1}$ for the bromo-bridged complexes and $10^{-7} \sim 10^{-8}\ \Omega^{-1}cm^{-1}$ for the chloro-bridged complexes, and are significantly higher than those of Pt and Pd analogs.

Table I. Binding Energy (eV)

	$2p_{3/2}$			Cl2p		
	Ni(II)	Ni(III)	Ni(IV)	Cl^{-a}	Cl^{-b}	ClO_4^-
$[Ni^{II}([14]aneN_4)](ClO_4)_2$	855.1	—	—	—	—	207.6
$[Ni^{III}Br_2([14]aneN_4)]ClO_4$	—	855.9	—	—	—	
$[Ni^{III}Cl_2([14]aneN_4)]ClO_4$	—	855.9	—	—	197.6[e]	207.5
$Ni(pn)_2Cl_3$[c]	855.6	—	857.7	196.9	198.4[f]	—
$Ni([14]aneN_4)Br(ClO_4)_2$[d]	855.2	—	856.9	—	—	207.9

a, counter anion; b, axial or bridged; c, $[Ni^{II}(pn)_2][Ni^{IV}Cl_2(pn)_2]$ (pn=1,2-diaminopropane); d, $[Ni^{II}([14]aneN_4)][Ni^{IV}Br_2([14]aneN_4)]$; e, axial; f, bridged.

V-E-4 Structural Study of Ni(II)-Ni(IV) Mixed Valence Complexes by Means of Extended X-ray Absorption Fine Structure

Koshiro TORIUMI, Toshiaki KANAO *(Kumamoto Univ. and IMS)*, **Masahiro YAMASHITA, Akira OHYOSHI** *(Kumamoto Univ.)*, **and Tasuku ITO**

The one-dimensional Ni(II)-NI(IV) mixed valence complexes described in a preceding section (V-E-3) do not afford single crystals suitable for X-ray analyses. We are trying to detemine the structural parameters of the linear chain structures by means of EXAFS spectroscopy.

EXAFS spectra of $[Ni^{II}(pn)_2]$ $[Ni^{IV}Cl_2(pn)_2]Cl_4$, $[Ni^{II}(en)_2]$ $[Ni^{IV}Cl_2(en)_2](ClO_4)_4$, and $[Ni^{II}([14]aneN_4)]$ $[Ni^{IV}Br_2([14]aneN_4)](ClO_4)_4$ were obtained on a laboratory EXAFS spectrometer with a rotating anode X-ray source and LiF(220) bent crystal (II-E-3). Some examples of Fourier transforms of EXAFS spectra are presented in Figure 1. EXAFS parameters have been determined by the curve fitting techniques for Fourier-filtered $k^2\chi(k)$ waves, using the theoretical phases and amplitudes tabulated by Teo and Lee.[2] The analyses were made with the aid of EXAFS spectra of Ni(II) and Ni(III) complexes having the same coordination environments, structures of which have been known by X-ray diffractometry. For $[Ni^{II}(pn)_2][Ni^{IV}Cl_2(pn)_2]Cl_4$, we obtained two Ni-Cl distances of 2.46 and 3.04 Å, which correspond to Ni(IV)-Cl and Ni(II)···Cl separations along the chain. Further studies are now in progress.

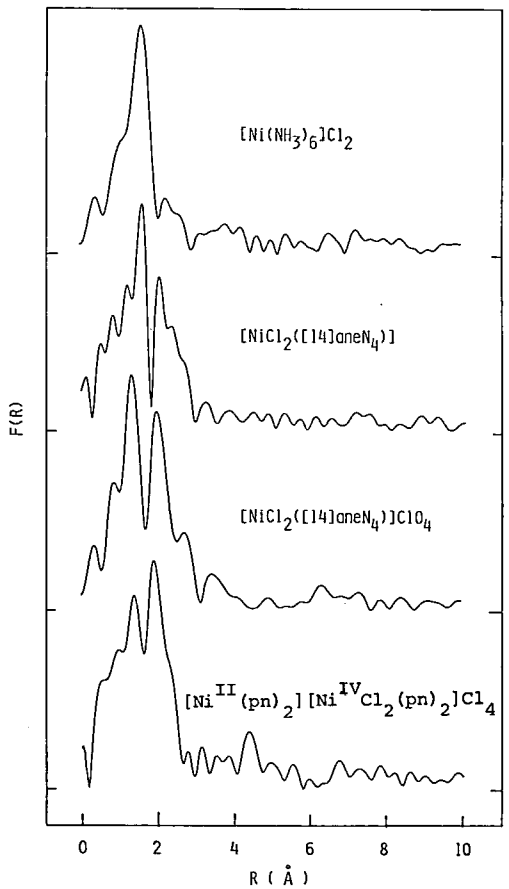

Figure 1. Fourier transforms of EXAFS spectra.

Reference

1) IMS Graduate Student from Kumamoto University for 1983.
2) B.-K. Teo and P.A. Lee, J. Am. Chem. Soc., **101**, 2815 (1979).

V—F Nuclear Magnetic Study of Ion-Ion Interaction in Solutions of Metal Complex Salts

The nuclear magnetic resonance technique provides a useful tool for investigating the static and dynamic features of ion-ion interactions in solutions. Thus interaction between ions such as ion-pair formation and hydrophobic aggregate formation may cause a change in the chemical shift of the resonance frequency and in the relaxation rate of magnetic nuclei. This reseach project was undertaken to disclose the effects of the electrostatic and the hydrophobic interaction on the static and dynamic features of ion-ion interaction in solutions. The 1,10-phenanthroline and the 2,2'-bipyridine complexes of ruthenium (II) and cobalt (III) in the forms of chloride and sulfate were selected as probes for the reasons: (1) They are large ions and are adequately treated by the hydrodynamic model. (2) They are similar in shape but different in charge. (3) They have bulky hydrophobic ligands.

V-F-1 Proton Chemical Shift Study of the Hydrophobic Interaction between Tris(1,10-phenantroline)ruthenium(II) Ions in Aqueous Solution

Yuich MASUDA *(Nagoya Univ.)*, **and Hideo YAMATERA** *(Nagoya Univ. and IMS)*

[*Bull. Chem. Soc. Jpn.*, **57**, (1984) in press]

The proton NMR chemical shifts were measured in the D_2O solutions of $[Ru(phen)_3]SO_4$. The proton resonances of the phenanthroline ligand showed up-field shifts with increasing concentration of *rac*-$[Ru(phen)_3]SO_4$, but they were not significantly affected by the addition of Na_2SO_4. The profile of the up-field shifts for the Λ-$[Ru(phen)_3]SO_4$ solution was different from that for the *rac*-$[Ru(phen)_3]SO_4$ solution. These results give the evidence that the up-field shifts were caused by the interaction between $[Ru(phen)_3]^{2+}$ ions. Assuming the formation of the triple and quadrupole aggregates containing two $[Ru(phen)_3]^{2+}$ ions, we determined the association constants of these aggregates as well as the magnitudes of the up-field shift in the aggregate. The obtained up-field shifts for the racemic aggregate were largest in the 5 and 6 positions (1 ppm) and smallest in the 2 and 9 positions (0.2 ppm). A probable structure of the aggregate (Figure 1) was deduced from the measured chemical shifts by attributing the up-field shift in the aggregates to the ring-current effect of the phenanthroline ligands. The importance of the hydrophobic interaction between $[Ru(phen)_3]^{2+}$ ions in aqueous solution was thus indicated.

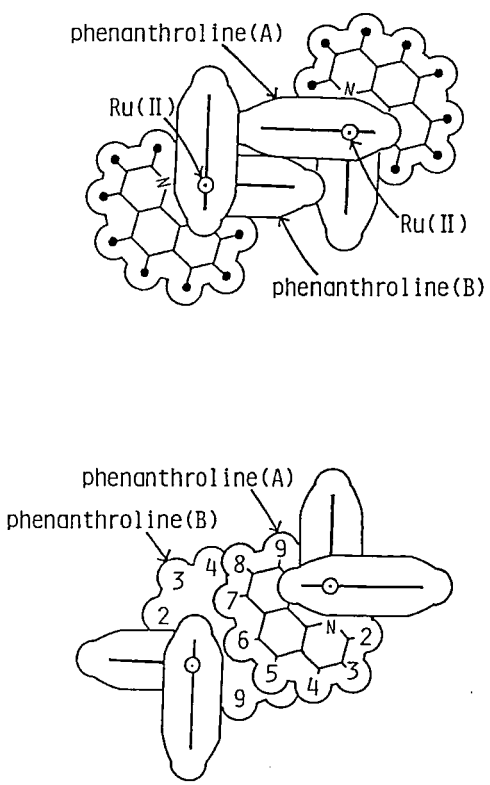

Figure 1. Probable configuration of a pair of Λ- and Δ-$[Ru(phen)_3]^{2+}$ ions in the M_2X and M_2X_2 aggregates: the elevation (top) and the plan (bottom).

V-F-2 Rotational Motion of the Tris(1,10-phenanthroline) and Tris(2,2-bipyridine) Complexes of Ruthenium (II) and Cobalt (III) Ions in Solutions

Yuichi MASUDA *(Nagoya Univ.)*, **and Hideo YAMATERA** *(Nagoya Univ. and IMS)*

Rotational motions of hydrophobic complex ions, $[Ru\ L_3]^{2+}$ in D_2O and CD_3OD, and $[Co\ L_3]^{3+}$ in D_2O (L = 1,10-phenanthroline and 2,2'-bipyridine) were investigated by the nuclear mag-

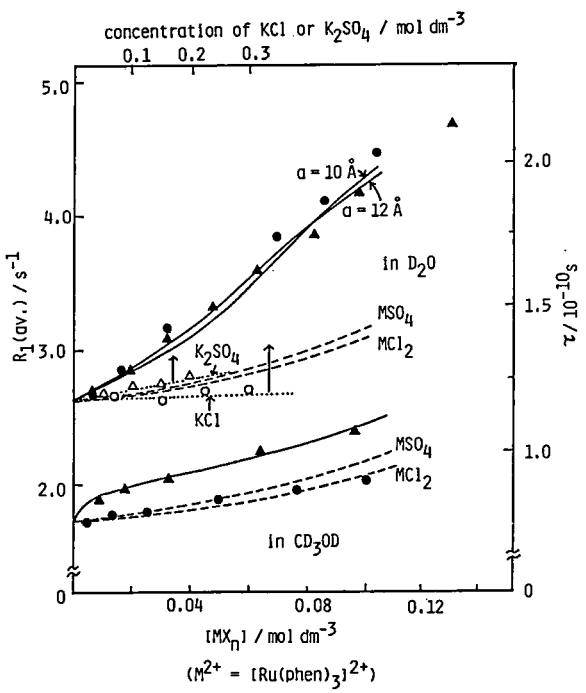

Figure 1. Plots of the R_1 (av.) and τ values of $[Ru(phen)_3]^{2+}$ in D_2O and CD_3OD at 33.0 °C vs. the concentration of the chloride (●) and the sulfate (▲) of $[Ru(phen)_3]^{2+}$ and vs. the concentration of KCl (○) and K_2SO_4 (△) added to the 0.005 mol dm $^{-3}$ D_2O solution of the chloride and the sulfate of $[Ru(phen)_3]^{2+}$. Broken and dotted lines indicate the τ values as a linear function of the viscosity.

netic relaxation technique. The measured spin-lattice relaxation rates of the ^{13}C nuclei of the complex ions showed that the rotational motions of the ions were nearly isotropic. At infinite dilution, the dependences of the τ values of the complex ions on temperature were approximately represented by the Stokes-Einstein equation. In the CD_3OD solution of $[Ru(phen)_3]SO_4$, the τ value was appreciably larger than that predicted from the change in the viscocity of the solution, which was shown by the broken line in Figure 1. Similar increases in the τ values were also observed in the CD_3OD solution of $[Ru(bpy)_3]SO_4$ and in the D_2O solutions of $[Co\ L_3]_2(SO_4)_3$. These increase of the τ values were attributed to the formation of the 1 : 1 ion-pairs with the sulfate ion. The τ value of the $[Ru(phen)_3]^{2+}$ ion in D_2O remarkably increased with increasing concentration of the complex salts. This increase in τ was attributed to the formation of the aggregate containing two $[Ru(phen)_3]^{2+}$ ions. The τ values of the complex ions were 20 − 30% larger in the ion-pairs and about 200% larger in the aggregate than those of unassociated complex ions.

V—G Organic Reactions Initiated by Photoinduced Electron Transfer

Exploratory and mechanistic studies have been carried out on the rearrangements, additions, and cyclizations of organic compounds initiated by intramolecular electron transfer in the photo-excited state. As an extension of the photo-Smiles rearrangement, the nitrobenzene chromophore carrying ω-anilinoalkyl group at the meta position has now been studied.

V-G-1 Photocyclization of ω-Anilinoalkyl *m*-Nitrophenyl Ethers

Kiyoshi MUTAI *(Univ. of Tokyo and IMS)*, **Kenji YOKOYAMA** *(Inst. Phys. Chem. Res.)*, **and Keiji KOBAYASHI** *(Univ. of Tokyo)*

[*Tetrahedron,* in press]

Irradiation of 1-(*m*-nitrophenoxy)-ω-anilinoalkanes (**1**, n = 2 and 3) and their 1-(2-methoxy-5-nitrophenoxy) analogs (**2**) induced intramolecular cyclization in which the hydrogen or methoxyl group at the para position with respect to the nitro group is replaced by the anilino nitrogen, giving **3** as only isolable products.

Laser flash photolysis of **1** (n = 2) showed generation of transient species with half-lives of 50 ns and 20-30 μs. The intermediate with shorter lifetime has been confirmed as a radical ion pair composed of nitrophenoxyl radical anion and anilino radical cation moieties, by comparison of its transient absorption spectrum with that of a reference. This fact, together with several other reaction features, suggests that the photocyclization starts with intramolecular electron transfer, followed by recombination of a radical ion pair thus formed. The regiospecificity observed is rationalized by this mechanism.

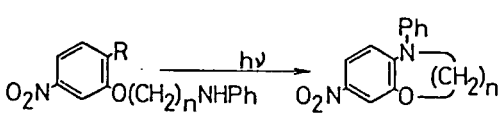

1, R=H; 2, R=OMe 3

RESEARCH ACTIVITIES VI

COMPUTER CENTER

VI—A Theoretical Investigations of Metalloporphyrins by the *Ab Initio* SCF MO Method

Metalloporphyrin complexes are interesting polyatomic systems because of their complicated electronic structure and because of their catalytic function. Heme and chlorophyll are prominently important as an active center of energy conversion processes in biological systems. In this project the electronic structure and the fundamental functions are studied for several complexes by performing *ab initio* MO computations.

VI-A-1 *Ab initio* MO Study of Mössbauer Spectra of Fe-Porphyrin Complexes

Hiroshi KASHIWAGI, Shigeyoshi YAMAMOTO, Minoru SAITO *(IMS and Nagoya Univ.)* **and Shigeru OBARA** *(Kyoto Univ.)*

Ab initio LCAO SCF MO calculation have been carried out on five Fe-portphine-pyridine-L_6 complexes (L_6: none, CO, pyridine, F^- and CN^-), which are ferrous and ferric compounds and have various spin angular momentum. Observable quantities of Mössbauer spectra, i.e. isomer shift (IS), quadrupole splitting (QS), etc. have been calculated for these complexes. Three empirical parameters in the expresions of IS and QS are redetermined by comparison between the observed and the calculated values of the five complexes. On the whole, the calculated values are in good agreement with the experimental ones as shown in Table I.

A new relation which was found in the previous paper[1] is confirmed even for ferric complexes. This relation is that the diagonal component of the EFG tensor along the perpendicular axis to the portphine plane consists of two terms, i.e. the contribution from d-electrons of iron and a constant term C depending on axial ligands.

Table I. Calculated and observed data of Mössbauer spectra of Fe-porphyrin complexes

calc. obs.	Compound State		IS (mm/sec)	QS (mm/sec)	V_{zz} sign	direction	η
calc.	FeP(py)	5B1	0.80	2.35	+	y	0.77
obs.	FeTPP(2-MeIm)		0.93	2.28			
	deoxy Mb				+	in plane	
	deoxy Mb			2.28	+	in plane	0.7
	deoxy Mb			2.22	−	in plane	0.7
calc.	FeP(py)CO	$^1A_1$	0.41	0.09	−	z	0.43
obs.	FePFP-(1-MeIm)CO		0.27	0.27			
	MbCO		0.27	0.36	+	z	0.2-0.4
calc.	$FeP(py)_2$	^1A_g	0.62	0.96	+	z	0
obs.	$FeOEP(py)_2$		0.46	1.13	+		~0
	$FeTPP(py)_2$		0.41	1.15			
	$FePP(py)_2$		0.45	1.21			
calc.	$FeP(py)F^-$	$^6A_1$	0.28	0.39	+	z	0
obs.	MbF^-		0.46	0.70	+		~0
calc.	$FeP(py)CN^-$	$^2B_2$	0.19	1.48	−	x	0
obs.	$HbCN^-$		0.17	1.39			

Reference

1) S. Obara and H. Kashiwagi, *J. Chem. Phys.*, 77, 3155 (1982).

CHEMICAL MATERIALS CENTER

VI—B Synthesis and Characterization of 1 - [Bis(cyclopentadienyl)zircona] - 2 - oxacyclopentanes. X-Ray Crystal Structure of $[(\eta\text{-}C_5H_5)_2ZrOCH_2CH_2CHCH_3]_2$

Hidemasa TAKAYA, Masashi YAMAKAWA, and Kazushi MASHIMA

[*J. Chem. Soc., Chem. Commun.*, in press]

Metallacycle compounds continue to attract an increasing interest because of their importance as

intermediates in many useful transition metal catalyzed organic reactions. Only a limited number of papers, however, have been reported on the preparations and reactions of metallacycles which contain an oxygen atom in their rings. We have studied the synthesis and thermal reactions of the parent 1-[bis(cyclopentadienyl)zircona]-2-oxacyclopentane (**1a**) and its derivatives.

Treatment of $(\eta\text{-}C_5H_5)_2ZrHCl$ with potassium allyl alcoholate (**2a**) in THF at room temperature followed by recrystallization of the product from chloroform afforded (**1a**). Similar reaction with (**2b**) gave (**1b**), whereas reaction with (**2c**) afforded only (**1c**). No ten-membered metallacycle such as (**3**) was isolated. The structure of (**1c**) was unequivocally established by a single crystal *X*-ray diffraction study, which revealed that it has a dimeric and five co-ordinate bent metallocene structure (Figure 1).

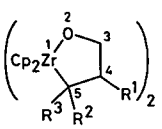

(1)

a; $R^1 = R^2 = R^3 = H$
b; $R^1 = CH_3$, $R^2 = R^3 = H$
c; $R^1 = R^2 = H$, $R^3 = CH_3$
d; $R^1 = H$, $R^2 = R^3 = D$

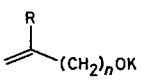

(2)

a; $n = 1$, $R = H$
b; $n = 1$, $R = CH_3$
c; $n = 2$, $R = H$

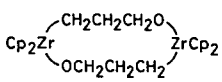

(3)

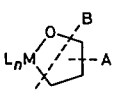

(4)

Thermal decomposition of (**1a–c**) and their deuterated derivatives have been carried out at 240–250°C under reduced pressure. The results indicated that the thermal decomposition of (**1**) follows two reaction modes, A and B (see formula

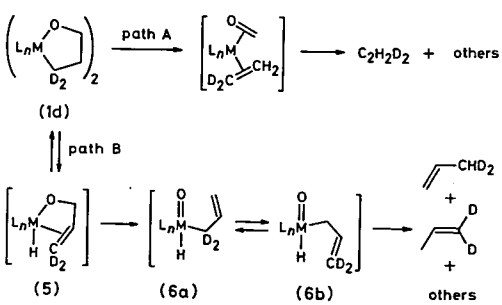

Scheme 1 L = cyclopentadienyl

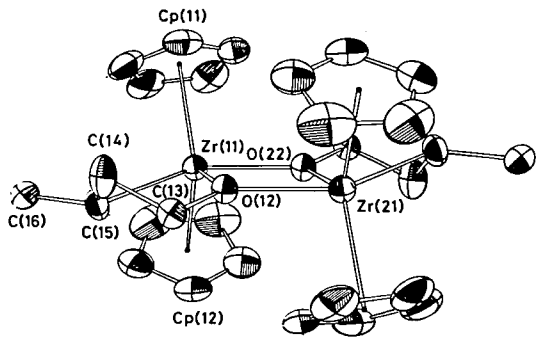

Figure 1. The molecular structure of **1c**.

(4)). A possible mechanism has been given in Scheme 1.

VI—C Characterization of the New Platinacycle Compounds Derived from Bicyclo[1.1.0]butanes and Platinum Complexes. An Isolation of a Novel Carbene—Pt(0) Complex

Akira MIYASHITA *(Saitama Univ.)* **and Hidemasa TAKAYA**

We have been interested in the mechanism of transition metal catalyzed reactions of bicyclo[1.1.0]butanes. In our former studies on this topic we reported the first isolation of new platinacycle compounds **4a—h** (eq 1) by the reaction of bicyclo[1.1.0]butanes (**1**) and Pt(II) complexes (**2**) and their intriguing chemical behaviors.[1,2] We furnished a sufficient evidence that Pt(II)-catalyzed isomerization of bicyclo[1.1.0]butanes takes place in a stepwise manner by way of metallacycle intermediates of the type **4**. This time our attention was directed to the effects of ligands and oxidation states of the metals on the stability and properties of the platinum complexes derived from **1**. Reduction of **4f** with 1% sodium amalgam in acetonitrile afforded isolable Pt(II) metallacycle **5** (eq 2), while similar treatment of **4g** resulted in the isolation of a novel allylcyanocarbene—Pt(0) complex **6** (Scheme I). The unique chemical properties of these complexes including the nucleophilic character of the carbenic carbon have been demonstrated (eq 2 and Scheme I).

The above results indicate that under controlled conditions 2-platinabicyclo[1.1.1]pentane complexes

isomerize easily to allylcarbene-platinum complex, which provides a strong support for the mechanism involving allylcarbene-transition metal intermediates proposed in the intra- and intermolecular reactions of bicyclo[1.1.0]butanes assisted by transition metals.

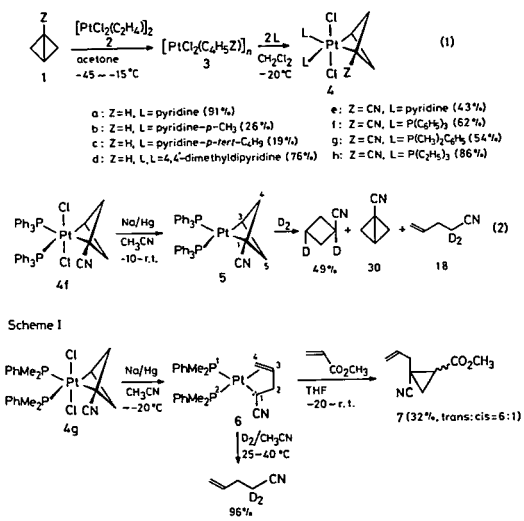

References

1) A. Miyashita, M. Takahashi, and H. Takaya, *J. Am. Chem. Soc.*, **103**, 6257 (1981).
2) A. Miyashita, Y. Watanabe, and H. Takaya, *Tetrahedron Lett.*, **24**, 2595 (1983).

VI—D Synthesis of New Atropisomeric Diphosphine Ligands and Their Use in Transition Metal Catalyzed Asymmetric Reactions

Akira MIYASHITA, Hidemasa TAKAYA, Toshiaki SOUCHI,* and Ryoji NOYORI*
*(*Nagoya Univ.)*

[*Tetrahedron Symposia In Print*, in press]

In our earlier reports[1-3] we communicated the synthesis of 2,2'-bis(diphenylphosphino)-1,1'-binaphthyl (**1**), a new atropisomeric bis(triaryl)phosphine and its use in Rh(I)-catalyzed asymmetric organic reactions. This time we have reported the full details of the successful preparation of this chiral diphosphine **1** and its use in Rh(I)-catalyzed asymmetric hydrogenations of α-(acylamino)acrylic acids. We are now making a continuous effort to develop new type of chiral diphosphine ligands bearing 1,1'-binaphthyl skeleton which are effective for asymmetric reactions other than olefin hydrogenations.

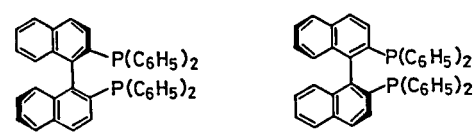

(*R*)-(+)-1 (*S*)-(-)-1

References

1) A. Miyashita, A. Yasuda, H. Takaya, K. Toriumi, T. Ito, T. Souchi, and R. Noyori, *J. Am. Chem. Soc.*, **102**, 7933 (1980).
2) K. Toriumi, T. Ito, H. Takaya, T. Souchi, and R. Noyori, *Acta Cryst.* **B38**, 807 (1982).
3) K. Tani, T. Yamagata, S. Otsuka, S. Akutagawa, H. Kumobayashi, T. Taketomi, H. Takaya, A. Miyashita, and R. Noyori, *J. Chem. Soc., Chem. Commun.* 600 (1982).

INSTRUMENT CENTER

VI—E Photophysical Dynamics of Highly-Ordered Molecular Assemblies

Polymers with helically arranged chromophores and liquid crystals are typical examples of molecular systems or assemblies with specifically organized arrangement. They in some cases provide us with analogues of supermolecular system in biological organisms. In molecular assemblies, photons are absorbed to produce excited species, which then engage in photophysical processes such as excitation energy tansfer, excimer formation and photochemical reaction. The focus is directed to new dynamical aspect of the photophysical and photochemical processes under the highly-ordered molecular assemblies. Recently, we have investigated the excitation energy transfer in bilepigment system of the photosynthetic organisms and the excimer formation of constituent molecules in the liquid crystal, by means of a picosecond time-resolved fluorescence spectroscopy.

VI-E-1 Picosecond Time-Resolved Fluorescence Spectroscopy of Photosynthetic Bilepigments

Iwao YAMAZAKI, Naoto TAMAI, Tomoko YAMAZAKI

[*Photochem. Photobiol.*, **38**, 658 (1983)]

Time-resolved fluorescence spectra of intact cells of red and blue-green algae *Porphyridium cruentum* and *Anacystis nidulans* were measured by means of a picosecond laser and a time-correlated photon counting system.[1] Fluorescence spectra were observed successively from various pigments in the light harvesting system in the order of phycoerythrin (PE), phycocyanin (PC), allophycocyanin (APC) and chlorophyll *a* (Chl *a*). The spectrum changes with time in the range of 0–400 ps in *P. cruentum* and of 0–1000 ps in *A. nidulans*. The time-resolved spectra were analyzed into components to obtain the rise and decay curve of each fluorescence component. Overall time behaviors of the sequential fluorescence emissions from various pigments can be interpreted with a decay kinetics of $\exp(-2kt^{1/2})$. The rate constants of the energy transfer show that the energy transfer takes place much faster in the red alga *P. cruentum* than in the blue-green alga *A. nidulans*, particularly in the step PC → APC. Similar results have been obtained for other series of algal intact cells such as *Toripos tenuis* (Figure 1) and *Flemyella diplosiphone*.

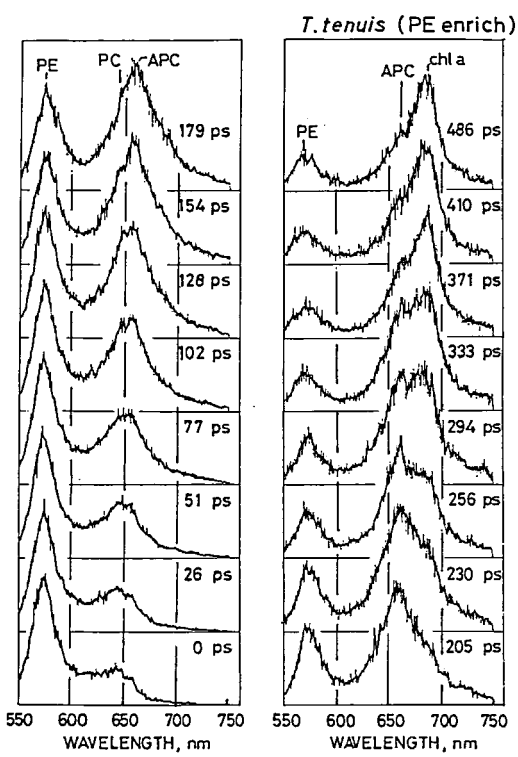

Figure. 1 Time-resolved fluorescence spectra of *T. tenuis* intact cells enriched in a content of phycoerythrin, following excitation at 540 nm. The time zero corresponds to the time at which the excitation laser pulse reaches maximum intensity.

Reference

1) T. Murano, I. Yamazaki, and K. Yoshihara, *J. Spectrosc. Soc. Japan*, **31**, 96 (1982).

VI-E-2 Picosecond Time-Resolved Fluorescence Spectroscopy of Liquid Crystals

Naoto TAMAI, Iwao YAMAZAKI

Liquid crystals are highly anisotropic media with their molecular arrangement being changed due to phase transition. Difference in orientational and spatial ordering of molecules define the mesophases such as smectic A and nematic phases. Such an effect in liquid crystals is now receiving increased attention in view of the photophysical and photochemical processes in highly ordered molecular assemblies.[1,2] The present study is directed toward dynamics of an intermolecular excimer formation between constituent molecules of the liquid crystal.

Dynamics of the excited state of 4-cyano-4-octoxybiphenyl (80CB) liquid crystal have been investigated as a function of temperature in relation to the phase transition. Figure 1 shows a typical example of picosecond time-resolved fluorescence spectra in the nematic phase at 343.2K. Monomer-like fluorescence with maximum at about 350–360 nm was observed immediately after excitation in smectic A, nematic and isotropic phases. It is seen from spectral change that the monomer-like state is relaxed to the excimer-like state within 200–300 ps. These results may be interpreted in terms of ground- and excited-state conformational differences depending on the phase.

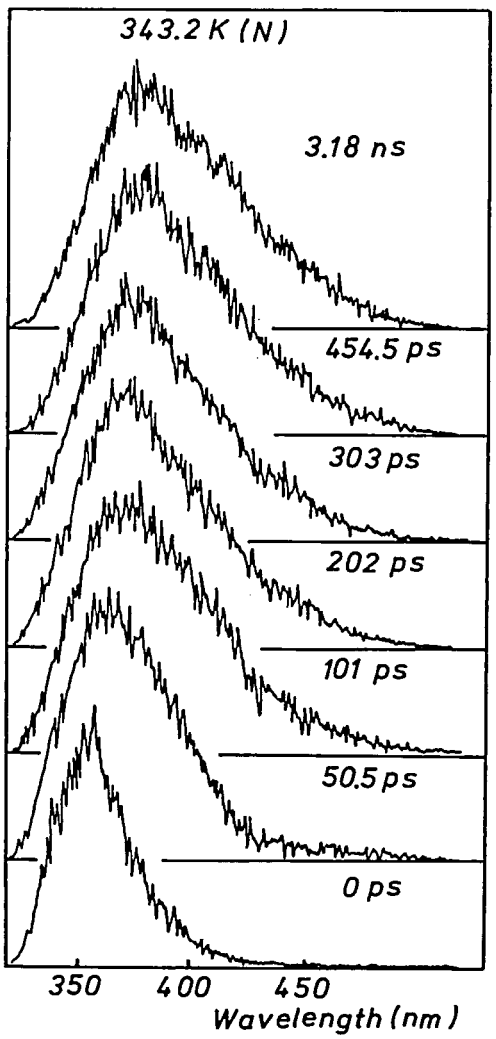

Figure 1. Time-resolved fluorescence spectra of neat 4-cyano-4'-octoxybiphenyl in nematic phase at 343.2K, following excitation at 300 nm. Delay times after exciting pulse are indicated in the figure.

References

1) V.C. Anderson, B.B. Craig, and R.G. Weiss, *J. Phys. Chem.* **86**, 4642 (1982).
2) R. Subramanian, L.K. Patterson, and H. Levanon, *Chem. Phys. Lett.*, **93**, 578 (1983).

VI—F Development of Picosecond Time-Resolved Fluorescence Spectrophotometer

Naoto TAMAI and Iwao YAMAZAKI

Previously we have constructed a picosecond time-resolved emission spectrophotometric system[1] which consists of a synchronously pumped, cavity-dumped dye laser, a time-correlated single-photon counting system and a computer system. The time resolution of this system was achieved to be ten times as high as that of usual fluorimeters, by using a microchannel plate photomultiplier instead of conventional photomultipliers with a dynode string: The pulse width of the laser scattering light is observed with a 70-ps fwhm.[2,3] This system enables us to measure the time-resolved spectrum in every 12.8-ps time interval as well as fluorescence decay curves. We now proceed experiment using various types of the fluorescence detection system, with a view to improving furthermore the time resolution of the system. The time characteristics of different detectors are summarized in Table I.

Table I. Time resolution and dynamic range in various types of detectors

Method	Detector	Observed pulse width of the laser (fwhm)	Dynamic range
Time-correlated photon counting system	Side-on photomultiplier RCA 1P28	600 ps	10^4
	MCP (non-proximity) photomultiplier HT R1294U	70 ps	10^4
	MCP (proximity) photomultiplier HT R1564U	60 ps	10^4
Synchroscan streak camera	HT C1587	20 ps	10^2

References

1) T. Murao, I. Yamazaki, and K. Yoshihara, *J. spectrosc. Soc. Japan*, **31**, 96 (1982).
2) T. Murao, I. Yamazaki, and K. Yoshihara, *App. Opt.* **21**, 2297 (1982).
3) I. Yamazaki, T. Murao, and K. Yoshihara, *Chem. Phys. Lett.*, **87**, 384 (1982).

VI—G Magnetic Resonance Study of Hydrogenase and Cytochrome c_3

Keisaku KIMURA, Hiroo INOKUCHI, Tatsuhiko YAGI *(Shizuoka Univ.)*, **Shinsuke NAKAJIMA** *(Yokohama Nat. Univ.)*, **and Katsumi NIKI** *(Yokohama Nat. Univ.)*

Hydrogenase is an enzyme for hydrogen cleavage reaction and cytochrome c_3 is a native electron

acceptor in this reaction. The active center of hydrogenase was reported to be an iron-sulfur cluster as found in ferredoxin. However the essential component in hydrogenase has not yet been settled. A nickel atom and also a zinc atom have recently been detected as a component of hydrogenase.[1] Therefore we examined an active center of hydrogenase of *Desulfovibrio vulgaris*.

The X-band ESR spectra of the hydrogenase preparation were recorded at temperatures raging from 4.2K to 42K at 1 mW microwave power and at microwave powers from 10 μW to 100 mW at 17K. The spectrum line shape was analysed by computer simulation. The model of the cluster was constructed from the analysis.

^{1}H-NMR measurement of cytochrome c_3 was studied at 400 MHz. The temperature dependence, redox titration, and pH titration classified the methyl protons of four hemes. The electron transfer rate was also elucidated.

Reference

1) H-J. Krüger, B.H. Huynh, P.O. Ljungdahl, A.V. Xavier, D.V. DerVartanian, I. Moura, H.D. Peck, Jr, M. Teixeira, J.J.G. Moura, and J. LeGall, *J. Biol. Chem.*, **257**, 14620 (1982).

VI—H The Study of Metal Fine Particles in Organic Solvents

Fine particles as a model of zero dimension substance are characterized by quantum size effect, surface effect on bulk properties and size effect on a superconducting transition temperature. These effects were studied as a function of metal species and solvents.

VI-H-1 Preparation Method and Optical Properties of Metal Particles

Keisaku KIMURA and Shunji BANDOW

[*Bull. Chem. Soc. Jpn.*, **56**, 3578 (1983)]

Three new methods for the preparation of metal colloid in organic solvent are presented. These methods were the matrix isolation method, the gas flow-cold trap method and the gas flow-solution trap method; The latter has three characteritics. One is the wide applicability to any metals/metal solid solutions with use of the same apparatus. It should be emphasized that this technique is not confined to metals but is applicable also to any thermally stable solid samples. The second is the simpleness of the system. This technique gives substantially a two-component pure system unless the metal does not react with solvent. The simpleness of the system may make it easy to understand the solid state properties of small metal particles in solution. The third one is that the colloid prepared by the present method is a sol, that is, the metal fine particles are in solution. This is a merit for the optical measurement in ultraviolet region, because the scattering effect is dominant in solid matrixes in this region.

This technique was applied to Pb, Sn, Al, Ca, In, Cu, Au, and Ag metal colloid in ethanol solution. All metals gave well dispersed colloids. The diameters of many samples fell in the region of 10 to 50 nm in the present experimental conditions. Some metal particles, Pb, Sn, Ca, and Cu were found to be unstable and others, Al, In, Au, and Ag, were stable. The optical spectra of these colloid solutions resembled the reported spectra of fine particles on matrix or on substrate, many of which were results of low temperature measurements.

VI-H-2 Reaction of Metal Fine Particles in Organic Solvents

Keisaku KIMURA

The instability of copper and lead colloids in ethanol solution was studied spectrophotometrically. In the beginning of the reaction, very small copper particles reacted with ethanol producing ethoxide, which was confirmed by the incremental increase of the 213-nm peak. As the reaction proceeded, the 577-nm characteristic copper band showed a red shift together with line broadening.

This was explained by the particle size dependence of the spectrum.

VI—I Development of Experimental Devices and Techniques

The Instrument Center is equipped with various types of instruments for molecular spectroscopy, solid-state chemistry and magnetic spectroscopy.[1] All of them are opened widely for researchers in universities and institutions as well as staffs in IMS. In view of efficient use of these instruments, the Center staffs are concerned with development of new experimental devices and techniques.

Reference

1) *List of Instruments*, No.4, IMS Instrument Center (1983).

VI-I-1 Spectrofluorimeter with Nanosecond Time Resolution by Means of a Transient Digital Memory

Takaya YAMANAKA and Iwao YAMAZAKI

A spectrofluorimeter with nanosecond time resolution has been constructed, for the purpose of mesuring the decay curves and the time-resolved spectra for fluorescence and phosphorescence. The system consists of transient digital memories (Biomation 6500 and NF WM-852) and microcomputer system. A schematic diagram is shown in Figure 1. The photoelectric signal associated with emission signal is recorded on the transient digital memory (1024 channels) in which the time history of emission intensity can be recorded with 2–50 ns/channel time resolution. The data are transferred to the computer and accumulated for successive excitations. The wavelength of the monochromator is driven under the control of the computer. After a series of rise and decay curve measurements at various wavelengths, time-resolved spectra are obtained for the minimum time interval of 2 ns. All these measurements and data processing are performed automatically with the aid of the computer. This system is applicable to the time-dependent molecular spectroscopy and the molecular dynamics in photochemical reactions.

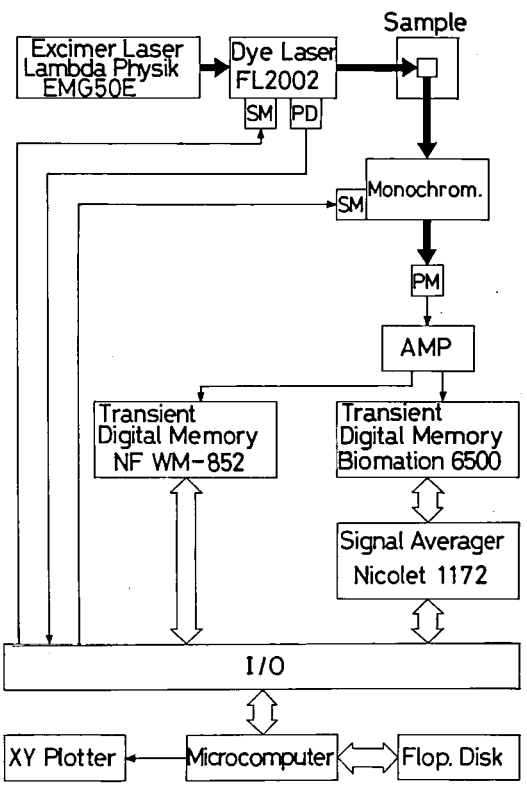

Figure 1. Schematic diagram of the spectrofluorimeter. PD, photodiode; SM, stepping motor; PM, phtomultiplier.

LOW TEMPERATURE CENTER

VI—J Hydrogen Chemisorption in Alkali Metal Complexes of Polycyclic Aromatic Hydrocarbons and Graphite

Alkali metal complexes of polycyclic aromatic hydrocarbons and graphite have catalytic activities for hydrogen and occude hydrogen in their solid chemisorptively and physisorptively. We are investigating the chemisorption mechanism and the static and dynamical behaviors of hydrogen in the complexes by means of ESR and electrical conductivities.

VI-J-1 Chemisorption of Hydrogen in Graphite-Alkali Metal Intercalation Compounds

Toshiaki ENOKI, Mizuka SANO *(Kumamoto Univ.)* **and Hiroo INOKUCHI**

[*J. Chem. Phys.*, **78**, 2017 (1983)]

The hydrogen chemisorption mechanism in the graphite-alkali metal intercalation compounds has been investigated by means of ESR and electrical resistivity under hydrogen atmosphere. In the first stage rubidium compound C_8Rb, hydrogen molecules are dissociated into atoms which are stabilized in the interstices of Rb atoms in the gaps of the graphite layers. C_8K has a two-stage hydrogen absorption. In the initial stage, the dissociated hydrogen atoms are transiently yielded and then, in the second stage, the formation of hydride ions H^- takes place through the charge transfer from C_8K to H. C_8Cs shows no change in the ESR signal under hydrogen atmosphere. This finding suggests that its catalytic activity for an H-D exchange reaction is due to the surface activity. For the second stage compounds $C_{24}K$ and $C_{24}Rb$, there exists a one-stage hydrogen absorption process, i.e., absorbed hydrogen directly becomes hydride ion H^-. $C_{24}Cs$ shows no change in the ESR signal under hydrogen atmosphere. For the chemisorption activity, the order of the strength is K>Rb>Cs in both first and second stage compounds.

VI—K Solid State Properties of Organic Conductors

New types of donors and acceptors were synthesized in order to develop organic conductors. Solid state properties of the charge transfer complexes with these donors and acceptors have been investigated.

VI-K-1 Synthesis of Cyclobutane-fused Tetracyanoquinodimethanes

Shunro YAMAGUCHI,* Hitoshi TATEMITSU,* Yoshiteru SAKATA,* Toshiaki ENOKI, and Soichi MISUMI* *(*Osaka Univ.)*

[*J. Chem. Soc., Chem. Commun.*, 1065 (1982)]

The preparation of the title π-acceptors (1)–(3) from the corresponding cyclohexane-1,4-diones and the electrical conductivities of their charge transfer complexes with tetrathiafulvalene are described.

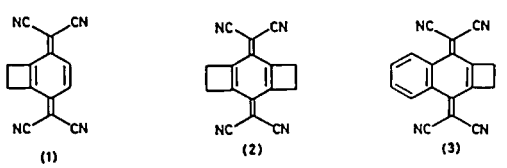

VI-K-2 The Synthesis of 2,7-Bis(dimethylamino)pyrene and -tetrahydropyrene and the Electrical Conductivities of Their Complexes

Naomi UEDA,* Bunji NATSUME,* Kazumi YANAGIUCHI,* Yoshiteru SAKATA,* Toshiaki

ENOKI, Gunzi SAITO, Hiroo INOKUCHI, and Soichi MISUMI* *(*Osaka Univ.)*

[*Bull. Chem. Soc. Jpn,* **56**, 775 (1983)]

New π-donors containing a pyrene or a tetraphydropyrene ring shown in Figure 1, were synthesized by means of a unique transannular reaction of the corresponding [2,2]metacyclophane derivatives. The charge-transfer complexes of these donors with a series of TCNQ derivatives different in electron affinity were prepared and their electrical conductivities on single crystals were measured. The highest conductivity ($0.36\Omega^{-1}cm^{-1}$) was that of the tetraphydropyrene derivative-TCNQ complex. It was reconfirmed that the partial charge-transfer from a donor to an acceptor is very important for high conductivity.

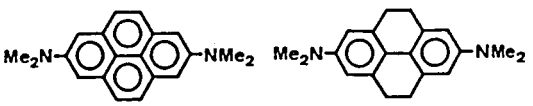

1 2

EQUIPMENT DEVELOPMENT CENTER

VI—L Development of Optical Apparatus

VI-L-1 Design and Construction of a Vacuum-UV Spectrophotometer

Kusuo SAKAI, Toshio HORIGOME, Kazuo HAYAKAWA, Masaaki NAGATA, Norio OKADA, Mitsukazu SUZUI, Hisashi YOSHIDA, Nobuo MIZUTANI, Shinji KATO and Tadaoki MITANI

The staff of the Equipment Development Center has been constructing a vacuum-uv spectrophotometer to be connected to the UVSOR beam line for common use. An outline of the spectrophotometer is shown in Figure 1. The ray trace calculations were performed through all optical elements on the

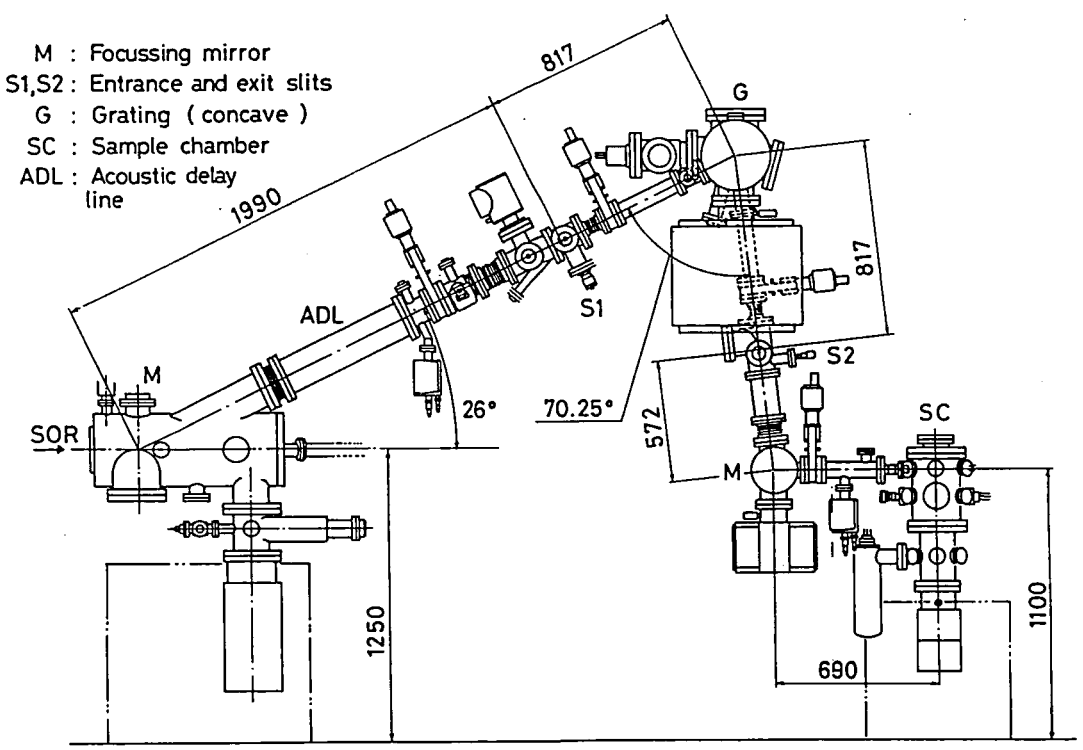

Figure 1. Schematic diagram of the vacuum-uv spectrophotometer.

line, including a 1m Seya-Namioka monochromator and toroidal focussing mirrors mounted in source and sample housings. In order to achieve maximum throughput and high resolution, we employed a new mechanical design in the monochromator; three concave gratings can be interchanged by precise linear motion in an ultrahigh vacuum. The choice of gratings and all scanning motions are controlled by a microcomputer, matching to wavelength and resolution required. This system is expected to provide a high intensity of 10^{12} photon/sec with a resolution of 3A or a high resolution of 0.2A with a 10^{10} photon/sec in a wide spectral range of 35–250 nm. A beam size on the sample is less than 1 mm^2 with a beam aperture of 26 mrad.

VI-L-2 Pressure Apparatus for Optical Measurements at Low Temperature

Tadaoki MITANI, Yoshio KANEKO *(Univ. of Tokyo)* **and Norio OKADA**

A clamp type pressure apparatus for optical measurements has been constructed. A specific mark of the apparatus lies in a design for a pressure measurement of reflectivity, which has not been done before, and use as a precise, reliable, routine instrument operating at low temperatures. An optical cell with three sapphire windows is mounted in a liquid He cryostat. Six electrodes inserted into the cell can be used for electroreflectance, conductivity and photoconductivity measurements. An accurate pressure in the cell is determined by a change of resistivity of manganese wire, which is caliblated by the ruby fluorescence pressure-measurement method. This cell is capable of generating hydrostatic pressure up to 25 kbar at 4.2K.

The first application of this apparatus was successfully made to study of the neutral-ionic phase transition observed in TTF-p-chloranil single crystals (see Special Research Project (1)). In this application, the second differential analysis of the reflectivity spectra was found to be effective to improve an experimental accuracy in an observation of spectral changes under a pressure.

VI-L-3 Electroreflectance Spectrometer

Tadaoki MITANI, Yoshiki WADA *(Univ. of Tokyo),* **and Kazuo HAYAKAWA**

We have constructed an electroreflectance spectrometer available in a wavelength region from infrared to vacuum-uv. Modulation RF (2 kHz) and DC electric fields of about 5 x 10^4 v/cm are applied to materials in the asymmetric coplanar electrode configulation. Since the electric fields are extremely high, the apparatus is usually operated at a low temperature (2 or 77K). A variation of intensity of incident light is compensated by the DC output constant method using an integrated programable high-voltage supplier and an output ($\Delta R/R$) is further averaged by using a microcomputer-based data-aquisition system. The maximum sensitivity of modulation signals is better than 10^{-5}.

An advantage of the electric-field modulation spectroscopy is to reveal fine structures out of a broad spectrum by using polarized light parallel or perpendicular to an applied field. Such a polarization-dependent spectrum provides detailed information of anisotropic electronic structures. In an application of electroreflectance to elongated cis- and trans-$(CH)_x$ polymers, it is at first confirmed that the Wannier exciton states delocalized along a polymer chain exist in the both polymers. The field-dependence of the spectra indicates that the modulation mechanism is not due to the Franz-Keldysh effect but due to the mixing effect within the isolated exciton transitions.

VI—M Experimental Confirmation of the Spin-Orbit Coupling-Assisted d-d Transition in Transition Metal Complex Ions

Yoshihiro TAKAGI

Optically induced spin orientation (OISO) has been observed in various complex ions of 3d group elements.[1] Due to Zeeman-selective absorption of the circularly polarized radiation from a pulsed laser, transient magnetization in the groud state was created at room temperature. The optical transitions used for the creation of the OISO are spin-allowed (except for Mn^{2+} and Fe^{3+}) electric dipole d-

d transitions. The creation of the OISO suggests that the spin-orbit coupling contributes to the transition moment. This contribution has never so far been confirmed experimentally for the case of the spin-allowed transition. Relative transition probabilities between various Zeeman levels of the ground and excited states were calculated using the formula given by KAMIMURA et al[2] assuming that the odd-parity component in the spin-orbit coupling of the type A_{1u}, E_u, T_{1u}, or T_{2u} (irreducible representation) is responsible for the electric dipole-allowed transition. From the dependence of the signal intensity and polarity on different materials, predominant component of the spin-orbit coupling was identified for some cases.

References

1) Y. Takagi, Laser Spectroscopy VI (Proceedings of Sixth Int. Conf. of Laser Spectroscopy, 1983), in press.
2) H. Kamimura, S. Sugano, and Y. Tanabe, "Ligand Field Theory and its Applications" (Shokabo, Tokyo 1972).

VI—N Picosecond High-Power Continuously Tunable Laser Ranging between 214 nm and 4.4 μm

Yoshihiro TAKAGI, Minoru SUMITANI, Nobuaki NAKASHIMA, Desmond O'CONNOR, and Keitaro YOSHIHARA

Tunability range of 227–244 nm in the picosecond laser system previously reported[1] has been extended to 214–460 nm by using different combinations of mixing sources. One of the mixing lights is the picosecond tunable radiation of 850–1450 nm from a single-pass optical parametric generator which is pumped by the second harmonic of the mode-locked Nd:YAG laser. The other mixing beam is the second (532 nm), third (355 nm), or fourth (266 nm) harmonic of the same laser or stimulated Raman radiation of high pressure hydrogen or nitrogen gas pumped by these harmonics. Wavelength dependence of the output energy is shown in Figure 1. The ouptut energy exceeded 0.1 mJ in almost entire tuning range. The spectral bandwidth of about 10 cm^{-1} is determined by that of the optical parametric radiation. The spectral range of 230–250 nm is especially important in our laboratory as a picosecond tunable light source for studying so called "channel three" mechanism in benzene molecule.[2,3] Combining the spectal region of the longer wavelength previously developed,[4] the available tunability of the system is now from 214 nm in the UV to 4.4 μm in the IR without interruption.

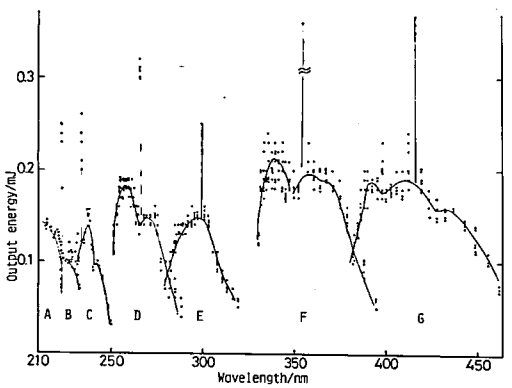

Figure 1. Wavelength dependence of the output energy based on optical frequency mixings. Combinations are: A: OPR and FH, B: OPR and FH-pumped N_2 Raman, C: OPR and FH-pumped H_2 Raman, D: OPR and TH, E: OPR and TH-pumped H_2 Raman, F: OPR and SH, and G: OPR and SH-pumped H_2 Raman (OPR; optical parametric radiation, FH; fourth harmonic, TH; third harmonic, SH; second harmonic)

References

1) Y. Takagi, M. Sumitani, N. Nakashima, D. O'Connor, and K. Yoshihara, *App. Phys. Lett.*, **42**, 489 (1983).
2) Y. Takagi, M. Sumitani, N. Nakashima, D. O'Connor, and K. Yoshihara, *J. Chem. Phys.*, **77**, 6337 (1982).
3) M. Sumitani, D. O'Connor, Y. Takagi, N. Nakashima, K. Kamogawa, Y. Udagawa, and K. Yoshihara, *Chem. Phys. Lett.*, **97**, 508 (1983).
4) Y. Takagi, M. Sumitani, N. Nakashima, and K. Yoshihara, *Rev. Laser Engineering* (in Japanese), **10**, 57 (1982).

ULTRAVIOLET SYNCHROTRON ORBITAL RADIATION FACILITY

VI—O Construction of UVSOR (Ultraviolet Synchrotron Orbital Radiation) Light Source

Makoto WATANABE, Toshio KASUGA, Akira UCHIDA, Osamu MATSUDO, Masami HASUMOTO, Hiroto YONEHARA, Toshio KINOSHITA, Kusuo SAKAI, Hiromichi YAMAMOTO,* Kiyoshi TAKAMI, Takeshi KATAYAMA,*** Katsuhide YOSHIDA,*** and Motohiro KIHARA,****** *(*Fukui Univ. and IMS, **Kyoto Univ., ***Univ. of Tokyo, ****Nat. Lab. High Energy Phys. and IMS)*

UVSOR light source is a 600 MeV (max. 750 MeV) electron storage ring dedicated to synchrotron radiation research, the injector of which is a 600 MeV synchrotron with a 15 MeV linac. In 1981, its construction was started. At present, the synchrotron is under test operation. The current is 10 mA. The injection into the storage ring will be started in this October. The present status of the UVSOR light source is given in "Ultraviolet Synchrotron Orbital Radiation Facility" in this issue.

RESEARCH FACILITIES

For the sake of brevity of the present issue are included only the newly installed facilities and the activities since September 1982. Concerning the activities and facilities before September 1982, please refer to IMS Annual Review (1982).

Computer Center

The main facilities of the Computer Center are two HITAC M-200H computers, which have a processing capacity of over 10 million instructions per second. They have 16 and 12 mega byte main memory and 13 giga byte disk memory. The computers are used not only by the research staff at IMS but also by the staff at nearby Nagional Institutes as well as by scientists outside the Institutes in the related fields. As of March 1983, the number of project groups was 211 consisting of 522 users. In the twelve month period ending March 1983, 239771 jobs were processed with 8205 hours of the CPU time.

A porogram library for molecular science has been established under a unique library management system, with which users can search on their TSS terminal whereabouts and guides of wanted programs. Until March 1983, 96 programs have been registered on the disk memory and are being used frequentry. NUMPAC (Nagoya University Mathematical Package, including 603 programs) has newly been registered. All of the QCPE programs has been obtained and will be so on the continued basis. The center is in service of four data bases, QCLDB (Quantum Chemistry Literature Data Base), IRDC (Infra-Red spectral Data Base), CHEMICS (Automated Organic Chemical Structure Elucidation System) and CMQCA (Carnegie-Mellon Quantum Chemistry Archive).

Chemical Materials Center

In July, 1982, Dr. Akira Miyashita was promoted to associate professor of the Department of Applied Chemistry, Saitama Univ. Mr. Kazushi Mashima moved to this Center from Osaka University in October, 1982, to fill the position. He is working on the subjects of synthesis and reactions of new metallacycle compounds and asymmetric synthesis catalyzed by new chiral transition metal complexes.

Instrument Center

For the efficient use of instruments, the Center is equipped with various types of instruments for general use.[1] Two instruments have been newly installed in 1983.

1) 400-MHz FT NMR Spectrometer (JEOL GX-400)

This is a multinuclear FT NMR spectrometer equipped with a super-conductivity magnet of 9.4 Tesla. The whole system is controlled with a disk-based computer of 32-bit precision. A wide variety of software is available for data processing.

2) Nanosecond Time-Resolved Spectrofluorimeter

In a combination with the pulsed dye laser as an excitation source, the system can be used for measuring decay curves and time-resolved spectra of fluorescence and phosphorescence with 2–50 ns/channel time resolution.

Reference
1) *List of Instruments*, No.4, IMS Instrument Center (1983).

Low Temperature Center

Two manuals have been published for users to facilitate low temperature experiments. The one concerns experimental techniques at liquid helium temperature and the cryostats developed in this institute are introduced. The other has to do with liquid nitrogen, where the instructions are described for beginners of low temperature experiments.

Equipment Development Center

A number of research instruments have been designed and constructed by making use of the mechanical, electric and glass-blowing technologies available at this Facility. Representative instruments developed during this fiscal year of 1982 are listed below.

1) Molecular Beam Chemistry Apparatus (MBC-I) (see Research Activities IV-M-2)
2) Cryostat of Adiabatic Calorimeter
3) Electron Beam Monitor of the UVSOR storage ring
4) Improved Acoustic Delay Line
5) Microcomputer-controlled CAMAC System
6) Developed Interfaces of a 16 bits microcomputer
7) Spherical Glass Collector for the photoelectron measurements
8) Various Kinds of optical cell

Ultraviolet Synchrotron Orbital Radiation Facility

The injector synchrotron has been completed in March 1983. Figire 1 gives its picture. The pre-accelerator linac supplies 15 MeV electrons with peak current of 40 mA to the synchrotron. The pulse width is 1.5 μs and the repetition rate is 1–3 Hz. The synchrotron accelerates 15 MeV electrons up to 600 MeV. The current of 10 mA was already achieved at the end of August.

The light source, a 600 MeV (max. 750 MeV) electron storage ring, is under construction. The building accomodating the storage ring has been completed in March of this year. Magnets were precisely aligned in August. An RF cavity and vacuum torus-type tube were installed in September. Test injection of the electrons into the storage ring will be made in October. Figure 2 illustrates the arranged picture of the storage ring.

Manufacturing nine synchrotron radiation outlets, each of which consists of a water cooled shutter, a slow closing valve and a fast closing valve, will be finished at the end of October. At the beginning of 1984, following monochromators will be connected to the synchrotron radiation outlets; three 1m Seya-Namioka, two plane-grating, one 3m normal incidence, two 2.2m grazing incidence and one double crystal monochromators.

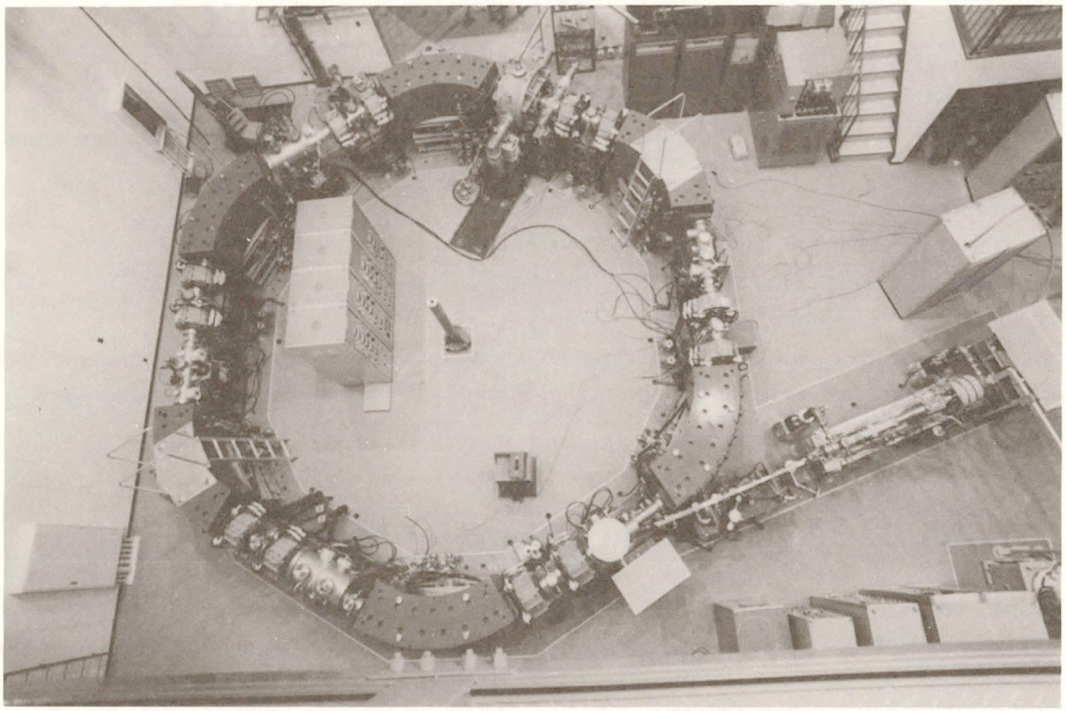

Figure 1. The injector synchrotron for UVSOR storage ring.

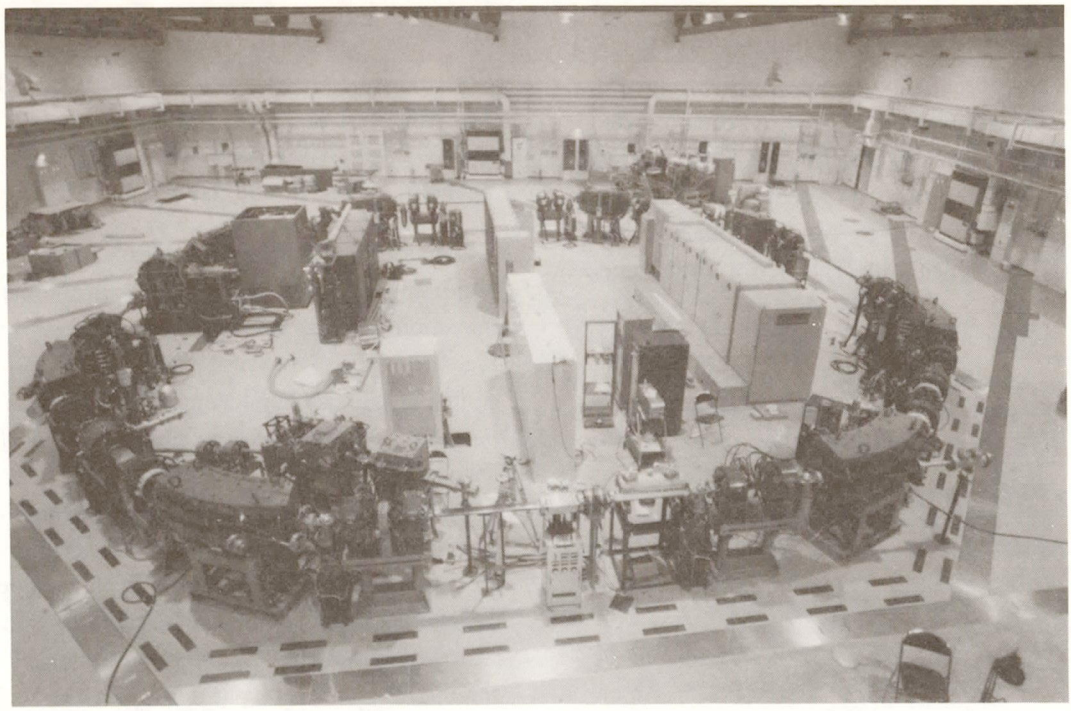

Figure 2. UVSOR storage ring.

SPECIAL RESEARCH PROJECT

IMS has special research projects supported by national funds. Two projects presently in progress under the second five year plan (1980–1985) are:

(1) The development and control of molecular functions,

(2) Energy transfer and energy conversion through molecular processes.

The third special research project started in the 1982 fiscal year is:

(3) Molecular science of primordial chemical evolution.

These projects are being carried out with close collaboration between research divisions and facilities. Collaborators from outside also make important contributions. Research fellows join these projects. In this report, the results in 1982 are reviewed.

(1) The Development and Control of Molecular Functions

Construction of a Laboratory EXAFS Spectrometer for Catalyst Study

Kazuyuki TOHJI and Yasuo UDAGAWA

[*Rev. Sci. Instum.*, in press]

A convenient and reliable in-laboratory EXAFS spectrometer which consists of a Johansson cut bent dispersing crystal and a fast SSD has been constructed. The use of a bent crystal has made it possible to collect x-ray photons intense enough for EXAFS measurement, and the SSD can completely discriminate higher overtones which can seriously deteriorate the spectra if present. Fast electronics modules are employed to keep up with high x-ray intensity. Combined with a 12 kW rotating anode x-ray generator, the spectrometer can provide an EXAFS spectrum of enough quality for practical analysis typically in about 2 hours. By selecting a higher order reflection such as Ge(440), a resolving power as high as 2 ev can be achieved.

As an example, an EXAFS spectrum of CoO crystal which is a model compound for Co/TiO_2 catalyst is shown in Figure 1.

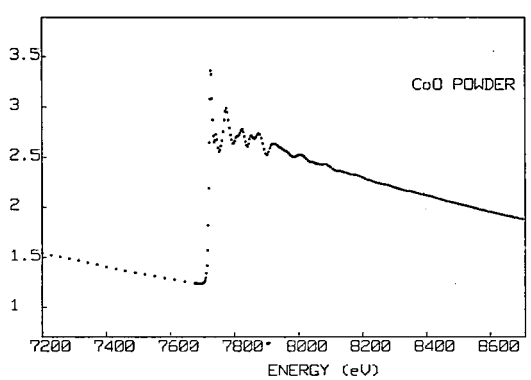

Figure 1. EXAFS spectrum of CoO powder at R. T. LiF(220) reflection was used with slit width of 200μ.

Control of Molecular Function in Charge-Transfer Solids

Tadaoki MITANI and Gunzi SAITO

Some charge-transfer complexes with acceptor-donor mixed stacks undergo a neutral-ionic phase transition as a function of temperature and pressure. The physical properties of these complexes drastically change near the transition points, suggesting a possibility of a feature development of molecular design in this field. From the optical, X-ray and ESR measurements on the TTF-p-chloranil single crystals, it was found that the transition induced by lowering temperature causes the dynamically dimerized distortions in a lattice system. The discontinuous change of the conductivity and the spin density at the transition temperature can be interpreted in terms of a soliton kink of dimerizations. In order to get an insight into such an electron-phonon coupling, we have been investigating the hydrostatic pressure effects on the optical and conductive properties of

these crystals up to 20 kbar. Preliminary results surports the dimerization model mentioned above. The pressure cell used was designed to be mounted in the liquid ^{3}He cryostat for operation temperature down to 0.3K. The low temperature apparatus is being constructed, which allows us to expand an object of our investigations to different kinds of charge-transfer system from the TTF-p-quinone system.

High-Spin Hydrocarbons as a Model for Organic Ferromagnets

Hiizu IWAMURA,* Tadashi SUGAWARA and Akira IZUOKA

A series of high-spin hydrocarbons have been designed by taking advantage of triplet diphenylcarbene as a building block and connecting the units in non-Kekule fashion. Linear, cyclic and network-shaped aromatic polyketones were synthesized and converted via the polyhydrazones to the corresponding poly(diazo) compounds. The polycarbenes matrix-isolated or oriented in single crystals of benzophenone were obtained by irradiation of the poly(diazo) compounds at cryogenic temperature. The nonet species of the linear tetracarbene was confirmed by ESR spectroscopy to be the ground electronic state (V-A-4). Polycarbenes expected to have higher spin multiplicity were also generated.

Kinetic studies and product analyses have revealed an interesting mode of the release of nitrogen molecules from the poly(diazo) compounds in the photo excited state. While only one nitrogen molecule was released in fluid solutions at ambient temperature, all the C-N bonds were cleaved by one photon in matrices and crystals at cryogenic temperature.

A study of magnetic properties of these high spin hydrocarbons is in progress.

Dynamical Molecular Structure and Control of Reactive Molecules

Eizi HIROTA,* Shuji SAITO,* Chikashi YAMADA, Yasuki ENDO, Kentarou KAWAGUCHI, and Tetsuo SUZUKI

In order to facilitate the observation of singlet-triplet transitions in simple carbenes (e.g. HCF and HCCl) and HNO, spectroscopic techniques in the near-infrared and infrared regions have been developed and improved: (1) new near-infrared diode lasers were added, (2) the dye laser (CR 599-21) has been extended in wave number region down to 14 700 cm^{-1} by introducing DCM dye (II-B-1), and (3) an infrared diode laser with an external cavity was designated to cover a wide wavelength region without mode-hopping. The lifetime of the diode will then be significantly increased, because temperature changes which have otherwise been necessary to tune the diode, but often caused deterioration or damage to the diode, can be minimized.

Preparation of Functionally Responsible Materials with Heat-treatment Method

Hiroo INOKUCHI and Naoki SATO

A new type of carbon filaments has been grown from graphitic material in argon plasma. (S. Tamura, ISSP, University of Tokyo) The filaments heat-treated at high temperature were found to consist of the concentric stacking of graphitic layer planes, all the individual c-axes being perpendicular to the filament axis. For more well-controlled heat-treatment, a Xe-lamp infra-red radiation focused type furnace (>3000°C) has been constructed.

Synthesis of Highly Functional Transition Metal Complexes and Their Use in Organic Reactions

Hidemasa TAKAYA,* Kazushi MASHIMA, and Masashi YAMAKAWA

We have been working on the synthesis of new chiral transition metal catalysts useful for asymmetric organic reactions. We prepared 2,2′-bis(diphenylphosphino)-1,1′-binaphthyl, an atropisomeric chiral diphosphine. This new chiral ligand has been shown to be quite effective for Rh(I)-catalyzed asymmetric hydrogenations of α-(acylamino)acrylic acids and asymmetric 1,3-hydrogen shift of allylamines into enamines. An

effort has been made to develop new chiral diphosphine ligands effective for asymmetric catalytic reactions other than olefin hydrogenations.

Elucidations of the mechanisms of transition metal catalyzed organic reactions are also the subjects of our major interest. We have studies the Pt(II)-catalyzed isomerization of bicyclo[1.1.0] butanes and showed, for the first time, that the reaction proceeds in a stepwise manner involving 2-platinabicyclo[1.1.1]pentanes and allylcarben-platinum complexes. We have also synthesized and characterized 1-[bis(cyclopentadienyl)zircona]-2-oxacyclopentane and its derivatives. Parts of these results are presented in the Section VI–B, C and D.

Syntheses and Solid State Properties of Superconductive Fine Particles with Chemically Modified Surface

Keisaku KIMURA,* Shunji BANDOW, Toshiaki ENOKI, and Gunzi SAITO

The superconductive transition temperature of fine particles is enhanced when the surface of the particles is oxidized or modified by other chemical substances. In 1964, Little suggested that the interaction between conduction electrons and molecules with large polarizable moiety caused high T_c super conduction and in 1973, Bardeen proposed another high T_c model at semiconductor surface. Therefore, the ultra fine particles with chemically modified surface might be a good test probe to check the above mentioned models.

We have developed three new preparation methods of ultra fine particles in organic solution. (1) matrix isolation method. (2) gas flow-cold trap method. (3) gas flow-solution trap method. With the use of these methods, several kinds of chemically modified metal fine particles were obtained; Lead fine particles with porphyrin compounds and with TTF derivatives. The electronic properties of these materials are now under investigation.

One-Dimensional M(II)—M(IV) Mixed Valence Complexes of Palladium and Nickel

Tasuku ITO,* Masahiro YAMASHITA, Koshiro TORIUMI, and Haruko ITO *(Aichi Kyoiku Univ.)*

The chemical consequences of ligand macro-cyclizations in tetraazacycloalkane complexes and their applications are the subject of our continued interest. Previously we studied the stabilization of high-oxidation states of metal ions by taking advantage of the chemical characteristics arising from their cyclic nature. Our studies along this line have now been extended to the chemistry of one-dimensional M(II)–M(IV) mixed valence complexes. So far, halogen-bridged M(II)–M(IV) mixed valence complexes of Pt and Pd have been studied widely from a variety of viewpoints. In this study, we are aiming at syntheses of new Pd and Ni complexes of this type. On going from Pt to Ni, it is expected that the electronic interaciton between M(II) and M(IV) through a bridged halogen ion increases and thereby the electric conductivity would be enhanced, though it becomes more difficult to synthesize the compounds because of the instability of the M(IV) state. A part of our results are presented in V–F.

(2) Energy Transfer and Energy Conversion through Molecular Processes

Intramolecular Energy Transfer in Vibrationally Excited Molecular Clusters and Molecular Beam Studies of Reaction Dynamics of Chemically Reactive Atoms and Free Radicals

Kosuke SHOBATAKE,* Kiyohiko TABAYASHI, and Shigeru OHSHIMA

This project consists of two seemingly different subjects but has a common approach to study the dynamics of atomic and molecular interactions in that the energy transfer processes and reaction dynamics are strongly dependent upon the potential surface(s) on which the system moves and the initial conditions of motion for the interacting system.

An arc-heated nozzle beam source developed for the last one year and a half has been applied to the study of reactions involving active nitrogen atoms $N^*(^2D,^2P)$. So far the chemiluminescent reactions $N^*(^2D,^2)$ + HI, HBr, H_2S producing nascent $NH(A^3\pi)$ molecules have been studied (see IV-M-1). A crossed molecular beams apparatus with a rotatable mass spectrometer detector has been completed (see IV-M-2). To begin with, we have measured the differential cross sections for the non-reactive scattering of NO from Ar to determine accurate intermolecular potentials (see IV-L-1). This machine (Model MBC-I) is to be used to study predissociation dynamics of van der Waals molecules as well as to carry out reactive scattering experiments involving active nitrogen atoms.

Photocatalytic Effect of Semiconductor and Dyes: Its Application to Hydrogen Production and Organic Reactions

Kazuhiro HASHIMOTO, Tomoji KAWAI and Tadayoshi SAKATA*

Efficient photocatalytic hydrogen production systems without any electron relay was constructed by using halogenated fluorescein derivatives in the presence of a reduction catalyst and various reducting agents. They are stable and efficient in the pH region. The quantum yield of hydrogen production for erythrosine as a photocatalyst are 12% and 0.15% with triethanol amine(TEOA) and ethanol, respectively. The mechanism of hydrogen production was investigated by the transient absorption spectrum and the time behavior of the intermediate species.

The photocatalytic oxidation of aliphatic hydrocarbons, benzene and organic acids were investigated using powdered semiconductors. The possibility of direct oxidation of benzene and the new reaction paths were proposed. In the case of organic acids, products, in which the number of carbon is increased compared with that in the starting material, were produced. For instance, propionic acid and succinic acid were accumulated in the aqueous medium for the photocatalytic reaction of acetic acid. Formation of succinic acid from fumaric acid was also succeeded in by the hydrogen addition to the unsaturated bond with powdered semiconductor photocatalyst.

The catalytic role of RuO_2 on n-type semiconductor under irradiation and the transient response of a semiconductor-electrolyte circuit were also investigated (see III–D).

Vibrationally Highly Excited ("Hot") Molecule — Its Photochemical Formation, Energy Transfer, and Reaction

Keitaro YOSHIHARA, Nobuaki NAKASHIMA, Minoru SUMITANI, Nobuo SHIMO, and Noriaki IKEDA

Vibrationally highly excited ("hot") molecules and radicals are found to be efficiently formed in benzene derivatives and alkenes. For example, excitation of gaseous benzene itno S_2 state with an ArF excimer laser (193 nm) leads to a "hot" state ($S_0^{\dagger}$) with internal energy of 624 kJ/mol and temperature of 3390K. The quantm yield of formation was close to unity. The high internal energy is relaxed by collision. This process was well approximated by an energy-dependent energy transfer model. Excitation of benzyl halides leads to formation of "hot" benzyl radicals and alkenes to "hot" allyl-type radicals.

Photochemical formation of "hot" molecules and radicals has the following characteristics, 1) non-Boltzmann excitation, 2) narrow temperature distribution, 3) extremely rapid heating (less than 10 picosecond), and 4) extremely high temperature. The details of the results are described in III–A.

Effects of External Magnetic Field on Photodissociation of NaK and Conservation of Angular Momentum

Hajime KATÔ *(Kobe Univ. and IMS),* **Masaaki BABA, and Ichiro HANAZAKI**

Beside molecular fluorescence, the fluorescence of the D lines of Na and K atoms were observed when NaK molecule was excited by 4765 Å line. The absolute and the relative intensities of the atomic D_1 and D_2 lines have been found to be different between the Na and K atoms. The intensities of the emission from the dissociated $Na(3^2P_{3/2})$, $Na(3^2P_{1/2})$,

$K(4^2P_{3/2})$, and $K(4^2P_{1/2})$ are found to change remarkably when a magnetic field is applied, and each line changed individually depending on the field strength. The correlation of molecular electronic state with the separated molecular state has been established through the conservation of angular momentum. The most likely pathway as the source of the sodium D_1 line has been identified as a direct photodissociation.

$$NaK(X^1\Sigma^+) + h\nu \rightarrow NaK(D^1\Pi\text{:continuum}) \rightarrow Na(3^2P_{1/2}) + K(4^2S_{1/2})$$

The intensity of the sodium D_2 line increased remarkably as the external magnetic field was increased, and the effects of magnetic field on the collisional breakup or on the atom-atom interchange are estimated to be most important.

Multiphoton Ionization Photoelecton Spectroscopy and Its Application to Photochemistry of Molecular Clusters

Katsumi KIMURA,* Yohji ACHIBA, and Kenji SATO

In order to study excited-state photoelectron spectroscopy of molecules and molecular cluster, we have been developing a technique of resonant multiphoton ionizatio in this laboratory since 1979. Although the first stage of this project is to establish the technique of such excited-state photoelectron spectroscopy, our final goal is to apply this technique to photochemistry of photophysics of molecular clusters. During the last one year, we have further extended our work to the following subjects. (1) The mechanism of autoionization of NO molecule in the resonant multiphoton ionization process through the excited B state at $v = 9$. (2) Vibrational relaxation of the E_{1u} state of benzene. (3) Photodissociaton of iron pentacarbonyl and ferrocene. (4) Vibrationally resolved photoelectron spectra of Rydberg excited state of methyliodide. (5) Vibrational relaxation of the S_1 and S_2 excited states of naphthalene. (6) The van der Waals complex formed between Ar and NO.

(3) Molecular Science of Primordial Chemical Evolution

Research Report

Chemical Evolution on Icy Solids Initiated by UV Irradiation: Formation of Precursor Molecules for Prebiotic Syntheses

Nobuyuki NISHI,* Hisanori SHINOHARA and Tohru OKUYAMA

Intersteller grains are thought to be cold enough to accreate mantles of ices composed of intersteller molecules. Comet is one example of icy objects including intersteller molecules in the mantle. Input of UV photon energy to molecular solids may induce chemical reactions initiated by electronical excitation of some moleucles. Here we report preliminary results of the photochemical reactions found in (1) $NH_3 + CH_3CN$(1:4) and pure C_2H_2 solid systems at 77 ~ 120K. Figure 1 illustrated the low temperature reaction cell used in the preliminary experiment. The cell was evacuated by a diffusion pump equipped with a molecular sieves oil trap. Ultra-low pressure mercury lamp (mostly 185 nm and 248 nm) was used as a light source.

In contrast with gas phase reactions internal excess energy in an excited molecule or in a reaction intermediate in the solid can be dissipated into phonon field. So, formation of bigger molecules occurs efficiently in solid state. Identification of the products were done by using GC-MS and HPLC. The products detected in the system (1) were acetoamidine, diaminomaleonitrile (DAMN), five-membered heterocyclic compounds such as 4-aminoimidazole, 5-carbonitrile(AICN), and other hetrocyclic compounds. DAMN and AICN are known as precursor molecules in the prebiotic synthesis of purines, amino acids and peptides. Pure solid acetylene gave diacetylene, vinylacetylene, $C_2H_3(C{\equiv}C)_3H$, $H(C{\equiv}C)_4H$, and some other polyacetylene compounds as well as saturated hydrocarbons. Hydrogen disproportionations occured quite drastically in this solid.

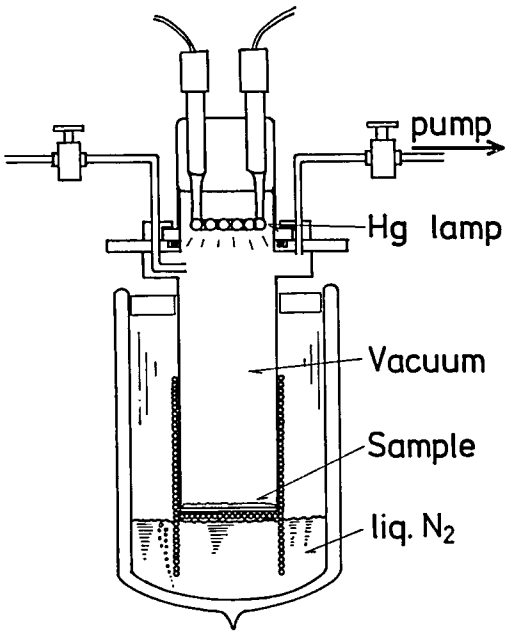

Figure 1. Vacuum photolysis cell used for the study of low temperature solid reactions.

Symposium Report
"Formation and Evolution of Intersteller Molecules"
(January 28, 29, 1983)

Organizer: I. HANAZAKI, I. KOYANO, S. SAITO, and N. NISHI

In the time of the first year at this project, a symposium was organized for the purpose of reviewing the present states and possible future developments of the study on "Formation and Evolution of Intersteller Molecules." speakers are specialists in the fields of astronomy, astrophiscs, geophysics, geochemistry, physical chemistry, organic chemistry, and biology. Quite hot results using the 45m radio telescope at the Nobeyama Radio Observatory were reported by Prof. Kaifu. We saw great advances in getting microwave emission spectra covering wide ranges around 90 GHz and 40 GHz where many molecular lines were observed. Prof. Nakano discussed the formation process of stars from intersteller molecular clouds. The present state of infrared astronomy was reported by Prof. Okuda. In the second session, Prof. Tanaka and Prof. Ogawa introduced the studies of atomospheric molecular processes. Prof. Masuda discussed the formation processes of meteorites and the origin of the anomalies of Cs and Ba contents. Prof. Harada reported high efficiency synthesis of aminoacids by argon ion plasma. Prof. Shimizu presented his own theory of the formatin of proteins and nucleic acids in space and also advanced a unique model on the genesis of genetic code. Various topics on free radical reactions, ion-molecule reaction, formation of carbonations compounds from high energy radicals, formation of cometary ices, and chemical evolution in primitive ocean were reported.

As a separate program of this symposium, Prof. C. Ponnamperuma (University of Maryland) gave a special lecture entitled "Cosmochemistry and the origin of life."

OKAZAKI CONFERENCES

"Okazaki Conferences" are principal symposia at IMS, which are held on the subjects related to the "Special Research Projects". They are held usually twice a year, with a moderate number of participants around 50, including several invited foreign speakers. The formal language for the conference is English. Outlines of the fifteenth and sixteenth conferences are as follows:

The Fifteenth Okazaki Conference

Spectroscopy and Dynamics of Molecules and Clusters in Molecular Beams

(November 15—17, 1982)

Organizers: M. Ito *(Tohoku Univ.),* **K. Kaya** *(Keio Univ.),* **T. Kondow** *(Univ. of Tokyo),* **K. Kimura** *(IMS),* **I. Hanazaki** *(IMS)*
Invited Speakers: J. Jortner *(Tel-Aviv Univ.),* **R.N. Zare** *(Stanford Univ.),* **J.P. Simons** *(Univ. of Nottingham),* **R.E. Smalley** *(Rice Univ.)*

The conference was held for the purpose of discussing recent progress in spectroscopical and dynamical studies with molecular beams, in particular, with the supersonic nozzle beam technique. It was divided into three main sessions; (1) High resolution spectroscopy of large molecules using the super-cooling of internal degrees of freedom with the supersonic jet technique. (2) Formation and nature of clusters in a super-cooled molecular beam. (3) Dynamical processes under the collision-free condition.

In session (1), Professor Jortner talked on a slit pulse beam source to measure the absorption spectra of super-cooled large molecules as well as

the fluorescence spectra. In (2), Professor Smalley discussed the formation of metal cluster beam by the UV laser irradiation. In session (3), Professor Zare talked about the reaction of alkali earth metal beam with hydrogen halides and discussed the effects of molecular geometry, rotational quantum number, impact parameter and translational energy on the reaction cross section. Professor Simons presented a method for producing metastable atomic beam with his rotor-accelerated beam technique and discussed the reaction of the metastable atom with halogen molecules.

With about 80 attendants, the conference seems to have been successful in reviewing the recent rapid progress in the field and in clarifying a number of important points to be solved in the future.

The Sixteenth Okazaki Conference

Magnetic Field Effects upon Dynamic Behaviour of Molecules

(January 17—19, 1983)

Organizers: H. Hayashi *(Inst. Phys. Chem. Res.),* **K. Yoshihara and N. Nishi** *(IMS)*
Invited Speakers: Yu. N. Molin *(Inst. Chem. Kinet. Combus., Academy of Sci.),* **G.L. Closs** *(Univ. of Chicago),* **A. Tramer** *(Univ. Paris-Sud),* **and M. Lombardi** *(Univ. Sci. Med. Grenoble)*

Study of magnetic field effects on chemical reactions and relaxation processes has achieved a tremendous advance during the past decade. Many reactions through radical pair states have been confirmed to show magnetic field effects on the reaction yields, which in turn gave us significant information on the mechanistic studies of chemical reactions. The fluorescence from the singlet state, which has no magnetic property originally, is now known to show magnetic field effects.

The conference was started with the opening lecture by Prof. Nagakura and followed by various lectures under the following four sessions; 1) excited state dynamics of molecules in the gas phase, 2) magnetic resonance studies of chemical reactions, 3) excited state dynamics of molecules in the condensed phase, and 4) new developments in the studies of magnetic effects. In the session 1), Prof. Tramer demonstrated that the use of supersonic jets and dye lasers has great advantage for the study of the mechanism of gas phase processes. Prof. Lombardi gave a theoretical analysis to the preceding lecture. Prof. Closs and Prof. Molin showed the application of new methods (Reaction Yield Detected Magnetic Resonance, and Optical Detection of Magnetic Resonance of Ion-radical Pair, respectively). Various aspects of magnetic field effects such as quantum beats of fluorescence, photochemical reactions, exciton-exciton annihilations, CIDNP, combustion, bimolecular reactions, isotope separation, and catalytic reaction have been discussed. More than ninety scientists attended to this meeting, which would reveal the activities in this field.

JOINT STUDIES PROGRAMS

As one of the important functions of an inter-university research institution, IMS undertakes joint studies programs for which funds are available to cover research expenses as well as travel and living expenses of individuals. The proposals from domestic scientists are reviewed and controlled by the inter-university committee. The programs are carried out under one of four categories:

1) Joint Studies on special projects (a special project of significant relevance to the advancement of molecular science can be carried out by a team of several groups of scientists).
2) Research Symposia (on timely topics in collaboration with both outside and IMS scientists).
3) Cooperative Research (carried out in collaboration with both outside and IMS scientists).
4) Use of Facility (the Computer Center, Instrument Center and other research facilities at IMS are open to all researchers throughout the country).

In the fiscal year 1982, numbers of joint studies programs accepted amounted to 3, 8 and 181 for categories 1) ~ 3), respectively.

1) Joint Studies

UV Photoelectron Spectroscopy of Polymers Containing Functional Groups

Coordinators: **Hiroo INOKUCHI** *(Department of Molecular Assemblies)*
Hiroshi MIKAWA *(Osaka University)*

UV photoelectron spectra were measured for 1:1 alternating copolymers, photoconductive polymers and also some basic polymers. From these experiments, the accurate threshold ionization potentials of these polymers could be obtained. Futher, from these findings, we found valuable information for understanding their photoconductivities and for designing photoreceptors for use in electrophotography.

Primary Photochemical Processes of Benzene and Related Compounds

Coordinator: **Keitaro YOSHIHARA** *(Department of Electronic Structure)*

Under present program, we intended to encourage both information exchange and actual experimental studies on the subject area. Current particular interest is intramolecular energy redistribution upon excitation of single vibronic or rovibronic levels under collision free conditions. Aza-benzenes are of interest since they fall into a typical intermediate coupling case. A few tens of picosecond from single vibronic level (SVL) fluorescence of pyridine vapor was measured at IMS in collaboration with Hokkaido group. In relation to the channel three threshold in radiationless transition of benzene, fluorescence quantum yield and decay times together with excitation and emission spectra have been measured following excitation by a picosecond tunable laser. The characteristic channel three effect was observed (see III–B). The fate of this channel was investigated by a laser flash photolysis with an excimer laser. Vibrationally highly excited state was found to be efficiently formed in benzene and fluorobenzenes (see III–1). Kinetic studies of photodissociation of halogenated benzenes were performed with flash photolysis at IMS in collaboration with TIT group.

A one-day discussion meeting was held and various activities were reviewed by the members. Dr. I. Fujimura (Tohoku Univ.) was invited as a speaker of the theoretical aspect on the present subject area.

The members of the program are H. Baba, H. Ohta, M. Fujita (Hokkaido Univ.), I. Tanaka, Y. Mori, T. Ichimura (Tokyo Ins. Tech.), K. Yoshihara, N. Nakashima, M. Sumitani, N. Shimo, N. Ikeda, D.V. O'Connor, I. Hanazaki, I. Yamazaki, and T. Murao (IMS)

Spectroscopic Study using Variable Temperature Molecular Beam Sources

Coordinator: **Katsumi KIMURA** *(Department of Molecular Assemblies)*

Since 1981, in this project we have designed and constructed several variable temperature supersonic nozzle beam sources to produce van der Waals molecules efficiently. The low temperature nozzle beam source constructed by Shobatake and Tabayashi has been used to measure differential cross-sections for the non-reactive scattering of NO and O_2 from Ar at two collision energies $\bar{E} = 1.32$ and 1.02 kcal/mole, in order to determine accurate intermolecular potentials for NO + Ar and O_2 + Ar. An arc-heated beam source constructed by Tabayashi and Shobatake has been used for the molecular beam chemiluminescence studies involving metastable active nitrogen atoms $N^*(^2D,^2P)$ in the range of collision energies $\bar{E} = 0.45 \sim 1.1$ eV (see IV-M-1).

Furthermore, two other supersonic nozzle beam sources have been constructed in this project. One is a pulsed beam source capable of controlling the temperature up to 100°C. This has been constructed by Sato, Achiba and Kimura in connection of studies of multiphoton ionization photoelectron spectroscopy (see IV-K-1 ~ 5). The other is a supersonic nozzle beam source used at liquid-nitrogen temperature, constructed by Koyano and Tanaka in connection of studies of ion-molecule reaction (see IV-H-1).

2) Research Symposia

1. Design and Development of Conceptually New Organic Compounds. A Perspective of Structural and Solid State Physical Organic Chemistry.
   (January 22nd — 23rd, 1982)
   Organizer: I. Murata (Osaka Univ.)
2. Picosecond Phenomena
   (January 11th — 13th, 1982)
   Organizer: S. Shionoya (The Institue for Solid State Physics, Univ. of Tokyo)
3. Molecular Functions where metal Ions Play Important Roles.
   (January 8th — 10th, 1982)
   Organizer: Y. Yoshikawa (Nagoya Univ.)
4. Electron Transfer and Proton Transfer in the Excited State
   (October 27th, 1981)
   Organizer: K. Yoshihara (IMS)
5. Multiple Bondings Between Group IV Atoms
   (March 14th — 15th, 1982)
   Organizer: E. Hirota (IMS)
6. Electronic Properties of One-Dimentional Insulators
   (January 27th, 1982)
   Organizer: T. Mitani (IMS)
7. Photoionization Spectroscopy of Molecules and Molecular Clusters
   (June 18th, 1982)
   Organizer: K. Kimura (IMS)
8. Photochemical Solar Energy Conversion
   (April 26th, 1982)
   Organizer: K. Yoshihara (IMS)

3) Cooperative Research

This is one of the most important programs IMS undertakes for conducting its own research of the common interest to both outside and IMS scientists by using the facilities at IMS. During the first half of the fiscal year of 1982 ending on September 30, 84 outside scientists including 10 invited collaborated with IMS scientists; and during the second half of the fiscal year, 74 outside scientists including 13 invited worked in collaboration with IMS scientists. The names and the affiliations of these collaborators are found in the Research Activities.

4) Use of Facility

The number of projects accepted for the Use of Facility Program of the Computer Center during the fiscal year of 1982 amounted to 121(319 users), and the computer time spend for these projects is 3988 hours (52% of the total annual CPU time).

Fifty five projects(140 users) were accepted for the Use of Facility Program of the Instrument Center during the fiscal year of 1982.

FOREIGN SCHOLARS

Visitors from abroad play an important role in research activities and are always welcomed at IMS. The following is the list of foreign scientists who visited IMS in the past year (Aug. 1982 – July 1983). The sign *1 indicates a visitor invited to attend an Okazaki Conference, *2 a visitor on the Invited Foreign Scholars Program, and *3 a councillor of IMS.

Dr. A.R.W. Mckellar	Herzberg Inst. of Astrophys.	(Canada)	Aug. – Oct. 1982
Dr. S.I. Choi	Univ. of North Carolina	(USA)	Aug. 1982
Prof. G. Klumpp	Univ. of Amsterdam	(Netherland)	Aug. 1982
Prof. Y.H. Kim	KAIST	(Korea)	Aug. 1982
Prof. C.S. Kim	KAIST	(Korea)	Aug. 1982
Prof. M. Makosza	Polish Academy of Science	(Poland)	Aug. – Sep. 1982
Prof. O. Johnson	Univ. of Pittsburg	(USA)	Sep. 1982 – Apr. 1983
Prof. P. Coppens	State Univ. of New York	(USA)	Sep. 1982
Prof. H. Jones	Univ. of Ulm	(W. Germany)	Sep. 1982
Prof. A.E. Underhill	Univ. of Coll. North Wales	(UK)	Sep. 1982
Prof. A. Schweig	Univ. Marburg	(W. Germany)	Sep. 1982
Dr. M. Linna	CSTP	(Finland)	Sep. 1982
Prof. L. Couture	Univ. of Paris	(France)	Sep. 1982
Dr. B. Dees	Franklin Inst.	(USA)	Oct. 1982
Prof. A. San Pietro	Univ. of Indiana	(USA)	Oct. 1982
Dr. C. Wallas	NSF	(USA)	Oct. 1982
Dr. E. Gantt	Smithonian Inst.	(USA)	Oct. 1982
Prof. A.C. Ley	Rockefeller Univ.	(USA)	Oct. 1982
Prof. D. Lundell	Univ. of California	(USA)	Oct. 1982
Dr. R. MacColl	New York State Dept. of Health	(USA)	Oct. 1982
Prof. B. Mulligan	Harvard Univ.	(USA)	Oct. 1982
Prof. R.M. Sweet	Univ. of California	(USA)	Oct. 1982
Prof. R.F. Troxler	Boston Univ.	(USA)	Oct. 1982
Prof. H. Zuber	Eidg. Tech. Hochsch. Zurich-Hoenggerberg	(Switzerland)	Oct. 1982
Prof. T.Y. Mi	Inst. of Chem., Acad. Sinica	(China)	Oct. 1982
Prof. G. Smets	Katholic Univ. Leuven	(Belgium)	Oct. 1982
Prof. F.A. Gianturco	Univ. di Roma	(Italy)	Oct. 1982
Prof. M. Kasha*[3]	Florida State Univ.	(USA)	Oct. 1982
Prof. A.J. Freeman	Northwestern Univ.	(USA)	Oct. 1982
Mr. B.M. Schmid	Univ. Stuttgart	(W. Germany)	Nov. 1982 – Jul. 1983
Dr. J.E. Butler	Naval Res. Lab.	(USA)	Nov. 1982 – Nov. 1983
Prof. S. Mrozowski	New York State Univ.	(USA)	Nov. 1982
Dr. J.P. Hobson	National Research Council	(Canada)	Nov. 1982
Prof. J.K. Thomas	Univ. of Indiana	(USA)	Nov. 1982
Prof. K.D. Sen	Univ. Hyderabad	(India)	Nov. 1982
Prof. R.E. Smalley*[1]	Rice Univ.	(USA)	Nov. 1982
Prof. J.P. Simons*[1]	Univ. Nottingham	(UK)	Nov. 1982
Prof. R.N. Zare*[1]	Stanford Univ.	(USA)	Nov. 1982
Prof. J. Jortner*[1]	Tel-Aviv Univ.	(Israel)	Nov. 1982
Dr. M. Faubel*[2]	Max-Planck Inst.	(W. Germany)	Nov. 1982 – Mar. 1983

Prof. M. Halmann	Weizmann Inst.	(Israel)	Nov. 1982
Prof. D.G. Whitten	Univ. of North Carolina	(USA)	Nov. 1982
Prof. R.S. Davidson	City Univ. of London	(UK)	Nov. 1982
Dr. D. Guérard	Univ. de Nancy	(France)	Nov. 1982
Dr. R.H. Wilson*[2]	General Electric	(USA)	Dec. 1982 – Feb. 1983
Dr. V. Rehn	Michelson Lab.	(USA)	Dec. 1982
Prof. C.K. Suzuki	Univ. of Campinas	(Brazil)	Dec. 1982
Prof. S.M. Wang	National Tsing Hua Univ.	(Taiwan)	Dec. 1982
Prof. A. Tramer*[1]	Univ. Paris-Sud	(France)	Jan. 1983
Prof. M. Lombardi*[1]	Univ. Sci. Med. Grenoble	(France)	Jan. 1983
Prof. G.L. Closs*[1]	Univ. of Chicago	(USA)	Jan. 1983
Prof. Yu. N. Molin*[1]	Inst. Chem. Kinetics Combusion	(USSR)	Jan. 1983
Dr. F. Webster	Univ. of Chicago	(USA)	Jan. 1983
Prof. C. T. Chang	National Tsing Hua Univ.	(Taiwan)	Feb. 1983
Prof. Ponnamperuma*[1]	Univ. of Maryland	(USA)	Feb. 1983
Prof. F.C. De Schryver*[2]	Katholic Univ. Leuven	(Belgium)	Feb. – Mar. 1983
Dr. R.J. Butcher	Univ. of Cambridge	(UK)	Mar. – Jun. 1983
Dr. B. Ke	Kettering Inst.	(USA)	Mar. 1983
Prof. H. Ratajczak	Univ. of Wrocław	(Poland)	Mar. 1983
Dr. R. Comès	Univ. de Paris Sud	(France)	Mar. 1983
Dr. J.T. Hougen	N.B.S.	(USA)	Apr. 1983
Prof. M.S. Jhon	KAIST	(Korea)	Apr. 1983
Prof. H. Fischer	Inst. der Univ. Zurich	(Switzerland)	Apr. 1983
Dr. E. Roduner	Inst. der Univ. Zurich	(Switzerland)	Apr. 1983
Prof. W.G. Schneider	National Research Council	(Canada)	Apr. 1983
Prof. A. Perez-Masia	Inst. Quim. Fis. "Rocasolano" Cons. Super. Invest. Cient.	(Spain)	Apr. 1983
Prof. R.H. Gleiter	Univ. Heidelberg	(W. Germany)	Apr. 1983
Prof. Govindjee	Univ. of Illinois	(USA)	Apr. 1983
Prof. G. Porter*[3]	Royal Institution	(UK)	Apr. 1983
Prof. G.E. Zaikov	Inst. of Chem. Phys.	(USSR)	Apr. 1983
Dr. J.T. Hougen	NBS	(USA)	Apr. 1983
Prof. I.G. Csizmadia	Univ. of Toronto	(Canada)	May – Jun. 1983
Prof. E.M. Voigt*[2]	Simon Fraser Univ.	(Canada)	May – Aug. 1983
Prof. O. Eisenstein	Univ. of Michigan	(USA)	May – Jun. 1983
Prof. B.F. Sonntag	Univ. of Hamburg	(W. Germany)	May 1983
Prof. R. Hoffmann	Univ. of Cornell	(USA)	May 1983
Prof. C. D. Zhao	Northeast Normal Univ.	(China)	May 1983
Prof. R.A. Poirier	Univ. of Toronto	(Canada)	May – Jun. 1983
Prof. G.Y. Jian	Acad. Sinica	(China)	May 1983
Prof. H. Lin	Acad. Sinica	(China)	May 1983
Prof. C.C. Zu	Acad. Sinica	(China)	May 1983
Prof. D.G. Liang	Acad. Sinica	(China)	May 1983
Prof. Z.C. Da	Acad. Sinica	(China)	May 1983
Prof. G.F. Huei	Acad. Sinica	(China)	May 1983
Prof. L.W. Cheng	Acad. Sinica	(China)	May 1983
Prof. R.D. McKelvey	Univ. of Wisconsin La Crosse	(USA)	May – Nov. 1983
Prof. H. Johansen	The Technical Univ. of Denmark	(Denmark)	May – Jun. 1983

Dr. A.M. Anderson	Nature Macmillan Journals Ltd.	(UK)	Jun. 1983
Prof. C-H.H. Schiel	Deutsche Forschungsgemeinshaft	(W. Germany)	Jun. 1983
Dr. N.S. Ham	CSIRO	(Australia)	Jun. 1983
Prof. G.A. Russell	Iowa State Univ.	(USA)	Jun. 1983
Prof. W.T. Borden	Univ. of Washington	(USA)	Jun. – Jul. 1983
Dr. T.A. Miller*[2]	Bell Lab.	(USA)	Jun. – Sep. 1983
Prof. A.J. Yencha	State Univ. of New York	(USA)	Jul. 1983
Prof. R.J. Donovan*[2]	Univ. of Edinburgh	(UK)	Jul. – Sep. 1983
Mr. C.T. Owens	NSF	(USA)	Jul. 1983
Dr. A. Milsap	NSF	(USA)	Jul. 1983
Prof. J.E. Fischer	Univ. of Pennsylvania	(USA)	Jul. 1983
Prof. S.C. Shim	KAIST	(Korea)	Jul. – Aug. 1983

AWARD

Prof. Eizi Hirota received the Bourke Lectureship in 1983 from the Royal Society of Chemistry, Faraday Division. Prof. Hirota gave lectures entitled "Recent Progress in High Resolution Spectroscopic Studies of Reaction Intermediates" and "Dipole Moment as a Means of Talking to Molecules", in several Universities in England.

Prof. Hirota's Scientific Achievement:

In 1976 Prof. Hirota moved to IMS from Kyushu University. Since then he has devoted himself to the construction of new laboratories to conduct microwave spectroscopy, infrared and visible laser spectroscopy, as well as to the establishment of the newly started Institute for Molecular Science itself. His main interest has been to characterize the various transient intermediates in chemical reactions by means of high resolution spectroscopy, covering as wide a wavelength region as possible.

More than 50 free radicals including HO_2, CH_2, CH_3, CH_3O, NO_3 etc. have been detected and analyzed to give indispensable information about each of the intermediates, molecular structure, electronic structure through the hyperfine interacions, and so on.

Another interest of his has been the isotopically induced dipole moment of non-polar molecules, for example CH_4, C_2H_4, CO_2 etc. These molecules have been studied by means of microwave spectroscopy, in spite of their weak absorption.

Prof. Hirota and his coworkers have thus contributed much to improving and developing spectroscopic methods for free radical studies. Prof. Hirota's contributions have motivated similar researches in other laboratories all over the world.

Drs. Yoshihiro Takagi, Minoru Sumitani, Nobuaki Nakashima, and Keitaro Yoshihara have received the Seventh Progress Award of the Laser Society of Japan in 1983 for their contribution to "Development of a High-power UV-Visible-IR Continuously Tunable Picosecond Laser System Using Optical Parametric conversion"

Drs. Takagi, Sumitani, Nakashima, and Yoshihara's Scientific Achievement

They constructed a high-power continuously Tunable picosecond laser system based on techniques of optical parametric generation and amplification, stimulated Raman scattering, and sum frequency generation. The obtained picosecond light pulse is in 10 picosecond duration 100 μJ ~ 3 mJ output power, and it covers wavelength range of 214 ~ 4,400 nm continuously. High output power was obtained by their detailed consideration of the optical characteristics of nonlinear crystals and geometrical configuration, and very high efficiencies of more than 30% are achieved at each process of wavelength conversion. Their method is more advantageous than the use of dye laser, since high power picosecond pulse can be obtained in much wider wavelength region. Among various tunable wavelength regions, UV light toward shorter wavelength region is expected to be very useful since it is difficult to achieve by other means. This laser system is now used as a powerfull tool to elucidate various problems of photophysical and photochemical primary processes in molecules.

Dr. Kenichiro Tanaka received a Mass Spectroscopy Society of Japan Award for Young Scientists in 1983 for his contribution to "Studies on state-selected ion-molecule reactions by photoionization mass spectrometry."

Dr. Tanaka's Scientific Achievement:

Dr. Tanaka, since his graduation, has actively been engaged in the study of gas-phase ion chemistry and has made several important contributions in this research field. These are divided into the following two major categories.

(i) Studies of State Selected Ion-Molecule Reactions by the TESICO Technique. He established the Threshold Electron-Secondary Ion Coincidence (TESICO) technique as a novel and versatile technique for the selection of internal states of reactant ions. This technique is unique in that it yields information on state selected reaction cross sections directly. By this technique, he investigated the vibrational-state dependence of various fundamentally and practically important reactions of diatomic molecular ions, such as H_2^+, N_2^+, O_2^+, and CO^+, spin-orbit-state dependence in the reactions of Ar^+, and vibronic-state dependence in the reactions of $O_2^+(a^4\Pi_u)$, $NO^+(a^3\Sigma^+)$, and $NO^+(b^3\Pi)$. Impact of these studies on the field of dynamics of chemical reactions is enormous.

(ii) Studies of Thermal Energy Ion-Molecule Reactions Using the Flowing Afterglow Technique. Using a flowing afterglow apparatus of York University, Dr. Tanaka extensively investigated the gas-phase proton transfer and other important S_N2 reactions of the type $X^- + CH_3Y \rightarrow CH_3X + Y^-$, where $X^- = H^-, O^-, C^-, ...$, and Y = F, Cl, and Br. In particular, he pointed out the imprtance of the spin conservation in ion-molecule reactions, showing that the neutral product CH of the proton transfer.reacion $C^- + HX \rightarrow CH + X^-$, where HX = HCl, HCN, etc., is in the $a^4\Sigma$ state rather than the $X^2\Pi$ state whenever the former state is attainable energetically.

LIST OF PUBLICATIONS

K. OHNO and K. MOROKUMA, ed., "Quantum Chemistry Literature Data Base, Supplement 1. – Bibliography of ab initio Calculations for 1981", *THEOCHEM*, **8**, 1 (1982).

M. AIDA, C. NAGATA, I. OHMINE, and K. MOROKUMA, "Ab initio Molecular Orbital Study of the Thermostability of the Extreme Thermopile t-RNA: Role of the Base Stacking", *J.Theo. Biol.*, **99**, 599 (1982).

K. ICHIKAWA, Y. HAMADA, Y. SUGAWARA, M. TSUBOI, S. KATO, and K. MOROKUMA, "Ab Initio Study on Cyanamide and Isocyanamide", *Chem. Phys.*, **72**, 301 (1982).

Y. HAMADA, N. TANAKA, Y. SUGAWARA, A.Y. HIRAKAWA, M. TSUBOI, S. KATO, and K. MOROKUMA, "Force Field in the Methylamine Molecule from Ab Initio MO Calculation", *J. Mol. Spectr.*, **96**, 313 (1982).

K. MOROKUMA, S. KATO, K. KITAURA, S. OBARA, K. OHTA, and M. HANAMURA, "Potential Energy Surfaces of Chemical Reactions", in *"New Horizons of Quantum Chemistry"*, ed. P. O. Löwdin and B. Pullman, p.221 (1983).

S. SAKAKI, K. KITAURA, K. MOROKUMA, and K. OHKUBO, "Ab Initio MO Study of Nickel(0) Complexes: Stereochemistry of $Ni(PH_3)_2L$ (L = H_2CO or $(CO)_2$) and Comparison of Coordinate Bonds of Various Ligands", *Inorg. Chem.*, **22**, 104 (1983).

N. WASHIDA, M. SUTO, S. NAGASE, U. NAGASHIMA and K. MOROKUMA, "Emission Spectra of CF_3 Radicals. IV. Excitation Spectra, Quantum Yields, and Potential Energy Surfaces of the CF_3 Fluorescences", *J. Chem. Phys.*, **78**, 1025 (1983).

S. KATO, R.L. JAFFE, A. KOMORNICKI, and K. MOROKUMA, "A Theoretical Study on the Mechanism of Electronic to Vibrational Energy Transfer in $Hg(^3P)$ + CO Collisions", *J. Chem. Phys.*, **78**, 4567 (1983).

S. KATO, K. MOROKUMA, D. FELLER, E.R. DAVIDSON, and W.T. BORDEN, "Ab Initio Study of m-Benzoquinodimethane", *J. Am. Chem. Soc.*, **105**, 1791 (1983).

Y. WAKATSUKI, O. NOMURA, K. KITAURA, K. MOROKUMA, and H. YAMAZAKI, "Cobalt Metallocycles. 11. On the Transformation of Bis(acetylene) cobalt to Cobaltacyclopentadiene", *J. Am. Chem. Soc.*, **105**, 1902 (1983).

S. SAKAKI, K. KITAURA, K. MOROKUMA, and K. OHKUBO, "Reaction Paths of CO Insertion into Pt(II)-CH_3 Bond. An MO Study", *J. Am. Chem. Soc.*, **105**, 2280 (1983).

Y. NISHIMURA, T. MIZUGUCHI, M. TSUJI, S. OBARA, and K. MOROKUMA, "Theoretical Studies on Low-lying Electronic States of the CCl^+, $SiCl^+$, and $GeCl^+$ Ions", *J. Chem. Phys.*, **78**, 7260 (1983).

I. OHMINE and T. TANAKA, "Salt Effects on Phase Transition of Ionic Gels", *J. Chem. Phys.*, **77**, 5725 (1982).

M. TSUKADA, H. ADACHI, and C. SATOKO, "Theory of Electronic Structure of Oxide Surface", *Progress in Surface Science*, **14**, (1983).

H. NAKAMURA, "Dynamical-state Representation and Nonadiabatic Electronic Transitions in Atomic Collisions", *Phys. Rev.*, **A26**, 3125 (1982); **A28**, 486 (1983).

H. TAKAGI and H. NAKAMURA, "Two-electron Excited States and Adiabatic Quantum Defects of H_2: Analysis of Elastic Scattering of Electrons from H_2^+.", *Phys. Rev.*, **A27**, 691 (1983).

Y. ITIKAWA, H. TAKAGI, H. NAKAMURA, and H. SATO, "Theoretical Studies of Photoionization of Hydrogen Molecules.", *Phys. Rev.*, **A27**, 1319 (1983).

H. NAKAMURA, "Semiclassical Theory of Predissociation Induced by Rotational (Coriolis) Coupling.", *Chem. Phys.*, **78**, 235 (1983).

R.E. WYATT, G. HOSE, and H.S. TAYLOR, "Mode-selective Multiphoton Excitation in a Model System.", *Phys. Rev.*, **A28**, 815 (1983).

K. NASU, "Dynamical Theory of Electron-Lattice Relaxation", *Semiconductors and Insulators*, **5**, 201 (1983).

K. NASU, "Extended Peierls-Hubbard Model for One-Dimensional N-Sites N-Electrons System. I. —Phase Diagram by Mean Field Theory—", *J. Phys. Soc. Jpn.*, **52**, 3865 (1983).

H. ADACHI, M. TSUKADA, I. YASUMORI, and M. ONCHI, "Cluster Model Calculations of Oxygen Chemisorption on (001) Surfaces of bcc V, Cr, and Fe", *Surf. Sci.*, **119**, 10 (1982).

M. TSUKADA and T. HOSHINO, "On the Electronic Structure of the Polar Surface of Compound Crystals", *J. Phys. Soc. Jpn.*, **51**, 2562 (1982).

T. HATTORI, Y. HISAJIMA, H. SAITO, T. SUZUKI, H. DAIMON, Y. MURATA, and M. TSUKADA, "Initial Stage of Sputtering in Silicon Oxide", *Appl. Phys. Lett.*, **42**, 244 (1983).

M. MORINAGA, H. ADACHI, and M. TSUKADA, "Electronic Structure and Phase Stability of ZrO_2", *J. Phys. Chem. Solids*, **44**, 301 (1983).

M. TSUKADA, "Theory of Non-Adiabatic Processes of Adsorbates", *J. Phys. Soc. Jpn.*, **51**, 2927 (1982).

M. TSUKADA, "Present Status and Problems in the Theory of Desorption, in 'Desoption and Related Phenomena Relevant to Fusion Devices", *IPPJ-AM-22 Inst. of Plasma Phys. Nagoya Univ.*, **139**, (1982).

T. HOSHINO and M. TSUKADA, "Electronic Structure of TiC(111) Polar Surface", *J. Magnetism and Mag. Materials*, **31—34**, 901 (1983).

T. AMANO, K. KAWAGUCHI, M. KAKIMOTO, S. SAITO, and E. HIROTA, "Infrared-Optical Double Resonance Spectroscopy of the NH_2 Radical", *J. Chem. Phys.*, **77**, 159 (1982).

Y. ENDO, C. YAMADA, S. SAITO, and E. HIROTA, "The Microwave Spectrum of the Trifluoromethyl Radical", *J. Chem. Phys.*, **77**, 3376 (1982).

T. AMANO, P.F. BERNATH, C. YAMADA, Y. ENDO, and E. HIROTA, "Difference Frequency Laser Spectroscopy of the ν_3 Band of the CH_3 Radical", *J. Chem. Phys.*, **77**, 5284 (1982).

E. HIROTA and C. YAMADA, "Intramolecular Motions and Molecular Structure of the CH_3 Radical", *J. Mol. Spectrosc.*, **96**, 175 (1982).

S. SAITO, Y. ENDO, M. TAKAMI, and E. HIROTA, "The Microwave Spectrum of the CF Radical", *J. Chem. Phys.*, **78**, 116 (1983).

C. YAMADA and E. HIROTA, "The Transition Dipole Moment of the ν_2 Band of the Methyl Radical", *J. Chem. Phys.*, **78**, 669 (1983).

M. KAKIMOTO, S. SAITO, and E. HIROTA, "Doppler-Limited Dye Laser Excitation Spectroscopy of HCCl", *J. Mol. Spectrosc.*, **97**, 194 (1983).

Y. ENDO, S. SAITO, and E. HIROTA, "The Microwave Spectrum of the PH_2 Radical", *J. Mol. Spectrosc.*, **97**, 204 (1983).

Y. ENDO, K. NAGAI, C. YAMADA, and E. HIROTA, "Diode Laser Spectroscopy of the SF Radical", *J. Mol. Spectrosc.*, **97**, 213 (1983).

C. YAMADA and E. HIROTA, "Infrared Diode Laser Spectroscopy of the CF_3 ν_3 Band", *J. Chem. Phys.*, **78**, 1703 (1983).

A.R.W. McKELLAR, C. YAMADA, and E. HIROTA, "Infrared Diode Laser Spectroscopy of the FO Radical ($^2\Pi_{3/2}$)", *J. Mol. Spectrosc.*, **97**, 425 (1983).

C. YAMADA, Y. ENDO, and E. HIROTA, "Difference Frequency Laser Spectroscopy of the ν_1 Band of the HO_2 Radical", *J. Chem. Phys.*, **78**, 4379 (1983).

S. SAITO, Y. ENDO, and E. HIROTA, "The Microwave Spectrum of the DO_2 Radical", *J. Mol. Spectrosc.*, **98**, 138 (1983).

Y. MORINO, M. TANIMOTO, S. SAITO, E. HIROTA, R. AWATA, and T. TANAKA, "Microwave Spectrum of Nitrogen Dioxide in Excited Vibrational States—Equilibrium Structure", *J. Mol. Spectrosc.*, **98**, 331 (1983).

S. SAITO, Y. ENDO, and E. HIROTA, "The Microwave Spectrum of the SiN($^2\Sigma^+$) Radical", *J. Chem. Phys.*, **78**, 6447 (1983).

K. KAWAGUCHI, S. SAITO, and E. HIROTA, "Microwave Spectroscopy of the NCO Radical in the $v_2 = 1$

$^2\Sigma$ State", *Mol. Phys.*, **49**, 663 (1983).

K. KAWAGUCHI, S. SAITO, and E. HIROTA, "Far-Infrared Laser Magnetic Resonance Detection and Microwave Spectroscopy of the PO Radical", *J. Chem. Phys.*, **79**, 629 (1983).

J. TERAOKA, T. OGURA, and T. KITAGAWA, "Resonance Raman Spectra of the Reaction Intermediates of Horseradish Peroxidase Catalysis.", *J. Am. Chem. Soc.*, **104**, 7354 (1982).

H. OKABAYASHI, T. YOSHIDA, T. IKEDA, H. MATSUURA, and T. KITAGAWA, "PO_2^- Symmetric-Stretching Raman Line and Molecular Aggregation States of Barium Dialkyl Phosphates.", *J. Am. Chem. Soc.*, **104**, 5399 (1982).

K. NAGAI, T. KAGIMOTO, A. HAYASHI, F. TAKETA, and T. KITAGAWA, "Resonance Raman Studies of Hemoglobins M: Evidence for Fe-Tyrosine Charge Transfer Interactions in the Abnormal Subunits of Hb M Boston and Hb M Iwate.", *Biochemistry* **22**, 1305 (1983).

T. KITAGAWA, S. HASHIMOTO, J. TERAOKA, S. NAKAMURA, H. YAJIMA, and T. HOSOYA, "Distinct Heme-Substrate Interactions of Lactoperoxidase Probed by Resonance Raman Spectroscopy: Difference between Animal and Plant Peroxidases", *Biochemistry* **22**, 2788 (1983).

N. ITO, T. FUJIYAMA, and Y. UDAGAWA, "Study of Local Structure Formation in Binary Solutions of 2-Butoxyethanol and Water by Rayleigh Scattering and Raman Spectra.", *Bull. Chem. Soc. Jpn.*, **56**, 379 (1983).

M. TANAKA, K. NISHIKAWA, K. TOHJI, and T. FUJIYAMA, "X-Ray Diffraction Study of Mixing States in the Carbon Tetrachloride Solution of Methanol and Pentane.", *Bull. Chem. Soc. Jpn.*, **56**, 1273 (1983).

S. HYODO, U. NAGASHIMA, and T. FUJIYAMA, "On the Effect of the Finite Size of the Solvent Molecule in Dielectric Friction Theory.", *Bull. Chem. Soc. Jpn.*, **56**, 1041 (1983).

K. TOHJI and Y. UDAGAWA, "Development of a Laboratory EXAFS Facility.", *Jpn. J. Appl. Phys.*, **22**, 882 (1983).

S. TANABE, A. UENO, K. TOHJI, and Y. UDAGAWA, "EXAFS Study on the Local Structure Changes around Ni atom during the Ni/SiO_2 Catalyst Preparation Procedures.", *Chem. Lett.*, 1089 (1983).

K. TOHJI and Y. UDAGAWA, "Measurements of EXAFS in the Laboratory (in Japanese)", *Bunko* Kenkyu **32**, 255 (1983).

H. ABE, N. MIKAMI, M. ITO, and Y. UDAGAWA, "Vibrational Energy Redistributions in Jet Cooled Hydrogen Bonded Phenols.", *Chem. Phys. Lett.*, **93**, 217 (1982).

T. KATO, N. ITO, T. FUJIYAMA, and Y. UDAGAWA, "Light Scattering Study of Local Structure Formation in Aquaous Solutions of Nonelectrolytes", *Studies in Phys. Theor. Chem.*, **27**, 175 (1983).

T. KATO, T. FUJIYAMA, and H. NOMURA, "Estimation of Parameters, G_{11}, G_{22}, and G_{12} in the Kirkwood-Buff Solution Theory on the Basis of the Concentration Fluctuation Data Obtained from Rayleigh Scattering.", *Bull. Chem. Soc. Jpn.*, **55**, 3369 (1982).

T. IIJIMA, K. NISHIKAWA, K. TOHJI, and Y. MURATA, "Premelting Process of Benzene (in Japanese)", *J. Cryst. Soc. Jpn.*, **24**, 336 (1983).

K. TOHJI and Y. MURATA, "X-Ray Diffraction Study of the Melting of Benzene.", *Jpn. J. Appl. Phys.*, **21**, 1199 (1982).

K. NISHIKAWA, K. TOHJI, and Y. MURATA, "Energy-Dispersive X-Ray Diffractometry and Its Application. Structural Correlation between the Liquid and the Plastic Crystal of Carbon Tetrachloride.", *Studies in Phys. Theor. Chem.*, **27**, 165 (1983).

N. NAKASHIMA, and K. YOSHIHARA, "Laser Photolysis of Benzene. V. Formation of Hot Benzenen", *J. Chem. Phys.*, **77**, 6040 (1982).

Y. TAKAGI, M. SUMITANI, N. NAKASHIMA, D.V. O'CONNOR, and K. YOSHIHARA, "Laser Flash Photolysis of Benzene. VII. Fluorescence Decay in the Channel 3 Region", *J. Chem. Phys.*, **77**, 6337 (1982).

D.V. O'CONNOR, M. SUMITANI, J.M. MORRIS, and K. YOSHIHARA, "Non-Exponential Picosecond Fluorescence Decay in Isolated Pentafluorobenzene and Hexafluorobenzene", *Chem. Phys. Lett.*, **93**,

350 (1982).

K. KAMOGAWA, J.M. MORRIS, Y. TAKAGI, N. NAKASHIMA, K. YOSHIHARA and I. IKEGAMI, "Picosecond Fluorescence Studies of P700–Enriched Particles of Spinach Chloroplasts", *Photochem. Photobiol.*, **37**, 207 (1983).

T. OKAMURA, M. SUMITANI, and K. YOSHIHARA, "Picosecond Dynamic Stokes Shift of α-Naphthylamine", *Chem. Phys. Lett.*, **94**, 339 (1983).

N. SHIMO, N. NAKASHIMA, and K. YOSHIHARA, "Laser Flash Photolysis of Benzene. VI. Photolysis in Aqueous Solution", *Bull. Chem. Soc. Jpn.*, **56**, 389 (1983).

M. TANAKA, I. TANAKA, S. TAI, K. HAMANOUE, M. SUMITANI, and K. YOSHIHARA, "Temperature Dependence of the Nonradiative Relaxation Process of the Lowest Excited Singlet States of Meso-Substituted Bromoanthracenes", *J. Phys. Chem.*, **87**, 813 (1983).

K. YAGI, F. TANAKA, N. NAKASHIMA, and K. YOSHIHARA, "Picosecond Laser Fluorometry of FAD of D-Amino Acid Oxidase-Benzoate Complex", *J. Biol. Chem.*, **258**, 3799 (1983).

H. INOUE, K. IKEDA, H. MIHARA, M. HIDA, N. NAKASHIMA, and K. YOSHIHARA, "Photoreduction of Polyhalogenated Anthraquinones by Direct Electron Transfer from Alcohol", *Chem. Phys. Lett.*, **95**, 60 (1983).

M. SUMITANI, D.V. O'CONNOR, Y. TAKAGI, N. NAKASHIMA, K. KAMOGAWA, Y. UDAGAWA, and K. YOSHIHARA, "Fluorescence Quantum Yields of S_1 Benzene in the Channel 3 Region", *Chem. Phys. Lett.*, **97**, 508 (1983).

K. HAMANOUE, T. HIDAKA, T. NAKAYAMA, H. TERANISHI, M. SUMITANI, and K. YOSHIHARA, "Solvent Effects on the Nonradiative Relaxation Processes of the Lowest Excited Singlet States of Meso-Substituted Bromoanthracenes", *Bull. Chem. Soc. Jpn.*, **56**, 1851 (1983).

N. NAKASHIMA, and D. PHILLIPS, "Intramolecular Charge-Transfer Fluorescence from 9,9′-Bianthyl Adsorbed on Porous Glass", *Chem. Phys. Lett.*, **97**, 337 (1983).

N. NAKASHIMA, and K. YOSHIHARA, "Laser Flash Photolysis of Benzene. VIII. Formation of Hot Benzene from the S_2 State and its Collisional Deactivation", *J. Chem. Phys.*, **79**, 2727 (1983).

Y. TAKAGI, M. SUMITANI, D.V. O'CONNOR, N. NAKASHIMA, K. KAMOGAWA, Y. UDAGAWA, and K. YOSHIHARA, "Assignment of the E Absorption Transitions in C_6D_6 by Means of Isolated-Molecule Fluorescence Spectra", *Chem. Phys. Lett.*, **99**, 445 (1983).

T. KAJIWARA, K. HASHIMOTO, T. KAWAI, and T. SAKATA, "Dynamics of Luminescence from $Ru(bipy)_3Cl_2$ Adsorbed on Semiconductor Surfaces", *J. Phys. Chem.*, **86**, 4516 (1982).

K. HASHIMOTO, T. KAWAI, and T. SAKATA, "Hydrogen Production with Visible Light by using Dye-Sensitized TiO_2 Powder", *Nouv. J. Chim.*, **7**, 249 (1983).

K. HASHIMOTO, T. KAWAI, and T. SAKATA, "Efficient Hydrogen Production from Water by Visible Light Excitation of Fluorescein-Type Dyes in the Presence of a Redox Catalyst and a Reducing Agent", *Chem. Lett.*, 709 (1983).

T. SAKATA, T. KAWAI, and K. HASHIMOTO, "The Catalytic Properties of RuO_2 and Pt on n-Type Semiconductors", *Denki Kagaku* (in Japanese), **51**, 79 (1983).

R. NAKAGAKI, and I. HANAZAKI, "Inequivalent Methyl CH Oscillators in Methyl-substituted Conjugated Compounds as Revealed by Higher Overtone Spectra", *Chem. Phys.*, **72**, 93 (1982).

M. ITOH, Y. HANASHIMA, and I. HANAZAKI, "Excitation Energy Dependence of Intramolecular Excimer Formation in N,N,N′,N′-Tetramethylpropanediamine Vapor", *J. Phys. Chem.*, **87**, 569 (1983).

R. NAKAGAKI, and I. HANAZAKI, "Substituent Effects in Benzene Derivatives –A Local Mode Analysis of Ring CH Stretching Overtone Spectra of Methylated and Chlorinated Benzene", *Spectrochim. Acta.*, in press.

M. ITOH, Y. HANASHIMA, N. WADA, and I. HANAZAKI, "Excitation Energy Dependence of Intramolecular Exciplex Formation and Electronic Relaxation in the Collision-free Vapor", *Bull. Chem. Soc. Jpn.*, **56**, 1944 (1983).

M. UMEMOTO, H. SHINOHARA, N. NISHI and R. SHIMADA, "UV Laser Photolysis of C_3O_2 at 193 nm:

Emission from Electronically Excited C, CO and C_2", *J. Photochemistry*, **20**, 277 (1982).

K.Y. CHOO, H. SHINOHARA, and N. NISHI, "Molecular Beam Multiphoton Ionization Studies on Ammonia-Water Binary Clusters", *Chem. Phys. Letters*, **95**, 102 (1983).

M. KAWASAKI, K. KASATANI, H. SATO, H. SHINOHARA, and N. NISHI, "Photodissociation of Molecular Beams of SO_2 at 193 nm", *Chem. Phys.*, **73**, 377 (1982).

N. IWASAKI, N. NISHI, and M. KINOSHITA, "$T_1 \leftarrow S_0$ Excitation Spectra of 1,4-Dichloronaphthalene", *Chem. Lett.*, 1105 (1983).

M. KAWASAKI, K. KASATANI, H. SATO, H. SHINOHARA, and N. NISHI, "Photodissociation of Molecular Beams of N_2O_4", *Chem. Phys.*, **78**, 65 (1983).

H. SHINOHARA, "Two-Photon-Ionization Mass Spectroscopy of Ammonia Clusters in a Pulsed Supersonic Nozzle Beam", *J. Chem. Phys.*, **79**, 1732 (1983).

R. NAKAGAKI, "Orientation and Mechanism in Photochemical Aromatic Substitutions.", *J. Syn. Org. Chem. Jpn.*, (Yuki Gosei Kagaku), **40**, 651 (1982) (in Japanese).

R. NAKAGAKI, D.C. FROST, and C.A. MCDOWELL, "Shake-up Satellites in the Nitro-Nls Spectra of Highly Polar Nitro-Aromatic Amines.", *J. Electron Spectrosc. Relat. Phenom.*, **27**, 69 (1982).

H. KATÔ and H. KOBAYASHI, "Laser-induced Fluorescence of the RbCs Molecule.", *J. Chem. Phys.*, **79**, 123 (1983).

K. ONOMICHI and H. KATÔ, "Laser-induced Fluorescence of the NaCs Molecule.", *Bull. Chem. Soc. Jpn.*, **56**, 3533 (1983).

S. HINO, T. VESPREMI, K. OHNO, H. INOKUCHI, and K. SEKI, "Absorption Spectra of Volatile Aromatic Hydrocarbon Films in the Vacuum Ultraviolet Region", *Chem. Phys.*, **71**, 135 (1982).

K. SEKI and H. INOKUCHI, "The Ultraviolet Photoelectron Spectroscopy of Aliphatic Hydrocarbons and Tetramethylsilane in the Solid State", *Bull. Chem. Soc. Jpn.*, **56**, 2212 (1983).

CHEN SHANG XIAN, K. SEKI, H. INOKUCHI, SHI ZURONG, QIAN RENYUAN, "Ultraviolet Photoelectron Spectra of α- and β-Poymorphs of Copper Phthalocyanine", *Bull. Chem. Soc. Jpn.*, **56**, 2565(1983).

Y. SHIROTA, Y. MATSUMOTO, H. MIKAWA, K. SEKI, and H. INOKUCHI, "Ionization Potentials of 1:1 Alternating Copolymers Containing a Pendant Carbazolyl Group as Determined by UV Photoelectron Spectroscopy", *Chem. Phys. Lett.*, **97**, 57 (1983).

N. SATO, G. SAITO, and H. INOKUCHI, "Ionization Potential and Polarization Energies of Tetraselenafulvalene (TSF) Derivatives Determined with Ultraviolet Photoelectron Spectroscopy", *Chem. Phys.*, **76**, 79 (1983).

N. KARL, N. SATO, K. SEKI, and H. INOKUCHI, "UV Photoelectron Spectroscopy of Several One- and Two-component Organic Photoconductors", *J. Chem. Phys.*, **77**, 4870 (1982).

N. SATO, H. INOKUCHI, K. SEKI, J. AOKI, and S. IWASHIMA, "Ultraviolet Photoemission Spectroscopic Studies of Six Nanocyclic Aromatic Hydrocarbons in the Gaseous and Solid States", *J.* Chem. *Soc., Faraday Trans.* 2, **78**, 1929 (1982).

G. SAITO, T. ENOKI, H. INOKUCHI, H. KUMAGAI, and J. TANAKA, "Organic Conductors: Electrical Properties of HMTTeF (Hexamethylenetetratellurafulvalene) Complexes", *Chem. Lett.*, 503 (1983).

H. KOBAYASHI, A. KOBAYASHI, Y. SASAKI, G. SAITO, T. ENOKI, and H. INOKUCHI, "Crystal Structure of a New Type of Two-Dimensional Organic Metal, $(C_{10}H_8S_8)_2ClO_4(C_2H_3Cl_3)_{0.5}$", *J. Am. Chem. Soc.*, **105**, 297 (1983).

S. KAGOSHIMA, J.P. POUGET, G. SAITO, and H. INOKUCHI, "X-Ray Evidence for a Structural Phase Transition in the Organic Two-Dimensional Conductor $(BEDT\text{-}TTF)_2ClO_4(C_2H_3Cl_3)_{0.5}$", *Solid State Commun.*, **45**, 1001 (1983).

T. MORI, A. KOBAYASHI, Y. SASAKI, H. KOBAYASHI, G. SAITO, and H. INOKUCHI, "Two-Dimensional Band Structure of an Organic Metal, Perchlorate Salt of Bis(ethylenedithiolo)-tetrathiafulvalene $(BEDT\text{-}TTF)_2ClO_4(C_2H_3Cl_3)_{0.5}$", *Chem. Lett.*, 1963 (1982).

H. KOBAYASHI, R. KATO, T. MORI, A. KOBAYASHI, Y. SASAKI, G. SAITO, and H. INOKUCHI, "Crystal Structure of α-$(BEDT\text{-}TTF)_2PF_6$", *Chem. Lett.*, 759 (1983).

H. KOBAYASHI, T. MORI, R. KATO, A KOBAYASHI, Y. SASAKI, G. SAITO, and H. INOKUCHI, "Transverse Conduction and Metal-Insulator Transition in β-(BEDT-TTF)$_2$PF$_6$", *Chem. Lett.*, 581 (1983).

Y. MARUYAMA, R. HIROSE, G. SAITO, and H. INOKUCHI, "Tunneling Spectroscopic Study on the Superconductivity of (TMTSF)$_2$ClO$_4$ Crystals", *Solid State Commun.*, **47**, 273 (1983).

K. OSHIMA, H. BANDO, H. KOBAYASHI, and G. SAITO, "Precise Determination of Critical Field Anisotropy in (TMTSF)$_2$ClO$_4$" *J. Magnetism and Magnetic Materials*, **31—34**, 1147 (1983).

K. MURATA, T. UKACHI, H. ANZAI, K. KAJIMURA, T. ISHIGURO, and G. SAITO, "Anomalous Longitudinal Magnetoresistance in Quasi 1-D Organic Conductor (TMTSF)$_2$ClO$_4$", *J. Magnetism and Magnetic Materials*, **31—34**, 1145 (1983).

K. MURATA, K. KAJIMURA, H. TOKUMOTO, T. UKACHI, M. TOKUMOTO, H. ANZAI, T. ISHIGURO, and G. SAITO, "Superconducting Transition of Organic Metal (TMTSF)$_2$ClO$_4$: Effects of Thermally Induced Microcracks", *Proc. Int. Cryog. Mater. Conf.*, 434 (1982) Ed. K. Tachikawa, A.F. Clark, Butterworth, UK.

T. ISHIGURO, T. UKACHI, K. KATO K. MURATA, K. KAJIMURA, M. TOKUMOTO, H. TOKUMOTO, H. ANZAI, and G. SAITO, "Kink Deformation of (TMTSF)$_2$ClO$_4$ Single Crystal and Its Influence on Electrical Resistivity", *J. Phys. Soc. Jpn.*, **52**, 1585 (1983).

K. KAJIMURA, H. TOKUMOTO, M. TOKUMOTO, K. MURATA, T. UKACHI, H. ANZAI, T. ISHIGURO, and G. SAITO, "Spin-Density-Wave and Superconducting States in Thermally Quenched (TMTSF)$_2$ClO$_4$", *Solid State Commun.*, **44**, 1573 (1982).

S. KAGOSHIMA, T. YASUNAGA, T. ISHIGURO, H. ANZAI, and G. SAITO, "Quenching Effect on the Anion Ordering in the Organic Superconductor (TMTSF)$_2$ClO$_4$ ··· An X-Ray Study ···", *Solid State Commun.*, **46**, 867 (1983).

M. NAKATSUKA, K. NAKASUJI, I. MURATA, I. WATANABE, G. SAITO, T. ENOKI, and H. INOKUCHI, "3,7-Dihalo-2H, 6H-benzo[1,2-b:4,5-b']dithiophene-2,6-dione: New Wurster-Type Acceptors Isoelectronic with 2,6-Anthraquinone", *Chem. Lett.*, 905 (1983).

H. KOBAYASHI, T. MORI, R. KATO, A. KOBAYASHI, Y. SASAKI, G. SAITO, and H. INOKUCHI, "Highly Conductive Poly(Carbon Diselenide)", *Chem. Lett.*, 1407 (1983).

K. TANAKA, T. KATO, and I. KOYANO, "Analysis of the Autoionization Structure of N$_2$ Using Ar Charge Exchange Detection", *Chem. Phys. Lett.*, **97**, 562 (1983).

K. TANAKA, T. KATO, P.-M. GUYON, and I. KOYANO, "State Selected Ion-Molecule Reactions by a TESICO Technique. VII. Isotope Effect in the Reactions $O_2^+(X^2\Pi_g, a^4\Pi_u) + HD \rightarrow O_2H^+(O_2D^+) + D(H)$", *J. Chem. Phys.*, **79**, 4302 (1983).

T. KATO, K. TANAKA, and I. KOYANO, "State Selected State Ion-Molecule Reactions by a TESICO Technique. VIII. Vibronic-State Dependence of the Cross Sections in the Reaction $NO^+(a^3\Sigma^+,v;b^3\Pi,v) + Ar \rightarrow NO + Ar^{+*}$", *J. Chem. Phys.*, **79**, No. 12 (1983).

I. KOYANO, K. TANAKA, and T. KATO, "Vibronic and fs State Selected Charge Transfer Reaction: $O_2^+ + Ar \rightleftharpoons Ar^+ + O_2$ and $NO^+ + Ar \rightleftharpoons Ar^+ + NO$ Systems", *Electronic and Atomic Collisions*, edited by J. Eichler et al., 625 (1983).

S. TOMODA, Y. ACHIBA, K. NOMOTO, K. SATO and K. KIMURA, "Photoelectron Spectroscopic Study of Simple Hydrogen-bonded Dimers. I. Supersonic Nozzle Beam Photoelectron Spectrometer and the Formic Acid Dimer", *Chem. Phys.*, **74**, 113 (1983).

S. TOMODA and K. KIMURA, "Photoelectron Spectroscopic Study of Simple Hydrogen-bonded Dimers. II. The Methanol Dimer", *Chem. Phys.*, **74**, 121 (1983).

S. TOMODA and K. KIMURA, "A Photoelectron Spectroscopic Estimation of the Concentrations of Simple Hydrogen-bonded Dimers Produced in the Temperature-controlled Supersonic Nozzle Beam", *Bull. Chem. Soc. Jpn.*, **56**, 1768 (1983).

S. TOMODA and K. KIMURA, "Ionization Energies of the Water Dimer and Clusters", in "Ions and Molecules in Solution", Ed. N. Tanaka, H. Ohtaki and R. Tamamushi, Elsevier, Amsterdam (1983),

p.13.

S. TOMODA, "Comments on the "Usage of the Term 'Angle of Incidence'" by J.H. Beynon, D. Cameron and J.F. Todd", *Int. J. Mass Spectrom. Ion Phys.*, **49**, 87 (1983).

K. SATO, S. TOMODA, K. KIMURA, and S. IWATA, "Electronic and Molecular Structure of the Water Dimer Cation. A Theoretical Study", *Chem. Phys. Lett.*, **95**, 579 (1983).

Y. NAGANO, Y. ACHIBA, K. SATO, and K. KIMURA, "Photoelectron Spectra and Angular Distribution in Resonant Three-photon Ionization of Atomic Iron: J Dependence", *Chem. Phys. Lett.*, **93**, 510 (1982).

Y. ACHIBA, K. SATO, K. SHOBATAKE, and K. KIMURA, "A Photoelectron Spectroscopic Study of (3 + 1) Resonant Multiphoton Ionization of NO and NH_3", *J. Chem. Phys.*, **78**, 5479 (1983).

K. KOBAYASHI, Y. KODAMA, M. NISHIO, T. SUGAWARA, and H. IWAMURA, "The Conformations of Several 1-Phenylethyl and 1-Phenylpropyl Aryl Sulfoxides. Evidence for Attractive Aryl/Aryl Interaction.", *Bull. Chem. Soc. Jpn.*, **55**, 3560 (1982).

W. NAKANISHI, Y. IKEDA, and H. IWAMURA, "Structure of 2-Carboxyphenyl Methyl Selenoxide, Its Sodium Salt and Related Compounds in Solution, Studied by ^{1}H, ^{13}C and ^{77}Se NMR.", *Org. Magn. Reson.*, **20**, 117 (1982).

E. LIPCZYŃSKA-KOCHANY and H. IWAMURA, "Oscillation in Fluorescence Intensity from Irradiated Solution of *N*-Methylanthranilohydroxamic Acid in Methanol.", *Chemistry Lett.*, 1825 (1982).

A. SEKIGUCHI, W. ANDO, T. SUGAWARA, H. IWAMURA, and M.T.H. LIU, "10-Silaanthracen-9(10H)-ylidene and Anthracen-9(10H)-ylidene.", *Tetrahedron Lett.*, **23**, 4095 (1982).

K. MARUYAMA, H. FURUTA, H. IWAMURA, and T. OTSUKI, "Complex Formation between Chlorophyll and Quinone is Suggested to be Important in Light-Induced Electron Transfer.", *Photobiochem. Photobiophys.*, **4**, 47 (1982).

E. LIPCZYŃSKA-KOCHANY and H. IWAMURA, "Oxygen-17 Nuclear Magnetic Resonance Studies of the Structures of Benzohydroxamic Acids and Benzohydroxamate Ions in Solution.", *J. Org. Chem.*, **47**, 5277 (1982).

W. NAKANISHI, A. SAKAUE, Y. IKEDA, and H. IWAMURA, "Novel Reduction of Chlorine Adducts of Aryl and Alkyl Selenides with Dimethyl Sulfoxide.", *Chemistry Lett.*, 33 (1983).

T. SUGAWARA, M. INADA, and H. IWAMURA, "Different Photolytic Behavior of 1,3-Bis (α-diazobenzyl)benzene in Solutions vs. in Crystals and Matrices.", *Tetrahedron Lett.*, **24**, 1723 (1983).

T. SUGAWARA, N. NAKASHIMA, K. YOSHIHARA, and H. IWAMURA, "Low-Temperature and Time-Resolved Absorption Spectral Studies on the sp- and ap-2-(9-Fluorenyl)phenylnitrenes Generated from 1-Azatriptycene and 2-(9-Fluorenyl)phenyl Azide.", *J. Am. Chem. Soc.*, **105**, 858 (1983).

Y. KAWADA, H. IWAMURA, Y. OKAMOTO, and H. YUKI, "Stereoisomerism in Molecular Bevel-Gears. Optical Resolution of the DL Isomers of Bis(2- and 3-chloro-9-triptycyl)methanes and Ethers.", *Tetrahedron Lett.*, **24**, 791 (1983).

Y. KAWADA and H. IWAMURA, "Correlated Rotation in Bis(9-triptycyl)-methanes and Bis(9-triptycyl) Ethers. Separation and Interconversion of the Phase Isomers of Labeled Bevel Gears.", *J. Am. Chem. Soc.*, **105**, 1449 (1983).

N. KOGA, Y. KAWADA, and H. IWAMURA, "Recognition of the Phase Relationship between Remote Substituents in 9,10-Bis(3-chloro-9-triptycyloxy)triptycene Molecules Undergoing Rapid Internal Rotation Cooperatively.", *J. Am. Chem. Soc.*, **105**, 5498 (1983).

S. MURATA, T. SUGAWARA, and H. IWAMURA, "Contrasting ESR and UV Spectroscopic Properties and Reactivities between the Conformationally Restricted *o*-(9-Fluorenyl)phenylnitrenes at Cryogenic Temperatures.", *J. Am. Chem. Soc.*, **105**, 3723 (1983).

W. NAKANISHI, Y. YAMAMOTO, Y. KUSUYAMA, Y. IKEDA, and H. IWAMURA, "The Structure of Halogen Adducts of Some Selenides and a Telluride in Solution Studied by ^{1}H and ^{13}C NMR Spectroscopy. Evidence for the Formation of a Molecular Complex of Selenoxanthone with Bromine.", *Chemistry Lett.*, 675 (1983).

T. SUGAWARA, H. IWAMURA, H. HAYASHI, A. SEKIGUCHI, W. ANDO, and M.T.H. LIU, "Time-Resolved and Low-Temperature Absorption Spectroscopic Studies on 10,10-Dimethyl-10-silaanthracen-9(10H)-ylidene.", *Chemistry Lett.*, 1257 (1983).

T. SUGAWARA, H. IWAMURA, H. HAYASHI, A. SEKIGUCHI, W. ANDO, and M.T.H. LIU, "Time-Resolved Absorption Spectroscopic Detection of 10,10-Dimethyl-10-silaanthracen-9(10H)-one Oxide.", *Chemistry Lett.*, 1261 (1983).

M. SUGIMOTO, H. ITO, K. TORIUMI, and T. ITO, "Structure of *cis*-Bisisothiocyanato[1,4,7,10-tetraazacyclotetradecane]nickel(II). Electronically Controlled cis-Coordination", *Acta Crystallogr.*, **B38**, 2453 (1982).

M. SUGIMOTO, M. NONOYAMA, T. ITO, and J. FUJITA, "Tetraaza Mactocyclic Metal Complexes Containing a Medium Size Chelate Ring. I. Syntheses and Characterization of Nickel(II) Complexes with 1,4,7,10-Tetraazacyclo-tetradecane, -pentadecane, and -hexadecane", *Inorg. Chem.*, **22**, 950 (1983).

M. SUGIMOTO, J. FUJITA, H. ITO, K. TORIUMI, and T. ITO, "Tetraaza Macrocyclic Metal Complexes Containing a Medium Size Chelate Ring. II. X-ray Structural Studies of *trans*-Dichloro(1,4,7,10-tetraazacyclotetradecane)nickel(II) Monohydrate, 1,4,7,10-Tetraazacyclopentadecanenickel(II) Perchlorate, and *trans*-Dichloro(1,4,7,10-tetraazacyclohexadecane)nickel(II)", *Inorg. Chem.*, **22**, 955 (1983).

T. ITO, M. SUGIMOTO, H. ITO, K. TORIUMI, H. NAKAYAMA, W. MORI, and M. SEKIZAKI, "A Chelate Ring Size Effect on Spin State of Iron(III) Complexes with Hexadentate Ligands Derived from Salicylaldehyde and 4,8-diazaundecane-1,11-diamine (3,3,3-tet) or 4,7-diazadecane-1,10-diamine (3,2,3-tet), and Their X-ray Structures", *Chem. Lett.*, 121 (1983).

S. ONAKA, Y. KONDO, N. FURUICHI, K. TORIUMI, and T. ITO, "Photochemistry of Metal-Metal Bonds. I. Isolation, X-ray Molecular Structure Analyses of Orthometalated Triphenylphosphite Manganese Carbonyl Derivatives and Reaction Mechanism of Orthometalation from Photodegradation of Manganese Carbonyl Derivatives with Sn-Mn Bond", *Bull. Chem. Soc. Jpn.*, **56**, 87 (1983).

M. YAMASHITA, H. ITO, K. TORIUMI, and T. ITO, "Syntheses and Structure of a One-dimensional Pd(II)-Pd(IV) Mixed Valence Complex and Its Parent Pd(II) and Pd(IV) Complexes with 1,4,8,11-Tetraazacyclotetradecane", *Inorg, Chem.*, **22**, 1566 (1983).

M. YAMASHITA, H. ITO, and T. ITO, "A Binuclear Copper(II) Complex with Both Metal Ions Bound within a 22-Membered Homologue of Curtis-type Tetraazamacrocyclic Ligand", *Inorg. Chem.*, **22**, 2101 (1983).

M. TANAKA, I. TSUJIKAWA, K. TORIUMI, and T. ITO, "The Structure of Linear Chain Tetraammineplatinum(II)-dibromotetraamineplatinum(IV) Hydrosulfate, $[Pt(NH_3)_4][PtBr_2(NH_3)_4](HSO_4)_4$", *Acta Crystallogr.*, **B38**, 2793 (1982).

T. OHISHI, K. KASHIWABARA, H. ITO, and T. ITO, "Preparation and Molecular Structure of cis-β, trans(sec-N,P)-{(2-Aminoethyl)dimethylphosphine}(3,7,-diazanonane-1,9-diamine)cobalt(III) Bromide Dihydrate", *Bull. Chem. Soc. Jpn.*, **56**, 1551 (1983).

H. SHIOI, S. YANO, K. TORIUMI, T. ITO, and S. YOSHIKAWA, "The Reaction of $[Ni(tn)_3]^{2+}$(tn = trimethylenediamine) with Carbonhydrates: X-ray Crystal Structure of Bis{1-[(3-aminopropyl)amino]-1,6-dideoxy-L-mannose}nickel(II) Dibromide Dihydrate Methanol Soluvate, $[Ni(L\text{-rham-tn})_2]Br_2{\cdot}2H_2O{\cdot}CH_3OH$", *J. Chem. Soc., Chem. Commun.*, 201 (1983).

S. OBARA and H. KASHIWAGI, "*Ab Initio* MO Studies of Electronic States and Mössbauer Spectra of High-, Intermediate-, and Low-Spin Fe(II)-Porphyrin Complexes", *J. Chem. Phys.*, **77**, 3155 (1982).

M. SANO, H. KASHIWAGI, and H. YAMATERA, "*Ab Initio* MO Calculations for Hexacyano Complexes", *Inorg. Chem.*, **21**, 3837 (1982).

K. OHNO, K. MOROKUMA, F. HIROTA, H. HOSOYA, S. IWATA, H. KASHIWAGI, S. OBARA, Y. OSAMURA, S. YAMAMOTO, N. KOSGI, K. NISHIMOTO, K. TANAKA, M. TOGASHI, and S. YAMABE, "Quantum Chemistry Literature Data Base — Bibliography of Ab Initio Calculations for 1981", *Theochem.*, **91**, 1 (1982).

Y. WATANABE, K. NISHIMOTO, and H. KASHIWAGI, "*Ab Initio* MO Study of the Stacking Complexes,

Flavin-Tyrosine, Flavin-Tryptophan, and Flavin-NADH", in "Flavins and Flavoproteins", Vincent Massey and Charles H. Williams, Editors, Elsevier North Holland Inc., New York, 1982, p.537.

T. NOZAWA, M. HATANO, U. NAGASHIMA, S. OBARA, and H. KASHIWAGI, "Electronic States of Dioxygen Heme Complex Revealed from ab initio LCAO-SCF-MO Calculations", *Bull. Chem. Soc. Jpn.*, **56**, 1721 (1983).

Y. WATANABE and H. KASHIWAGI, "*Ab Initio* MO Calculations of Benzen + TCNE and Naphthalene + TCNE complexes with STO-3G π-Split Basis Set", *Int. J. Quant. Chem.*, **23**, 1739 (1983).

E. MIYOSHI, S. OBARA, T. TAKADA, H. KASHIWAGI, and K. OHNO, "Theoretical Study of Degree of Covalency in Some CoF_6(n-) Complexes (n = 4, 3, and 2)", *Int. J. Quant. Chem.*, **23**, 1753 (1983).

E. MIYOSHI and H. KASHIWAGI, "Theoretical Study of Equilibrium Co-F Bond Distance of CoF_6(n-) (n = 4, 3 and 2) Clusters in Crystal", *Int. J. Quant. Chem.*, **24**, 85 (1983).

A. MIYASHITA, Y. WATANABE, and H. TAKAYA, "Isolation and Characterization of 2-[bis(pyridine)dichloroplatina]-1-cyanobicyclo[1.1.1.]pentane Derived from 1-Cyanobicyclo[1.1.0]butane and Pt(II) Complexes", *Tetrahedron Lett.*, **24**, 2595 (1983).

I. YAMAZAKI, T. MURAO, T. YAMANAKA, and K. YOSHIHARA, "Intramolecular Electronic Relaxation and Photoisomerization Processes in the Isolated Azabenzene Molecules Pyridine, Pyrazine and Pyrimidine", *J. Chem. Soc., Faraday Discussion*, **75**, 380 (1983).

I. YAMAZAKI, M. MIMURO, T. MURAO, T. YAMAZAKI, K. YOSHIHARA, and Y. FUJITA, "Excitation Energy Transfer in Light Harvesting Antenna System of the Red Alga Porphyridium cruentum and the Blue-Green Alga Anacystis nidulans: Analysis of Time-Resolved Fluorescence Spectra", *Photochem. Photobiol.*, **38**, 658 (1983).

K. SUSHIDA, M. FUJITA, I. YAMAZAKI, and H. BABA, "Electronic Relaxation Processes from Single Vibronic Levels in the $S_1(n,\pi^*)$ State of Pyridine Vapor", *Bull. Chem. Soc. Jpn.*, **56**, 228 (1983).

T. IKEYAMA, T. AZUMI, T. MURAO, and I. YAMAZAKI, "Shift of Emission Band upon the Excitation at the Long Wavelength Absorption Edge. IV. Time Dependent Fluorescence Shift of Fluid Ethanol Solution of 6-Methoxyquinoline", *Chem. Phys. Lett.*, **96**, 419 (1983).

H. MASUHARA, N. MATAGA, S. TAZUKE, T. MURAO, and I. YAMAZAKI, "Time-Resolved Total Internal Reflection Fluorescence Spectroscopy of Polymer Films", *Chem. Phys. Lett.*, **100**, 221 (1983).

N. TAMAI, H. MASUHARA, and N. MATAGA, "The Excited and Ionic States of Polymers with Pendant Phynanthryl Groups in Solution. Model Systems for Photophysics in Phenanthrene Aggregates", *J. Phys. Chem.*, **87**, 4461 (1983).

H. MASUHARA, N. TAMAI, N. MATAGA, F.C. DE SCHRYVER, J. VANDENDRIESSCHE, and N. BOENS "Excimer Formation in Poly(N-Vinylcarbazole) and its Model Compounds as Revealed by Picosecond Time-Resolved Absorption Spectroscopy", *Chem. Phys. Lett.*, **95**, 471 (1983).

K. KIMURA, "A New Formalism of Chemical Exchange Near the Region of Intermediate Rate", *J. Mag. Res.*, **52**, 13 (1983).

R. INOUE, T. ENOKI, and I. TSUJIKAWA, "Physical Properties of a Quasi One-Dimensional Conductor $Pt_6(NH_3)_{10}Cl_{10}(HSO_4)_4$: Partially Oxidized Salt of the Magnus Green Salt", *J. Phys. Soc. Jpn.*, **51**, 3592 (1982).

S. YAMAGUCHI, H. TATEMITSU, Y. SAKATA, T. ENOKI, and S. MISUMI, "Synthesis of Cyclobutane-fused Tetracyanoquinodimethanes", *J. Chem. Soc., Chem. Commun.*, 1065 (1982).

T. ENOKI, M. SANO, and H. INOKUCHI, "Hydrogen in Aromatics III. Chemisorption of Hydrogen in Graphite-Alkali Metal Intercalation Compounds", *J. Chem. Phys*, **78**, 2017 (1983).

N. UEDA, B. NATSUME, K. YANAGIUCHI, Y. SAKATA, T. ENOKI, G. SAITO, H. INOKUCHI, and S. MISUMI, "The Synthesis of 2,7-Bis(dimethylamino)pyrene and -tetrahydropyrene and the Electrical Conductivities of their Complexes", *Bull. Chem. Soc. Jpn.*, **56**, 775 (1983).

Y. TOKURA, T. KODA, T. MITANI, and G. SAITO, "Neutral-ionic Transition in Tetrathiafulvalene-p-Chloranil as Investigated by Optical Reflection Spectra", *Solid State Commun.*, **43**, 757 (1982).

Y. TAKAGI, M. SUMITANI, N. NAKASHIMA, D. O'CONNOR, and K. YOSHIHARA, "Generation of

High-Power Picosecond Continuously Tunable Radiation between 215 and 245 nm by Mixing of Raman and Optical Parametric Light.", *App. Phys. Lett.*, **42**, 489 (1983).

Y. TAKAGI, "Optical Parametric Conversion and Picosecond Tunable Laser." *Bunkōkenkyu* (in Japanese), **32**, 263 (1983).

Review Articles and Textbooks

C. SATOKO, "Surface Electronic Structures and Geometries", *Butsuri* (in Japanese), **22**, 179 (1983).

H. HAYASHI and K. NASU, "Tunnel Self-trapping Process of Exciton", *Gekkan Physics*, (in Japanese), **4**, 688 (1983).

M. TSUKADA, "Theory of Electronic Structure and Chemisortion of Semiconductor Surfaces, to be published in 'Recent Topics from the Progress of Semi-Conductors", *World Scientific Publishing Co.*

S. SAITO, "New Molecules Formed in Interstellar Space", Kagaku (in Japanese), **52**, 633 (1982).

E. HIROTA, "Molecular Science of C_1 Organic Free Radicals. Methylene and Methyl", Kagaku (in Japanese), **38**, 302 (1983).

E. HIROTA, "Laser Molecular Spectroscopy" in "Laser Spectroscopy", K. Shimoda, Ed., Gakkai Shuppan (in Japanese), 1983, p.38.

T. KITAGAWA, "The Iron-Histidine Stretching Raman Line as a Probe of the Proximal Histidine of Hemoproteins" in "Oxygenases and Oxygen Metabolism", M. Nozaki, S. Yamamoto, Y. Ishimura, M.T. Coon, L. Ernster, and R.W. Estabrook eds. Academic Press pp.451–456 (1982).

T. KITAGAWA and J. TERAOKA, "Coordination Characteristics of Proximal Histidine of Plant Peroxidases and Their Relevance to the Heme-Linked Ionization" in "The Biological Chemistry of Iron" H.B. Dunford, D. Dolphin, K. Raymond, and L. Sieker eds. D. Reidel, pp.375–389 (1982).

T. KITAGAWA, "Resonance Raman Spectra of Hemoproteins and Flavoproteins" *Kagakuno Ryoiki* (in Japanese) M. Tsuboi, M. Tanaka, and M. Tasumi, eds. **140**, pp.83–100 (1983).

K. YOSHIHARA and N. NAKASHIMA, "Fast Chemical Reactions", in Laser Handbook (*Laser Society of Japan* (Ohmu Co. Inc., Tokyo, 1982)) (in Japanese), pp.747–753.

T. SAKATA, "Photocatalytic Water Splitting and Hydrogen Production from Organic Resources", *Chemical Industry* (in Japanese), **33**, 1068 (1982).

T. SAKATA and T. KAWAI, "Photosynthesis and Photocatalysis with Semiconductor Powders" in "Energy Resources through Photochemistry and Photocatalysis", M. Grätzel Ed., Academic Press, 1983, pp.331–358.

T. SAKATA, "Chemical Conversion of Solar Energy by Using Semiconductor Electrode or Photocatalyst", *Energy and Resources* (in Japanese), **4**, 320 (1983).

T. KAWAI and T. SAKATA, "Photochemical Reactions on the Semiconductor Surfaces" in "Technology of VLSI-VII. The Fundamental Processes – Studies of Semiconductors, vol. 20", (in Japanese), Kogyo Chosakai Publishing Co., Ltd., Tokyo, 1983, pp.37–47.

T. SAKATA, "Semiconductor Particulate Photocatalyst-Present State, Problems and its Views in the 21st Century", *Denki Kagaku*, (in Japanese), **51**, 104 (1983).

T. KAWAI and T. SAKATA, "Hydrogen Production with Semiconductor Photocatalyst" in "Future Industrial Technology, vol. 3", Kagakugijyutsu Koho Zaidan (in Japanese), pp.320–332, (1983).

T. SAKATA, "Photocatalysis" in "Inorganic Phtochemistry; Kagakusosetsu No.39" (in Japanese), Japan Chemical Society, Gakkai Shuppan Publishing Co., Ltd., 1983, pp.118–135.

T. SAKATA, "Photocatalytic Hydrogen Production" in "Biomass Energy Conversion" (in Japanese), S. Suzuki Ed., Kodansha Publishing Co., Ltd., 1983, pp.172–186.

S. HASHIMOTO and K. SEKI, "Electronic Properties of Polyethylene" *Kagaku* (in Japanese), **37**, 425 (1982).

H. INOKUCHI, "Metals" (in Japanese), *Baifukan*, (1982).

T. YAGI, H. INOKUCHI, and K. KIMURA, "Cytochrome c_3, a Tetrahemoprotein Electron Carrier Found in Sulfate-Reducing Bacteria", *Acct. Chem. Res.*, **16**, 2 (1983).

T. NIKI, T. YAGI, and H. INOKUCHI, "Electrochemical Studies of Cytochrome c_3 of Desulfovibrio vulgaris", *Advan. Chem. Ser. Am. Chem. Soc.*, **201**, 199 (1983).

H. INOKUCHI, "Cytochrome c_3: Electron Carrier in Biological System" in Studies Org. Chem., Elservier and Kodansha, **13**, 101 (1983).

I. KOYANO, "State Selected Reaction Dynamics", *Bunko Kenkyu* (in Japanese), **31**, 341 (1982).

K. SHOBATAKE, "Experimental Methods for Studying Elementary Chemical Reaction Processes", *Semiconductor Research*, Vol. 20 "VLSI Technology; No.7. Basis for VLSI Processes." ed. J. Nishizawa (Semiconductor Research Inst., Sendai, 1983), pp.3–28.

H. IWAMURA, "Molecular Dynamics of Triptycene Framework.", *Yuki Gosei Kagaku Kyokaishi*, (in Japanese), **41**, 168 (1983).

H. IWAMURA, "Polycarbenes in the Ground Multiplet States Derived from Diphenyldiazomethane Homologs." *Kagaku no Ryoiki* (in Japanese), **37**, 146 (1983).

H. IWAMURA, "Molecular Design of Correlated Internal Rotation.", *Kagaku no Ryoiki* (in Japanese), **37**, 252 (1983).

H. KASHIWAGI, "Utilization and Development of Library Programs for Atoms and Molecules", *Butsuri* (in Japanese), **37**, 779 (1982).

Institute for Molecular Science, Myodaiji, Okazaki 444, Japan